Chemical Kinetics Modelling Study on Fuel Autoignition in Internal Combustion Engines

by

Zhen Liu

A Doctoral Thesis

submitted in partial fulfilment of the requirements for the award of

Degree of Doctor of Philosophy of Loughborough University

July 2010

Abstract

Chemical kinetics has been widely acknowledged as a fundamental theory in analysis of chemical processes and the corresponding reaction outputs and rates. The study and application of chemical kinetics thus provide a simulation tool to predict many characteristics a chemical process. Oxidation of hydrocarbon fuels applied in internal combustion engines is a complex chemical process involving a great number of a series of chained reaction steps and intermediate and simultaneous species. Symbolic and Numerical description of such a chemical process leads to the development and application of chemical kinetics models. The up-to-date application of chemical kinetics models is to the simulation of autoignition process in internal combustion engines.

Multi-zone thermodynamic combustion modelling has been regarded as a functional simulation approach to studying combustion process in IC engines as a decent compromise between computation accuracy and efficiency. Integration of chemical kinetics models into multi-zone models is therefore a potential modelling method to investigate the chemical and physical processes of autoignition in engine combustion.

This research work has been therefore concerned with the development, validation and application of multi-zone chemical kinetic engine models in the simulation of autoignition driven combustion in SI and HCCI engines. The contribution of this work is primarily made to establish a mathematical model based on the underlying physical and chemical principles of autoignition of the fuel-air mixture in SI and HCCI engines. Then, a computer code package has been developed to numerically solve the model. The derived model aims at improving the understanding of autoignition behaviour under engine-like conditions and providing an investigative tool to autoignition characteristics. Furthermore, as part of the ongoing program in the research of free piston engines, the results of this work will significantly aid in the

investigation and simulation of the constant volume autoignition applied in free piston engines.

Keywords: Autoignition, Knock, SI, HCCI, Chemical Kinetics, Multi-zone, Modelling, IEGR, LUCKS, Mixing, DVODE

Figure List

Table List

Dedication

This thesis is what it is today because of a few special people, and I would like to thank them for everything they have done in support my accomplishment of the thesis. First and foremost, to Professor Rui Chen, my supervisor who has been the most respectable master and friend in my life, I cannot fully express my gratitude for his care, faith, and superb guidance.

My gratitude especially to my aunts and uncles who have supported and had faith in me, without them, I would not have been typing this work in English.

Thank you especial to my dearest wife, Shanshan, who believed this work from the start and gives her full heart and soul to our life.

To my colleagues and friends, Pratap Rama, Paul Osei-Owusu and Anna Liu, for their help, kindness and trust, I am not able to be grateful enough.

I would be remiss and reproved if I did not mention the two extraordinary couples who have been of paramount importance in my life: first, my parents who are forever the best parents in the world for me and my parents-in-law, who treat me like a beloved son.

Last but not the least, lots of thanks to those friends and relatives whose name are not mentioned in this dedication, their help, understanding, and faith is considerably important.

Nomenclature

Abbreviations

1D	One Dimensional
AFR	Air-Fuel Ratio
AFER	Air-Fuel Equivalent Ratio
ATAC	Active Thermo-Atmosphere Combustion
AVT	Active Valve Train
BDC	Bottom Dead Centre
BMEP	Brake Mean Effective Pressures
BTDC	Before Top Dead Centre
CA	Crank Angle
CAD	Computer Aided Design
CAI	Controlled Auto-Ignition
CCD	Charge Coupled Device
CFD	Computational Fluid Dynamics
CI	Compression-Ignition
CIDI	Compression-Ignition Direct Injection
CIHC	Compression Ignited Homogeneous Charge
CO	Carbon Monoxide
CO_2	Carbon Dioxide
CPU	Central Processing Unit
DI	Direct Injection
DME	Dimethyl Ether
DTBP	Di-tertiary Butyl Peroxide
EGR	Exhaust Gas Recirculation
EEGR	External Exhaust Gas Recirculation
EVC/EC	Exhaust Valve Closing
EVO	Exhaust Valve Opening
FVVT	Fully Variable Valve Train
GDI	Gasoline Direct Injection
GUI	Graphics Users Interface
HC	Hydrocarbons
HCCI	Homogeneous Charge Compression Ignition
HCDC	Homogeneous Charge Diesel Combustion
IAPAC	Injection Assisted Process Air Compressed
IC	Internal Combustion
ICE	Internal Combustion Engine
IEGR	Internal Exhaust Gas Recirculation
IMEP	Indicate Mean Effective Pressures
IVC	Inlet Valve Closing

IVO/IO	Inlet Valve Opening
LUCKS	Loughborough University Chemical Kinetics Simulation
MMT	Methylcyclopentadienyl Manganese Tricarbonyl
NO_X	Oxides of Nitrogen
NTC	Negative Temperature Coefficient
NVO	Negative Valve Overlapping
NZ	Total Zone Number
ODE	Odinary Differential Equation
ON	Octane Number
PCCI	Premixed Charged Compression Ignition
PDA	Particle Dynamics Analysis
PM	Particulate Matter
PPM	Parts Per Million
PRF	Primary Reference Fuels
PVO	Positive Valve Overlapping
RCM	Rapid Compression Machine
RGF	Residual Gas Fraction
RON	Research Octane Numbers
SI	Spark-Ignition
SOC	Start of Combustion
SOI	Start of Injection
TDC	Top Dead Centre
TEL	Tetraethyl Lead
UHC	Unburned Hydrocarbon
VCR	Variable Compression Ratio
VVT	Variable Valve Timing
WOT	Wide Open Throttle

Definitions

CHEMKIN	Chemical Kinetics Modelling Code
FLUENT	Commercial CFD code
KIVA	Open-source CFD code for engine modelling
SENKIN	Closed-Volume, Gas-Phase Chemistry Code
DVODE	Double-precision Variable-coefficient Ordinary Differential Equation Solver
LUCKS	Loughborough University Chemical Kinetic Simulation

Arabic Symbols

a	Stoichiometric Coefficients
b	Stoichiometric Coefficients
c	Stoichiometric Coefficients
d	Stoichiometric Coefficients
c_v	Specific Heat Capacity at Constant Volume [J/kg/K]
c_p	Specific Heat Capacity at Constant Pressure [J/kg/K]
h	Specific Enthalpy [J/kg]
j	The step number
k	Reaction Rate Coefficient
m	Mass/Parameter [kg]

n	The time step number/Parameter/moles
p	Pressure [Pa]
r	Reaction Rate
t	Time [s]
Δt	The calculation time step [s]
u	Specific Internal Energy [J/kg]
v	Specific Volume [m3/kg]
x	Burned Mass Fraction
A	Area/Reactant/ Pre-exponential Factor/Parameter Matrix [m2]
B	Cylinder Bore/Reactant/Parameter Matrix [m]
C	Product
C_{wsh}	Woschni's Heat Transfer Rate Constant
C_p	Heat Capacity at Constant Pressure [J/kg]
C_h	Heat transfer rate constant
D	Product/Character Length
E	Activation Energy [J/mole]
K	Pressure slope Change Rate [Pa/CA]
M	Third Body Molecule/Molar Mass [kg/mole]
N	Total Number
N_u	Nusselt Number
P	Products
ΔP_c	Instantaneous Pressure Rise [Pa]
P_o	Pressure at IVC [Pa]
Q	Heat Loss [J]
R	Universal Gas Constant/Species [J/kg-K]
R_e	Reynolds Number
S	Species
$\overline{S}_p$	Mean Piston Speed [m/s]
T	Temperature [K]
U	Internal Energy [J]
$\overline{U}_g$	Average Gas Velocity [m/s]
V	Volume [m3]
V_d	Displaced Volume [m3]
V_o	Cylinder volume at IVC [m3]
X	Mole Fraction
Y	Mass Fraction
T_o	Temperature at IVC [K]

GREEK

α	Stoichiometric Coefficients/Angle

β	Stoichiometric Coefficients/ Radiation Heat Transfer Coefficient/Angle
$\dot{\omega}$	Molar Rate of Production
σ	Stefan-Boltzmann Constant
λ	Gas Conductivity
ρ	Density
ν	Net Stoichiometric Coefficient
θ	Crank Angle in degree
γ	Specific Heat Ratio - Relationship between the Heat Capacities c_p / c_v
τ	Correlation of Ignition Delay
μ	Gas Viscosity
w	Characteristic Speed
Δ	Gradient/Difference

SUBSCRIPTS

$auto$	Autoignited
b	Burned Gas
bl	Blowby
cly	Cylinder
$conv$	Convective
f	Burning/Forward/Function
$flame$	Flame Propagation
g	Global
ht	Heat Transfer
i	Reaction/Zone/Mass Flow Index
in	Entering
j	Species Index/ Step Number
$initial$	Beginning Point
k	Reaction Index
l	Heat Loss/Flow Index
out	Existing
r	Reverse
rad	Radiation
$total$	Total
u	Unburned Gas
w	Cylinder Wall
$weibe$	Weibe Function
$Fuel$	Fuels
$Oxidizer$	Oxidizer
A	Area
BL	Bounday Layer
H	High

L	Low
Z	Zone

Publications

The following publications have been achieved in relation to this research.

Zhen, Liu and Chen, Rui.; Multi-Zone Kinetic Model of Controlled Auto Ignition Combustion, SAE World Congress & Exhibition, April 2009, Detroit, MI, USA. SAE 2009-01-0673

Zhen, Liu and Chen, Rui (2009) 'A Zero-Dimensional Combustion Model with Reduced Kinetics for SI Engine Knock Simulation', Combustion Science and Technology, 181:6, 828-852

Contents

Chapter One: **Introduction**

1.1 Motivation

Autoignition phenomenon in spark ignition (SI) engines was first recognized in the early 1900's, which is the major cause of engine knock that is identified as a limitation on engine output and fuel efficiency. Since then, the understanding of autoignition is restricted to its negative impact on the new design of SI engines. Many potential approaches for improving SI engine performance and reducing emissions such as increasing compression ratios, boosting inlet pressure and raising EGR temperature are limited by their undesirable contribution to engine knock

Autoignition has been regarded as the setback for gasoline engine development till the emergence of a new combustion concept, Homogeneous Charge Compression Ignition (HCCI). HCCI engines utilize homogeneous charge of gasoline and air as in traditional spark ignition (SI) engines; however, the charge is compressed to autoignite as in traditional compression ignition (CI) engines. This new combustion concept provides the fuel efficiency as high as that in CI engines and the much lower NO_X and particulate emissions than that in SI engines. For the first time, autoignition is applied positively as an ignition approach in gasoline engines.

In conclusion, the roles of autoignition in gasoline combustion engines have been twofold: limitation to SI engines and solution to HCCI engines. Therefore, tremendous research effort has been devoted to the study of autoignition. Investigation of engine knock in SI engines aims at restraining knock either mechanically by improving the chamber design or chemically by changing the molecular structure of fuels. Research on HCCI combustion studies the

characteristics of autoignition and the relative influential factors so that the ignition timings and combustion rates can be controlled for consistent application.

Autoignition is acknowledged as a phenomenon, in which a combustible mixture of fuel and oxidizer reacts in a self-accelerating manner, and eventually spontaneously ignite leading to combustion. This ignition process is kinetically driven by the chemical reactions of fuel-air mixture rather than externally supplied ignition sources. When the energy released from the oxidation of hydrocarbon fuels is larger than the heat lost to the surroundings, the temperature of the mixture gradually increases and accelerates at temperatures high enough to supply the activation energy for the thermal explosion. Both of the physical and chemical properties of the mixture are critical to the autoignition process.

In SI and HCCI engines, autoignition occurs in different combustion scenarios. In SI engines, chemical reactions with heat release occur in the end gas ahead of the advancing flame front as the result of the combination of compression from piston motion and the propagating flame front. This raises the temperature of the end gas to a thermally and chemically stressed condition triggering autoignition that produces a rapid rise in local temperature and pressure. The autoignition process is thus significantly influenced by the flame propagation speed and thermal properties of the end gas. However, in HCCI engines, combustion is initiated by autoignition of the in-cylinder charge, which is dominated by local chemical-kinetic reactions with no requirement for flame propagation. Therefore, temperature of in-cylinder charge has a considerable effect on the combustion process due to the sensitivity of chemical kinetics to temperature.

Though studies of autoignition in SI and HCCI engines have involved a lot of research effort, research progress is still limited by inadequate understanding of the physical and chemical processes that lead to autoignition. It has been a big challenge to characterize autoignition due to the complexity involved in the physical and chemical process. Modelling of autoignition in SI and HCCI engine is to address both the physical and chemical processes so that the autoignition behaviour can be theoretically described and numerically characterized. Moreover, modelling work in relation with autoignition chemistry provides a convenient tool in engine design and development in terms of control of the chemical kinetic behaviour of hydrocarbon combustion.

Combustion chemistry of gasoline used in SI and HCCI has been widely studied and can be generally interpreted as an oxidation process of hydrocarbon fuels involving a series of complex degenerate chain branching, carrying and terminating reactions with stable and intermediate radical species. Chemical kinetics modeling has been investigated and acknowledged as an important tool in the analysis of the rates of chemical processes and the factors that affect these rates. A chemical kinetics model contains the important elementary reactions and individual species and uses the best available rate parameters and thermochemical data. The size of such a model is decided by the numbers of reactions and species included in the model, which ranges from reduced models with only a few species and reaction steps to detailed models consisting of hundreds of chemical species and thousands of reactions.

One of the major challenges in using chemical kinetics models is the uncertainties in the selection of species, reactions and rate parameters. Most of the available models can only be validated over a rather limited range of conditions. When necessary and possible, optimization of the reaction rate parameters has to be conducted to improve the fit of modeling results against experimental data. However, it will suffer from expensive computation resource even for the models of moderate size, for example, containing a few hundreds of parameters, which could turn the number of algorithm dimensions to hundreds or even thousands. Another challenge for applying chemical kinetics modeling comes from the concern over computation cost. The computational power of modern computers has not been developed well enough to handle in an efficient and effective manner the chemical kinetics calculation in cooperation with multidimensional modeling. In the simulation of combustion in SI or HCCI engines, the integration of computational fluid dynamics (CFD) model with detailed chemical kinetics models, theoretically, provides unparalleled simulation accuracy and details in presenting combustion chamber geometries and combustion behaviour. However, numerical modeling of this scale requires substantial computer resources. Though, a few CFD codes such as FLUENT, CHEMKIN-CFD etc. have been equipped with some kind of chemistry models, but the size of the models implemented are limited to a much-reduced level. Moreover, the computational time of this approach is still costly and unacceptable for both engine research and design.

To the challenges presented above, one of the solutions could be integration of the downsized chemical kinetics models into the zero-dimensional multi-zone models that can describe adequately the in-cylinder combustion scenarios in SI and HCCI

engines. Firstly, in contrast to the prevailing single zone models, the multi-zone approach stands out through taking account of the inhomogeneity of the in-cylinder mixture by dividing the combustion chamber into multiple zones and models the zonal changes of volume and mass caused by the in-cylinder flow dynamics. When coupled with chemical kinetics models, multi-zone modelling is capable of describing chemically the combustion process so that the major characteristics of autoignition such as ignition timing and heat release rate etc. can be more accurately predicted. With chemical kinetics modelling, in addition, emissions e.g. CO and HC can be better modelled in multi-zone models.

Secondly, the multi-zone models represent much lower computational cost in comparison with the CFD approach. Even though Incorporation with detailed chemical kinetics models may result in increased computation time over reduced chemical models, it is still of time scales of tens of minutes to hours, which is more reasonable and acceptable in contrast to the computational cost by the approach coupling CFD and chemical kinetics.

Finally, though chemical kinetics modelling has prevailed in simulating kinetic combustion processes since the last two decade, research work on its incorporation into thermodynamic modeling of IC engine is lagging. The major hindrance used to be the inadequate understanding of combustion chemistry under IC engine combustion conditions and the underdevelopment of chemical kinetics models of the real fuels used in IC engines. However, with advances in relevant knowledge and computer-aided technologies in developing downsized kinetic models, it has been achievable task for researchers to develop multi-zone chemical kinetics models.

This research work consequently puts emphasis on incorporation of chemical kinetics models with zero-dimensional multi-zone models in the simulation of SI and HCCI combustion so that autoignition behaviours in both types of combustion processes can be better understood and numerically described.

1.2 Goals and Scope of Present Work

The overall purpose of this study was to establish, develop and program multi-zone chemical kinetics models for the simulation of combustion processes in SI and HCCI engines.

The model for SI combustion is to develop a diagnostic tool for engine knock analysis. The incorporation of chemical kinetics with three-zone thermodynamic model (burned, unburned and burning) provides an approach of simulating the thermodynamic states of the three zones under knocking conditions. Through the model, the major knock characteristics (i.e. knock tendency and knock onset timing, etc.) can be predicted and related influential factors (i.e. spark timings and air-fuel ratios, etc) can be analyzed and investigated.

The model for HCCI combustion is to simulate HCCI combustion process in consideration of inhomogeneous distribution of in-cylinder temperature and mixture compositions. The effort is mainly put on the application of chemical kinetics models to provide chemical analysis of the autoignition-driven ignition process and the post-ignition combustion processes, and the application of the zonal model to describe the thermodynamic and physical behavior of the in-cylinder mixture during the combustion. The developed model provides a numerical prediction method for examining and studying ignition and combustion behaviors and emissions of major products of interest. The results from the modeling work can help to improve the understanding of HCCI combustion and provide important information on overcoming the challenges limiting the HCCI engine as a standalone production engine and good knowledge base for further computational studies and experimental work.

The achievements of both of the above objectives form the basis of the computer simulation work for the ongoing project to investigate free piston engines that apply constant volume autoignition as the ignition and combustion approaches. This new engine type has the potential for high efficiency, low emissions, and low manufacturing cost. Its main applications are likely to be in series hybrid vehicles and portable power generation. The technology is based around a single-cylinder free-piston internal combustion engine (ICE), which is run on a 4-stroke cycle, with an integral linear electromagnetic machine and electromagnetically operated poppet valves. By freeing the piston from crank shaft motion, it removes most of the constraints of crankrod-slider internal combustion engines, and facilitates many advanced combustion strategies - by enabling variable compression ratio operation, throttle-free operation, different piston strokes during compression and expansion, and other previously unattainable piston trajectories. Furthermore, a free-piston engine is capable of operating on a variety of fuels. Last but not least, the HCCI approach is adopted and applied to free-piston engines for the mixture ignition, so it

has a similar combustion scenario to HCCI engines, in which combustion is dominated by chemical kinetic reactions.

So far, most of the available and validated computer codes for chemical kinetics modeling of IC engine combustion apply single zone approaches such as the SENKIN code in the CHEMKIN package. However, due to the assumption of the homogeneous mixture properties and the ignorance of the mixture dynamics, it suffers from its ability to predict major combustion characteristics such as heat release rate, emissions, combustion completeness and peak cylinder pressure, etc. Moreover, most software companies do not publish the source code of the developed software, which disallows the end-users to get access to the core of the software. This surely best protects the software companies' interest, but it hinders the end-user development to make modifications and additions to the software for more advanced modeling. Therefore, another interest in this research work is to translate the established model from the algorithm form into a computer program. The work is oriented to develop a computer code of a well-designed structure so that it is easy for end-users to read and revise. This computer code can be able to facilitate the application, improvement and generalization of the developed multi-zone model.

The main objectives of this research work with relevant chapters in this thesis are summarized as follows:

- Review the studies of autoignition-driven combustion phenomenon in SI and HCCI engines and the modelling and experimental work in the field. (**Chapter 2** and **3**)
- Summarize the chemical kinetics theories and review the chemical kinetics modelling work on hydrocarbon fuels in relation to its application in SI and HCCI engines. (**Chapter 4**)
- Compare and review the computation methods applied on engine combustion modelling and develop the mathematical model of multi-zone chemical kinetics simulation of SI and HCCI engines. (**Chapter 5**)
- Investigate the numerical features of the system equations related with chemical kinetics simulation. The numerical methods and codes for the solution of the system equations are compared and discussed. (**Chapter 5**)
- Develop and interpret the LUCKS code designed for the multi-zone chemical kinetic simulation of SI and HCCI engine combustion. This is suggested to be

regarded as the core part of the research work. This code translates the mathematical description of the multi-zone to the computer language and is developed in a commercial-code-like style. (**Chapter 6**)

- Evaluate the LUCKS_SI code in the simulation of SI engine knock and validate the model through comparison of the simulation results against the experimental results. (**Chapter 7**)
  - Divide the in-cylinder mixture according to their difference of thermodynamic states and compositions.
  - Apply a reduced chemical kinetics model to model both post-flame heat release and pre-flame autoignition.
  - Modify the reduced chemical kinetics model to improve its prediction of autoignition characteristics under SI combustion.
- Evaluate the LUCKS_HCCI code in the simulation of HCCI engine combustion. (**Chapter 8**)
  - Model the inhomogeneity of in-cylinder mixture properties and mass and energy transfer caused by mixture dynamics.
  - Validate the model against experimental results at various Internal Exhaust Gas Re-circulation (IEGR) levels and investigate the thermal and chemical effect of the IEGR on the HCCI combustion.
- Summarize and conclude the work and make future recommendation. (**Chapter 9**)

Chapter Two: **Literature Survey on SI Engine Knock**

2.1 Introduction

The spark ignition engines are still the main power source in the road vehicles nowadays. However, with the increasing awareness of the dying-out of conventional fuel supply and environmental issues, improving the efficiency of SI engines has been the major research subject and a critical motivation in guiding engine design in the automotive industry.

The thermal efficiency of a spark ignition engine can be improved by either increasing compression ratio or boosting intake pressure through turbocharging or supercharging. However, both of the approaches are limited by knocking combustion. Compared with old-timed engines, modern engines have been designed to be more compact with much increased compression ratios. However, further increase of compression ratios is constrained by engine knock, which occurs when the end-gas is over compressed at high compression ratios. Knock is also a significant barrier to the design of high brake mean effective pressures (BMEP) engines through either turbocharging or supercharging due to the high sensitivity of knock to intake pressure.

Engine knock is an unacceptable combustion phenomenon causing unpleasant and undesirable sound to the passengers in a vehicle and at a high enough intensity, engine damage. Knock has been a long term problem for engine designers. It is believed that occurrence of knock is associated with spontaneous ignition (autoignition) of the unburned mixture ahead of the flame front before the arrival of

the propagating flame or preignition caused by the glowing combustion chamber deposit [1]. Figure 2-1 compares the normal and abnormal combustion phenomenon occurring in SI engines.

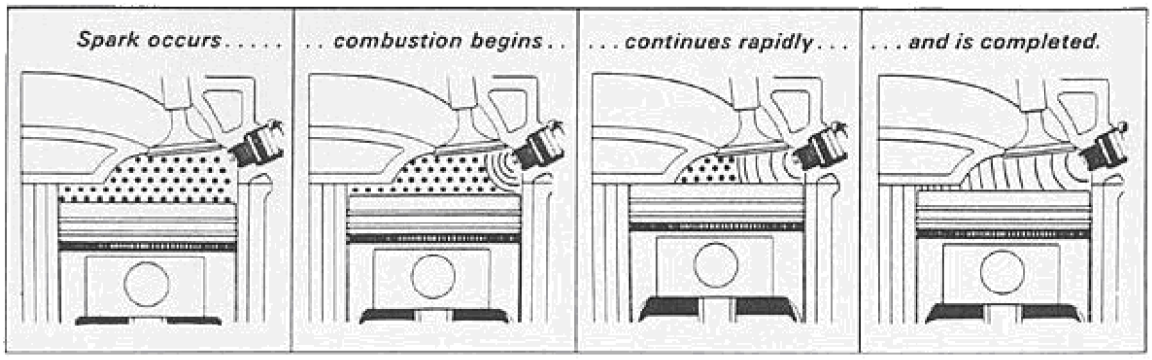

a: Normal Combustion

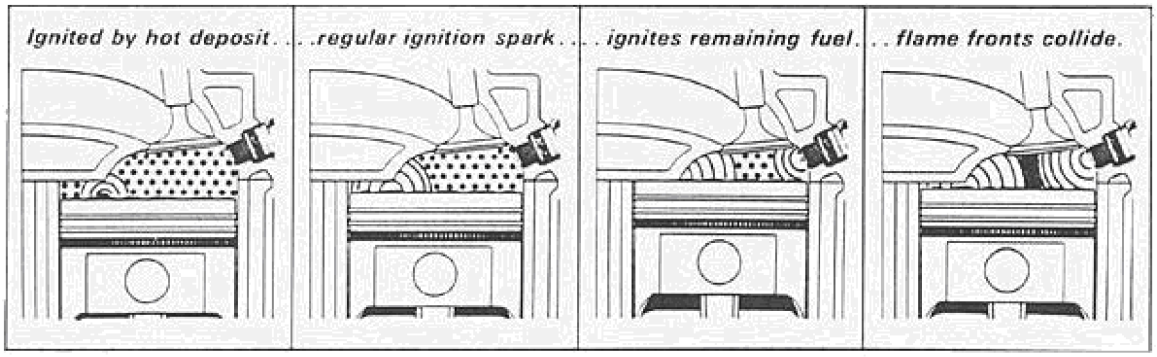

b: Abnormal Combustion caused by Surface Ignition

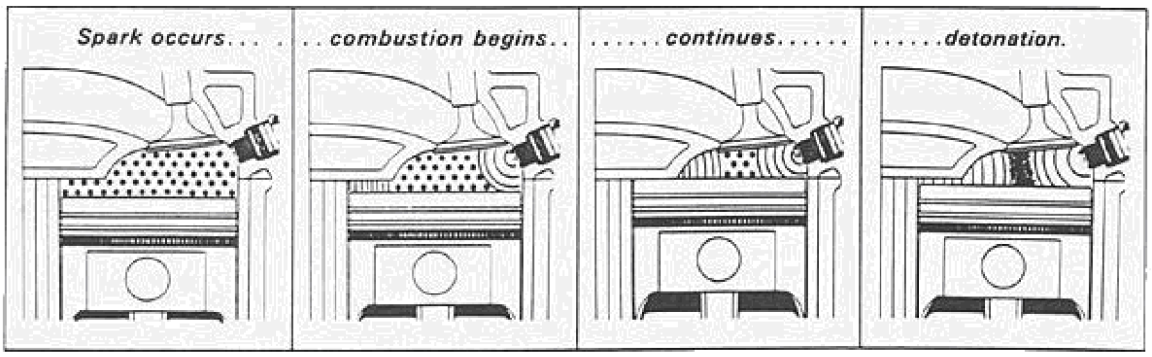

c: Abnormal Combustion caused by End-Gas Autoignition

Figure 2-1: Comparison of normal (a) and abnormal (b and c) combustion phenomenon in SI engines [2].

Studies of engine knock have involved a lot of research effort in order to restrain knock either mechanically by improving the chamber design or chemically by changing the molecular structure of fuels. However, extension of knock limit in SI

engines is still limited by inadequate understanding of the physical and chemical processes that lead to knock. It is also a big challenge to characterize knock further due to the significant cyclic variation of knock characteristics. In addition, modelling work is even farther lagged behind.

2.2 Spark Ignition Engine Combustion and Knock

Combustion in SI engines is initiated at the precise moment towards the end of the compression stroke at the spark plug by an electric discharge. When the spark plug fires, a flame kernel is formed, and then the kernel continues to grow into a fully developed self-sustained flame and propagates through the homogenous charge [3-5].

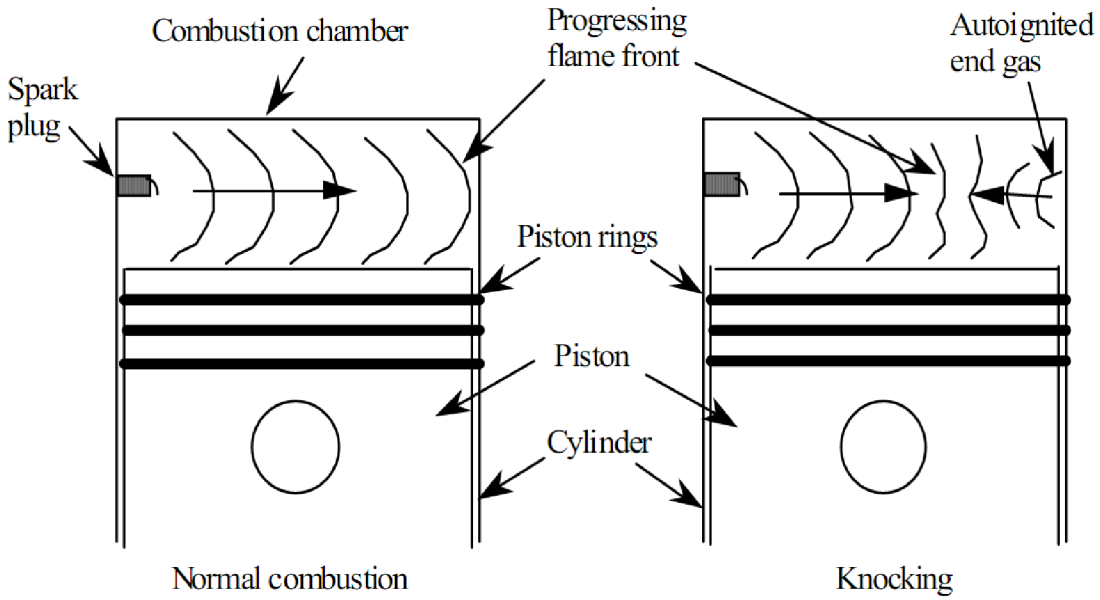

Figure 2-2: Schematic of combustion process with and without knock [6].

When flame propagation speeds exceeds a limited value, the end-gas is compressed by both the propagating flame front and upward moving piston to a sufficiently high pressure and temperature for fuel oxidation to spontaneously occur, which starts with pre-flame chemistry and ends with rapid energy release. This phenomenon is generally termed as '**autoignition**' [1]. Whether or not, occurrence of autoignition depends on a race between the chemical consumption of the end-gas ahead of the flame front and the consumption by the propagating flame. If the end-gas is not consumed before the chemical reactions proceed to the point, at which bulk heat is

rapidly release, the resulting autoignition causes sharp increase of local temperatures and pressures. Figure 2-2 compares the combustion processes with and without knock.

A pressure wave then spreads outwards from the location of autoignition at a sound speed of sound and resonates within the engine cylinder. The pressure oscillations cause vibration of the head and block, resulting in a clanging or pinging sound. ***Knock*** is the term used to describe such physical manifestations. Audible knock is not acceptable, and the high local temperatures and pressures associated with heavy knock can cause engine damage. Autoignition of the end-gas limits the compression ratios in a position to achieve higher combustion efficiency and severe autoignition leads to knock, deteriorates engine efficiency, and thereby increases emissions.

Since knock causes damage to engine body and bring uncomfortableness to vehicle passengers, engine design and operating parameters have to be adjusted for its avoidance. It has been acknowledged that severe knock is subject to occur at high load, which creates high peak pressures, and low engine speed, which provides a long residence time for autoignition chemistry of the end-gas. In prevention of knock, peak in-cylinder pressure has to be reduced. For this, spark ignition delay has been widely applied to move location of peak pressure away from TDC position. However, over-delayed sparking ignition-timing leads to reduction of the forces from the ignited mixture on the downward piston, so to the engine torque and efficiency, and an increase of exhaust temperatures. To balance the avoidance of knock and achievement of maximum engine efficiency, compression ratios and boosted intake pressure have to be limited with sacrifice of their best benefit in improving engine efficiency.

2.3 Factors that Affect Engine Knock

The chemical kinetic reaction rates of the end-gas are dependent on temperature; however temperature is interactively affected by pressure. The following thermodynamic expression describes the P-T relationship for an adiabatic compression process.

$$T = T_{initial}\left(\frac{p}{p_{initial}}\right)^{\frac{\gamma-1}{\gamma}} \quad \textbf{(2-1)}$$

Where γ is specific heat ratio and the subscript $initial$ indicates the beginning point of compression stroke. Equation 2-1 dictates that an increase of end-gas pressure increases end-gas temperature, which in turn increases reaction rates. Any factor having influence on temperature and pressure therefore affects the thermodynamic and chemical kinetic states of the end-gas. Many factors are considered important in relation to autoignition development and knock. The following is a brief description of some of these factors [1,7-9]:

Spark Timing – Change of ignition timings affects combustion phasing. Retarded ignition timings cause lower overall in-cylinder pressure because the combustion phasing is shifted away from the TDC position, which leads to the main combustion with major heat release occurs within a larger and faster expanding volume as the piston is moving downward. As a contrast, advanced spark timings causes earlier combustion that results in higher cylinder pressures. Knock occurrence is more subject to earlier spark timings because of the maximum end-gas temperature is increased.

Compression Ratio – With increased compression ratios, the volume swept by the piston during the compression and combustion phases becomes smaller. This leads to more intense compression on the end-gas and higher heat release from the mixture. As a result, a higher compression ratio increases cylinder pressure and end-gas temperatures.

Air-Fuel Ratio – At different AFRs, the in-cylinder mixture shows different combustion strength. Change of the mixture composition and thermodynamic properties affects combustion rates and the energy release, which in turn affects cylinder pressure and end-gas temperatures.

Intake Pressure - A higher intake pressure forces a larger amount of air-fuel mixture into the cylinder with higher initial pressure and volumetric efficiency cylinder, which consequently leads to higher overall in-cylinder pressure and combustion temperature.

EGR - Using EGR increases the total heat capacity of the end-gas and consequently reduces the temperature rise of the gas, which thermally diminishes

knock tendency. However, the large number of reactive species present in the exhaust gas can also promote autoignition by chemical means.

Engine Speed - The chemical reactions of the end-gas takes time to proceed. At lower engine speeds, flame propagating speed become equivalent to or slower than the reaction characteristic time, so autoignition reactions is more likely to build up and advance.

Charge Preparation – The flow dynamic motion (turbulence, swirl, and tumble) affects the homogeneity of the mixture, which has a significant effect on combustion process. Local inhomogeneities of the mixture could lead to incomplete combustion or regionally high combustion temperature.

Combustion Chamber Geometry - The general shape of the combustion chamber, as well as spark plug location, affects the flame front area and the distance the flame front travels. Longer flame travel distance results in longer combustion duration and more time for autoignition chemistry to proceed.

Intake Temperature – It can be deduced from equation 2-1 that mixture temperature in the compression process scales closely with initial temperature. Higher initial temperatures lead to higher overall mixture temperatures throughout the compression and combustion processes, which promote the rates of autoignition reactions

2.4 Knock Theories

The cause of knock has been a research subject provoking many arguments. However, there is no yet a general agreement on the explanation of SI engine knock. Throughout the literatures, two major theories have been established and common accepted to explain knock phenomenon: ***autoignition theory***, ***detonation theory*** and ***surface ignition***.

2.4.1 End-Gas Autoignition

Autoignition in SI engines is the spontaneous self-ignition of the fuel-air mixture in the combustion chamber associated with high chemical reaction rates and heat release rates [1]. In the compression stroke, the in-cylinder mixture is compressed by the upward moving piston and the temperature is gradually increased until the spark plug

ignites the mixture at a certain crank angle position before TDC. The burned gases then expand in a form of propagating flame. As a result, the unburned gas in front of the flame front is compressed by both the movement of the piston and flame propagation. When the piston passes the TDC and moves downwards, the compression of the flame propagation is offset a bit, but the flame propagates at a higher speed than that of the piston in the early stage of the expansion stroke, so the unburned gas is still under compression. During the compression of the unburned gas, temperature and pressure gradually increases and the low temperature chemistry for the hydrocarbon fuels is initiated to produce accumulative reactive products that can lead to explosive autoignition when the temperature is increased to a critical value. Once the autoignition starts, it is accompanied by rapid energy release and sharp increase of temperature and pressure. Autoignition is a complex chemical process that involves thousands of reaction steps at different temperature regions [10-12]. Details of autoignition chemistry are provided in **Chapter 4**.

2.4.1.1 Autoignition Sites

Studies [13,14] claim that autoignition sites of the end-gas in SI engines are located at discrete exothermic centres (exothermic centres), from which autoignition chemical reactions proceed and propagate. Formation of autoignition centres can be caused by both temperature and composition heterogeneity. Temperature heterogeneity could arise from surface hot spots and inhomogeneously distributed gas residuals, or deposit, or temperature gradients due to heat transfer with cylinder wall, or from a combination of these. The inhomogeneity of the mixture composition may result from imperfect mixing of the mixture of fuel, air and/or residual gases.

Later study from Hajireza and Konig [15] further confirmed the above point. They investigated the appearance of exothermic centres caused by inhomogeneities within the end-gas of SI engines. It is found that the gas near the exothermic centre is pre-reacted to produce products and intermediate products from low-and high-temperature reactions. As a result, a radical pool is formed as a reaction centre and reaction front propagates from this centre with a velocity of several meters per second. The velocity increases with decreasing temperature gradients in the inhomogeneous mixture.

Sheppard and Konig [14] concluded that autoignition centres occur either close to main flame where they engulfed by the flame, by the chamber or at random location

in the end-gas. Griffiths et al [16] showed that the sites at which autoignition occur are related to compression temperature, gas motion and associated heat transfer taking place in the chamber. Schrieber er al [17] found that at both low and high bulk end-gas temperatures the autoignition centres occurred in the adiabatic core, because the local gas temperature in this region was higher than at the chamber wall.

In a recent study, Nobuyuki et al [221] use a high-speed video camera to visualize flame propagation and autoignited kernels in the end-gas at knocking combustion. They found that auto-ignited kernels appeared near a negative curvature of the flame front, which related to low-temperature chemistry. The large amount of unburned mixture generated a strong pressure wave caused by the auto-ignited kernels explosion. Visualized images of a regular propagating flame front and auto-ignited kernels

2.4.1.2 Autoignition Modes

Theoretical studies [14,19-21] have suggested that in terms of magnitude of temperature gradients about autoignition centres, three autoignition modes can be identified as ***deflagration***, ***thermal explosion*** and ***developing detonation***. The three modes are characterized as follows;

2.4.1.2.1 Deflagration

In the deflagration mode, autoignition chemistry occurs takes places at low end-gas temperature and results in steep temperature gradient (>100K/mm). The reaction centre undergoes a sequent steady transition from an initial radical pool to a deflagration site and then to a propagating flame into the surrounding regions of the unburned gas. A weak pressure wave resulted from the temperature gradient then propagates away from the centre, but the resultant pressure wave attenuates as it propagates into the unburned gas. Deflagration of the end gas does not cause influence on autoignition chemistry of the other reaction centres, and leads to little or no knock and may actually be beneficial to combustion completion and clearance of unburned hydrocarbon left throughout engine cycles.

2.4.1.2.2 Thermal Explosion

Thermal explosion occurs at high end-gas temperature with small temperature gradients around the autoignition reaction centre. In this mode, the chemical reactions proceed in a high reaction speed and leads to a simultaneous autoignition

throughout the end-gas. As a result of fast heat release, it is likely to produce strong pressure waves and moderate or strong knock. However, there is no coalescence of pressure and reaction fronts, so the pressure waves resulted from this autoignition mode not intense enough to cause major engine damage.

2.4.1.2.3 Developing Detonation

The developing detonation occurs at moderate end gas temperatures with moderate temperature gradients. As there is insufficient time or space for a detonation to fully develop, this mode is described as a developing detonation. In this mode, the autoignition reaction front propagates at approximately the acoustic velocity and becomes coupled with pressure waves leading to mutual enhancement. The latter is damaging. A developing detonation comprises supersonic combustion with very high peak pressures, which, although short lived, may cause damage to the engine, as is observed with severe conventional spark ignition engine knock. Of the three, it is the mode that can lead to the most damaging form of knock.

2.4.1.3 Autoignition Chemistry

The unburned gas starts to get chemically active the moment the compression process begins. Chemical reactions steadily proceeds, but at rather low rates. With the ignition of the unburned mixture, a flame then begins to propagate across the chamber and impose further compression on the unburned gas (end-gas), which promotes the chemical reaction rates of the end-gas. Under normal operation, the chemistry in the end-gas will stay steady and only consumes very a small fraction of the unburned gas. However, under extreme conditions when pressure or temperature exceeds a critical level, the chemical reactions of the end-gas will accelerate and release significant amount of heat that is greater than what can absorbed by the surroundings, which then leads to a full-scale autoignition of the end-gas.

It has been widely acknowledged that oxidation of hydrocarbon fuels is a complex chemical reaction process involving a large number of simultaneous, interdependent and intermediate species and reactions. The process is normally initiated from a group of reactions abstracting H atoms from or decomposing the hydrocarbon molecules to produce highly reactive intermediate species (radicals). This is then followed by propagation reactions where the generated radicals react with the reactant molecules to form products and other radicals. Propagation reactions are characterised by producing more radicals than the ones they consumed, which is

called chain branching reactions. Chain branching reactions Increase the number of radicals and accelerate the chemical process. Finally, radical accumulation is suppressed by termination reactions that transform the active radicals to stable products [10,22-24].

In terms of the temperature ranges, in which the reactions proceed, the whole chemical process can be separated by three temperature regimes. The following section gives a brief description of these temperature regimes and more details of the chemistry of hydrocarbon oxidation can be referred to **Chapter 4**.

2.4.1.3.1 Temperature Regimes

The chemical processes of autoignition may be generally described as a series of complex degenerate chain branching, carrying and terminating reactions involving stable and radical species (See **Chapter 4** for more details). It is commonly accepted that for hydrocarbon oxidation, these reactions may be separated into three distinct temperature regimes: low, intermediate and high temperature regimes [25].

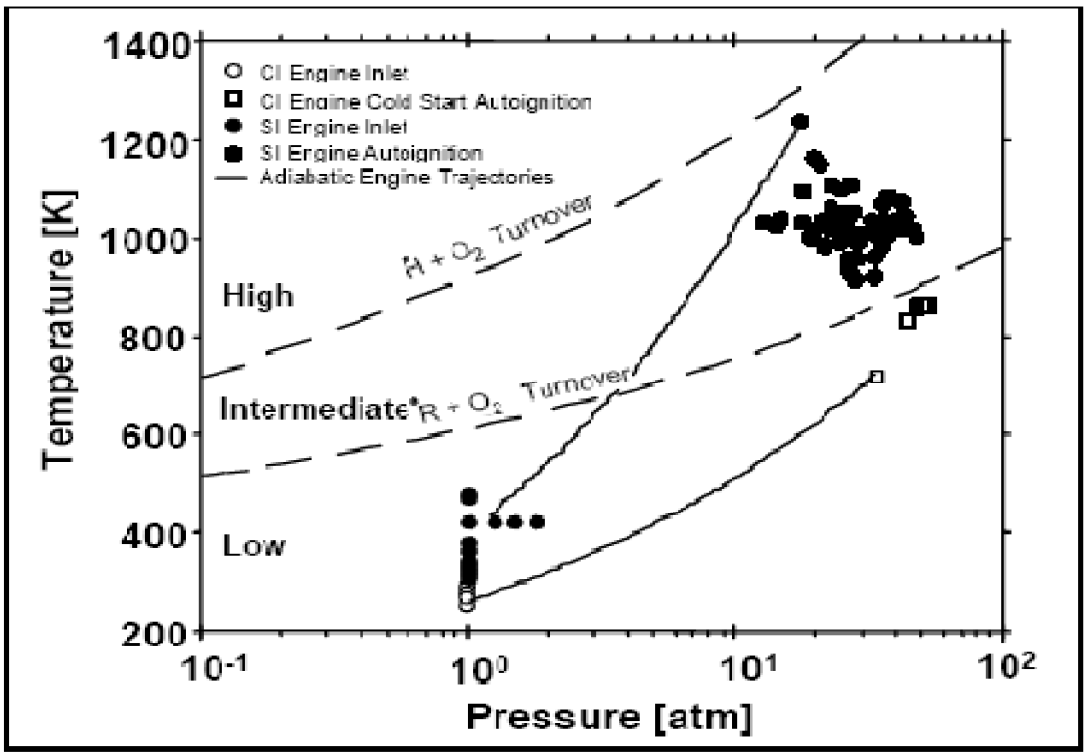

Figure 2-3: Typical SI engine envelope of end gas temperature and pressure histories leading up to the point of knock [26].

Each regime is dominated by reactions involving different radical species and

different pathways. Naturally, the combustion environment, temperature, pressure and equivalence ratio affects the location of the boundaries between each regime. The boundaries between regimes shift slightly to higher temperature as the pressure is increased. The typical range of temperature and pressure that unburned gas experiences before knock in SI engines is illustrated in Figure 2-3.

2.4.1.3.2 Low Temperature Regime

During the compression process, temperature of the unburned gases drops in a range between about 450K and 650K, within which, the chemical reactions of the unburned gases only have low reaction rates. However, due to the low piston speed during this period, the residence time for the unburned mixture staying within this temperature range is long enough to activate some chemical reactions and release chemical energy. This phenomenon is getting more evident at low engine speeds.

In the low temperature regime, the overall reaction takes place primarily through the formation of various alkyl-peroxy radicals via addition of molecular oxygen to alkyl radicals (R•), followed by production of alkyl hydro-peroxides (QOOH•) and subsequent reactions [10]. A schematic diagram for the branching pathways of low and intermediate temperature chemistry is shown in Figure 2-4.

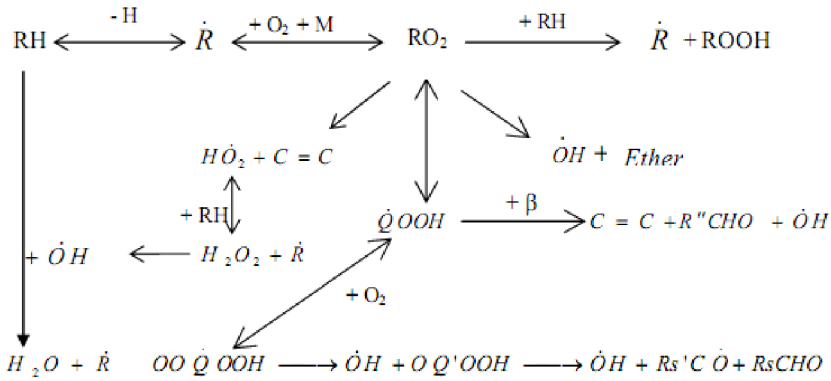

Figure 2-4: Branching pathways for hydrocarbon oxidation at low and intermediate temperatures [27].

2.4.1.3.3 Negative Temperature Coefficient (NTC) Regime

When temperature reaches a regime between ca 650-850 K, further increase in temperature produces a fall in reaction rates, which is called Negative Temperature Coefficient (NTC) or cool-flame regime, where combustion chemistry shows nonlinear responses to the temperature change. In the NTC regime, Alkyl-peroxy

radicals (RO2•) become unstable and react reversely to the oxidation of alkyl radicals (R•+ O2 <=> RO2•) and another reaction pathway for the consumption of alkyl radicals (R•) become competitive, which produces more stable C=C and HO2• and leads to consequently a retarded chain branching of the reactions [10,11,28].

Through the NTC regime, the chemistry moves from the low temperature regime to intermediate temperature regime and then to the final ignition. Thus, NTC behaviour is important in controlling this transition and the chemical reactions in the NTC regime play a critical role in determining ignition induction time and ignition timing.

2.4.1.3.4 Intermediate Temperature Regime

As the temperature increases, the chemistry enters intermediate temperature regime (ca. 800-1000K) and the NTC region eventually disappears. In this regime, autoignition chemistry is dominated by the reactions of HO2• radicals to produce H2O2 radicals that decompose as rapidly as they are formed and produce OH radicals that are responsible for reaction chain branching as depicted in Figure 2-4.

Based on end-gas temperature history measured by Smith et al [29], knock occurs within the intermediate temperature regime. Therefore, the chemical behaviour in the low and intermediate temperature regimes plays a critical role in determining the characteristics of autoignition.

2.4.1.3.5 High Temperature Regime

When the process reaches the high temperature region (above 1000K), the dominant chain branching reactions in hydrocarbon ignition are dominated by OH•, O•, and H• radicals produced by thermal decomposition of radicals such as ethyl, vinyl, formyl, isopropyl and others.

High temperature chemistry leads to fast exothermal chain branching effect and propagate active radicals, which consequently accelerates the overall rate of ignition with explosively released energy.

2.4.1.3.6 Single-stage and Two-stage Autoignition

From the concise introduction of autoignition chemistry, one can learn that autoignition is not a spontaneous process as known by intuition. The real chemical process involves a series of complex chemical reactions. Typically autoignition of hydrocarbon fuels can be characterized by one or two-stage ignition depending on the fuel structure and carbon number in the fuel molecule. Figure 2-5 [30] shows the

evolution of pressure in the combustion chamber of a rapid compression machine for n-heptane oxidation. Two-stage autoignition, an important characteristic of alkane autoignition, is clearly visible. The first stage of ignition, which occurs after an induction period, t_1 meassured from TDC, is characterized by a pressure increase of about 1 bar. This has been acknowledged as the result of the NTC chemistry. After this NTC event, the intermediate and high temperature reactions leads to fully developed hot ignition and a sharp and significant increase of pressure. A total delay time t measured from TDC is observed for this phenomenon.

However, for some hydrocarbons at high temperature and pressure such as iso-octane, the amount of heat released by exothermic reactions at low temperatures is very small, which results in the reduced duration of the NTC stage. Furthermore, when the temperature is sufficiently high, the degenerate branching at low temperatures (the first-stage ignition) is high enough to induce hot ignition directly. This autoignition process is manifested as a single stage ignition [6].

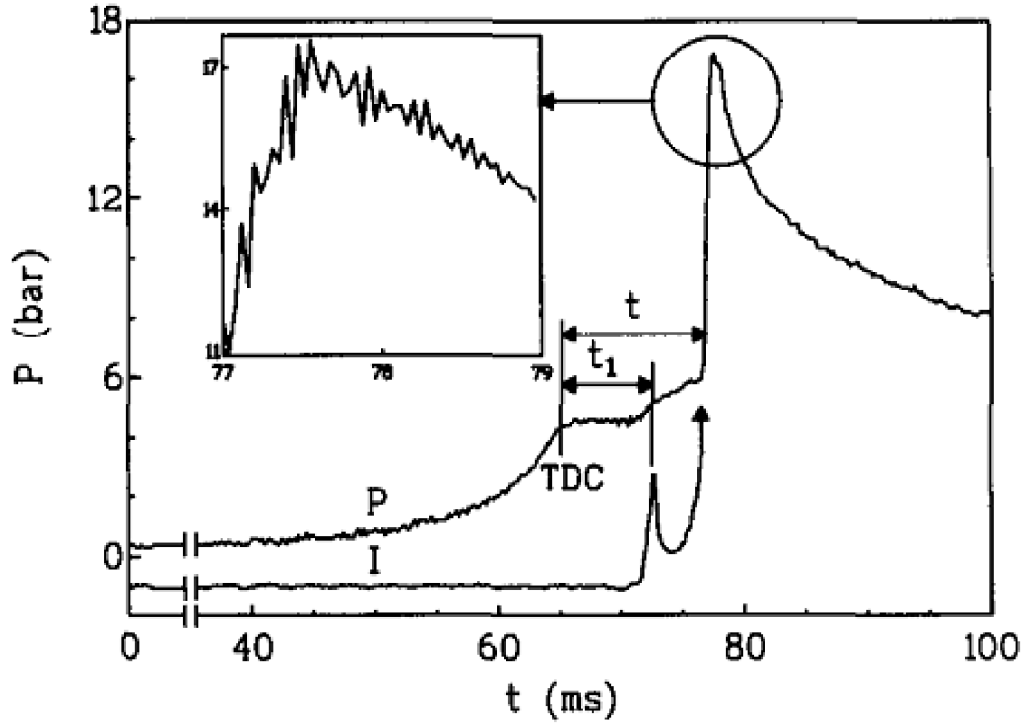

Figure 2-5: Pressure history during the two-stage autoignition [30].

For most of hydrocarbon fuels, at low compressed gas temperatures, ignition exhibits a two-stage ignition phenomenon, however, as the overall compressed temperature increases, the ignition delay associated with the first-stage ignition becomes smaller

and eventually ignition becomes single stage. In general, the induction period of ignition is dependent on the fuel octane number. Hydrocarbon of a higher octane number exhibits an overall increase in ignition delay time

2.4.1.4 Modelling of End-Gas Autoignition

Modelling methods of end gas autoignition can be generally categorized into ***empirical correlation*** and ***chemical kinetics modelling*** [1]. The experimental methods and empirical correlations had been used to study the auto-ignition process back to the time when the chemical understanding of autoignition was limited. Over the last decade, however, numerical modelling using chemical kinetics has gained in importance as a new approach to model auto-ignition behaviour of gas mixtures thanks to both the improved understanding of hydrocarbon chemistry and the advanced computer technologies, by which numerical computations can be achieved at an acceptable cost. As a comparison to the experimental methods, numerical modelling is cheap and time saving, and additionally is able to offer autoignition data in regions where an experimental approach would simply fail. However, since numerical models need to be validated with experimental data, they can never fully replace the experimental studies.

2.4.1.4.1 Empirical Correlation

The empirical correlations were derived by matching an Arrhenius function to measured data on ignition delay times and ignition timing. For given fuel-air mixtures, over the relevant mixture pressure p and temperature T, the correlations have the form

$$\tau = A \cdot p^{-n} \cdot \exp\left(\frac{B}{T}\right) \qquad \textbf{2-2}$$

where τ indicates the ignition delay time, A and B are fitted parameters dependent on fuel types. To predict knock occurrence with time dependent temperature and pressure histories, the Equation 2-2 is integrated. Autoignition is deemed to occur if the value of the integral of τ exceeds a given threshold. A number of these empirical relations have been developed from engine studies of autoignition [31,32] the most extensively tested correlation is that proposed by Douaud and Eyzat [32].

$$\tau = 17.68 \cdot \left(\frac{ON}{100}\right)^{3.402} \cdot p^{-n} \cdot \exp\left(\frac{3800}{T}\right) \qquad \textbf{2-3}$$

where τ is the induction time in milliseconds and ON is the motor octane number of the fuel. Models of this type have been used in conjunction with thermodynamic models for engine combustion [31]. However, the ability of this type of models to predict the onset of autoignition and knock with sufficient accuracy is still unclear and empirical correlation are too simple to give any information of the reaction process and at best only fit the data over a limited range.

2.4.1.4.2 Chemical Kinetics Modelling

The end-gas autoignition is a complex chemical kinetic process that may involve thousands of elementary reaction steps and species [33]. Should all of the reaction steps and rate coefficients were known and very fast computation resources were available at low cost, the prediction of autoignition characteristics (ignition timing, ignition delay time, location of autoignition centres, the heat release, the reaction intermediate, and the final products of combustion etc.) can be achieved via numerical simulation. However, this ideal numerical approach has not been achieved and applied, as the lack of knowledge of the elementary reaction steps and rate coefficients and expensive computation time caused by the difficulty of analyzing thousands of equations have been playing a restrictive role in the development of chemical kinetics modelling.

Even so, in the past two decades, chemical kinetics modelling has still been prompted to be an important tool in the analysis of combustion systems. Correspondingly, there are four factors that are considered to be the major driving force contributing to the increasing application of chemical kinetics modelling [34], which are summarised as

- Availability of large amounts of elementary kinetic data
- Improved techniques for estimating specific reaction rates
- Development of efficient "stiff equation" solution techniques
- Continual growth in the size, speed, and availability of large computers

Chemical kinetics modelling, according to the scale of the numbers of reactions and species enclosed in the model, can be classified into detailed, lumped, reduced, skeletal and global models. The basic characteristics of hydrocarbon chemistry include cool flame and low and high temperature chemistry as is briefly introduced in the earlier context. More of the information of hydrocarbon combustion chemistry and

its modelling is reported in **Chapter 4**.

2.4.2 End-Gas Detonation

In contrast to the autoignition theory as a major cause of engine knock, some researchers [35,36] believed that it was the advancing flame front that accelerated to sonic velocity and consumed the end-gas at a rate much faster than would occur with normal flame speed, which resulted in high pressure and strong pressure wave. This theory suggested that any autoignition observed in the end gas was only an intermediate stage in the knocking mechanic and not the cause. However, full detonation is unlikely to occur in spark ignition engine, this due to the lack of unbumed gas and space available for full detonation to occur. Curry [35] claimed the observation of abnormally accelerated flame font speeds in the range of 100 to 400 m/s. However his experimental work was conducted only with ion probes, without photographic corroboration, and consequently his findings are considered unreliable. In summary, detonation has led many to call knock "Detonation". But there is much less evidence to support the detonation theory than the autoignition theory as the initiating process. Most recent evidence indicates that knock originates with the spontaneous or autoignition of one more local regions within the end gas. Thus the autoignition theory is most widely accepted.

2.4.3 Surface Ignition

The other important abnormal combustion phenomenon is surface ignition. Surface ignition originates from ignition of fuel air charge caused by overheated valves or spark plugs or glowing combustion chamber deposits, or by any other hot spot in the engine combustion chamber. Mostly surface ignition is due to carbon deposits. Surface ignition may take place before the spark plug ignites the charge (preignition) or after normal ignition (postignition). It leads to the formation of one or multiple propagating flame fronts opposite the one originating from spark caused by spark ignition. Surface ignition may lead to a more rapid and high rise of pressure and temperature than in case of normal combustion, because the flame either starts propagating sooner, or it does from more than one sources. Consequently, surface ignition is likely to cause knock. To identify whether surface ignition causes knock or not, the term "knocking surface ignition" and "non-knocking surface ignition" are used. Since knocking surface ignition usually caused by glowing combustion chamber deposits rather than spark ignited flame propagation, it can not be

controlled by retarding the spark timing. The non-knocking surface ignition occurs late in the operating cycle [1].

2.5 Fuel Effect

Automotive fuels, which have different structure and composition, feature different resistance to knock. In this section, the effect of fuel structure and composition on propensity of knock occurrence and knock intensity are interpreted.

2.5.1 Octane Number

The measure of fuels resistance to knock is defined by that fuel's Octane Number (ON). In 1927, Graham Edgar suggested using two hydrocarbons that could be produced in sufficient purity and quantity. These were normal heptane that was already obtainable in sufficient purity from the distillation of Jeffrey pine oil, and an octane, named 2,4,4-trimethyl pentane that he first synthesized, which is called as iso-octane today. Dr. Edgar devised the octane scale by testing the knocking tendency of every compound that was similar to gasoline. He found that isooctane would not knock in any engine under any operating conditions, while n-heptane would always knock in any engine. By mixing isooctane and n-heptane in different amounts, he obtained fuels of all qualities, the percentage of isooctane in the mixture being the octane number. Commercial gasoline was compared to these mixtures in test engines to determine their octane number. When the scale was developed, commercial gasoline had octane ratings between 40 and 75, and the best were brought up to a rating of 87 by the addition of tetraethyl lead, making leaded gasoline. Today, due to environmental reasons, tetraethyl lead has been outlawed. However, we do not really need it, because new and better processes allow oil companies to make gasoline for our automobiles with octane ratings as high as 97 [37].

The reason for using normal heptane and iso-octane was because they both have similar volatility properties, specifically boiling point, thus the varying ratios 0:100 to 100:0 should not exhibit large differences in volatility that could affect the rating test.

There are several octane rating methods. The two most common are the "motor" method and the "research" method. The motor octane number (MOR) testing uses a similar test engine to that used in RON testing, but with a preheated fuel mixture, a

higher engine speed, and variable ignition timing to stress the fuel's knock resistance.

Therefore, SI engines require fuel of a minimum octane level that depends upon the design of the engine. If such an engine is operated on a gasoline fuel that has an octane number lower than the minimum requirement for the engine, knock will occur.

2.5.2 Chemical Interpretation of Octane Number

During the oxidation of a hydrocarbon fuel, the hydrogen atoms are removed one at a time from the molecule by reactions with small radical species (such as OH and HO2), and O and H atoms, which is depicted by chemical Equation 2-4.

$$RH \xrightarrow{\text{H abstraction}} R\bullet \qquad \textbf{2-4}$$

The strength of carbon-hydrogen bonds depends on how the carbon atoms are connected in the molecule structure. Straight chain H-Cs such as n-heptane as shown in Figure 2-6a, have secondary C-H bonds that are significantly weaker than the primary C-H bonds present in branched chain H-Cs like iso-octane as shown in 2-6b.

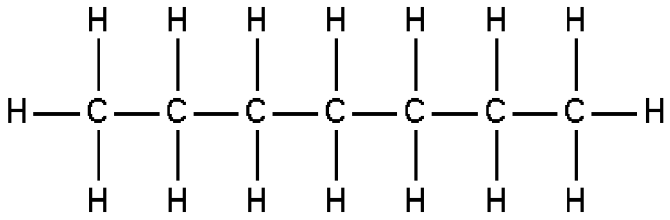

a

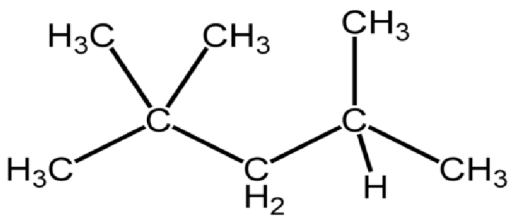

b

Figure 2-6: Molecular structures of n-heptane (a) and iso-octane (b).

Consequently, the octane rating of hydrocarbon fuels is determined by the structure of the molecule, with long and straight hydrocarbon chains producing large amounts of easily self-ignitable pre-flame decomposition species, while branched and

aromatic hydrocarbons are more resistant. This explains why the octane rating of paraffin decreases with carbon number [38].

Perdih et al [39] summarized the empirical rules of ON dependence on the molecular structure of alkane and they concluded

- ON decreases with the number of CH2 groups and increases with the number of CH3 groups, the number of adjacent CH2 groups has the highest ON.
- ON decreases with the separation between branches (i.e. of the number of adjacent methylene groups)
- ON increases with the more central position of the branches.
- ON increases with the bulkiness of the branched structure.
- Ethyl group as a branch can express apparently contradictory effects: If it increases the number of CH2 groups, ON decreases; if not, ON increases.

2.5.3 Fuel Additives

Gasoline can be refined to have sufficiently high octane numbers to run today's high compression engines, but such refining is expensive and energy intensive. The addition of anti-knock additives such as alkyl lead and oxygenates can significantly change autoignition characteristics primarily by interfering at different points in the chemical reaction pathway. The oxygenates are capable of retarding undesirable low temperature reactions, and the alkyl lead compounds react in the intermediate temperature region to deactivate the major undesirable chain branching sequence. .

The problem with metallic anti-knock gasoline fuel additives, however, is the high toxicity of their combustion products. For example, the first widely used metallic additives were Tetraethyl Lead (TEL). They were widely adopted until the late 1960s, their use starting phasing out with the change of legislation on automotive emission in response to rising public concern about environmental pollution. The negative aspects in use of TEL are

- Most lead compounds in the combustion products from TEL are toxic at low levels to human and animal life.
- Most TEL additives poison the catalyst used to reduce exhaust pollution

It would therefore be desirable to identify non-metallic anti-knock agents which would produce little toxic combustion products compared to metallic anti-knock agents, and

which would provide a needed increase in octane ratings to eliminate knock. The most popular anti-knock oxygenate additives include isooctane, toluene, etc.

2.6 Knock Detection

To improve engine design and numerical modelling; it is important to have accurate and reliable indicators for knock onset and intensity. A great amount of work has been reported in literature [40-42], which varies in the degree of sophistication of the equipment needed and the complexity of the computations to be carried out on the acquired data. These methods can be generally classified into two categories:

- Signals of accelerometers mounted on the cylinder block
- Cylinder pressure cranks angle records

Both of the methods have its keen users in light of its application merits. In modern production engine applications, the mounted accelerometers are popularly implemented to measure structural vibrations associated with knock, which is used as an indicator of knock. The sturdiness of the accelerometer and its low cost are the main advantages. However, the high sensitivity to noise makes detection difficult at high engine speeds [41].

The pressure based methods provide a much more direct and reliable way of knock detection and the information on knock intensity. Moreover, this method is widely used in laboratories. Its disadvantages are mainly the high cost of in-cylinder pressure probes with high signal/noise ratio. It is likely that for this reason methods based on pressure analysis have not yet been applied on a large scale. Nevertheless, recent progresses in non-intrusive probes may make its use possible on real applications in the near future [40,41].

2.7 Summary

The knock phenomenon in SI engines has constituted a major and the most serious limitation upon increasing efficiency of SI engines by increasing the compression ratio. The occurrence of knock is subject to the factors such as sparking timings, AFR, intake pressure etc. that affect the thermodynamic and chemical kinetic states

of the end-gas.

Generally, "knocking" occurs when a fuel, especially gasoline, spontaneously and prematurely ignites or detonates in an engine prior to spark plug initiated ignition.

Knock is currently believed is the result of the autoignition of a certain amount of fuel-air mixture in the end gas before it can be consumed by a primary flame propagating through the cylinder charge. In the view of chemists, it may be further characterized as a non-homogeneous production of free radicals that ultimately interfere with a flame wave front. The autoignition occurs randomly at discrete exothermic centres (exothermic centres), from which autoignition chemical reactions proceed and propagate. Formation of autoignition centres can be attributing to surface hot spots of the cylinder body and/or inhomogeneous distribution of mixture properties such as gas residuals and deposit etc.

The chemical process of autoignition is a series of complex degenerate chain branching, carrying and terminating reactions involving stable and radical species. These reactions may be separated into three distinct temperature regimes: low, intermediate and high temperature regimes. Each regime is dominated by reactions involving different radical species and different pathways.

Chemical kinetics modelling has been regarded as an ideal numerical approach in the analysis of autoignition chemistry and in the prediction of autoignition characteristics. A chemical kinetics model is composed of information of selected species, elementary reactions, and reaction rate parameters that can be used to numerically depict a chemical process. Chemical kinetics models can be classified according to the numbers of reactions and species contained in the model.

The ability of a fuel to resist knock is scaled by octane number. Fuels with higher octane numbers exhibit higher knock resistance. The addition of anti-knock additives such as alkyl lead and oxygenates can be used to reduce engine knocking and increase the fuel's octane rating. The typical antiknock agents in use include Tetra-ethyl lead, Methylcyclopentadienyl manganese tricarbonyl (MMT),Ferrocene, Iron pentacarbonyl, Toluene, Isooctane.

Engine knock identification methods can be classified into two categories: Signals of accelerometers mounted on the cylinder block and Cylinder pressure cranks angle records. Each of method has its particularity in different application fields.

Chapter Three: **Literature Survey on HCCI Combustion and engines**

3.1 HCCI Combustion and Engines

3.1.1 Definition of HCCI combustion

Homogenous charge compression ignition (HCCI) is a sparkles and flameless burning process of premixed fuel-air mixture, which combines homogeneous (premixed) intake charges as in SI engines with the autoignited combustion as CI engines [43]. Unlike a traditional S.I. or Diesel engine, HCCI combustion takes place spontaneously and homogeneously without flame propagation, which eliminates heterogeneous air/fuel mixture regions. In Figure 3-1, these three combustion processes are illustrated. To achieve HCCI combustion, generally the engine run on a lean, diluted mixture of fuel, air, and combustion products, which results in lower peak burned gas temperature. The low combustion temperature dramatically reduces NO_X emissions [9]. As HCCI combustion is an autoignition process, compression ratios are not limited by the occurrence of knock as in SI engines. As known, a high compression ratio is the most critical factor to increase thermal efficiency for an engine. As a result, with relatively higher compression ratios and less heat lose due to low combustion temperature, the thermal efficiency of HCCI engines approaches the levels of CI engines. Furthermore homogeneous mixture leads to no rich fuel regions in the charges, which is essential to minimize the Particulate Matter (PM) emission.

HCCI is first termed by Rob Thring [44] and has now been world widely recognised,

especially in USA. Another name having the similar popularity as HCCI is Controlled Autoignition (CAI), which is used more in Europe. However, throughout the years, HCCI has coexists with many other names in the literature; Onishi, et al [45] called it ATAC, which stands for Active Thermo-Atmosphere Combustion. Najt and Foster [46] called it CIHC, which stands for Compression Ignited Homogeneous Charge. Aoyama, et al [5] named it PCCI for Premixed Charged Compression Ignition and this term is more accepted in Japan.

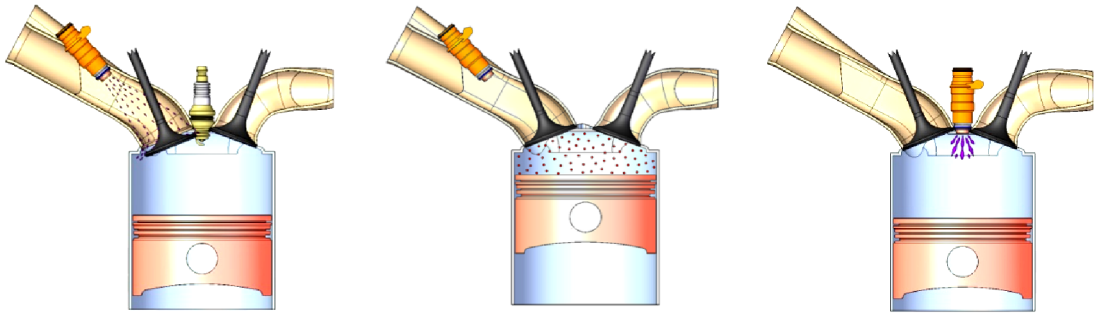

SI Process with Port-Fuel Injection	**HCCI Process with Port-Fuel Injection (Red spots represent multiple ignition and reaction sites)**	**CI Process with Direct Fuel Injection**

Figure 3-1: Comparison of SI, HCCI and CI combustion engines.

3.2 Fundamental Principles of HCCI Combustion

Najt and Foster [46] proclaimed that HCCI combustion were fully dominated by chemical kinetics with negligible influence from physical effects (turbulence, mixing). This is probably the most widely acknowledged opinion regarding the nature of HCCI combustion so far. Other studies also provided experimental [47-51] evidences in favour of this opinion. These studies indicate that HCCI combustion is a simultaneous multipoint ignition process with no flame propagation and the order of radical formation in HCCI combustion corresponds to that of self-ignition rather than flame propagation.

However, some researchers [52-54] believe that although turbulence has little effect on HCCI combustion, it may be most important as a factor in determining

temperature gradients and boundary layer thickness inside the cylinder, and as a result, influencing autoignition timing and emission formation. Furthermore, heat transfer and mixing process are critical issue in forming the conditions of the charge prior to ignition.

Najt and Foster also concluded in their work that HCCI combustion is a chemical kinetic combustion process, in which HCCI autoignition is controlled by the same low temperature (below 1000 K) chemistry as that occurring during SI engine knock and in which most of the energy release is controlled by the high temperature (above 1000 K) chemistry. This is consistent with the results from the studies of chemical kinetics of HCCI combustion [10,12,55], which conclude that little heat is released prior to this main ignition event at 1050-1100 K; however, significant heat-producing reactions begin at temperatures of about 1100 K. Although the amount of energy liberated is too small to be considered ignition, these low-temperature reactions quickly drive the mixture up to the 1050-1100 K temperature necessary for main ignition.

3.3 Characteristics of HCCI combustion

HCCI engines has the advantage of the application of premixed homogeneous gas mixture, throttle-less operation, high compression ratio, low NO_X and particulate emission, diesel-like efficiency, etc. However, HCCI engines confront a few challenges like high UHC and CO emissions, narrow operation range, high load limitation and uncontrolled heat release rate, etc. this section describe the main characteristics of HCCI combustion as comparison of those in SI and CI engines

3.3.1 Advantage of HCCI combustion

As introduced in the previous section, HCCI combustion has the potential to be the next generation combustion concept applied in IC engines thanks to its advantages in emission reduction and combustion efficiency in comparison with SI and CI engines. A brief overview of the advantages from HCCI engines is given below followed by a summary

3.3.1.1 In Comparison to SI engines

3.3.1.1.1 Higher Efficiency

HCCI engines are characteristic of higher combustion efficiency over SI engines and approaching the efficiency of a CI engine. The following factors are believed to contribute to high efficiencies in HCCI engine.

Application of High Compression Ratios – A high compression ratio is the most critical condition to increase thermal efficiency for IC engines. Since HCCI combustion is not limited by the knock problem as in SI engine, the compression ratios applied in HCCI engines can be applied as high as in CI engines.

Elimination of the Throttling Losses - Operation with no throttle in HCCI engine leads to a reduction in pumping loss, and thus a significant efficiency improvement in comparison to SI engine operation.

Lower Overall Combustion Temperature – As HCCI engines are normally operated with lean and diluted mixtures, they have much lower combustion temperatures in contrast to SI engines, which reduce the energy loss due to the heat transfer.

Shorter Combustion Duration – The Multi-point simultaneous autoignition of mixtures eliminates the existence of flame propagation in HCCI engine, which leads to faster combustion, and consequently shorter combustion duration. This shorter combustion duration makes HCCI combustion more like theoretical constant volume combustion and therefore have the advantage of higher efficiency.

3.3.1.1.2 Lower NO_X emission

HCCI combustion is characteristic of lower combustion temperature due to application of lean and dilute mixture compared to SI combustion, which leads to a significant reduction in NO_X emissions. Experimental study [56] showed that much lower NO_X was generated with HCCI combustion even compared with that from SI engines with three-way catalyst technology.

3.3.1.2 In Comparison to CI engines

3.3.1.2.1 Lower NO_X and PM emissions

HCCI engines relative to CI engines, has the advantage of significantly lower NO_X and PM emissions because of both dilute and homogeneous mixture properties and low combustion temperature, which take the advantage of the following factors

No Fuel Rich Regions - The homogeneous distribution of fuel- air mixture in HCCI engine eliminates the fuel rich regions as in CI engines.

Lean Charge - Charge in HCCI engines can be diluted to be very lean but capable of sustain the ignition by using Exhaust Gas Recirculation (EGR), or stratified charge, or by both of these strategies.

High Dilution Level - Since combustion of the charge in HCCI engines is driven by multi-point autoignition rather than one driven by flame propagation as in SI and CI engines, the mixture employed can be significant diluted to a higher level than that in SI or CI engines

Lower Ignition Temperature - Compression induced autoignition in HCCI engines has a much lower threshold ignition temperature (at 800 to 1100 K and fuel-type dependent) compared with SI and CI engines. As combustion occurs, the temperature will rise above the ignition temperature, but the peak temperature (at around 1800 K) is maintained below the level for significant formation of NO_X, In contrast, the combustion CI engines is high enough (above 2000K) to produce NO_X to a unacceptable level.

3.3.1.2.2 Higher Efficiency

As HCCI combustion is characteristic of a simultaneous combustion process due to the lack of flame propagation, the combustion duration in HCCI engines is much shorter than CI engines, which leads to a decreased heat rejection to the engine. In addition, the low combustion temperature also contributes to lower energy loss through the heat transfer. As a result, HCCI combustion features higher combustion efficiencies.

3.3.1.2.3 Lower cost

With higher combustion efficiency and lower emission relative to SI and CI engines, HCCI engines have the advantage of lower costs for pollution cleanup, engine cycle operation and fuel.

3.3.1.3 Additional advantages

In addition to the advantages presented above, Application of HCCI engines also benefited from the following factors.

3.3.1.3.1 Fuel Flexibility

Since HCCI combustion is not constrained by knock as in SI engines, a wide range of fuels have been tested on HCCI combustion which include gasoline [57,58], diesel fuel [59,60], natural gas [61-64], propane [65-67], and Primary Reference Fuel (PRF)

[48,56,68-72], and most alternative fuels such as methanol [73,74], ethanol [58,70], Dimethyl Ether (DME) [62,75-77]. The real benefit of HCCI lies in its compatibility with current engine architectures and ability to run on everyday fuel.

3.3.1.3.2 Smooth engine cycle Operation

Test results proved that under optimised conditions, HCCI combustion can be very repeatable, resulting in smooth engine operation [78,79]. The simultaneous multi-point ignition in HCCI combustion eliminates the influence of flame propagation on combustion as that in CI and SI engines. As a result, cycle-by-cycle variation is significantly minimized in HCCI combustion.

3.3.1.3.3 High Compatibility

Further benefit of HCCI seems to be its compatibility with current engine architectures and ability to run on everyday fuel. HCCI combustion can be applied in internal combustion engines and electric series hybrid vehicles or fuel cell hybrid vehicles. With the combination with other energy supply systems, engine can be optimized for operation over a limited range of speeds and loads, at which HCCI combustion is more suitable. This enables elimination of many of the control issues normally associated with HCCI and creation of highly efficient hybrid vehicles.

3.3.1.4 Summary

The inherent advantages of HCCI engines are summarized as follows:

- High thermal efficiency (some studies have reported over 50%) associated with un-throttled, ultra-lean operation:
  - High compression ratios
  - Lower dissociation losses
  - Increased ratio of specific heats during expansion stroke
  - Reduced cooling losses
  - Decreased heat loss
- Very low NO_X emissions (<10ppm, some studies have suggested that less than 1ppm may be attainable) resulting from low combustion temperature with ultra-lean operation
- Next to zero emissions of particulate matter thanks to pre-mixed

homogeneous charge operation

- Small cycle-by-cycle variation
- High compatibility of with current engine architectures and ability to run on everyday fuel.

3.3.2 Challenges of HCCI combustion

HCCI engine technology has received increasing attention in recent years due to its intrinsic benefits in terms of high efficiency and low NO_X and soot emissions. However, unresolved issues include combustion phasing (i.e., the control of the start and duration of combustion), high CO and HC emissions, limited load-speed operating window, etc. The major challenges of HCCI are briefly overviewed and summarised in this section.

3.3.2.1 Hydrocarbons and Carbon Monoxide (HC and CO)

Although HCCI combustion is characterised by low NO_X and PM emissions because of the distributed low-temperature reactions of the fuel-lean mixture, this low-temperature combustion typically results in higher HC and CO emissions than conventional CI combustion [80,81]. Two important mechanisms for HC emissions from HCCI engines are crevices and liquid fuel effect. Fuel that is packed into the crevices and impinged into the boundary layer close to the cylinder wall normally escapes the major combustion. However, the lean mixture operation in HCCI engines leads to a very low post-combustion temperature, at which any fuel that escapes from the major combustion has very low chance of undergoing complete post-combustion oxidation. Furthermore, significant CO emission is formed in the partial oxidation of the unburned HC.

3.3.2.2 Control of Combustion Phasing and Rate

One of the major barriers to wide and general application of HCCI combustion is control of combustion phasing and rate. Since HCCI combustion is an instantaneous autoignition process of homogeneous mixture, both of the direct control methods in SI and CI engine (spark timing control and fuel injection timing control) used in controlling start of combustion are not applicable in HCCI engines.

Ideally, autoignition in HCCI occurs at the point where the piston reaches top dead center to provide optimum power and efficiency; therefore, the timing of the autoignition is critical. Without the help of an external triggering event, HCCI has a

problem in controlling the ignition timing.

Autoignition is a fully reaction rate controlled process. The reaction rates of kinetic chain branching reactions that are in control of initiation and heat release rate of combustion are primarily determined by composition of the fuel-oxidiser mixture and by time-temperature history to which the mixture is exposed. The following factors have been claimed to be the major influences on the charge composition and temperature

Mixture Homogeneity – As aforementioned, turbulence and mixing play a important role determining stratification of charge temperature and composition inside the cylinder, as a result, influencing autoignition timing and combustion phasing.

Fuel Property - Each type of fuel has unique chemical and physical properties, so the chemistry of autoignition varies from fuel to fuel.

Fuel-Air Ratio – Load control in HCCI engines is achieved by varying fuel-air ratios of the mixture, which causes change of charge composition and temperature.

EGR Rate – While using EGR technique, a fresh air-charge is mixed with hot trapped exhaust gases, increasing the temperature and changing the composition of the newly formed charge mixture (Fuel/Air/EGR), and thus influencing the ignition timing and heat release rate.

Heat Transfer – Heat loss from the charge to the surroundings also leads to the regional inhomogeneities of the mixtures prior to ignition.

Compression Ratio – An increased compression ratio elevates the temperature of the in-cylinder charge during the compression process, which enhances the chemical reaction rates. As a result of this, ignition delay is shortened and ignition timing is advanced.

Inlet Temperature – Inlet temperature has the significant influence on ignition timing and energy release rate. An increased intake temperature enhance the chemical reaction rates and thus advances ignition timing and vice versa.

Engine Speed – Changing engine speed changes the amount of time for the autoignition chemistry to occur relative to the piston motion. Ignition timing retards with increased engine speed and vice versa

3.3.2.3 Operation Range

Another drawback of HCCI combustion is the operating range, which is currently limited at low and medium loads with fuel lean mixtures. When fuel rich mixtures are applied at high load, the combustion stability degrades, heat release rates increase, knock-like oscillations in the cylinder pressure appear, and the emissions benefits vanish [5,60]. Therefore, it is highly in demand to achieve controlled operation at high load condition in HCCI engines.

One of the solutions to overcome the load range limitations of HCCI is hybrid combustion mode, by which HCCI mode is used at part load and then transitions into SI or CI modes at high load conditions [82]. This hybrid operation takes advantage of benefits of HCCI combustion at low and medium loads and makes use of SI or CI combustion as a substitution at high loads. Exploration of the fundamental nature of the hybrid mode combustion has been limited so far and raised much research awareness.

Another method has the potential of extending the operating range of HCCI engine to higher loads is charge stratification, both thermal and compositional. At locally stratified temperature and fuel-air ratios, combustion event at high load conditions can be stretch out. Several strategies for mixture control have been devised and are currently being considered to help overcome load range limitation in HCCI engines. These include diverse fuel injection schemes such as port fuel injection and single or multistage direct injection (DI or MDI), new intake and in-cylinder mixing processes to obtain non-uniform fuel/air/residual mixtures, as well as external exhaust gas recirculation (EGR), variable valve timing, and variable compression ratio, etc. [27,83]

3.3.2.4 Homogeneous Mixture Preparation

Mixture preparation has a significant effect on combustion chemistry and thus is a critical issue to achieve satisfactory control of HCCI combustion [84,69]. Homogeneous mixture preparation is most difficult for fuels with low volatility such as diesel, which require elevated intake air temperatures to evaporate the fuel [60].

3.3.2.5 Cold-Start Capability

During engine cold start, HCCI combustion is almost impossible due to lack of preheating to the intake charge and high heat transfer to the cold combustion chamber. Without some compensating mechanism, the low compressed-charge temperatures could prevent an HCCI engine from firing.

Various mechanisms for cold starting in HCCI mode have been proposed such as using glow plugs, using a different fuel or fuel additive, and increasing the compression ratio using VCR or VVT. It has proven preferable to employ spark ignition at cold start and then transition to HCCI mode after warm-up, though it adds cost and complexity [43]. VCR and VVT systems are usable for cold start conditions by changing the effective compression ratio and/or the amount of hot exhaust gases retained in the cylinder in order to raise the inlet charge temperature.

3.3.2.6 Summary

The technical obstacles to implementing HCCI engines are summarized as follows:

- Operating range is significant narrower than those for SI and CI engines with difficulties at cold start and high load conditions.
- High energy release rate and short combustion duration lead to difficulties in control of combustion phasing
- High CO and UHC emissions, resulting from low combustion temperature, particularly at lower load conditions, and from crevices and boundary layer
- Load range limitation exists under both cold start and high load conditions
- High peak pressures.
- The combustion of highly dilute mixtures in these engines results in relatively low power density (unless supercharged).
- In addition, lean-burn exhaust composition is incompatible with the current state of the art NO_X reduction catalyst technology. Consequently, reaching very low levels of NO_X emissions hinges on achieving stable controllable operation at ultra-lean conditions ($\Phi < 0.5$)

3.4 Research Work in HCCI Engines

It has been 30 years, since HCCI combustion was discovered and considered as a alternative combustion concept to conventional SI and CI engines. Since then, research work on the development and application of HCCI combustion has not been stopped. A great deal researcher have dedicatedly done essential work, both experimental and modeling, to establish fundamental understanding of HCCI

combustion and developed feasible technical solutions for control of HCCI combustion. The following section chooses to present some of the typical work done in this field.

3.4.1 Fundamental Studies

HCCI combustion was first discovered as an alternative combustion mode in 1979 by Onishi et al [45]. They successfully achieved stable autoignition under fuel lean and part load conditions by throttling the exhaust to increase the amount of trapped EGR and initial mixture temperature. The stabilized lean autoignition combustion was proven to provide significant reduction in exhaust emissions, specifically UHC and fuel consumption and termed 'Active Thermo-Atmosphere Combustion' (ATAC).

As a pioneer study in HCCI combustion, Onishi's work established a fundamental understanding of the characteristics of HCCI combustion and had a significant influence on all the subsequent research. A few critical points made in Onishi's work are summarized below.

- Peak pressure in ATAC combustion shows a very small fluctuation resulting in little cycle-by-cycle variation, which leads to improved thermal efficiency
- ATAC is initiated by a controlled autoignition; hence, the occurrence or absence of an electric spark has no effect on the combustion pattern.
- Intermediate radicals (OH, CH, and C2) were formed earlier during the compression stroke in ATAC combustion, and had higher concentrations and a longer life than those in normal spark ignition engine operations.
- High-speed Schlieren photographs indicated no distinct flame propagation through the chamber and small density variations during the combustion period
- ATAC combustion was initiated by a special type autoignition where chemical combustion reactions occurred at many points and time differences regarding the start of combustion of these points are very small,
- The attainment of ATAC combustion depended on uniform mixture properties and high in-cylinder temperature, and proper ratios of new fuel-air charge to EGR.

Noguchi et al. [85] in the same year presented similar results with decreased fuel

consumption and decreased emissions of unburned hydrocarbons and they also confirmed the similarities of reaction chemistry between autoignition in HCCI engines and autoignition of the end-gas in SI engines through the analysis of formation of the radicals associated with autoignition in both the engines

Najt and Foster [46] in 1983 first applied HCCI combustion technology to a four-stroke gasoline engine with blends of paraffinic and aromatic fuels over a range of engine speeds and dilution levels. From simplified chemical kinetically controlled modeling and heat release analysis, they concluded that HCCI combustion is a chemical kinetic combustion process, in which start of autoignition is governed by low temperature (< 950 K) hydrocarbon oxidation kinetics and energy release is controlled by high temperature (above 1000 K) chemistry. They also concluded the limitation of ignition control and operating range in HCCI combustion.

Thring [44] in 1989 first proposed the term of Homogeneous Compression Charge ignition (HCCI) for this newly discovered combustion concept in internal engines. He studied the operating parameters of a four-stroke engine running with compressed homogeneous charge through mapping the operating regime by varying equivalence ratios, EGR rates, engine speeds and inlet temperatures. In Thring's work concluded that stable HCCI combustion could only be achieved at low speed, part load conditions in a four-stroke engine in the absence of advanced operating strategies and mechanisms.

Aoyama et al [5] in 1996 operated a single cylinder engine with inlet port injection of gasoline, a compression ratio of 17.4 and premixed lean mixture. They named the combustion method Premixed Charge Compression Ignition (PCCI) and concluded that under conditions of stable combustion, the test engine was able to achieve equivalent fuel economy and much lower NO_X emission compared with CI engines. In their work, they also studied the effects of intake air heating and supercharging on extending the range of stable combustion and found both of the effects are found to be significant.

Oguma et al. [48] in 1997 and Christensen et. al. [68] in 1999 studied HCCI performance with a variety of fuels (Iso-octane, ethanol and natural gas) operating at various compression ratios and intake temperatures. They found that HCCI combustion is of intrinsic fuel flexibility. Under proper operating conditions, fuels with any octane or Cetane number are theoretically applicable for HCCI combustion.

Autoignition conditions vary from fuel to fuel. However, octane number of a fuel is a critical parameter to determine the characteristics of autoignition such as ignition delay, combustion duration, and heat release rate, etc.

3.4.2 Technologies in HCCI engine

Though HCCI combustion was regarded as an alternative combustion concept to conventional SI and CI, a few major obstacles limit its application. However, during the past 30 years, technologies applied in HCCI engines aim at overcoming all these limitations have been widely developed

3.4.2.1 Variable Compression Ratio (VCR)

Compression ratio is a critical engine design parameter for HCCI engines. A high compression ratio elevates the charge temperature, advances the start of combustion, and shortens the combustion duration. Therefore, variable compression ratios (VCR) engine can be used to control combustion phasing and widen operation range of a HCCI engine [59,68,86]. Furthermore, high compression ratios with resultant high expansion ratios contribute to high thermal efficiencies. Christensen et al [68] varied the compression ratio from 10:1 to 28:1 with a constant air/fuel equivalence ratio of 3.0 using a port injection system. They concluded that gasoline required a compression ratio of 22.5:1 for satisfactory operation without the use of inlet air preheating. The results showed that no smoke was generated and that NO_X emissions were very low with increased compression ratio. However, compression ratios beyond 12 are likely to produce severe knock problems for the rich mixtures used at high load conditions. It seems that the best compromise is to select the highest possible CR to obtain satisfactory full load performance from SI fuels [46]. it should also be noted that VCR would add some cost and complexity to the engine.

A major technical issue for VCR is to achieve the fast response to handle rapid transients in vehicle application. A few relative options have been developed and examined in IC engines:

- One option is to mount a plunger in the cylinder head whose position can be varied to change the compression ratio [68].
- The second option is to vary the CR using an opposed-piston engine design having variable phase-shifting between the two crankshafts [87].
- SAAB has also announced the development of another method that is based

on a hinged, tilting cylinder arrangement [86].

While any of these systems or some other mechanism might succeed, only the variable-position plunger system has been demonstrated in an HCCI engine [68]. For these tests, the plunger was controlled by a hydraulic system allowing its position to be varied during engine operation. The data show that the VCR system is capable of controlling HCCI ignition timing to maintain optimal combustion phasing across a very wide range of intake temperatures and fuel types of various octane number.

3.4.2.2 Variable Valve Timing (VVT)

Variable valve timing (VVT) strategy offers an efficient promising approach to control the amount of trapped EGR and the effective compression ratio, and consequently the engine performance parameters [88,89]. By varying the amount of hot EGR, temperature and composition of the new charge mixture (fuel, air, and EGR) can be adjusted. The heating effect of EGR on the charge can be used to initiate HCCI combustion even with relatively low geometric compression ratios or under cold-engine conditions [90,91,146,147].

Law et al. [90] examined the effect of internal EGR ratios on controlled autoignition (CAI) combustion using a Lotus active valve train (AVT) on a single-cylinder engine. They concluded that increased internal EGR leads to the advanced start of combustion and shortened combustion duration and that there was no need to pre-heat either the intake air or the intake air-fuel mixture as long as enough internal EGR is used.

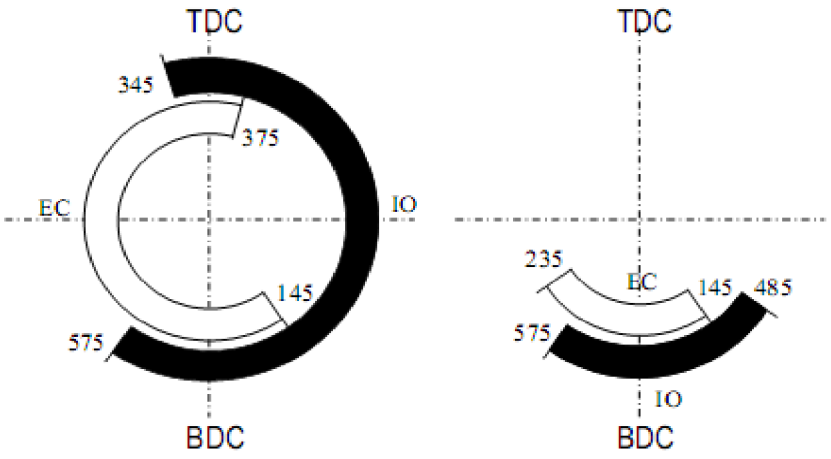

Figure 3-2: The depiction of the positive (left) and the negative valve (right) overlaps; EC: Exhaust valve closing and IO: intake valve opening.

Conventionally, the intake and exhaust valves of a typical four-stroke cycle engine are actuated by lobes fitted on camshafts. The configuration of these lobes primarily controls the valve events (timing, lift and duration). The standard valve strategy in SI and CI engines involves high lift, long duration and positive valve overlapping (PVO), while the modified valve strategy that is compatible with the HCCI combustion mode implies low lift, short duration and negative valve overlapping (NVO) [92]. The typical PVO and NVO overlaps are shown in Figure 3-2. The latter is used to facilitate the autoignition by trapping a proportion of the hot exhaust gases in the engine cylinder during the gas exchange process. The NVO is normally created by closing the exhaust valves relatively early in the exhaust stroke and opening the intake valves relatively late in the intake stroke.

During the course of NVO, the trapped exhaust gases are in compression throughout the final stage of exhaust stroke, called re-compression stage, and then expand on the early stage of intake stroke as the piston moves downwards, called re-expansion stage. The NVO is called symmetric when the timing of exhaust-valve-closing (EVC) is coupled with a symmetric degree of intake-valve-opening (IVO), measured with respect to the piston top dead centre (TDC) position [92].

VVT can be implemented in an engine with mechanical, magnetic, or hydraulic valve actuators [90,93]. Furthermore, modeling studies are being conducted to enhance VVT operation for the control of the HCCI process [94,95]. However, Similar to VCR, a VVT system would add cost and complexity to the engine.

3.4.2.3 Supercharging and Turbocharging

Supercharging or turbocharging technologies have been widely developed and applied in high performance SI and CI engines to improve the engine output power. Therefore, research effort have been put on the application of intake pressure boosting on HCCI engines

The influence of supercharging on HCCI was first experimentally investigated by Christensen et al [19], which concluded that supercharging dramatically, increases the attainable IMEP for HCCI. The highest attainable IMEP obtained in the study was up to 14 bars with ultra low NO_X emissions using natural gas as fuel. This was achieved with a 2 bar boost pressure and a compression ratio of 17:1. The subsequent studies used EGR [71] and a pilot fuel [153] to improve the ignition properties of the mixture in an attempt to extend the upper load limit for HCCI. The

study concluded that HCCI load limit could be extended when a supercharger is applied in combination with EGR, without increasing the maximum cylinder pressure.

Hyvönen et al [96] investigated the HCCI operation ranges with both mechanical supercharging and simulated turbocharging, and compared the operation range with a natural aspirated SI with gasoline as fuel. It is found that the operating range could be more than doubled with supercharging and higher brake efficiency was achieved at the same loads in comparison of the natural aspirated SI engine.

Canakci [97] conducted experimental studies on the effect of inlet air pressure on the performance and exhaust emissions of a DI-HCCI gasoline engine. The experiments were performed at three different inlet air pressures while operating the engine at the same equivalence ratio and intake air temperature as in normally aspirated HCCI engine condition at different engine speeds. He concluded that intake pressure boosting leads to earlier start of ignition, increased engine torque and brake thermal efficiency, and decreased CO and NO_X emission; and an increase in boost pressure causes the need of leaner mixture, and requires more advanced injection timing to achieve the maximum engine torque.

Application of supercharging and turbocharging still confront technical obstacles such as that typical low exhaust temperatures of HCCI require special care in turbocharger design in order to achieve high load/high efficiency operation and the higher cylinder pressures make autoignition control at high loads even more critical, which limits its potential application.

3.4.2.4 Stratified Charge

Stratified charge is a possible solution to the control and operating range challenge of HCCI engines. A controlled stratified charge produces a range of fuel concentrations throughout the combustion chamber by proper fuel injection and in-cylinder mixing. In another word, charge stratification modifies local mixture properties (temperature and composition, equivalent ratio). As a result, mixture stratification leads to sequent autoignition of fuel-air-EGR mixture, thus smooth combustion heat release and extended upper load operating limit [98,99]. Stratification of the fuel/air mixture improves emissions and combustion efficiency during part-load operation [100].

However, local high temperature regions in stratification combustion results in an increase of NO_X emissions. Therefore, one of the challenges for stratification combustion is to meet requirements of combustion control and load range extension

while keeping low NO_X emissions.

Optical studies [101], with high-speed CCD camera, showed that an increase in stratification leaded to poor combustion quality near the cylinder walls, due to leaner mixtures near the cylinder walls, which resulted in higher HC and CO emissions. The maximum rate of heat release depends on stratification amount - a larger amount gives a lower rate of heat release but the main heat release is advanced.

Charge stratification results in staged combustion, and thus leads to a larger operating range, due to its effect on combustion phasing and rate of heat release. This is because that the upper load limits originates from high heat release rates that leads to high-pressure oscillations and the low load limits from late combustion phasing that leads to high cycle-to-cycle variations [101].

Several potential mechanisms exist for achieving this partial charge stratification, including varying in-cylinder fuel injection, injecting water, varying the intake and in-cylinder mixing processes to obtain non-uniform fuel/air/residual mixtures, and altering cylinder flows to vary heat transfer.

3.4.2.5 Direct Injection (DI)

Direct injection (DI) has been widely investigated to control the spontaneous combustion as well as to expand the engine-operating region [102-105].

Standing et al [104] demonstrated the possibility of utilizing HCCI combustion in a multi-cylinder GDI engine using substantially standard production parts and also showed that the timing of the fuel injection could be used to control engine parameters such as ignition timing. Also the effect that the timing of the fuel injection as well as the valve timings, has on factors such as NO_X and HC emissions, as well specific fuel consumption and combustion duration

In early in-cylinder injection, fuel is injected early during the compression stroke. Vaporization of the injected fuel is an endothermic, so it consumes the energy released from the early stage reaction of fuel oxidation. As a result, the heat reaction rates are decreased by this effect and the temperature time history of the mixture is affected significantly. However, early injection timing results in a more homogeneous mixture, and it can lead to thermodynamically unfavourable advanced combustion timing under high load [105].

Dual-injection [106] or multiple-injection [105] has also been investigated to improve

the control of combustion phasing. The second or the subsequent fuel injection can function as an ignition trigger and can help to limit pressure rise rates caused by too rapid combustion. Standing, et al [105] carried out an investigation on a Ricardo Hydra single cylinder research engine equipped with early exhaust valve closing timing and three fuel injection timings. The earliest injection was set to coincide with exhaust valve closure, while the 'mid' injection event occurred at IVO. The late injection timing was set at BDC of the intake stroke, as shown in Figure 3-3. Results from Zhao, et al confirmed the effect of multiple-injection timings on mixture ignitibility, mixture quality and charge cooling.

Elsewhere, other research work on the effect of direct injection on combustion control include the studies of injection pressure [107], spray angle and shape [108], impingement spray [109,108] and pulse injection modes [110].

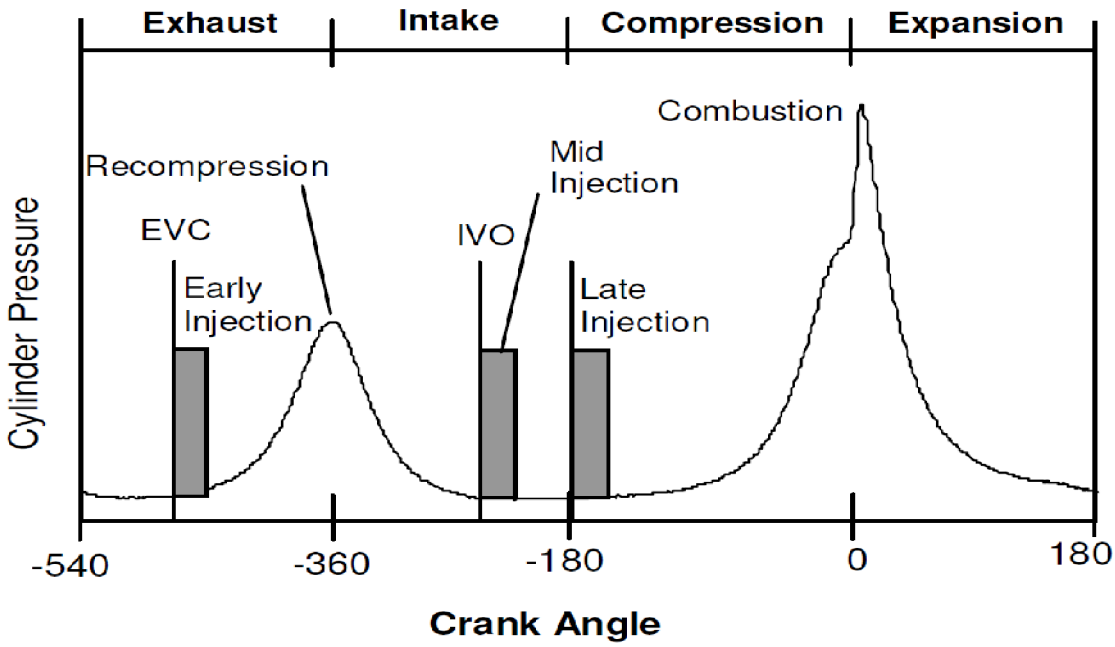

Figure 3-3: Typical cylinder pressure vs. crank angle showing injecting timing windows [105].

3.4.3 Engine-Input Parameters

Studies have shown that the combustion process of HCCI is significantly affected by different engine-input parameters e.g. fuel type, pressure, temperature composition of the in-cylinder mixture, etc. In this section, the effects of fuel composition, EGR, inlet temperature air-fuel ratio, coolant temperature and additives on HCCI combustion and emission are summarized and discussed.

3.4.3.1 Fuel Composition

As introduced in the early section, one of the advantages of HCCI combustion is its fuel flexibility. It is a well-accepted fact that autoignition process of HCCI combustion is primarily controlled by a series of complex chain branching, carrying, and terminating reactions involving stable and radical species. Thus, fuel molecular structure plays a crucial role in determining the formation of these radical species and affects the autoignition behaviour of the fuel.

Milovanovic [82] investigated the effects of four different types of fuels on ignition time and heat release rate in HCCI engine. The four types of fuels are n-heptane, iso-octane, ethanol and methane, which have different composition, molecular size and structure and octane number (ON). They concluded that fuels with different octane numbers exhibit various chemical reactivity. Fuels with low octane number like n-heptane are more reactive and characterised with two-stage ignition with Negative Temperature Coefficient (NTC) behaviour followed with main ignition. As a contrast, fuel with high octane number like iso-octane is less reactive and featured with single-stage ignition only. The reasoning behind the difference is the amount of heat released prior to the main ignition event. High ON fuels release very little heat during the early combustion stage. However, for the low ON fuels, significant heat is released from low temperature reaction at around 800 K; although the amount of the energy is not sufficient enough to lead to main ignition, it is capable of elevate mixture temperature to 1050-1100 K, which is a threshold temperature for H_2O_2 decomposition and the start of main ignition. This is the reason that HCCI combustion is sensitive to fuel types.

3.4.3.2 EGR

Exhaust Gas Recirculation (EGR) has been perhaps the most commonly investigated method for the control of HCCI combustion. As aforementioned, HCCI combustion is an autoignition process controlled by chemical kinetics, so change of composition, temperature, thermal properties of in-cylinder mixture has a significant influence on chemical reaction rates, which control ignition timing and energy release rate of the combustion.

EGR offers a way to control the engine charge temperature, mixture and pressure. Types of EGR are distinguished by location of mixing process between fuel-air charges and exhaust gases. Hot exhaust gases trapped inside the cylinder prior to

the compression stroke is commonly termed Internal EGR (IEGR) [89,90,111,112] and can be obtained through Variable Valve Train (VVT) system. However, hot exhaust gases recycled into intake manifold and mixed with the fresh charge mixture before its induction into the engine cylinder is known as External EGR (EEGR) [81,113].

Studies [56,63,81,112,114,115] claim that EGR has the effect on depleting the rate of chemical reactions and thus delaying the ignition time, reducing the heat release rate and lowering the peak cylinder pressure.

The effect of EGR on HCCI combustion can be divided into three aspects: a dilution effect (inert gasses present in the EGR), a thermal effect (heat exchange, thermal loss to the wall, EGR ratio mixture quality, EGR temperature, heat capacity), and a chemical effect [82,115].

Thermal Effect – In the event of high load conditions, in order to control ignition timing and combustion rate, cooled EEGR can be used to reduce the mixture temperature during the compression stroke. However, under lean mixture conditions, the high temperature of hot IEGR increases the temperature of the resulting charge in the mixing process with the fresh air-fuel mixture and therefore influences the start of ignition and further combustion. A higher temperature boosts kinetic reactivity (chemical reactivity) with consequent advanced autoignition. The thermal effect of the IEGR could be beneficial for HCCI combustion since it reduces the need of intake air preheating and eliminates the dependence on the operating conditions.

Furthermore, the total heat capacity of mixture of EGR, air, and fuel will be higher owing to the higher heat capacity of carbon dioxide and water vapour. This will lead to a reduction of gas temperature at the end of the compression stroke

Dilution Effect – the volumetric occupation of EGR leads to a substantial reduction of oxygen concentration in the mixture.

Chemical Effect – the introduction of EGR changes mixture composition and species concentration and provides additional species such as UHC, CO, CO_2, NO, etc. taking part in the chemical reactions. As a result, chemical reaction rates will be affected, which leads to the influence on ignition timing and combustion rate

3.4.3.3 Inlet temperature

HCCI combustion is predominated by chemical reaction, so the combustion event is

highly sensitive to temperature. Intake charge temperature is one of the important factors that affect ignition timing and heat release rate. Influence of intake charge temperature on the HCCI ignition timing, burn duration, and the emissions have been evaluated by many researchers [81,82,116]. Higher intake temperature boost kinetic reactivity, the heat release grows and autoignition is accelerated. On the other hand, decrease of inlet temperature delays ignition and for each fuel there exist a minimum inlet temperature, below which ignition cannot be initiated.

However, intake temperature boost has its limitation of application due to its negative effect on the indicated thermal efficiency, volumetric efficiency and trapped mass. An increase in the intake temperature reduces trapped mass and volumetric efficiency, which in turn adversely affect torque and power output [117]. Also advanced ignition increases compression effort and combined with reduced volumetric efficiency leads to the reduction in net indicated efficiency [82]. Furthermore, variation of intake temperature is generally a slow process, so this method is not really practical, especially under a transient condition.

3.4.3.4 Air-Fuel Equivalent Ratio (AFER)

Since HCCI combustion is initiated by autoignition of the air-fuel mixture by the piston compression, no supplementary ignition source is required and therefore considerably fuel lean mixture can be employed in HCCI engines. This refers to AFER as lean as $\phi = 0.2$ [68] and wider AFER ranges over the ones applied in SI engines. Thus, changing AFR directly influences the fuel concentration, effective pressure, and mixture specific heats, which have significant impact on ignition timing and fuel consumption rate and combustion rate. It has been found [56,81,82,95,113,118,119] that decreasing AFER results in longer ignition delay and lower combustion rate. This is because that excess air in the leaner mixture (AFER increases) acts as a diluent absorbing heat and reducing the temperature rise from the low temperature reaction, and the amount of compression heating is reduced due to the lower mixture specific heat of leaner mixtures.

3.4.3.5 Coolant Temperature

Controlling the coolant temperature is another possible approach in extending the operational range for a HCCI combustion mode [120,121]. It has been found that coolant temperature influences the in-cylinder heat transfer process, which in turn influences the charge mixture temperature and therefore the HCCI combustion

process. With the increase of coolant temperate, the combustion phase advances and the maximum heat release rate increases. Moreover, the maximum combustion pressure also increases. Overall, coolant temperature has a similar but smaller thermal effect on HCCI combustion compared with intake charge temperature.

3.4.3.6 Fuel Additives

As aforementioned, one of the critical obstacles to apply HCCI combustion is control of ignition timing. One option for ignition control is to use small amounts of ignition-enhancing additives to alter the ignition properties [122-125]. Most effective additives are thermally unstable and their thermal decomposition could generate radicals through thermal decomposition during the initiation stage of combustion, which strongly affect the HCCI combustion of the air/fuel mixture [123]. The additives having been investigated in the studies of HCCI combustion so far includes formaldehyde [125], methane and DME [122], Di-tertiary Butyl Peroxide (DTBP) [27], 2-ethyl-hexyl-nitrate and di-tertiary-butyl-peroxide [123], etc.

3.5 Modelling Methods on HCCI combustion

Though HCCI was identified as a distinct combustion phenomenon about 30 years ago, the modeling work had been somewhat late developed until 10 years ago, when it was consistently accepted that HCCI combustion was purely controlled by chemical kinetics with little effect of turbulence [126]. A pile of early experimental studies had provided insight into the HCCI combustion, from which physical understanding of the combustion process has been achieved. However, chemical understanding of the combustion process has to be obtained through detailed chemical kinetics modeling of the hydrocarbon oxidation process. CFD codes have the highest potential for predicting realistic results when the geometry of the combustion chamber is resolved in full detail. Thus, the ideal tool for HCCI analysis is a combination of a CFD code with a detailed chemical kinetics code. However, the required computational resources can become enormous, which is well beyond our current computational capabilities. Reducing calculation times can be achieved by reducing CFD mesh quality or/and downsizing the reaction mechanism implemented. Based on this point, a variety of numerical models has been developed for different usage purposes in the simulation of HCCI combustion and investigation of its characteristics. Major model

types falls into three categories based on their physical descriptions of the combustion processes.

- Single-Zone Models
- Multi-Zone Models
- Multi-Dimensional CFD Models

This section is giving an overview of the models of the above types. Note that the classification of the chemical kinetics mechanisms implemented in the simulation is discussed with details in the following chapter.

3.5.1 Single-Zone Models

Single-zone models has been widely developed and applied to study the characteristics of HCCI combustion [114,127,128]. This is mainly due to the simplicity of such models and requirement of less computation time, even when they are coupled with detailed chemical mechanisms.

In a single-zone HCCI model, the whole in-cylinder mixture is treated to be spatially homogeneous and applies ideal gas law. Heat transfer to/from cylinder walls is calculated by conductive heat transfer models, in general, using the Woschni's correlation [129]. The cylinder is considered as a closed chamber and the volume is varied with time according to the slider-crank relationship [1]. Mass loss from the cylinder and turbulence effect is negligible. By applying the conservation of mass, energy and species and chemical kinetics principles, the governing equations can be derived. Since such models have been widely investigated and are plentiful in the literature [82,114,117,128], the governing equations are not presented here.

It has been claimed in literatures listed above that single-zone models have been a valid approach in the studies of HCCI process. The main usability of single-zone models are summarized as follows：

- Single-zone models have shown ability in predicting the start of combustion process (ignition timing), peak cylinder pressure, indicated power etc.
- Single-zone models have been proved a useful tool for investigating certain fundamental aspects of HCCI combustion, such as a parametric analysis of the influence of engine parameters and fuel types. Eliminating the complexities of walls, crevices, and mixture inhomogeneities simplifies the

analysis of the kinetic and thermodynamic behaviours, which allows the studies on individual effects of the chemical kinetics and bulk-gas thermodynamics on in-cylinder combustion processes. Overall, use of single-zone model allows cause-and-effect relationships to be more easily identified.

- The simplicity of single-zone models allows the application of detailed chemical kinetics mechanisms without cost of expensive computation time.
- Single-zone models provide a fundamental base of numerical modeling of HCCI combustion, based on which, more complex models such as multi-zone models have been well developed and investigated.

However, there are arguments that single-zone models oversimplify the combustion processes in a real engine. In reality, in-cylinder charge is not possible to be spatially homogeneous, because fuel-air–EGR mixture will never be completely mixed and heat transfer from/to the cylinder walls will always cause temperature inhomogeneities across the cylinder. Furthermore, the engine cycle is not a closed the cycle at all, blowby leads to mass loss of in-cylinder charge, and mass trapped in the crevices and boundary layers will not get involved in the main combustion and is major source of HC and CO emissions. All these effects will alter the heat release rate, the peak pressure, and the actual amounts of HC and CO emissions. As a result, the single-zone model suffers from its ability to predict these values.

3.5.2 Multi-Zone Models

In theory, HCCI combustion is described as an instantaneous combustion process dominated by chemical kinetic reactions of the homogeneous in-cylinder mixtures. However, in reality, ignition is normally initiated at the hottest region inside cylinder and then the ignited part of the mixture compresses the rest of the charge, which subsequently ignites after a short time lag [53]. Furthermore, mixtures trapped in crevices and boundary layers generally remain too cold to react, and result in substantial hydrocarbon and carbon monoxide emissions. In addition, though turbulence has little effect during the major combustion phase, spatial mixing of mixture caused by turbulence in the remainder of the cycle has significant influence on temperature and mixture composition distribution, which results in inhomogeneous in-cylinder conditions and thus affects combustion performance and emissions [130]. To take account of all these factors in a simulation of HCCI combustion, more complex and realistic models over single-zone models are

requisite.

Thermo-chemical based multi-zone model is different from single-zone models that treat the entire cylinder as a uniform region with homogenous temperature and compositions. This approach splits the cylinder volume into a series of zone of different temperature and compositions with inclusion of boundary layers and crevices. Therefore, a multi-zone model is capable of handling distribution of temperature and composition, where different zones can be assigned different initial temperatures, compositions, and EGR fractions, and simulating the effect of crevices and boundary layers.

Compared with single-zone model, advantages of the multi-zone models include modelling of crevices and the thermal boundary layer, as well as specifying temperatures or/and composition for each zone to simulate the inhomogeneities of the charge. Through this approach, the combustion process can be more realistically described, resulting in more accurate predictions of cylinder pressure and heat release rate. In addition, emissions such as CO and HC can be modelled more accurately.

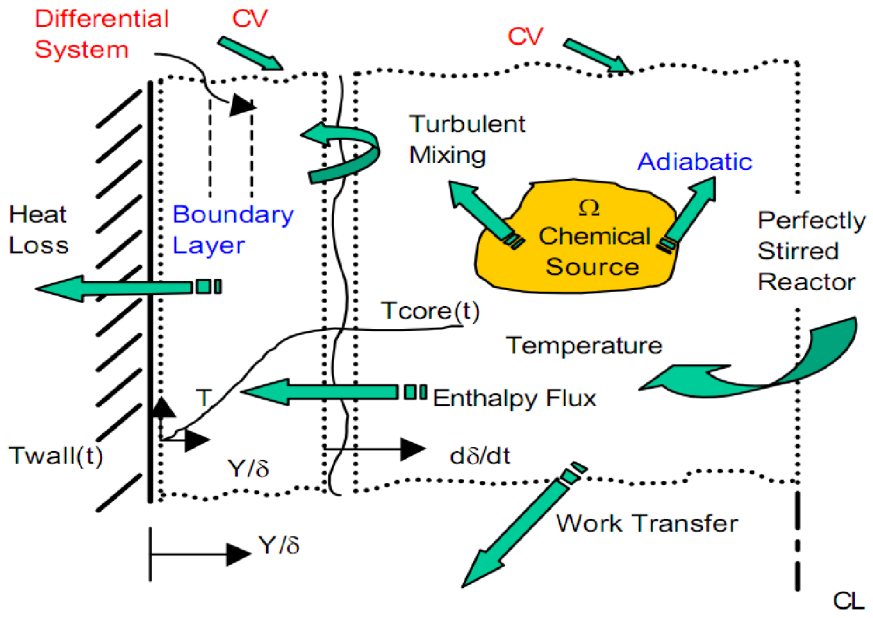

Figure 3-4: Interaction between the adiabatic core and the boundary layer [132].

Multi-zone modelling of HCCI engines has been investigated by a few group researchers [54,131]. The existing models can be summarized into three main categories according to the methods of the ***division of the combustion chamber***,

the consideration of mixing process and ***the initial condition setting***:

The model proposed by Scott and Dennis [132] established a fundamental base for zero-dimensional (0D) thermodynamic multi-zone models. The model separates the cylinder volume into two interacting regions: adiabatic core and thermal boundary layer. The general physics of the model are shown in Figure 3-4.

Ogink and Golovitchev [52] and Easley et al. [133] distributed the cylinder volume into several pockets at the beginning of the simulation, which consists of several core zones, one outer core zone, the boundary layer and the crevice as shown in Figure 3-5. The mass of each inner core zones is held constant throughout the simulation and mass transfer is considered only between the outer core zone and the boundary layer, and between boundary layer and the crevice. Mass exchange among the core zones is neglected. The initial temperature is assumed to distribute with a constant increment between every two adjacent zones and the mixtures are treated to distribute evenly across the combustion chamber.

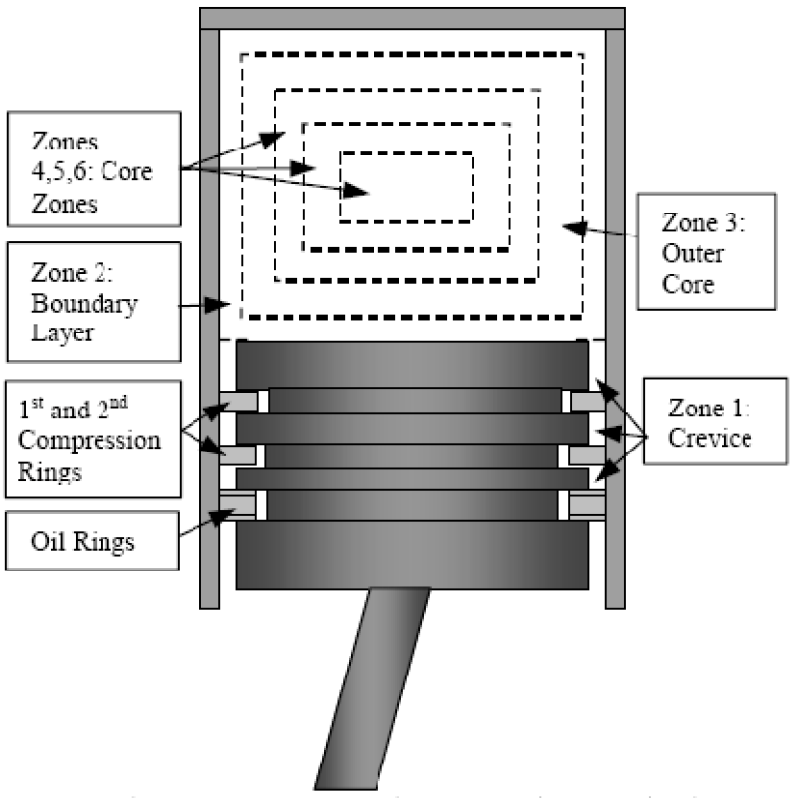

Figure 3-5: A Schematic drawing of a Multi-Zone model showing the Layout of the Different Zones [133]

Komninos et al. [131,134,135] separated the cylinder chamber into one cylindrical

core zone, several outer zones in the shape of cylindrical annulus and the crevice zone as illustrated in Figure 3-6. The thickness of the core zone and the outer zones evenly distribute the cylinder clearance height at TDC. The thickness of the core zone changes with piston motion and the outer zones' thickness are kept constant during the cycle. Mass exchange is taken into account across the zones. The in-cylinder temperature and composition at initial calculation point is assumed to be uniform throughout the cylinder

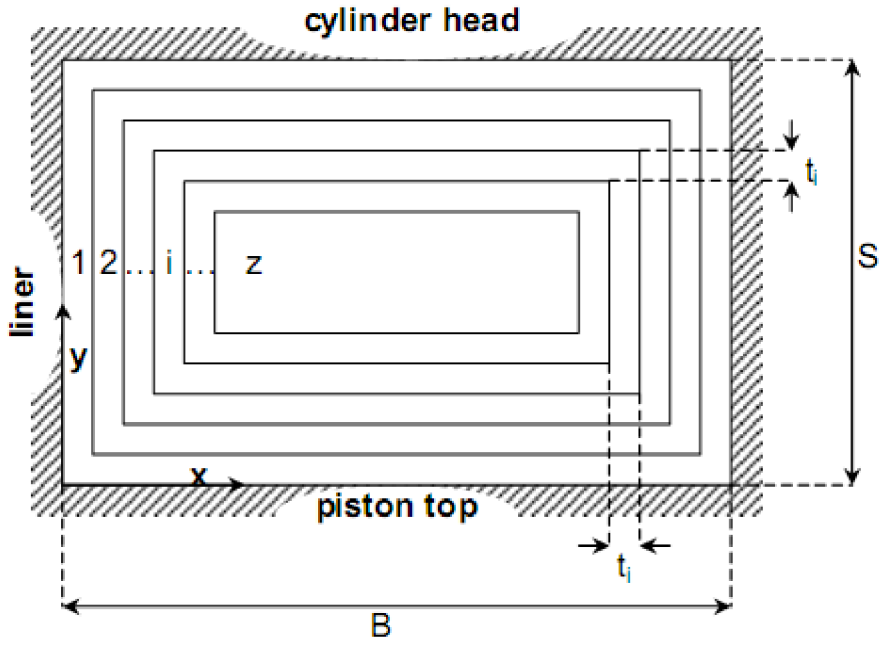

Figure 3-6: Geometric description of the multi-zone model proposed by Komninos et al [131].

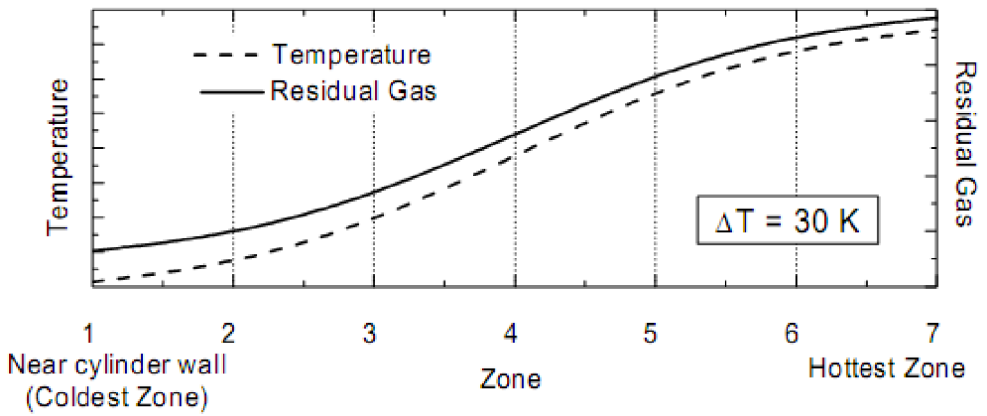

Figure 3-7: Distribution of EGR and mixture temperature over zones in the multi-zone model developed by Orlandini et al [136].

Orlandini et al. [136] zonally divided the combustion chamber into fixed mass zones, each zone is designated a volume percentage at beginning of the simulation. The mass mixing process is neglected, so the zones are interacted only through work. The inhomogeneous distribution of EGR and in-cylinder temperatures are defined by assigning a constant temperature gradient ΔT between the zones having the highest and smallest temperature as shown in Figure 3-7, and then temperatures of the other zone are arbitrarily adjusted to match the calculation results and experimental results. The EGR densities over the zones are assigned according to the temperature distribution, by which the zones of high temperature are assigned high EGR densities.

Despite the beneficial aspects of a multi-zone model, there are still unsolved technical problems of such model that hinder its extensive application. Firstly, with an increasing number of zones, calculation time becomes significantly increased, especially in the case of application of detailed chemical kinetics mechanisms, even for relatively simple multi-zone models, use of detailed mechanisms is computationally expensive.

Secondly, initial condition setting (normally at IVC) is still a major problem of HCCI multi-zone modeling. In order to evaluate the HCCI process, initial conditions for each zone must be defined for the multi-zone models. This means that the initial values for mixture composition, cylinder pressure, zone temperatures and EGR fractions etc in each individual zone have to be specified. Currently, three kinds of approaches in literatures have been investigated and applied in determining the IVC condition for multi-zone models.

Empirical data based adjustment [131,133,134,136] – this approach evaluates the IVC conditions in use of average empirical data and assigns the conditions of each zone in a experience-based manner.

Engine cycle simulation based adjustment [52] – a code for engine cycle simulation is applied in this approach to calculate the thermodynamic properties and mixture composition at IVC from gas exchange processes

CFD model based adjustment [53,65,137] - Computational Fluid Dynamics (CFD) calculations are performed in this approach to simulate the gas exchange processes and part of the compression till a computing point, from which a multi-zone model takes over to carry on the simulation for the rest of the engine processes

However, IVC conditions obtained from those approaches need to be arbitrarily adjusted (especially temperature) to match experimental results. This limits the confidence in such models in predicting HCCI combustion behaviour over any range of conditions wider than available experimental data [138].

3.5.3 Multi-Dimensional CFD Models

CFD modeling has been the dominant simulation and optimisation tool used in the modern engine design attributing to it powerful abilities in geometry representations. Thus, a full-scale integration of CFD model with detailed chemical kinetics model, theoretically, provides unparalleled simulation accuracy and details in presenting combustion behaviour. However, numerical modeling of this scale requires substantial computer resources in CPU speed, large-scale storage, and robust and fast numerical solution algorithm. Although, to date, the speed and power of computer resources has been significant improved, the simulation time for a CFD model with detailed chemical kinetics is still measured in weeks to months, which prevents the routine use of CFD models in the design process.

As a result, while CFD models have many great benefits, its implementation is markedly hampered by the size of chemical reaction mechanisms that can be incorporated with effectively. Typical CFD solutions are to sacrifice chemical accuracy for accuracy in geometry and flow by applying global (single-step) reactions or a set of severely reduced chemical reaction step [139-142]. However, this approach not only degrades the prediction accuracy but also is still computationally expensive. Another solution, as a contrast, is to reduce the full-scale CFD mesh to a one- or two- dimensional CFD mesh [52,143-145]. However, the computational time of such approach is still costly on current computers, especially when incorporated with detailed reaction mechanisms.

One of the solutions to the application of CFD code is the hybrid approaches, which incorporate the CFD models with multi-zone HCCI models in either **sequential** or **parallel** manners.

Aceves et al [53] firstly presented such a hybrid approach that formed a segregated sequential CFD Multi-zone thermo-kinetic Model. In their work, a hybrid approach integrating a Computational Fluid Dynamic (CFD) model (KIVA) with a multi-zone model with detailed chemical kinetics is presented. The CFD model is employed to solve the temperature and mixture composition until a transition time point prior to the

ignition, at which a multi-zone model substitutes for the CFD model to simulate the combustion and expansion process. The multi-zone model defines the zones by mass distribution and assumes no mixing between neighbouring zones. The initial conditions at the transition point for the multi-zone model are determined by the CFD model. The multi-dimensional results from the CFD model are reanalyzed and grouped to represent the temperature and mass, RGF distributions of a one-dimensional order. This process groups the cells of similar temperature and pressure history into a limited number of zones at the transition point.

The model was validated against experimental results and showed that the model predicts cylinder pressure and burn durations well, but HC and CO emissions were not predicted very accurately. Due to the application of the CFD model and the application of the detailed chemical kinetic mechanism in the multi-zone model, the computational time is still of a scale of hours or days which is usually unacceptably high for parametrical study. Moreover, this approach involves uncertainties in zone property definition and the selection of the transition point.

Another hybrid approach was presented by Flowers et al. [130], which combined a multi-zone model and a CFD model. In this approach, the two models are calculated in parallel during the compression and expansion strokes. At each time step, the CFD model carried out the computation of fluid dynamics, while the multi-zone model performed the calculations of detailed chemical kinetics. Information transfer between the two models took place at each time step. The advantage of this approach was that the fluid mechanic processes were calculated on a highly resolved grid, while the much more computationally expensive chemical kinetics processes could be solved for a limited number of computational zones [146].

Furthermore, the prediction of HC and CO emissions was significantly improved compared with the previous single-zone and multi-zone models. This results from the CFD simulation of the mixing process of the in-cylinder charge across zones during the expansion process, during which unburned or partially burned fuel and intermediates from low temperature regions (the crevices and boundary layers) diffused to hotter regions. Part of the released mixture is emitted as exhaust gases and the rest may further react at high temperature to convert to final oxidation productions.

In summary, CFD modeling allows for the provision of detailed information of initial

conditions and the incorporation of a CFD model with a multi-zone model offers a great advantage in computational time over a full integration of a CFD model with detailed chemical kinetics. However, the incorporative employment of the CFD model with the multi-zone chemical kinetics model is still under development and requires further investigation.

3.6 Summary

HCCI is a new combustion concept that can be applied in IC engines. In HCCI engines, the fuel and air are premixed to create homogeneous charge. During the compression stroke, the charge is compressed to autoignite around TDC. HCCI combustion is therefore an autoignition driven combustion process. As are results, the combustion process is primarily controlled by chemical kinetics of the fuel oxidation.

One of the major advantages of HCCI combustion is small cycle-to-cycle variations of the combustion process. The other advantages are low NO_X emissions and virtually no soot compared to diesel engines and higher part load efficiency compared with SI engines. However, due to the ignition occurs spontaneously at multiple points, HCCI features uncontrolled ignition timing. As autoignition has much shorter combustion, phase compared with flame propagation driven combustion as in SI engines, HCCI suffers from high combustion rate and high peak in-cylinder pressure at AFRs close to or above stoichiometric, which will cause damages to the engine body and produce unpleasant combustion noise. Consequently, HCCI is best operated at lean conditions. However, lean conditions leads to the relatively lower combustion temperature compared with that in SI engines, which results in relatively lower power density and high emissions of unburned hydrocarbon, especially at low loads.

In terms of the challenges presented with HCCI combustion, some technologies have been developed and applied for the solutions. EGR gases can be used to limit the rate of combustion. Adjustment of inlet temperature and EGR amount can be applied to control ignition timing. In the recent years, VVT systems emerged as a mean of controlling combustion rates as well. There are also many other technologies are developed to cope with the challenges with HCCI combustion such as turbocharging, stratified charge, direct injection, etc.

A variety of numerical models has been developed in the simulation of HCCI combustion to investigate its combustion characteristics. Major model types falls into three categories based on the dissimilarity of their physical descriptions of the combustion processes

- Single-Zone Models
- Multi-Zone Models
- Multi-Dimensional CFD Models

The single-zone models treat the combustion chamber as a closed system filed with homogeneous mixtures. It has been proven that single-zone models have been a valid approach in the studies of HCCI process in respect of numerical prediction of ignition timing and peak cylinder pressure, etc. and parametric analysis of the influence of engine parameters and fuel types. However, single-zone models oversimplify the real combustion scenario in HCCI engines, which results in inaccuracy in modelling heat release rate, CO and HC emissions, combustion completeness and peak cylinder pressure.

Multi-zone models stand out over single-zone models by embodying the description of the mixture inhomogeneity and the effect of the crevices and the thermal boundary layer and as well as in-cylinder mixture dynamics. Taking account of these aspects enable multi-zone models to model the combustion characteristics and emissions more accurately, but when coupled with chemical kinetics, the number of the variables needed to describe the system increases, which results in dramatic increase of computational time.

CFD modeling specializes detailing engine geometries and specifying mixture flow dynamics. When incorporated with chemical kinetics models, it provides unparalleled accuracy in the simulation of HCCI combustion. However, the major drawback of CFD model is the requirement of unacceptable and expensive computation cost. One of the solutions to the application of CFD code is hybrid approaches combining multi-zone models and CFD models, which is regarded as a compromise between simulation accuracy and computation cost.

Chapter Four: **Chemical Kinetics**

4.1 What is 'Chemical Kinetics'

The equilibrium composition of a reactive mixture can be predicted by the application of thermodynamic laws, In the case of that the chemical processes are much faster compared with the other processes like diffusion, heat transfer, flow etc. the thermodynamics alone allow the description of the system locally. In most cases, though, chemical reactions occur on timescales comparable with those of the flow and of the molecular transport processes. Therefore, information is needed about the rates at which the chemical reactions proceed. For this purpose, chemical kinetics has been investigated to study the rates of chemical processes in an effort to understand the factors that influence these rates and to develop theories that can be used to predict chemical processes.

In the research of internal combustion engines, chemical kinetics fulfils the needs for compact numerical models to represent hydrocarbon combustion and enables establish and development of numerical models for the design and prediction of performance of practical engine systems. In general, chemical kinetics forms a link between experimental observation and numerical interpretations of the combustion processes in internal combustion engines.

4.2 Rates, Rate laws and Rate Constants

In this section, three types of reactions that are global, elementary and chain

reactions and the terms, equations and basic laws applied to describe each reaction type are introduced.

4.2.1 Global Reactions

The chemistry in fuel oxidation can be expressed by a global reaction mechanism. Assuming that a mole of fuel reacts with a moles of oxidizer to produce b moles of combustion products, it yields

$$1 \cdot \text{Fuel} + a \cdot \text{Oxidizer} \rightarrow b \cdot \text{Products} \qquad \textbf{4-1}$$

The fuel consumption rate can be expressed by

$$\frac{d[X_{Fuel}]}{dt} = -k_G(T) \cdot [X_{Fuel}]^n \cdot [X_{Oxidizer}]^m \qquad \textbf{4-2}$$

where $[X_i]$ denotes the molar concentration of the ith species in the mixture. $k_G(T)$ is the global rate coefficient and is a strong function of temperature. The minus sign indicates that fuel concentration decreases with time. The exponent n and m relate to the reaction order.

Use of global reactions to express a chemical reaction system is frequently a 'black box' approach by providing the input-to-out perspective to the chemical process, which is not capable of providing a basis for understanding what is actually happening chemically in a system. The chemical equation 4-1 indicates that the oxidation process of the fuel is a one-step and instantaneous process. In reality, it is however a much more complex and sequential process. This process involves the breaking and formation of chemical bonds and production and destruction of intermediate species. A global equation consequently is not adequate to describe a chemical process in details, so a collection of *elementary reactions* has to be used to depict a chemical process, which will be considered in the following section.

4.2.2 Elementary Reactions

Elementary reactions express how actually molecules or ions react with each other. The equation in an elementary reaction represents the reaction at the molecular level rather than a global reaction. Based on numbers of molecules involved in the elementary reaction, there are three major types of elementary reactions: **Unimolecular** reactions, **Bimolecular** reactions, and **Trimolecular** reactions [147].

4.2.2.1 Unimolecular reactions

Unimolecular reactions describe the rearrangement or dissociation of a molecule, which can be expressed as

$$A \rightarrow \text{products} \qquad \textbf{4-3}$$

The rate, at which the reaction proceeds, is directly proportional to the concentration of the reactant species, i.e.

$$\frac{d[A]}{dt} = -k \cdot [A] \qquad \textbf{4-4}$$

where k symbolizes the rate coefficient, which generally applies throughout the context in this chapter.

4.2.2.2 Bimolecular reactions

Most elementary reactions of interest in combustion are bimolecular, that is, two molecules collide and react to form two different molecules, which can be generally expressed as

$$aA + bB \rightarrow c\mathrm{C} + d\mathrm{D} \qquad \textbf{4-5}$$

where a, b, c, and d are stoichiometric coefficients. The reaction rate is calculated by multiplying the reaction rate constant by the concentration of each of the reactants

$$\frac{1}{a}\frac{d[A]}{dt} = \frac{1}{b}\frac{d[B]}{dt} = -\frac{1}{c}\frac{d[C]}{dt} = -\frac{1}{d}\frac{d[D]}{dt} = -k \cdot [A] \cdot [B] \qquad \textbf{4-6}$$

Note that the negative rates indicate that the species are being consumed.

4.2.2.3 Termolecular reactions

A termolecular reaction involves the collision of three molecules. The general form of a termolecular reaction is

$$A + B + M \rightarrow \mathrm{C} + \mathrm{M} \qquad \textbf{4-7}$$

whose reaction rate can be expressed

$$\frac{d[A]}{dt} = -k \cdot [A] \cdot [B][M] \qquad \textbf{4-8}$$

where M may be any molecule and is frequently referred to as a third body.

4.2.2.4 Rate Constant

It has been observed from both kinetic theories of gases and experiments that the rate constant k for an elementary reaction is an exponential function of temperature and of the so-called Arrhenius form [148],

$$k(T) = A \cdot T^{b} \cdot \exp(-E_A / R_u T) \qquad \textbf{4-9}$$

where A is the pre-exponential factor. E is the activation energy for the reaction that is required to bring reactants to a reactive state such that the chemical bonds can be rearranged to form products. Both A and E need to be determined from experiment for most elementary reactions that occur in combustion.

4.2.3 Chain Reactions

Many gas-phase reactions are initiated by the formation, at very low concentration, of an extremely reactive species that sets off a series of reactions leading to a self-amplifying and self-sustaining chain of chemical events. Such a process is referred to as a chain reaction, and typically, it occurs after a short induction period to allow the formation of the reactive species [149]

4.2.3.1 Chain Reaction Mechanisms

The sequence of a reaction chain can be typically divided into four stages:

Initiation - in which a reactive intermediate, which may be an atom, an ion, or a neutral molecular fragment, is formed, usually through the action of an agent such as light, heat, or a catalyst.

Chain branching – whereby the intermediate reacts with the original reactants, producing stable products and another intermediate, whether of the same or different kind; the new intermediate reacts as before, so a repetitive cycle begins and more radicals are produced than destroyed

Propagation – in which, the number of radicals does not change significantly, but different radicals are produced

Termination – in which, radicals are destroyed either by gas-phase reactions or by collision with surfaces.

A simple chain reaction mechanism applicable to combustion can be illustrated by the following generic set

Initiation $S \underset{k_{r1}}{\overset{k_{f1}}{\Leftrightarrow}} R_1^{\bullet}$ **4-10**

Branching $R_1^{\bullet} + S \underset{k_{r2}}{\overset{k_{f2}}{\Leftrightarrow}} R_2^{\bullet} + R_3^{\bullet}$ **4-11**

Propagating $R_2^{\bullet} + R_3^{\bullet} \underset{k_{r3}}{\overset{k_{f3}}{\Leftrightarrow}} \alpha \cdot R_4^{\bullet}$ **4-12**

Termination $R_1^{\bullet} + R_2^{\bullet} + R_3^{\bullet} + R_4^{\bullet} \underset{k_{r3}}{\overset{k_{f3}}{\Leftrightarrow}} \beta \cdot P$ **4-13**

where indicates the fuel molecules, $\mathrm{R}_1^{\bullet}, \mathrm{R}_2^{\bullet}, \mathrm{R}_3^{\bullet}, \mathrm{R}_4^{\bullet}$ describe the intermediate species and P is the products. α and β are stoichiometric coefficients that have integer values greater than 1. k_f and k_r are the forward and reverse rate coefficients, respectively.

Note that the above chain scheme does not corresponding to any genuine chemistry but depicts the proceeding of a reaction chain, from which the reaction rates are derived in the following parts of the section.

4.2.3.2 Reaction Rates

Knowing rates of elementary reactions as expressed by Equation 4-4, 4-6 and 4-8, one can mathematically express the net rates of production or destruction for any species participating in a series of chain reactions. Taking the example of the mechanism in the above section, the net rate of production of $\mathrm{R}_1^{\bullet}$ is the sum of all of the individual elementary rates producing $\mathrm{R}_1^{\bullet}$ minus the sum of all of the rates destroying $\mathrm{R}_1^{\bullet}$, i.e.,

$$\begin{aligned}\frac{\mathrm{d}[\mathrm{R}_1^{\bullet}]}{dt} &= k_{f1}[\mathrm{S}] + k_{r2}[\mathrm{R}_2^{\bullet}][\mathrm{R}_3^{\bullet}] + k_{r4}[\mathrm{P}]^{\beta} \\ &\quad - k_{r1}[\mathrm{R}_1^{\bullet}] - k_{f2}[\mathrm{R}_1^{\bullet}][\mathrm{S}] - k_{f4}[\mathrm{R}_1^{\bullet}][\mathrm{R}_2^{\bullet}][\mathrm{R}_3^{\bullet}][\mathrm{R}_4^{\bullet}]\end{aligned} \quad \textbf{4-14}$$

And for $\mathrm{R}_2^{\bullet}$ atoms,

$$\begin{aligned}\frac{\mathrm{d}[\mathrm{R}_2^{\bullet}]}{dt} &= k_{f2}[\mathrm{R}_1^{\bullet}][\mathrm{S}] + k_{r3}[\mathrm{R}_4^{\bullet}]^{\alpha} + k_{r4}[\mathrm{P}]^{\beta} \\ &\quad - k_{f2}[\mathrm{R}_2^{\bullet}][\mathrm{R}_3^{\bullet}] - k_{f3}[\mathrm{R}_2^{\bullet}][\mathrm{R}_3^{\bullet}] - k_{f4}[\mathrm{R}_1^{\bullet}][\mathrm{R}_2^{\bullet}][\mathrm{R}_3^{\bullet}][\mathrm{R}_4^{\bullet}]\end{aligned} \quad \textbf{4-15}$$

With writing similar expression for each species participating in the mechanism, it yields a system of first-order ordinary differential equation that describes the evolution of the chemical system, i.e.,

$$\frac{\mathrm{d}[X_i](t)}{dt} = f([X_1](t),[X_2](t),...[X_n](t)) \qquad \textbf{4-16}$$

with known initial conditions

$$[X_i](t=0) = [X_i]_0 \qquad \textbf{4-17}$$

Together with equations describing conservation of mass and energy, and state, the set of equations can be numerically integrated using computerized methods. It should be noted that such a chemical system has an important feature of being stiff, which has one or more variables change very rapidly, while others change very slowly. The characterization of stiffness of a system of ordinary differential equations requires more complex numerical integration methods, i.e., Backward Euler method, to achieve stable numerical solution.

4.2.3.3 Matrix and Notation Expression

For mechanisms including many reactions and species, a notation expression can be used to represent the mechanism as

$$\sum_{j=1}^{N} \nu'_{ji} X_j \Leftrightarrow \sum_{j=1}^{N} \nu''_{ji} X_j \quad \textbf{for } i = 1, 2 \ldots L \qquad \textbf{4-18}$$

where ν'_{ji} and ν''_{ji} are the stoichiometric coefficients on the reactants and products side of the equation, respectively, for the jth species in the ith reaction. For example, consider the four reactions expressed by equations 4-10 - 4-13, involving six species: S, $\mathrm{R}_1^{\bullet}$, $\mathrm{R}_2^{\bullet}$, $\mathrm{R}_3^{\bullet}$, $\mathrm{R}_4^{\bullet}$ and P. Setting $[X] = \left[\mathrm{S} \quad \mathrm{R}_1^{\bullet} \quad \mathrm{R}_2^{\bullet} \quad \mathrm{R}_3^{\bullet} \quad \mathrm{R}_4^{\bullet} \quad \mathrm{R}_5^{\bullet}\right]^T$ and using j as the column index and i as the row index, the stoichiometric coefficient matrix can be written as

$$\nu'_{ji} = \begin{bmatrix} 1 & 0 & 0 & 0 & 0 & 0 \\ 1 & 1 & 0 & 0 & 0 & 0 \\ 0 & 0 & 1 & 1 & 0 & 0 \\ 0 & 1 & 1 & 1 & 1 & 0 \end{bmatrix} \qquad \textbf{4-19}$$

and

$$v''_{ji} = \begin{bmatrix} 0 & 1 & 0 & 0 & 0 & 0 \\ 0 & 0 & 1 & 1 & 0 & 0 \\ 0 & 0 & 0 & 0 & 1 & 0 \\ 0 & 0 & 0 & 0 & 0 & 1 \end{bmatrix} \qquad \textbf{4-20}$$

By applying the stoichiometric coefficient matrix, the net production rate of each species in a chain reaction mechanism can be expressed as

$$\dot{\omega} = \sum_{i=1}^{L} v \qquad \textbf{for } j = 1, 2 \ldots N \qquad \textbf{4-21}$$

where

$$v_{ji} = \left(v''_{ji} - v'_{ji}\right) \qquad \textbf{4-22}$$

and

$$q_i = k_{fi} \prod_{j=1}^{N} \left[X_j\right]^{v'_{ji}} - k_{ri} \prod_{j=1}^{N} \left[X_j\right]^{v''_{ji}} \qquad \textbf{4-23}$$

where the production rates, $\dot{\omega}$, corresponds to the left-hand-side of Equation 4-14 and 4-15 , which can also be expressed as $\dot{\omega}_j = \frac{d\left[X_j\right]}{dt}$. Equation 4-23 defines the rate-of- progress variable, q_i , for the ith elementary reaction.

The matrix and compact notations interpreted in Equations 4-18 - 4-23 provide a general expression of mathematical modeling of chemical kinetics, and consequently ease the computerization of solving chemical kinetics problems and facilitate the programming process. Thus, this pack of expression is applied in the in-house LUCKs code that is detailed in **Chapter 6**.

4.3 Chemical Kinetics of Hydrocarbon Autoignition

Auto-ignition in SI and HCCI engines as discussed earlier can be generally interpreted as an oxidation process of hydrocarbons, which is not initiated by any external ignition source. For either the conventional engines or HCCI engines, such a combustion process is not a single- or even a few-step chemical reactions; the actual autoignition process may be generally described as a series of complex degenerate

chain branching, carrying and terminating reactions involving stable and radical species.

This section is organized to discuss the gasoline composition and its surrogate first and the chemistry of hydrocarbon oxidation is next presented followed by the summarization of chemical kinetics models.

4.3.1 Gasoline Composition

Gasoline is a complex mixture of over 500 hydrocarbons that may have between 5 to 12 carbons. Alkanes type compounds of either straight chain or branched compounds are present in greatest amounts. Smaller amounts of alkane cyclic and aromatic compounds are present. Very small or trace amounts of alkenes are present in gasoline [150]. Typical composition of gasoline is given in Table 4-1. The data in Table 4-1 gives the volume fractions of the component groups in gasoline

Table 4-1: Typical Composition of Gasoline [150].

Typical Composition of Gasoline		
General Name	**Examples**	**Percentage %**
Aliphatic - straight chain	heptane	30-50
Aliphatic - branched	isooctane	
Aliphatic - cyclic	Cyclo-pentane	20-30
Aromatic	ethyl benzene	20-30

4.3.2 Gasoline Surrogates

Based on the above description, gasoline is a complex mixture of a large number of hydrocarbon species, including alkanes, cyclo-alkanes, alkenes, aromatics, and additives. For chemical kinetics modeling, all the species and corresponding reactions will lead to terribly long calculation times, so it is unpractical to include all of the species in the reaction mechanism, even if gasoline is analyzed thoroughly and its composition is exactly known. Therefore, the oxidation of simple blends or chemical surrogates has allowed a detailed examination of the combustion processes for fuels that either have too many compounds or have variable composition.

Based on the specific application of the surrogates to model gasoline combustion in internal combustion engines, the following criteria are judged to be of the most importance to form a fuel surrogate [146,151,152]

- A gasoline surrogate should have similar autoignition and burn rate

characteristics under SI, CI or HCCI conditions as real gasoline.

- The reaction mechanism for the surrogate should be of limited size to keep computation times reasonable.
- A (semi-)detailed reaction mechanism for the components of the surrogate to be included should be available or conceivable.
- Properties of the surrogate, such as the H/C ratio and the stoichiometric air/fuel ratio, should be as similar as possible to those of the full boiling range gasoline fuel.

A model surrogate does not necessitate having a chemical-class composition similar to that of the real gasoline, since any attempt to fulfill the first criterion concerning auto-ignition characteristics is expected to result in a fuel blend with a similar chemical-class composition to that of the real fuel [146].

A mixture of the two types of paraffin are wildly accepted and used to model gasoline; n-heptane and iso-octane (2, 2, 4-trimethyl-pentane). As well known, the volume fractions of the two components are used to indicate the Research Octane Number (RON). The Research Octane Number is determined by comparing the characteristics of a gasoline to iso-octane (2, 2, 4-trimethylpentane) and n-heptane.

In many publications on combustion models [127,133,153-155], Mixtures of n-heptane and iso-octane are stated as Primary Reference Fuels (PRFs) to represent gasoline. Iso-octane is assigned an octane number of 100, which is used as a reference for fuels that are very knock-resistant under SI engine conditions. In general, it is a highly branched module that burns smoothly with little knock. On the other hand, n-heptane, a straight chain, unbranched molecule is given an octane rating of zero because of its bad knocking properties. Thus, RON is chosen to be a measure of knocking resistance of fuels under standard conditions in a spark ignition engine.

However, the H/C and A/F ratios of blends of n-heptane and iso-octane are generally higher than those of gasoline. To improve the H/C and A/F ratios and make chemical composition more similar to real fuel, an aromatic compound e.g. toluene [146], can be added to the blends of n-heptane and iso-octane. However, research of development and validity of reaction mechanisms involving aromatic have been lagged behind, and in consequence, the blends of n-heptane and iso-octane are more generally applied to represent gasoline in modelling gasoline combustion in SI

and HCCI engines.

4.3.3 Hydrocarbon Oxidation Chemistry

The gas phase oxidation of hydrocarbons has been studied since the early 1900s. Since then, several theories have been forwarded as to the mechanism of hydrocarbon oxidation. The foundation of today's theory was forwarded by Semenov (1935), which is based on the concept of free radicals [156]. A radical is an atom or molecule with at least one unpaired electron in the outermost valence shell. Due to the unfilled valence shell, radicals are highly reactive. Since Semenov, the theory has been refined and enhanced, but the fundamental concept remains. Essentially, the oxidation process is controlled by a sequence of elementary chemical reactions in which radicals are created, propagated, or destroyed. These reactions can be grouped into several fundamental classifications [157].

- **Primary Initiation:** Formation of radicals from parent fuel molecule
- **Secondary Initiation:** Radicals formed from other "stable" intermediates
- **Chain Branching:** Reaction where the number of radicals increases
- **Chain Propagation:** Reaction where the number of radicals remain unchanged
- **Termination:** Removal of radicals from the reaction

Thus, the combustion process hydrocarbon may be generally described as a series of complex degenerate chain branching, carrying and terminating reactions involving stable and radical species. It is commonly accepted that for hydrocarbon oxidation these reactions may be separated into three distinct temperature regimes. Each regime, low, intermediate, and high temperature regime, is dominated by reactions involving different radical species and different pathways. Naturally, the combustion environment, temperature, pressure and equivalence ratio affect the location of the boundaries between each regime. For example, at one atmosphere, the hydrocarbon oxidation process can be divided along the following boundaries [6]:

- Low temperature regime: < 650 K
- Intermediate temperature regime: 650 – 1000 K
- High temperature regime: > 1000 K

4.3.4 The Oxidation of N-Heptane

The following flow chart gives the major reaction branches of the oxidation of n-heptane. Common agreement on this reaction system seems to be made by numbers of researchers involved in n-heptane oxidation chemistry [12,34,146,154,158-160] and similar diagrams are and arguments presented in their scientific papers.

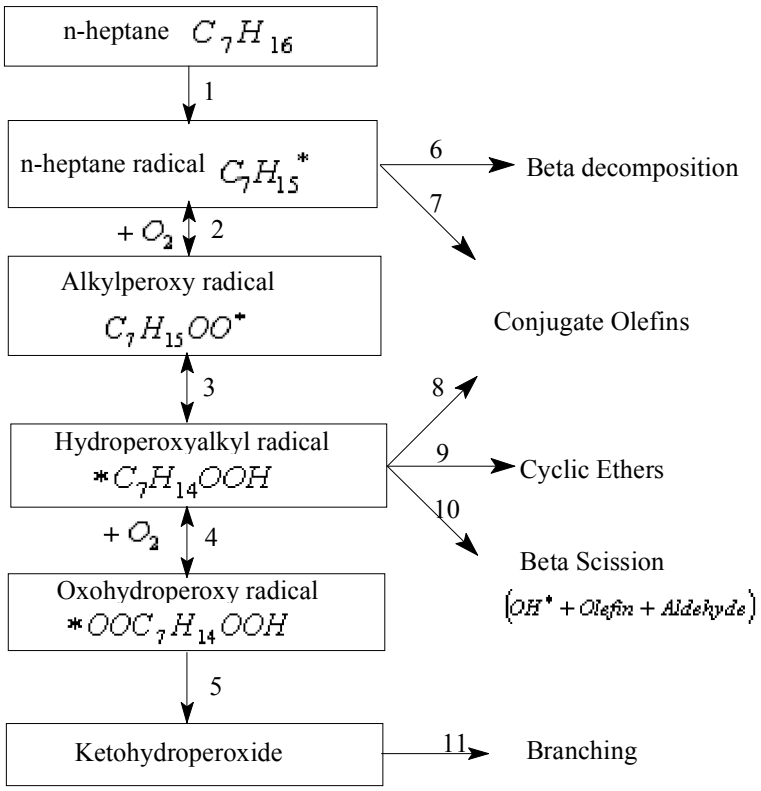

Figure 4-1: Major branches of n-heptane oxidation [6].

As stated in previous section, a hydrocarbon oxidation process can be classified by three distinct temperature regimes: low, intermediate and high temperature regimes. Each of them is dominated by reactions involving different radical species and different pathways shown in Figure 4-1.

4.3.4.1 Low Temperature Regimes

4.3.4.1.1 Reaction class 1

The chain reaction of oxidation of n-heptane in low temperature regime is initiated by the decomposition of the parent fuel molecule by molecular oxygen. This is achieved by the removal of a hydrogen atom by molecular oxygen.

$$C_7H_{16} + O_2 \rightarrow C_7H_{15}^* + HO_2^*$$

However, this step, named an abstraction reaction, is highly endothermic, roughly 180 – 230 kJ/mol, depending on the parent fuel and the bond energy of the abstracted H atom, and requires activation energy proportional to the endothermicity, thus this reaction is not a dominant route to form the n-heptane radical $C_7H_{15}^*$. Once the reaction system has created sufficient other radicals, such as OH^*, O^* and H^*, the abstraction reaction proceeds with the involvement of such radicals rather than molecular oxygen. The hydroxyl radical OH^* has the fastest attack rate due to its high reactivity [161].

$$C_7H_{16} + X^* \rightarrow C_7H_{15}^* + XH$$

In the hydrogen abstraction reactions, different heptyl radicals are formed. This is because any given hydrocarbon, the hydrogen atoms can be labelled in such a fashion as to indicate which abstraction sites will produce the same radicals and intermediates. For n-heptane, there are four distinct abstraction sites, “1”, “2”, “3” or “4” shown in Figure 4-2. The 1 are categorized to primary bond sites and, 2, 3 and 4 to secondary bond sites. A primary bond of C-H is defined as that a C atom is only connected with one other C atom, and a secondary one is indicated to a C atom is adjacent to two other C atoms.

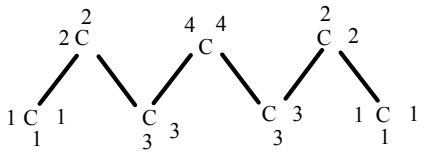

Figure 4-2: The four different sites for H abstraction in n-heptane.

4.3.4.1.2 Reaction class 2

Following H atom abstraction, an addition of an alkyl radical to O_2 is the most important reaction for low temperature oxidation, even though it does not immediately determine the overall rate of chain branching.

$$C_7H_{15}^* + O_2 \rightarrow C_7H_{15}OO^*$$

The activation energy for the addition reaction is taken to be zero but has a quite large value of approximately 30 kcal/mol in the reverse dissociation direction. Therefore, the equilibrium constant for this reaction is very strongly temperature dependent. At very low temperatures this reaction proceeds rapidly to produce the

alkylperoxy species very efficiently, however at high temperatures $C_7H_{15}OO$ dissociates rapidly and the concentration of $C_7H_{15}OO$ is very small [159].

4.3.4.1.3 Reaction class 3

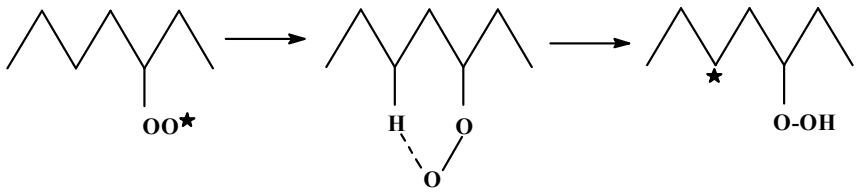

Figure 4-3: Reaction mechanism of isomerisation of $C_7H_{15}OO$.

Reaction mechanism proceeds with isomerisation of $C_7H_{15}OO$ by internal H-abstraction to form hydroperoxy alkyl radical [162], as shown in Figure 4-3.

$$C_7H_{15}OO \rightarrow {}^{*}C_7H_{14}OOH$$

An isomerisation process consists of a number of steps. Firstly, the radical site of OO^* attacks a hydrogen atom at the molecule chain and a ring-like structure is formed. Then the H atom that has connected with OO^* is abstracted from its original site to complete the isomerisation process. Fifteen different hydroperoxy alkyl radicals can be formed from the isomerisation of four kinds of $C_7H_{15}OO$ species.

According to Curran et al [159], the rate constants of isomerisation are determined by following factors.

- Ring strain energy barriers.
- The type and location of the abstraction H atom (primary or secondary)
- The degeneracy of number of H atoms at that site.

4.3.4.1.4 Reaction class 4 and 5

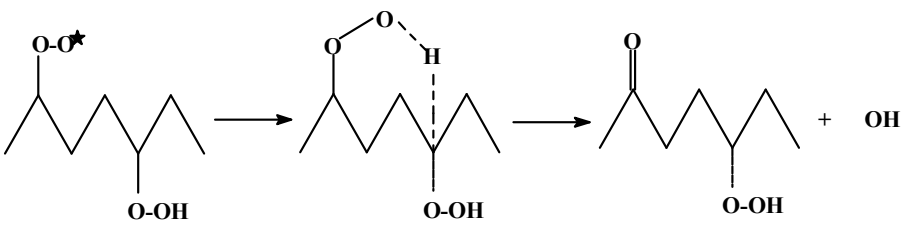

Figure 4-4: Reaction mechanism of isomerisation of ${}^{*}OOC_7H_{14}OOH$.

$$^{*}C_7H_{14}OOH + O_2 \rightarrow {}^{*}OOC_7H_{14}OOH \rightarrow {}^{*}OOC_7H_{14}O + {}^{*}OH$$

The hydroperoxy alkyl radicals $^{*}OOC_7H_{14}OOH$ formed in the previous isomerisation step reacts with molecule oxygen to produce oxohydroperoxide radicals. Then, $^{*}OOC_7H_{14}OOH$ dissociates to release OH and to form ketohydroperoxide species, $^{*}OOC_7H_{14}O$, via breaking the O-O bond. Different ketohydroperoxide species are formed depending on the different types of $^{*}C_7H_{14}OOH$. Figure 4-4 depicts 5-hydroperoxy-2-heptylperoxy radical undergoing isomerisation through a seven-member ring structure, forming 2-hydroperoxy-5-heptanone.

4.3.4.1.5 Reaction class 11

The ketohydroperoxide will remain until the temperature increases sufficiently for it to decompose [152]. This reaction group produces several kinds of radicals which contribute to the rapid chain branching process when the temperature reaches a certain high level (about 800K).

Generally speaking, oxidation of n-heptanes in the low temperature regime is exothermic. The heat release during the low temperature results in an increase of temperature by hundreds of degrees Kelvin and this phenomenon is referred as 'cool flame'.

4.3.4.2 Intermediate Temperature Regimes

As the temperature increases, the reaction scheme enters intermediate temperature regime. In this regime, reaction classes 8, 9 and 10 take over those 4, 5 and 11 to dominate the propagation of the reaction mechanism

4.3.4.2.1 Reaction class 8

$$^{*}C_7H_{14}OOH \rightarrow C_7H_{14} + HO_2^{*}$$

In intermediate temperature range, $^{*}C_7H_{14}OOH$ radicals that have a radical site beta to the hydroperoxy group can decompose to yield a conjugate olefin and HO_2^{*} radical. This reaction has proven to be quite sensitive, and is responsible for a large part of the NTC behaviour in n-heptane oxidation kinetics [159].

Note: a beta (β) radical site is referred to a radical site at a C atom located two

carbon atoms away from the O-O site; and NTC is an abbreviation for Negative Temperature Coefficient and refers to the temperature interval during which system reactivity decreases despite a rise in temperature. The reason that the chemistry slows down is that the low-temperature chain branching reactions are replaced by propagation reactions at intermediate temperatures, which does not lead to increasing numbers of reactive radicals [146].

4.3.4.2.2 Reaction class 9

$$^{*}C_7H_{14}OOH \rightarrow C_7H_{14}O + OH^{*}$$

This reaction sequence involves the breaking of the O-O bond, coupled with the formation of a cyclic compound including the remaining O atom and a hydroxyl radical.

4.3.4.2.3 Reaction class 10

$$^{*}C_7H_{14}OOH \rightarrow olefin + carbonyl + OH^{*}$$

Another channel shown above yields an olefin and an aldehyde, together with OH, and this is visualized as occurring by a β scission process, which will have somewhat higher activation energy due to the necessity of breaking a C-C bond in $^{*}C_7H_{14}OOH$ radicals [30,159]. The $^{*}C_7H_{14}OOH$ radicals, produced by $C_7H_{15}OO$ isomerisation with an intermediate ring structure of six atoms can undergo β - scission and scission products are chosen considering the weakest inner atomic bonds in the molecule.

In a conclusion, the main decomposition reactions of alkylhydroperoxy radicals are considered to proceed by the breaking of O-O bond, the scission of C-O bond and scission of C-C bond. Normally the C-C bond in $^{*}C_7H_{14}OOH$ is less probable to break than the O-O; however attention has to be paid to the β C-C bond, which is weakened by the present of O atom on β carbon.

4.3.4.3 High Temperature Regimes

When temperature increases further, the reaction mechanism enters high temperature range. First of all, the role of H_2O_2 played in the second ignition stage should be noticed. Hydrogen peroxide H_2O_2 is formed as a major product of cool

flame chemistry and plays a key role in promoting hot autoignition.

Hydrogen peroxide is formed from reactions of HO_2^*. The combination reaction of HO_2^* radicals to form H_2O_2 has been widely studied at low temperature, where it has small negative temperature dependence and a pressure effect [123].

$$HO_2 \bullet + HO_2 \bullet \rightarrow H_2O_2 + O_2$$

Alternative propagating reactions form H_2O_2 [163].

$$HO_2 \bullet + RH \rightarrow H_2O_2 + R$$

Amneus [164] explains that how a high temperature can be achieved when the reactions become slower during the NTC period. According to him, a pre-requisite for the cool flames to induce full combustion is that sufficient energy must be released by the low-temperature reactions to raise the system temperature to the high-temperature region. Furthermore, the temperature can be raised sufficiently by external effects as well: when the compression ratio is high enough, the gas temperature in the combustion chamber of an internal combustion engine will be forced into the high-temperature regime by means of the compression work during the compression stroke.

Reaction classes 6 and 7 represent the high temperature reaction paths. When the temperature is high enough to approximately 1000K, the conversion reactions of heptyl radicals to β decomposition products and conjugate olefins take over from the reaction of $C_7H_{15}\bullet$ forming $C_7H_{15}OO\bullet$ represented by reaction class 2 in the low temperature branch.

4.3.4.3.1 Reaction class 7

$$C_7H_{15} \bullet + O_2 \rightarrow \bullet C_7H_{15}OO \bullet$$

$$\bullet C_7H_{15}OO \bullet + M \rightarrow \bullet C_7H_{15}OO \bullet + M$$

$$\bullet C_7H_{15}OO \bullet \rightarrow C_7H_{14} + HO_2 \bullet$$

In this reaction class, a stable olefin and hydroperoxide are produced, thus it is responsible for NTC behaviour due to the sudden reduction in the concentration of alkyl radical, which is occurs when reaction class 2 is taken over by the reaction classes 6 and 7 [158].

4.3.4.3.2 Reaction class 6

Alkyl radical decomposition is important only at relatively high temperatures (T > 850 K), as the addition of alkyl radicals to molecular oxygen, even though a bimolecular reaction, is faster than β scission due to the relatively high activation energy barriers for alkyl radical decomposition (there is no energy barrier for the addition to O_2). β scission is considered to be the dominant decomposition path for alkyl radicals. In many cases there are two or more pathways possible for an alkyl radical, with different products [159].

Examples of alkyl radical decomposition reactions:

$$C_7H_{15}\bullet \rightarrow C_5H_{11}\bullet + C_2H_4$$

$$C_7H_{15}\bullet \rightarrow C_4H_9\bullet + C_3H_6$$

An essential high temperature chain branching reaction is the decomposition of H_2O_2 into two hydroxyl radicals. This is because hydrogen peroxide itself is considerably more stable than hydroperoxides, and can only act as a source of radicals at temperatures above 1000K, when the pressure dependent thermal decomposition becomes important [163]

$$H_2O_2 + M \rightarrow 2OH + M$$

When the temperature rises above 1200 K, the relatively high activation energy of the following reaction is overcome and becomes the dominant chain branching step [25, 28, 29]; the reactants, including one radical, lead to two product radicals. Since molecular oxygen participates in this reaction, lean fuel mixtures are more reactive in this high-temperature regime, whereas rich fuel mixtures are oxidized quickly at low temperatures due to chain branching which depends on radical species formed directly from the parent fuel [146,159].

$$H\bullet + O_2 \rightarrow O\bullet + OH\bullet$$

4.3.5 The Oxidation of Iso-octane

The scheme of iso-octane oxidation shown in Figure 4-5 is very similar to that for n-heptane. The main difference results from the molecular structure of the two fuels diagrammed in Figure 4-6. Four different CH groups can be recognized in iso-octane. Numerals are assigned to these positions in order to show their identity compared to

n-heptane. This difference of molecular structures leads to the different distribution of the mass flows through the different reaction branches, and thus the distribution of products changes accordingly

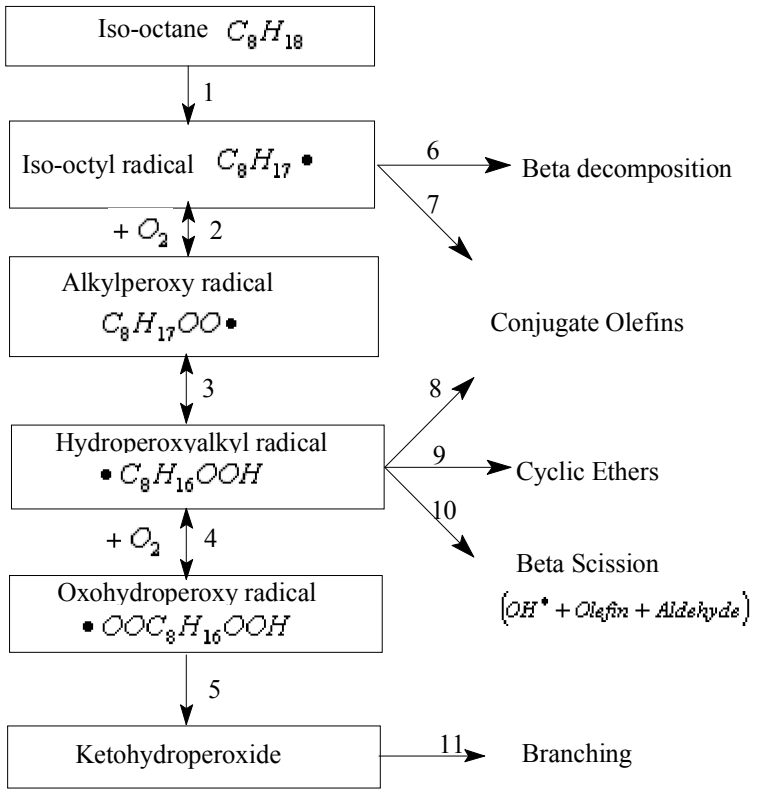

Figure 4-5: Major reaction branches of iso-octane oxidation [6].

Several researchers have discussed the differences between n-heptane oxidation and iso-octane oxidation, which are classified as follows:

Figure 4-6: Different types of CH groups in n-heptane (left) and iso-octane (right)

The sum of secondary and tertiary H atoms of iso-octane, which are more active than primary H atoms, is much lower than that of n-heptane. This is illustrated by Figure 2.8. Hence, the H abstraction and isomerisation reactions in the case of iso-octane are less likely to occur. Therefore, the propagation sequence through alkyl peroxy radicals (reaction class 2), hydroperoxy alkyl radicals (reaction class 3) and cyclic

ethers (reaction class 9) is favoured more for n-heptane than it is for iso-octane [165].

The difference in internal H abstraction rates between n-heptane and iso-octane is related to the different sizes of the transition ring with varied ring strain energy barrier shown in Figure 4-7

Figure 4-7: Different transition rings for internal H abstraction in n-heptane and iso-octane

4.3.6 Summary

As noted previously, the oxidation of hydrocarbons can be separated into three temperature regimes, the low, intermediate, and high temperature regimes. In the low temperature regime, the oxidation process is dominated by the alkylperoxy radical $R\dot{O}_2$, where R is the hydrocarbon molecule minus one hydrogen atom. The low temperature oxidation reactions are exothermic and can raise the temperature of the system, which forms 'cool flame', and can form an initial radical pool, which can promote branching decomposition and radical-initiated reactions at higher temperatures.

The intermediate temperature regime is dominated by the hydroperoxy radical. In the intermediate temperature regimes, the hydroperoxy alkyl radicals $\bullet ROOH$ are converted into conjugate olefins, cyclic ethers and β-scission products, instead of ketohydroperoxide, which is responsible for a large part of the NTC behaviour, and in the meantime accumulation of H_2O_2 takes place. The high temperature regime is dominated by several radicals, namely hydroxyl $\dot{O}H$, oxygen $\dot{O}$ and hydrogen H. These radicals can rapidly consume fuel and increase temperature, then results the ignition finally. In general, flames are considered high temperature phenomena; however, combustion related phenomena such as cool flames, the negative temperature coefficient (NTC) behaviour, and autoignition/knock are low and intermediate temperature phenomena [146].

4.4 Chemical Kinetics Model of Combustion

As has been stated in early sections, a chemical kinetics model that is capable of simulating fuel oxidation is a very useful tool to predict the characteristics of autoignition at SI or HCCI engine operation, e.g. autoignition timing, the heat release, the reaction intermediate, and the final products of combustion. There are five categories of chemical kinetics models: detailed, lumped, reduced, skeletal and global, and these have the general characteristics shown in Table 4-2.

Table 4-2: Categorization of chemical kinetics models [6].

Category	Description	Species	Reactions
Detailed	The latest 'comprehensive' reaction set	100's	1000's
Lumped	Uses a lumped description for larger species	100's	1000's
Reduced	A subset of the detailed model	10's	10's-100's
Skeletal	Employs class chemistry and lumping concepts	10's	10's
Global	Utilizes global reactions to minimize reaction set	<10	<10

4.4.1 Detailed Chemical kinetics models

In 1984, Westbrook and Dryer [34] introduced a detailed chemical kinetic mechanism for oxidation and pyrolysis of propane and propene. This model was later extended to lower temperatures and to much more complex fuels by Pitz et al [166]. Since then, there have been efforts from Curran et al [159,167-170] to develop detailed models for butane, pentane, up to n-heptane and iso-octane. Detailed models try to include all of the important elementary reactions and individual species using the best available rate parameters and thermochemical data. However, there are uncertainties in the selection of reactions and rate parameters, and detailed models are often developed for a single hydrocarbon and only validated over a rather limited range of conditions. Detailed models of hydrocarbon fuel oxidation, consisting of hundreds of chemical species and thousands of reactions, for an engine simulation require tremendous computational resources if coupled with engine CFD models. Several modeling studies simulating HCCI conditions using detailed chemical

mechanisms have been reported [53,130,146].

4.4.2 Lumped Chemical Kinetics Model

The other four model types are all driven by the desire to minimize the model size. Lumped models [151,171] use a simplified description of the primary propagation reactions and primary intermediates for large species and then treat the reactions of smaller species with a detailed elementary kinetic scheme, so that the model involves fewer intermediate species than a full detailed model.

4.4.3 Reduced Chemical Kinetics Model

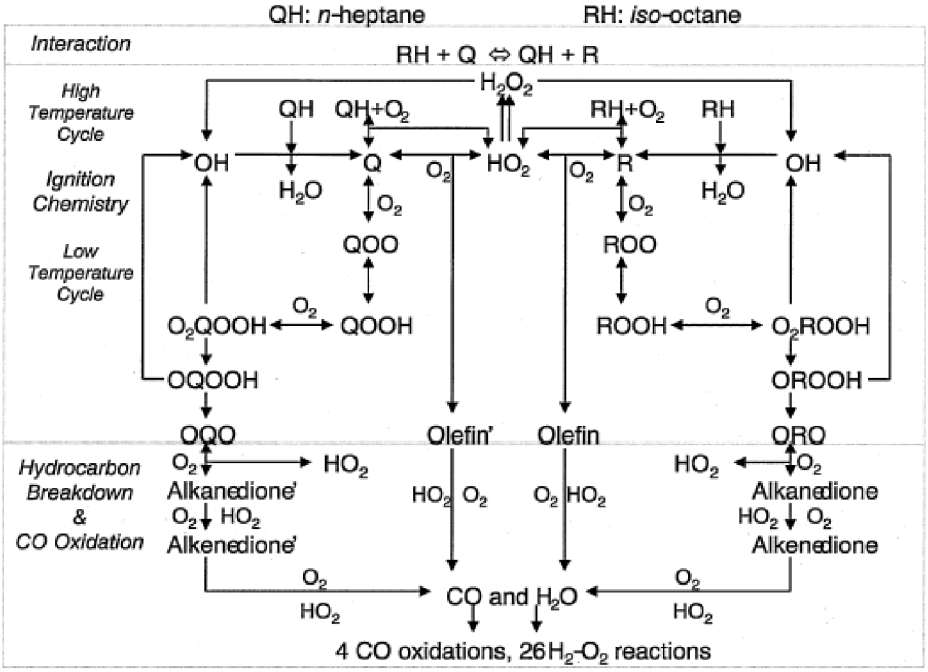

Figure 4-8: Reduced chemistry for oxidation of n-heptane and iso-octane mixtures [154].

A reduced model contains only the most critical elements of the full mechanism. A number of researchers, such as Frenklach and Wang [172], and Tanaka et al. [154] have developed different methods to reduce detailed reaction mechanisms in a systematical manner. In Shigeyuki's model, which oxidation mechanism is shown in Figure 4-8, 32 species and 55 reactions are used and the effect of wall heat transfer on the temperature of the adiabatic core gas is taken into account by adding the displacement volume of the laminar boundary layer to the cylinder volume. A simple interaction between n-heptane and iso-octane was also included. The results showed the well-known two-stage ignition characteristics of heavy hydrocarbons, which

involve low and high temperature cycles followed by a branched chain explosion. However, this may still be too large for detailed CFD calculations.

4.4.4 Skeletal Chemical Kinetics Model

The structure of a skeletal kinetic model is also based on the theories of degenerate-branched reaction chains illustrated by Figure 4-9. The kinetic steps can be elementary, generic, or global reactions. Rate parameters and thermochemistry are based on the best information but represent "classes" of reactions.

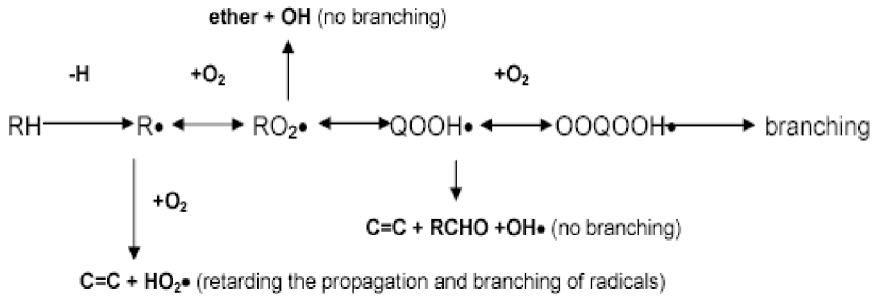

Figure 4-9: Structure of degenerate chain branching mechanism of a skeletal model.

In the 1970s, one of the earliest skeletal kinetic models, based on degenerate-branched-chain and class chemistry concepts, was developed at the Shell Thornton Research Center by Halstead et al [173,174]. This model consisted of 8 generalized reactions and 5 species (fuel, oxygen, total radical population, a branching agent B, and an intermediate species Q which forms B), where the primary interest is the ignition delay and the phenomenological complexity of hydrocarbon oxidation, such as cool flames, two stage ignition and NTC behavior were considered to be of secondary importance. A mathematical model of 6 coupled differential equations was developed and rate parameters were fitted for several fuels including primary reference fuel blends (iso-octane, PRF 90 and PRF 70) using ignition delay data obtained from a rapid compression machine. The rate of heat release was calculated assuming each CH_2 group is oxidized to form CO, CO2, and H_2O, which were not consistent with the oxidation products of CO, oxygenates and hydrocarbons in the first stage ignition. This work formed the basis for later developments and the model is widely used in engine applications.

Halstead et al [173,174] first developed the class chemistry concepts for prediction of autoignition delay time in a rapid compression machine, whose work formed the

basis for later development. Griffiths [175] has made a comprehensive review of skeletal kinetic models and their applications. A brief description of the models is given below.

Based on the existed knowledge of the alkane oxidation, Cox and Cole [160] formed a skeletal chemical kinetics model, which consists of 15 reactions and 10 active species and the rate of heat release was calculated in the same way as in the Shell model. The model was tested against the ignition data using iso-octane and PRF 90 in the Thornton rapid compression machine. The advantages of this model are a better representation of the chemical reactions and the reasonable rate parameters compatible with the existing kinetic information on the type of elementary processes involved. Hu and Keck [176] further developed a skeletal chemical kinetics model of 18 reactions and 13 active species. Keeping a better representation of the chemical reactions similar to Cox and Cole model, Hu and Keck treated exothermicity as enthalpy change in each of the elementary reactions. The rate parameters were calibrated using measured explosion limits in a combustion bomb. The fuels studied were C4-C8 straight chain paraffin and iso-octane. The effects of fuel structure are reflected in the rate parameter of the RO_2 isomerization reaction. The model was applied to predict selected data of ignition delay measured in the Thornton rapid compression machine.

The early work on skeletal chemical kinetics models showed that a relatively small number of rate limiting reactions can simulate two stage ignition processes and that models can generally reproduce the ignition delay for a specific hydrocarbon of interest based on simple adjustments of a fuel specific equilibrium constant. However, significant physical features such as pre-ignition fuel consumption, cumulative heat release, and key species concentrations were not modeled very well. To resolve these issues, an extended skeletal kinetic model, consisting of 13 active species and 29 reactions as shown in Figure , was developed by Li et al. [177,178] for application to PRF 87 (87% iso-octane and 13% n-heptane) and PRF 63 at selected engine conditions. In this model, oxidation of small species was considered and a formation path for CO was provided. The model was tested and validated in predicting the ignition delay and the pre-ignition heat release for these fuels within accuracy of up to 15%.

Zheng et al [127,179] further developed and extended Li's model to incorporate low, intermediate, and high temperature chemistry and successfully applied the model to

predict the pre-ignition behavior, ignition time, and combustion rate in HCCI engines. The results proved that skeletal models could be a useful tool to study HCCI engine operation. Nonetheless, if the kinetic model is to be combined with a CFD code, even simpler models are desirable to maintain acceptable computation times.

A. 20 Active Species

1. RH	2. O2	3. R•	4. RO2•	5. QOOH•
6. OOQOOH•	7. OQO•	8. OH•	9. HO2•	10. HOOH
11. OQ'OOH•	12. RCHO	13. C=C	14. RCO•	15. Rs•
16. RsO2•	17. RsOOH	18. RsO•	19. RO•	20. ROOH

B. 29 Reactions (units: mole, s, kcal)

Arrhenius parameters of rate constants $k=Ae^{-E/RT}$

		Equilibrium		k^+		k^-	
Reaction	$\Delta H°_{300}$	Log A	E	log A^+	E^+	log A^-	E^-
1. RH+O2 ⇔ R•+HO2•	46.4	1.5	46.0	13.5	46.0	12.0	0.0
2. R•+O2 ⇔ RO2•	–30.1	-1.4	-27.4	12.0	0.0	13.4	27.4
3. RO2• ⇔ QOOH•							
n-heptane	7.50	0.9	8.0	11.9	19.0	11.0	11.0
iso-octane	7.50	0.0	11.24	11.0	22.4	11.0	11.0
4. QOOH•+O2 <=> QOOHOO•	-30.1	-1.9	-27.4	11.5	0.0	13.4	27.4
5. OOQOOH• => OQ'OOH•+ OH•	–26.6			11.3	17.0		
6. OH•+RH => H2O+R•	-23.5			13.3	3.0		
7. OQ'OOH• => OQ'O•+OH•	43.6			15.6	40.0		
8. HO2•+HO2• => HOOH+O2	-38.5			12.3	0.0		
9. HOOH+M => 2OH•+M	51.4			16.88	46.0		
10. OQ'O• => 2RCHO+RCO•							
n-heptane	–17.5			14.0	15.0		
OQ'O• => 2RCHO+Rs•							
iso-octane	18.5			14.0	15.0		
11. QOOH• => C=C+RCHO+OH•	-3.0			14.4	31.0		
12. RO2•+RCHO => ROOH+RCO•	-0.6			11.45	8.6		
13. HO2•+RCHO => HOOH+RCO•	-0.6			11.7	8.64		
14. C=C+HO2• =>Epox+OH•	–0.23			10.95	10.0		
15. HO2•+RH ⇔ R•+HOOH	8.0	0.9	8.0	11.7	16.0	10.8	8.0
16. RO2•+RH ⇔ ROOH+R•	8.0	1.1	8.0	11.2	16.0	10.1	8.0
17. RCHO+OH• => RCO•+H2O							
n-heptane	-31.5			13.22	0.0		
iso-octane	-31.5			13.57	0.0		
18. RCO•+M => Rs•+CO+M	10.7			16.78	15.0		
19. Rs•+O2 ⇔ RsO2•	-31.0	-1.4	-27.4	12.0	0.0	13.4	27.4
20. RsO2• => C=C+OH•	17.5			11.75	28.9		
21. RCHO+RsO2• =>RsOOH+RCO•	-0.6			11.53	8.6		
22. RH+RsO2• ⇔ RsOOH+R•	8.0	1.18	8.0	11.28	16.0	10.1	8.0
23. RsOOH => RsO•+OH•	43.6			15.6	43.0		
24. RsO•+O2 => Rs'O+HO2•	-26.5			10.6	2.14		
25. C=C+OH• => 2OXY+OH•	–75.5			12.72	-1.04		
26. ROOH = RO•+OH•	43.6			15.6	43.0		
27. RO• => Rs•+RCHO	-10.0			13.3	15.0		
28. RO2• => C=C+HO2•	4.0			9.85	23.0		
29. RO2• => ether+OH•							
n-heptane	-25.0			9.48	18.0		
iso-octane	-25.0			8.78	18.0		

Figure 4-10: The skeletal chemical kinetics model of Li et al [178].

4.4.5 Global Chemical Kinetics Model

Global models describe the chemistry in terms of a few of the principal reactants and products in one or more overall functional relations [6]. The incentive to develop a global model is to minimize the number of species and reactions so that it can be applied in the combustion models e.g. multi-zone or CFD modeling that require enormous computation resource. The structure of a global model also follows the chain branching theory for hydrocarbon combustion. In general, the high temperature chemistry in a global model is described by one or two reaction steps and the other reaction steps are used to represent the low and intermediate temperature chemistry [26,180]. However, all these models can only be able to predict the preignition behavior, e.g. Ignition delay, but lack the ability in simulating the post-ignition behaviors and predicting combustion products. To enhance the use of global model, Zheng et al proposed a 7-step as listed in Table 4-3, to simulate the whole combustion processes in HCCI engine, and validated the model by reproducing the observed experimental behavior of real fuels.

Table 4-3: A proposed global kinetics model combining a low temperature sub-mechanism with a high temperature sub-mechanism [6].

Reaction	$Log_{10}A^+$	E^+	$Log_{10}A^-$	E^-
1. $F + 7.5O_2 \Rightarrow 8H_2O + 7CO$	12.36	39.70		
2. $CO + 0.5O_2 \Rightarrow CO_2$	14.0	40.00	7.08	40.00
3. $F + 2O_2 \Rightarrow I_1$	20.17	37.62	31.64	88.11
4. $I_1 \Rightarrow 2Y$	6.38	3.96		
5. $Y + 0.5F + 6.5O_2 \Rightarrow 8H_2O + 7CO$	18.00	32.67		
6. $I_1 \Rightarrow I_2$	10.45	13.86		
7. $I_2 \Rightarrow 2Y$	19.18	53.46		

4.4.6 Summary

Chemical kinetics models can be categorized according to the numbers of reactions and species enclosed in the model into detailed, lumped, reduced, skeletal and global. Detailed models detail a great number of identified important elementary reactions and individual species using the best available rate parameters and thermochemical data. The other four model types are all driven by the desire to minimize the model size. A lumped model simplifies parts of the chemistry paths to

exclude some unimportant intermediate species and reactions from the detailed model. A reduced model contains the most critical elements of the full mechanism and has a smaller size compared with lumped models. A skeletal model consists of a sequence of composite kinetic steps representing the chemistry path. A global model describes the chemistry in terms of a few of the principal reactants and products in one or more overall functional relations.

Selection of a chemical kinetics model should be a compromise of model sizes, model accuracy and model availability. For sample, in the application of CFD code, the size of the kinetic model has to be minimized in the consideration of computation cost; however, the model reduction sometimes is accommodated with degradation of model accuracy. Moreover, the chemical kinetics model have not been widely developed for all varieties of fuels, so availability check of the fuel of interest should always be conducted before modelling.

Chapter Five: **Modelling of Multi-zone Chemical Kinetics**

5.1 Introduction

Mathematical modelling of the systems involving chemical kinetics needs to integrate a kinetic solver to solve the mass and energy equations of the system. The levels of complexity of modelling processes are determined by the aspects related to the system properties and the computation methods applied. It could be a very simple model in describing the combustion chemistry of a homogeneous gas mixture in a constant volume reactor e.g. perfectly stirred reactor (PSR) or rapid compression machine (RCM), or complicated ones in simulating temperature and composition inhomogeneity of gas mixture in volume varying systems e.g. SI and HCCI engines.

The computation methods applied in modelling a combustion system can be categorized into the multi-dimensional CFD calculation and the zero-dimensional thermodynamic calculation. Both of the approaches can be incorporated with chemical kinetics models to simulate kinetic-controlled combustion events. The precision of the simulation depends on the accuracy of the representation of the chemical kinetics and more reliable numerical results can be obtained with more detailed reaction mechanisms.

5.1.1 CFD Approach

CFD model has been the dominant simulation and optimisation tool used in the modern engine design attributing to it powerful abilities in geometry representations. Thus, a full-scale integration of CFD model with detailed chemical kinetics model,

theoretically, provides unparalleled simulation accuracy and details in presenting combustion behaviour. However, numerical modeling of this scale requires substantial computer resources in CPU speed, large-scale storage, and robust and fast numerical solution algorithm. Although, to date, the speed and power of computer resources have been significant improved, the simulation time for a CFD model with detailed chemical kinetics is still measured in weeks to months, which prevents the routine use of CFD models in the design process.

As a result, although CFD models have many great benefits, its implementation is markedly hampered by the size of chemical reaction mechanisms that can be incorporated with effectively. Typical CFD solutions are to sacrifice chemical accuracy for accuracy in geometry and flow by applying global (single-step) reactions or a set of severely reduced chemical reaction step. However, this approach not only degrades the prediction accuracy but also is still computationally expensive. Another solution, as a contrast, is to reduce the calculation to a one- or two- dimensional CFD application. However, the computational time of this approach with the detailed reaction mechanism is still costly on current computers.

5.1.2 Zero-Dimensional Approach

As alternative to multi-dimensional approaches, a zero-dimensional thermodynamic model coupled with either detailed or reduced kinetic gains many researches interests due to its simplicity and relatively shorter computation time compared with CFD modelling.

For SI engine Combustion, the propagating flame front separates the in-cylinder mixture into two regimes: unburned and burned, in each of which the gas mixture are of different properties and the zone volume varies with the piston motion and mass entrained by flame front is transferred across the flame front from unburned zone to the burned zone. This two-zone model is the most simplified physical presentation of the combustion process in SI engines taking account of the flame propagation, mass transfer and volume change. An extension of the two-zone model could entail blowby, boundary layer, and local temperature and mixture composition inhomogeneity etc, which make it more requisite to apply multi-zone modeling.

Modelling of combustion in HCCI engine needs to take account of the temperature and mixture distribution across the combustion chamber, which is believed caused by heat transfer, boundary layer, crevice and spatial mixing as detailed in **Section 3.5.2**.

Simulation of combustion in HCCI engines necessitates the division of the combustion into multiple zones to represent these realistic circumstances.

In consequence, advantages of the multi-zone models include specifying the temperatures and compositions for each zone, which reflects the inhomogeneous prosperities of the in-cylinder mixture, modelling the volume and mass change caused by the in-cylinder flow dynamics, and as well as taking account of crevices and the thermal boundary layer. When coupled with chemical kinetics modelling of the local reacting gases, multi-zone modelling is capable of describing chemically the combustion process and predicting the autoignition timing and the energy release rate. In addition, emissions e.g. CO and HC can also be modelled with good accuracy. The drawback of multi-zone model is the increase in computational time when detailed chemical kinetics is applied, but compared with CFD approach, the CPU times is more reasonable by time scale of between tens of minutes and a few hours.

This research work consequently puts emphasis on the incorporation of chemical kinetics modelling with zero-dimensional multi-zone modelling of SI and HCCI combustion.

5.2 Mathematical Description of Multi-Zone Modelling

In multi-zone engine modeling, the cylinder volume is split into a series of zones of different thermal and composition properties. Each of zones is treated as homogeneous regions where kinetic chemistry can be applied. The multi-zone engine model handles distribution of temperature and composition, where different zones can have different starting temperatures and compositions. In this way, the inhomogeneity of the gas mixture in the combustion chamber can be simulated through a number of variable volume reactors, e.g. burned and unburned zone in Si engines and boundary layer, inner and outer core zones in HCCI engines. Pressure is assumed spatially uniform throughout the cylinder. The zones interact with each other through compression work e.g. the expansion of hotter zones compresses the colder zones in HCCI engine combustion and expansion of burned zone compresses the unburned zone in SI engine combustion. Zone interaction can also be induced through mass transfer, e.g. mass transfer from high-pressure zones to low-pressure

zones in HCCI combustion and mass entrainment from unburned zone to burned zone by propagating flame front in SI engines. Heat transfer between zones is considered in the type of convection in HCCI engine combustion and convection an radiation in SI engine combustion.

The manner, in which the multi-zone modeling of IC engine combustion is formed, has been discussed above. In general, a multi-zone model treats the cylinder as a combination of independent gas mixture zones. Each zone is treated as a variable volume combustion reactor, filled with homogeneous mixtures that act as a perfect gas, to which conservation of mass and energy are applied. Uniform pressure across the combustion chamber is also assumed.

5.2.1 Governing Equations

By applying law of conservation of mass and energy to each zone, a general zero-dimensional thermodynamic model for each zone is derived.

5.2.1.1 Ideal Gas Law

The gas mixture of each zone is supposed to conform to the ideal gas law,

$$p_i V_i = n_i R T_i \qquad \textbf{5-1}$$

Where

$p =$ pressure;

$n =$ the number of total moles of gas;

$R =$ universal gas constant

$T =$ temperature

$V =$ volume

$i =$ zone index

5.2.2 Conservation of Mass

The total mass inside the cylinder is presented by

$$m = \sum_{i=1}^{N_Z} m_i \qquad \textbf{5-2}$$

where

$m_i =$ mass of i - th zone

$N_Z =$ total number of the zones in the cylinder.

The mass change of the mixture in each open zone is affected by the mass flow entering and leaving the zone. Thus, the mass change rate of a single zone has the form

$$\frac{dm_i}{dt} = \sum_{l_{in}=1}^{N_{in}} \dot{m}_{l_{in},i} - \sum_{l_{out}=1}^{N_{out}} \dot{m}_{l_{out},i} \qquad \textbf{5-3}$$

where

$l_{in,}i =$ index of the flow of mass entering the i - th zone

$l_{out},i =$ index of the flow of mass existing the i - th zone

The total mass change rate in the cylinder is given by

$$\frac{dm}{dt} = \dot{m}_{out} \qquad \textbf{5-4}$$

where

$m_{out} =$ mass exiting the cylinder such as the blowby flow

5.2.3 Conservation of Species

The mass of an individual chemical species inside each zone is determined by the mass flux entering and exiting the zone and the formation and consumption by chemical reactions. Therefore, the mass change rate of a single species inside each zone is represented by

$$\frac{dm_{j,i}}{dt} = \sum_{l_{in}}^{N_{in}} \dot{m}_{j,l_{in},i} - \sum_{l_{out}}^{N_{out}} \dot{m}_{j,l_{out},i} + M_j \cdot V_i \cdot \dot{\omega}_{j,i} \qquad \textbf{5-5}$$

where

j = index of the species in the chemical reaction mechanism

$\dot{\omega}_{j,i} =$ molar production rate of the j - th species in i - th zone by the chemical reactions

$M_j =$ molar mass of the j - th species

V_i = volume of the i - th zone.

The mass fraction of species j in zone i is defined as

$$Y_{j,i} = \frac{m_{j,i}}{m_i} \qquad \textbf{5-6}$$

Substituting Equation (5.6) into Equation (5.5) yields

$$\frac{1}{m_i}\frac{d(Y_{j,i}m_i)}{\partial t} = \sum_{l_{in}}^{N_{in}} \frac{\dot{m}_{l_{in},i}}{m_i} Y_{j,l_{in},i} - \sum_{l_{out}}^{N_{out}} \frac{\dot{m}_{l_{out},i}}{m_i} Y_{j,l_{out},i} + \frac{M_j \cdot V_i \cdot \dot{\omega}_{j,i}}{m_i} \qquad \textbf{5-7}$$

Using the production rule of differentiation on term on LHS gives

$$\frac{dY_{j,i}}{dt} + \frac{1}{m_i}\frac{dm_i}{dt} \cdot Y_{j,i} = \sum_{l_{in}}^{N_{in}} \frac{\dot{m}_{l_{in},i}}{m_i} Y_{j,l_{in},i} - \sum_{l_{out}}^{N_{out}} \frac{\dot{m}_{l_{out},i}}{m_i} Y_{j,l_{out},i} + \frac{M_j \cdot \dot{\omega}_{j,i}}{\rho_i} \qquad \textbf{5-8}$$

where

ρ_i = density of zone i and $\rho_i = m_i / V_i$.

Using Equation (5.3) to replace the mass derivative in the second term on the LHS of Equation (5.8) yields

$$\frac{dY_{j,i}}{dt} + \frac{1}{m_i}\left(\sum_{l_{in}=1}^{N_{in}} \dot{m}_{l_{in},i} + \sum_{l_{out}=1}^{N_{out}} \dot{m}_{l_{out},i}\right) \cdot Y_{j,i} = \sum_{l_{in}}^{N_{in}} \frac{\dot{m}_{l_{in},i}}{m_i} Y_{j,l_{in},i} - \sum_{l_{out}}^{N_{out}} \frac{\dot{m}_{l_{out},i}}{m_i} Y_{j,l_{out},i} + \frac{M_j \cdot \dot{\omega}_{j,i}}{\rho_i} \qquad \textbf{5-9}$$

Noticing that the mixture leaving the zone has the same composition as the residual mixture inside the zone, which is

$$Y_{j,i} = Y_{j,l_{out},i} \quad , \; l_{out} = 1, N_{out} \qquad \textbf{5-10}$$

Thus, substituting Equation (5.10) into Equation (5.9) and eliminating repeated terms on both sides of the equation leads to

$$\frac{dY_{j,i}}{dt} + \frac{1}{m_i}\sum_{l_{in}=1}^{N_{in}} \dot{m}_{l_{in},i} Y_{j,i} = \sum_{l_{in}}^{N_{in}} \frac{\dot{m}_{l_{in},i}}{m_i} Y_{j,l_{in},i} + \frac{M_j \cdot \dot{\omega}_{j,i}}{\rho_i} \qquad \textbf{5-11}$$

Rearrangement of Equation (5.11) gives

$$\frac{dY_{j,i}}{dt} = \sum_{l_{in}}^{N_{in}} \frac{\dot{m}_{l_{in},i}}{m_i}\left(Y_{j,l_{in},i} - Y_{j,i}\right) + \frac{M_j \cdot \dot{\omega}_{j,i}}{\rho_i} \qquad \textbf{5-12}$$

Equation (5.12) indicates the composition of the gas mixture in each zone is decided

by both the chemical reactions and the composition difference between the inflow mixture and the residual mixture.

5.2.4 Conservation of Energy

The first law of the thermodynamics applies to the i - th zone yields

$$\underbrace{\frac{dU_i}{dt}}_{\text{Internal Energy}} = \underbrace{\frac{dQ_{ht,i}}{dt}}_{\text{Heat Transfer}} - \underbrace{p\frac{dV_i}{dt}}_{\text{Work}} + \underbrace{\sum_{l_{in}}^{N_{in}} \dot{m}_{l_{in},i} \cdot h_{l_{in},i}}_{\text{Inflow Energy}} - \underbrace{\sum_{l_{out}}^{N_{out}} \dot{m}_{l_{out},i} \cdot h_{l_{out},i}}_{\text{Outflow Energy}} \quad \textbf{5-13}$$

Where

$V_i =$ instantaneous volume of zone i.

5.2.4.1 Internal Energy

The total internal energy for the mixture of ideal gases is given by

$$\frac{dU_i}{dt} = \frac{d(m_i u_i)}{dt} = m_i \frac{du_i}{dt} + u_i \frac{dm_i}{dt} \quad \textbf{5-14}$$

where

$u_i =$ specific internal energy of the i - th zone

Based on definition of enthalpy, the specific internal energy can be expressed as

$$u_i = h_i - pv_i \quad \textbf{5-15}$$

where

$h =$ is the specific enthalpy

$v_i =$ is the specific volume of the i - th zone , expressed by $v_i = \frac{V_i}{m_i}$

then

$$\begin{aligned} m_i \frac{du_i}{dt} + u_i \frac{dm_i}{dt} &= m_i \cdot \frac{d(h_i - pv_i)}{dt} + (h_i - pv_i)\frac{dm_i}{dt} \\ &= m_i \cdot \frac{dh_i}{dt} - m_i \frac{d(pv_i)}{dt} + h_i \cdot \frac{dm_i}{dt} - pv_i \cdot \frac{dm_i}{dt} \\ &= m_i \cdot \frac{dh_i}{dt} + h_i \cdot \frac{dm_i}{dt} - \frac{d(pV_i)}{dt} \end{aligned} \quad \textbf{5-16}$$

The specific internal energy of the i - th zone is calculated from the gas-mixture species composition

$$h_i = \sum_j^{N_S} Y_{j,i} h_{j,i} \qquad \textbf{5-17}$$

where

$N_S =$ the total number of species in the chemical kinetic reaction mechanism applied.

From Equation 5.17, the change rate of the specific enthalpy is given by

$$\frac{dh_i}{dt} = \frac{d\left(\sum_j^{N_S} Y_{j,i} h_{j,i}\right)}{dt} = \sum_j^{N_S} Y_{j,i} \frac{dh_{j,i}}{dt} + \sum_j^{N_S} h_{j,i} \frac{dY_{j,i}}{dt} \qquad \textbf{5-18}$$

Assuming perfect gas, $dh_{j,i}$ can be written as

$$dh_{j,i} = c_{p,j,i} \cdot dT_i \qquad \textbf{5-19}$$

where

$T_i =$ temperature of the mixture in the i - th zone

$c_{v,j,i} =$ specific heat of the j - th species in the i - th zone evaluated at constant volume.

Substitution of Equations (5.11) and (5.19) into Equation (5.18) gives

$$\frac{dh_i}{dt} = \sum_j^{N_S} Y_{j,i} \cdot c_{p,j,i} \cdot \frac{dT_i}{dt} + \sum_j^{N_S} h_{j,i} \cdot \left(\sum_{l_{in}}^{N_{in}} \frac{\dot{m}_{l_{in},i}}{m_i} \left(Y_{j,l_{in},i} - Y_{j,i} \right) + \frac{M_j \cdot \dot{\omega}_{j,i}}{\rho_i} \right) \qquad \textbf{5-20}$$

Substituting Equation (5.20) into Equation (5.16) and using Equation (5.16) in Equation (5.14) yields

$$\frac{dU_i}{dt} = m_i \cdot \left(\sum_j^{N_S} Y_{j,i} \cdot c_{p,j,i} \cdot \frac{dT_i}{dt} + \sum_j^{N_S} h_{j,i} \cdot \left(\sum_{l_{in}}^{N_{in}} \frac{\dot{m}_{l_{in},i}}{m_i} \left(Y_{j,l_{in},i} - Y_{j,i} \right) + \frac{M_j \cdot \dot{\omega}_{j,i}}{\rho_i} \right) \right) - \frac{d\left(p \cdot V_i\right)}{dt} + h_i \cdot \frac{dm_i}{dt} \qquad \textbf{5-21}$$

Recalling and using Equation (5.3) and (5.17) in Equation (5.21) gives

$$\frac{dU_i}{dt} = m_i \cdot \left(\sum_j^{N_S} Y_{j,i} \cdot c_{p,j,i} \cdot \frac{dT_i}{dt} + \sum_j^{N_S} h_{j,i} \cdot \left(\sum_{l_{in}}^{N_{in}} \frac{\dot{m}_{l_{in},i}}{m_i} \left(Y_{j,l_{in},i} - Y_{j,i} \right) + \frac{M_j \cdot \dot{\omega}_{j,i}}{\rho_i} \right) \right)$$
$$- \frac{d\left(p \cdot V_i\right)}{dt} + \left(\sum_{l_{in}}^{N_{in}} \dot{m}_{l_{in},i} - \sum_{l_{out}}^{N_{out}} \dot{m}_{l_{out},i} \right) \cdot \sum_j^{N_S} Y_{j,i} h_{j,i} \cdot \quad \textbf{5-22}$$

Rearranging Equation (5.22) yields

$$\frac{dU_i}{dt} = m_i \cdot \frac{dT_i}{dt} \cdot \sum_j^{N_S} Y_{j,i} \cdot c_{p,j,i} - \frac{d\left(pV_i\right)}{dt} + \frac{m_i \cdot}{\rho_i} \sum_j^{N_S} h_{j,i} \cdot M_j \cdot \dot{\omega}_{j,i}$$
$$+ \sum_{l_{in}}^{N_{in}} \sum_j^{N_S} \dot{m}_{l_{in},i} \cdot h_{j,i} \cdot Y_{j,l_{in},i} - \sum_{l_{out}}^{N_{out}} \sum_j^{N_S} \dot{m}_{l_{out},i} h_{j,i} \cdot Y_{j,i}$$
$$\underbrace{- \sum_j^{N_S} \sum_{l_{in}}^{N_{in}} h_{j,i} \cdot \dot{m}_{l_{in},i} \cdot Y_{j,i}}_{6\text{th}} + \underbrace{\cdot \sum_j^{N_S} \sum_{l_{in}}^{N_{in}} h_{j,i} \cdot \dot{m}_{l_{in},i} \cdot Y_{j,i}}_{7\text{th}} \quad \textbf{5-23}$$

Cancelling the 6th and 7th terms on the RHS of Equation, one have

$$\frac{dU_i}{dt} = m_i \cdot \frac{dT_i}{dt} \cdot \sum_j^{N_S} Y_{j,i} \cdot c_{p,j,i} - \frac{d\left(pV_i\right)}{dt} + \frac{m_i \cdot}{\rho_i} \sum_j^{N_S} h_{j,i} \cdot M_j \cdot \dot{\omega}_{j,i}$$
$$+ \sum_{l_{in}}^{N_{in}} \sum_j^{N_S} \dot{m}_{l_{in},i} \cdot h_{j,i} \cdot Y_{j,l_{in},i} - \sum_{l_{out}}^{N_{out}} \sum_j^{N_S} \dot{m}_{l_{out},i} h_{j,i} \cdot Y_{j,i} \quad \textbf{5-24}$$

Using Equation (5.17), the last two terms on the RHS of Equation (5.13) can be expressed as

$$\underbrace{\sum_{l_{in}}^{N_{in}} \dot{m}_{l_{in},i} \cdot h_{l_{in},i}}_{\text{Inflow Energy}} - \underbrace{\sum_{l_{out}}^{N_{out}} \dot{m}_{l_{out},i} \cdot h_{l_{out},i}}_{\text{Outflow Energy}}$$
$$= \sum_{l_{in}}^{N_{in}} \sum_j^{N_s} \dot{m}_{l_{in},i} \cdot h_{j,l_{in},i} \cdot Y_{j,l_{in},i} - \sum_{l_{out}}^{N_{out}} \sum_j^{N_s} \dot{m}_{l_{out},i} \cdot h_{j,l_{out},i} \cdot Y_{j,l_{out},i} \quad \textbf{5-25}$$

Substituting Equation (5.24) and (5.25) into Equation (5.13) yields

$$m_i \frac{dT_i}{dt} \cdot \sum_j^{N_S} Y_{j,i} \cdot c_{p,j,i} - \underbrace{p \frac{dV_i}{dt}}_{\text{3th (LHS)}} - V_i \frac{dp}{dt} +$$

$$\frac{m_i}{\rho_i} \cdot \sum_j^{N_S} h_{j,i} \cdot M_j \cdot \dot{\omega}_{j,i} + \sum_{l_{in}}^{N_{in}} \sum_j^{N_S} \dot{m}_{l_{in},i} \cdot h_{j,i} \cdot Y_{j,l_{in},i} - \underbrace{\sum_{l_{out}}^{N_{out}} \sum_j^{N_S} \dot{m}_{l_{out},i} h_{j,i} \cdot Y_{j,i}}_{\text{5th (LHS)}} \quad \textbf{5-26}$$

$$= \frac{dQ_{ht,i}}{dt} - \underbrace{p \frac{dV_i}{dt}}_{\text{2nd (RHS)}} + \sum_{l_{in}}^{N_{in}} \sum_j^{N_S} \dot{m}_{l_{in},i} \cdot h_{j,l_{in},i} \cdot Y_{j,l_{in},i} - \underbrace{\sum_{l_{out}}^{N_{out}} \sum_j^{N_S} \dot{m}_{l_{out},i} \cdot h_{j,l_{out},i} \cdot Y_{j,l_{out},i}}_{\text{4th (RHS)}}$$

Since the mixture exiting the zone has the same composition as the one inside, one can obtain $h_{j,i} = h_{j,l_{in},i}$ and $Y_{j,i} = Y_{j,l_{in},i}$. Therefore, in Equation (5.16), the 5th term on the LHS and the 4th on the RHS of can be cancelled by each other. Eliminating the same terms on both side of the equation (3rd on the LHS and 2nd on the RHS) and rearranging the equation yield

$$m_i \frac{dT_i}{dt} \cdot \sum_j^{N_S} Y_{j,i} \cdot c_{p,j,i} = \frac{dQ_{ht,i}}{dt} + V_i \frac{dp}{dt} + \frac{m_i}{\rho_i} \cdot \sum_j^{N_S} h_{j,i} \cdot M_j \cdot \dot{\omega}_{j,i} + \sum_{l_{in}}^{N_{in}} \dot{m}_{l_{in},i} \sum_j^{N_s} Y_{j,l_{in},i} \cdot \left(h_{j,l_{in},i} - h_{j,i} \right) \quad \textbf{5-27}$$

The definition of mixture-average specific heat in mass unites gives

$$\bar{c}_p = \sum_j^{N_S} Y_{j,i} \cdot c_{p\,j,i} \quad \textbf{5-28}$$

and let $H_{j,i} = h_{j,i} \cdot M_j$, from which it follows

$$m_i \bar{c}_p \frac{dT_i}{dt} \cdot = \underbrace{\frac{dQ_{ht,i}}{dt}}_{\text{heat transfer}} + \underbrace{V_i \frac{dp}{dt}}_{\text{work}} + \underbrace{\frac{m_i}{\rho_i} \cdot \sum_j^{N_S} \dot{\omega}_{j,i} H_{j,i}}_{\text{chemical heat release}} + \underbrace{\sum_{l_{in}}^{N_{in}} \dot{m}_{l_{in},i} \sum_j^{N_S} Y_{j,l_{in},i} \cdot \left(h_{j,l_{in},i} - h_{j,i} \right)}_{\text{enthalpy difference}} \quad \textbf{5-29}$$

Equation (5.28) presents that the temperature change of each zone originated from heat transfer between the considered zone and surroundings, work done on the zone, heat released by chemical reactions and the enthalpy difference between the inflow of mixture and the resident mixture.

5.2.4.2 Pressure

By the assumption that pressure is uniform throughout the combustion chamber, one gets

$$p = p_1 = p_2 ... = p_i \qquad \textbf{5-30}$$

Then the pressure and its change rate are derived from the ideal gas equation as follows:

Rearranging Equation (5.1) yields

$$V_i = \frac{n_i R T_i}{p} \qquad \textbf{5-31}$$

The relationship between V_{cyl} and V_i follows that

$$V_{cyl} = \sum_{i}^{N_Z} V_i \qquad \textbf{5-32}$$

Substituting Equation (5.31) into (5.32) and rearranging the resulting equation yield

$$p = \frac{R \cdot \sum_{\mathrm{i}}^{NZ} T_i \cdot n_i}{V_{cly}} \qquad \textbf{5-33}$$

From Equation (5.33), one obtains the derivative of pressure

$$\begin{aligned} \frac{dp}{dt} &= R \frac{d\left[\sum_{\mathrm{i}}^{NZ} T_i \cdot n_i\right] \cdot V_{cly} - \left[\sum_{\mathrm{i}}^{NZ} T_i \cdot n_i\right] \cdot dV_{cly}}{V_{cyl}^2} \\ &= R \frac{\left[\sum_{\mathrm{i}}^{NZ} dT_i \cdot n_i + \sum_{\mathrm{i}}^{NZ} T_i \cdot dn_i\right] \cdot V_{cly} - \left[\sum_{\mathrm{i}}^{NZ} T_i \cdot n_i\right] \cdot dV_{cly}}{V_{cyl}^2} \\ &= \frac{R \cdot \sum_{\mathrm{i}}^{NZ} n_i \cdot dT_i}{V_{cly}} + \frac{R \cdot \sum_{\mathrm{i}}^{NZ} T_i \cdot dn_i}{V_{cly}} - \frac{p \cdot dV_{cly}}{V_{cly}} \end{aligned} \qquad \textbf{5-34}$$

The total number of moles of the zone mixture n_i is given by

$$n_i = \sum_{j}^{N_S} \frac{m_i \cdot Y_{j,i}}{M_j} \qquad \textbf{5-35}$$

The derivative of n_i required in Equation (5.35) is

$$\frac{dn_i}{d} = m_i \cdot \sum_j^{N_S} \frac{dY_{j,i}}{M_j} + dm_i \cdot \sum_j^{N_S} \frac{Y_{j,i}}{M_j} \qquad \textbf{5-36}$$

5.2.4.3 Volume

The cylinder volume and volume derivative, V_{cyl} and dV_{cyl}, are derived from the modelling of the engine geometrical properties [1].

5.2.4.4 Heat Transfer

Heat transfer between the in-cylinder gas mixture and the engine components attribute two major sources: convection throughout the engine operating cycle and radiation during combustion.

5.2.4.4.1 Convective heat loss

The heat transfer by convection Q_{ht_C} from the gas mixture to the cylinder components at temperature T_w is determined from the relation

$$Q_{ht\_C} = h_C \cdot A_C \cdot (T - T_w) \qquad \textbf{5-37}$$

where

$h_C =$ heat transfer coefficient

$A_C =$ heat transfer area

The heat transfer coefficient h_c is obtained from the Woschni's heat transfer correlation [129]. Woschni assumed the correlation of the form

$$N_u = 0.035 R_e^{0.8} \qquad \textbf{5-38}$$

where

$N_u =$ Nusselt number

$R_e =$ Reynolds number

The above two numbers are defined according to

$$N_u \equiv \frac{h_C D}{\lambda}$$

$$R_e \equiv \frac{D\rho}{\mu} \cdot \overline{U}_g \qquad \textbf{5-39}$$

where

$D =$ character length

$\lambda =$ gas conductivity

$\mu =$ gas viscosity

$\overline{U}_g =$ average gas velocity in the cylinder

In the case of a four-stroke IC engine, the cylinder bore B is taken as the characteristic length and the gas conductivity and gas and viscosity are assigned functional relationship with temperature T as $\lambda \propto T^{0.75}$ and $\mu \propto T^{0.62}$. The average gas speed $\overline{U}_g$ for use in evaluating the Reynolds number is determined by

$$\begin{aligned} &\text{For the gas exchange and compression period}: \overline{U}_g = 6.18 \cdot \overline{S}_p + 0.417 \cdot v_s \\ &\text{For the combustion and expansion period}: \overline{U}_g = 2.28 \cdot \overline{S}_p + 0.308 \cdot v_s + 0.00324 \frac{T_o V}{V_o} \frac{\Delta P_c}{P_o} \end{aligned} \qquad \textbf{5-40}$$

where

$\overline{S}_p =$ mean piston speed

$T_o =$ temperature at intake valve closing

$V_o =$ cylinder volume at intake valve closing

$\Delta P_c =$ instantaneous pressure rise due to combustion

$P_o =$ pressure at intake valve closing

$v_s = B\omega_P / 2$ and ω_P is the rotation speed of the paddle wheel used to measure the swirl velocity [1].

The pressure rise Δp_c due to combustion is the cylinder pressure in the firing engine minus the cylinder pressure in the motored engine at the same crank angle. The latter is estimated by use of the isentropic relation

$$PV^{\gamma} = P_o V_o^{\gamma} = \text{constan} \qquad \textbf{5-41}$$

Substituting Equation (5.39) into (5.38) and introducing $\rho = \frac{p}{RT}$ leads to

$$h_C = C_{wch} \cdot B^{-0.2} \cdot p^{-0.8} \cdot \overline{U}_g^{0.8} \cdot T^{-0.53} \qquad \textbf{5-42}$$

where

C_{wsh} = heat transfer rate constant

The exponential parameters in Woschni's correlation were determined by matching experimental results obtained using a particular diesel engine. When applied to any other engine with different combustion scenario, the constants should be adjusted to better suit the engine.

5.2.4.4.2 Radiation heat transfer

The heat transfer by radiation is predicted using the formula proposed by Annand [181], which is proportional to the fourth power of the absolute material temperature and is of the form

$$\dot{Q}_{ht\_R} = A_R \beta \sigma \left(T^4 - T_w^4 \right) \qquad \textbf{5-43}$$

where

A_R = Boundary surface area

σ = Stefan-Boltzmann constant equal to $5.67 \times 10^8 W / m^2 K^4$

β = Radiation heat transfer coefficient between 0.6 and 1.6 suggested by Heywood [1]

5.2.5 Summary

Examination of all the terms of Equation (5.12) and (5.13) just discussed reveals the following derivatives in those equations formulated for each single zone.

$$\frac{dY_{j,i}}{dt} \ , \ \frac{dT_i}{dt} \ , \ \dot{m}_i \ , \ \dot{m}_{l_{in},i} \ , \ \dot{\omega}_{j,i} \qquad \textbf{5-44}$$

And the following variables

$$\begin{gathered} T_i \ , \ Y_{j,i} \ , \ Y_{j.l_{in},i} \\ c_{p\,j,i} \ , \ h_{j,i} \ , \ h_{j,l_{in},i} \ , \ m \ , \ m_i \ , \ \rho_i \\ A_C \ , \ A_R \ , \ V_{cyl} \ , \ V_i \end{gathered} \qquad \textbf{5-45}$$

Where $i = 1, N_Z$, $j = 1, N_S$, $l_{in} = 1,\ N_{in}$

The thermodynamic variables $c_{p\,j,i}, h_{j,i}$ and $h_{j,l_{in},i}$ are calculated based on the assumption that the gas mixture in each zone has 'perfect' standard-state thermodynamic properties, by which these variables are functions of T_i . More details of the calculation are introduced in the next section.

The mass change rate of each zone is differently dealt with according to the engine type. For a SI engine, the mass transferred between zones can be known from an empirical burning law (Weibe Function) and for a HCCI engine, it is calculated by a mass mixing model in assumption of uniform pressure across the combustion chamber. All in all

The cylinder volume V_{cyl} is a known function of crank angle [1]. The zone volumes V_i and heat transfer related areas A_C and A_R are obtained from user-specified functions according to the engine type and operating characteristics, a discussion of which is deferred to **Chapter 7** and **Chapter 8**

The mass fraction and energy equations (5.12) and (5.29) are thus seen to be a relationship among the derivatives, $\frac{dY_{j,i}}{dt}$ and $\frac{dT_i}{dt}$, their integrals, $Y_{j,i}$ and T_i , and parameters A_i and B_i , dependent upon the integrals, which can be expressed as

$$\underbrace{\begin{pmatrix} \frac{dT_i}{dt} \\ \frac{dY_{1,i}}{dt} \\ \frac{dY_{2,i}}{dt} \\ \vdots \\ \frac{dY_{N_S,i}}{dt} \end{pmatrix}}_{(N_S+1)\times 1} = A_i \times \underbrace{\begin{pmatrix} T_i \\ Y_{1,i} \\ Y_{2,i} \\ \vdots \\ Y_{N_S,i} \end{pmatrix}}_{(N_S+1)\times 1} + B_i \qquad \textbf{5-46}$$

where the notes under the variable matrices indicates the matrix dimension. The A_i is the coefficient matrix and B_i is the parameter matrix, and they are expressed as

$$A_i = \begin{pmatrix} A_{1,1,i} & A_{1,2,i} & \cdots & A_{1,N_S+1,i} \\ A_{2,1,i} & A_{2.2,i} & \cdots & A_{2,N_S+1,i} \\ \vdots & \cdots & \cdots & \vdots \\ A_{N_S+1,1,i} & A_{N_S+1,2,i} & \cdots & A_{N_s+1,N_S+1,i} \end{pmatrix} \quad \text{and} \quad B = \begin{pmatrix} B_{1,i} \\ B_{2,i} \\ \vdots \\ B_{N_S+1,i} \end{pmatrix}$$

When Equation (5.46) is extended for a system with N_Z zones, the matrix expression of the governing equations is

$$\underbrace{\begin{pmatrix} \dot{Z}_1 \\ \dot{Z}_2 \\ \vdots \\ \dot{Z}_{N_Z} \end{pmatrix}}_{[N_Z\times(N_S+1)]\times 1} = A \times \underbrace{\begin{pmatrix} Z_1 \\ Z_2 \\ \vdots \\ Z_{N_Z} \end{pmatrix}}_{[N_Z\times(N_S+1)]\times 1} + B \qquad \textbf{5-47}$$

where

$$\underbrace{Z_i = \begin{pmatrix} T_i \\ Y_{1,i} \\ \vdots \\ Y_{N_S,i} \end{pmatrix}}_{(N_S+1)\times 1}, \quad \underbrace{A = \begin{pmatrix} A_1 \\ A_2 \\ \vdots \\ A_{N_Z} \end{pmatrix}}_{(N_Z\times(N_S+1))\times 1} \text{ and } \quad \underbrace{B = \begin{pmatrix} B_1 \\ B_2 \\ \vdots \\ B_{N_Z} \end{pmatrix}}_{(N_Z\times(N_S+1))\times 1}$$

5.3 Numerical Methods and Computation of Chemical kinetics

5.3.1 Introduction

In the previous chapter, a set of differential equations are summarized to express a multi-zone combustion system based on the conservation equations for mass and energy. This set of equations is treated as a time dependent initial value problem.

Equation 5-47 can also be expressed in a standard form as:

$$\mathrm{f}\left(\mathrm{t}, \frac{\mathrm{dy_{j,i}}}{\mathrm{dt}}, \frac{\mathrm{dT_i}}{\mathrm{dt}}, \mathrm{y_{j,i}}, \mathrm{T_i}\right) = 0 \qquad y(t_n) = y_n \qquad \textbf{5-48}$$

Where y is the vector of the system's unknowns, i.e. mass fraction and temperature and f is the vector containing the system's set of conservation equations, which are functions of the unknowns y and of time t. The following equation states an initial condition at a certain time t_n, in which n is the temporal discretization index.

The mathematical model of a combustion system with chemical kinetics is highly non-linear due to its Arrhenius expression exponential dependence and it is stiff. In a chemical kinetics model, reaction rates can differ by orders of magnitude from one reaction to another. The same is true for species concentrations, going from orders of 10^{-2} for fuel and oxidants, to 10^{-10} or 10^{-15} for many radicals. For such a system, even if the solution is slowly changing, very small calculation time steps are required just to maintain stability.

To computationally solve this kind of differential equations, several production-level soft ware is readily available, these software packages implement variable-order, variable-time step algorithms that compute efficiently and deliver high-accuracy solutions some of the widely used and well documented package are LSODE,VODE and DASSL.

5.3.2 Stiffness in Solution of ODEs of chemical kinetics

Chemical kinetics, especially for systems like combustion, is characterized by enormous disparities in the characteristic time scales for the response of different species. For some reactions, the rate constant k can be very large, resulting potentially in very rapid transient change in the concentrations of some species. On the contrary, the other species may be involved in some reactions that have relative low rates. In a flame, for example, the characteristic time scales for free-radical species (e.g., H atoms) are extremely short, while the characteristic time scales for other species (e.g., NO) are quite long. This huge time-scale disparity leads to a numerical property called stiffness [182].

Thus, stiffness occurs in problems where there are two or more very different scales of the independent variable, on which the dependent variables are changing. For example, consider the following set of equations derived from a chemical kinetic mechanism [183]:

$$u' = 998u + 1998v \qquad \textbf{5-49}$$

$$v' = -999u - 1999v \qquad \textbf{5-50}$$

With boundary conditions

$$u(0) = 1, v(0) = 0$$

The solutions are found as

$$u = 2e^{-x} - e^{-1000\,x}$$

$$v = -e^{-x} + e^{-1000\,x}$$

To integrate the system with a numerical method, the presence of the e^{-1000x} term would require a step size $h << 1/1000$for the method to be stable. This is so even though the e^{-1000x} term is completely negligible in determining the values of u and v as soon as one is away from the origin illustrated in Figure 5-1. This is the generic disease of stiff equations: the requirement of following the variation in the solution on the shortest length scale to maintain stability of the integration, even though accuracy requirements allow a much larger step size.

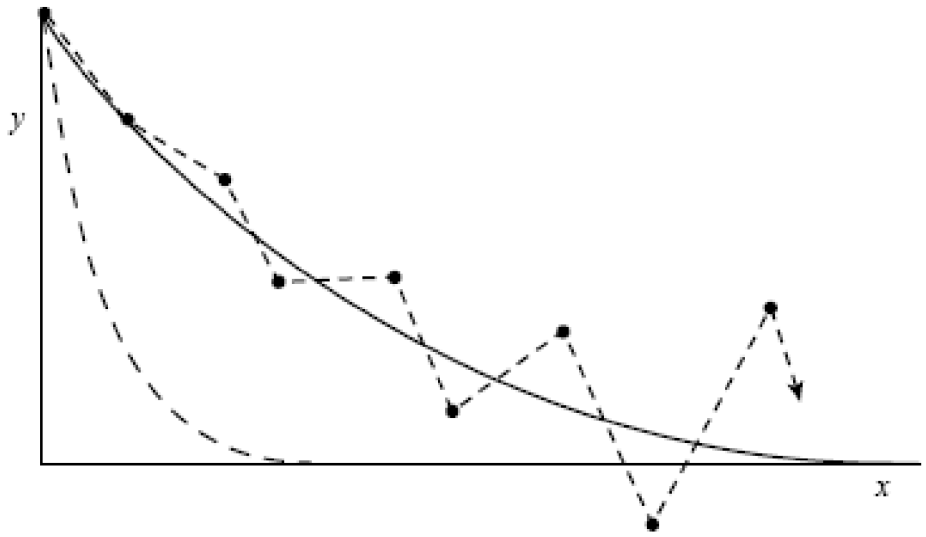

Figure 5-1: Example of instability encountered in integrating a stiff equation (schematic). Here it is supposed that the equation has two solutions, shown as solid and dashed lines. Although the initial conditions are such as to give the solid solution, the stability of the integration (shown as the unstable dotted sequence of segments) is determined by the more rapidly varying dashed solution, even after that solution has effectively died away to zero. Implicit integration methods are the cure [183].

5.3.3 Solution Methods

For stiff problem, one of the most popular currently used methods is Backward Differentiation Formula (BDF). The BDF method possesses the property of stiff stability and therefore does not suffer from the step size constraint once the rapid components have decayed to negligible levels. Throughout the integration, the step size is limited only by accuracy requirements imposed on the numerical solution.

(FYI: accuracy of a numerical method refers to the magnitude of the error introduced in a single step or, more precisely, the local truncation or discretization error.)

When a first-order ordinary differential equation is expressed as:

$$\frac{dy}{dt} = -\lambda y + g(t) \qquad \textbf{5-51}$$

Where the 'prime' indicates a time derivative, λ is a constant, and $g(t)$ is some function of time

An example of BDF method can be stated as follows:

$$\frac{y_{n+1} - y_n}{h_n} \approx y'_{n+1} = -\lambda y_{n+1} + g(t_{n+1}) \qquad \textbf{5-52}$$

where the time step is $h_n = t_{n-1} - t_n$ and the right-hand side function is evaluated at the advanced time level t_{n+1} and indicates the time level.

Then

$$y_{n+1} = h_n y'_{n+1} + y_n = h_n\left[-\lambda y_{n+1} + g(t_{n+1})\right] + y_n \qquad \textbf{5-53}$$

The nomenclature $y(t_{n+1})$ is used to mean the exact analytic solution evaluated at some time t_{n+1} and y_{n+1} to represent the numerical solution at t_{n+1}. It is clear that the true analytic solution must satisfy the differential equation 5-51 everywhere.

$$y'(t_n) = -\lambda y(t_n) + g(t_n) \qquad \textbf{5-54}$$

By adding the backward approximation to each side of this equation, both the backward algorithm and an expression for the local truncation error can be identified.

$$y'(t_{n+1}) + \frac{y(t_{n+1}) - y(t_n)}{h_n} = -\lambda y(t_{n+1}) + g(t_{n+1}) + \frac{y(t_{n+1}) - y(t_n)}{h_n} \qquad \textbf{5-55}$$

An algebraic rearrangement yields:

$$\begin{aligned} y(t_{n+1}) = y(t_n) + h_n\left[-\lambda y(t_{n+1}) + g(t_{n+1})\right] \\ + y(t_{n+1}) - y(t_n) - h_n y'(t_{n+1}) \end{aligned} \qquad \textbf{5-56}$$

The first three terms represent the backward algorithm and the remaining term

represents the local truncation error. A Taylor series expansion about t_{n+1} (in the negative t direction) yields an expression for $y(t_n)$

$$y(t_n) = y(t_{n+1}) - h_n y'(t_{n+1}) + \frac{h_n^2}{2} y''(t_{n+1}) + O(h_n^3) \qquad \textbf{5-57}$$

It can be seen that the local truncation error for the interval $\boldsymbol{h_n = t_{n+1} - t_n}$ is

$$d_n \equiv \frac{h_n^2}{2} y''(t_{n+1}) + O(h_n^3) = -\left[y(t_{n+1}) - y(t_n) - h_n y'(t_{n+1})\right] \qquad \textbf{5-58}$$

The global error is defined as $e_n = y_n - y(t_n)$. A recursion relationship for the global error can be found by using equations 5-53 and 5-56

$$e_{n+1}(1 + h_n\lambda) = e_n + d_n \qquad \textbf{5-59}$$

For the method to be stable, the error e_{n+1} must be less than e_n, which leads to the stability criterion as

$$\left|\frac{1}{1 + h_n\lambda}\right| < 1 \qquad \textbf{5-60}$$

It is obvious from this expression that the method is unconditionally stable for all λ and all time steps h_n (for linear problem). A consequence of the strong stability is that the time step can be chosen primarily to maintain accuracy. In slowly varying regions of stiff problems, the time steps can be very large compared those required to maintain stability for an explicit algorithm.

5.3.4 Numerical Code Packages

Various computer programs have been developed to solve the chemical kinetics model that consists of a set of stiff ordinary differential equations as described in the previous section. The first algorithm that is capable of handling stiff ODE systems was proposed by William Gear in the 1970's [184]. The state-of-the-art numerical codes that are now available and well regarded for solving large stiff ODE systems are VODE, LSODE, and DASAC.

5.3.4.1 Livermore Solver for Ordinary Differential Equations (LSODE)

For stiff problems, the LSODE (Livermore Solver for Ordinary Differential Equations)

package uses the Backward Differentiation Formula (BDF) method. To satisfy accuracy requirements, the BDF method may have to use small step sizes of order $1/\max(\lambda)$ in regions where the most rapid exponentials are active. However, for the regions, which have relative small change rates of the solutions, larger step sizes may be used. The LSODE package also includes the implicit Adams method, which is well suited for non-stiff problems. Both integration methods belong to the family of linear multi-step methods. As implemented in LSODE these methods allow both the step size and the method order to vary (between the Adams method and the BDF method) throughout the problem. The capability of dynamically varying the step size and the method order is very important to the efficient use of linear multi-step methods. The LSODE package consists of 21 subprograms and a BLOCK DATA module. The package has been integrated into a single FORTRAN 77 code, and in normal circumstances, the user needs to communicate with the code by calling only a single subroutine, also named LSODE for convenience, into the user-supplied program. Communication between different subroutines in the package is accomplished by means of both call sequences and the two common blocks.

5.3.4.2 Variable-coefficient Ordinary Differential Equation solver (VODE)

VODE (Variable-coefficient Ordinary Differential Equation solver) is an initial value ODE solver for stiff and non-stiff systems. It uses variable-coefficient Adams-Moulton and BDF methods in Nordsieck form, treating the Jacobian as full or banded. Unlike the older codes, VODE has a highly flexible user interface that is nearly identical to that of the LSODE package. As a comparison with LSODE, several algorithmic improvements have been made in VODE [185]:

- First, a change in step-size and/or order that is decided upon at the end of one successful step is not implemented until the start of the next step, so that interpolations performed between steps use the more correct data.
- Secondly, a new algorithm for setting the initial step size has been included, which uses somewhat more data and makes a more genuine attempt to approximate the initial second derivative vector, whose availability is the difficulty with the initial step selection
- Efficiency is greatly enhanced by an added algorithm for saving and reusing the Jacobian matrix $\boldsymbol{J}$ as it, under certain conditions, occurs in the Newton matrix. As an option, this Jacobian-saving feature can be suppressed if the

required extra storage is prohibitive.

- VODE offers a choice between functional iteration (where no matrices are involved) and a modified Newton iteration in which the Jacobian matrix $\boldsymbol{J}$ is treated as full or banded, and as either supplied by the user or approximated internally by difference quotients.

VODE demonstrates that multi-step methods with fully variable step-sizes and coefficients can outperform fixed-step interpolatory methods on problems with widely different active time scales. In one comparison test, on a 1-D diurnal kinetics-transport problem with a banded internal Jacobian, the run time for VODE was 36% lower than that of LSODE without the J-saving algorithm and 49% lower with it. The fixed-leading-coefficient version ran slightly faster, by another 12% without J-saving and 5% with it [185].

5.3.4.3 Differential Algebraic Sensitivity Analysis Code (DASAC)

DASAC (Differential Algebraic Sensitivity Analysis Code) solves nonlinear initial-value problems involving stiff implicit systems of ordinary differential and algebraic equations. Purely algebraic nonlinear systems can also be solved, given an initial guess within the region of attraction of a solution. Options include automatic reconciliation of inconsistent initial states and derivatives, automatic initial step selection, direct concurrent parametric sensitivity analysis, and stopping at a prescribed value of any user-defined functional of the current solution vector. Local error control (in the max-norm or the 2-norm) is provided for the state vector and can include the sensitivities on requires

5.3.4.4 Summary

In the old version of CHEMKIN II package, The LSODE code is employed, to solve the initial value problem for stiff or non-stiff systems of first order ordinary differential equations. The updated version of CHEMKJN II package and all the later versions handle the chemical kinetic systems using the VODE code to calculate the temperature and species concentrations at various residence times. In the SENKIN program, the DASAC code is implemented to solve the nonlinear ODE that describes the temperature and species concentrations and reaction sensitivities.

All the solver packages discussed above are widely used and have been proved to produce efficient computation and high computation accuracy as dealing with stiff

differential equations related to chemical kinetics. Upon closer examination of results, no method is found always superior to the others, the VODE code exhibits slightly better performance in calculation speed, but for zero-dimensional models, this benefit should not be highlighted since the overall computation time is only of time scale in minutes. As for calculation accuracy, no significant difference has been reported. Selection of the solvers might also be of users' personal preference in consideration of their familiarity to the code. In this work, the VODE code is applied as the numerical solver to the system equations.

Chapter Six: **Loughborough University Chemical Kinetics Simulation (LUCKS) Code**

6.1 Introduction

This chapter describes the packaged code - LUCKS (Loughborough University Chemical Kinetics Simulation) designed for the numerical solution of the set of first order ODEs describing the chemical and physical processes of gas-phase hydrocarbon combustion in SI and HCCI engines. The LUCKS code offers a flexible approach of incorporating chemical kinetics modelling with thermodynamic modelling in the simulation of SI and HCCI engine combustion. The mathematical background that the code employed is presented in **Chapter 5.**

The purpose-driven development of the LUCKS code is to overcome the limitation of the commercial codes that are developed to solve chemical kinetics in the simulation of IC engine combustion. So far, the typical commercial codes have been well packaged to predict the time-dependent chemical kinetics behaviour of a homogeneous gas mixture in a closed system. However, combustion in a real engine is a more complex scenario. Firstly, the in-cylinder mixtures are not spatially homogenous due to heat transfer and gas mixture motion. Secondly, a combustion chamber could not be a closed system owing to engine blowby. Thus, the LUCKS code has been designed for the following features on IC engine modelling

- Combustion system with the volume being a specified function of time parameters (e.g. IC engines)

- Simulation of open combustion systems via modelling of blowby
- Multi-zone modelling of inhomogeneity of in-cylinder gas mixture (burned, burning and unburned zones for SI engines and crevice zone, boundary layer and core zones for the HCCI engines)
- Modelling the effects of EGR on combustion and pollutant formation in HCCI engines
- Simulation of locally homogeneous gas-phase chemical kinetics
- Compatible with either detailed or reduced chemical kinetic mechanisms

The LUCKS code has been so far developed for the simulation of SI and HCCI engine combustion, each of which is represented by one of the two subordinate packages: **LUCKS_SI** and **LUCKS_HCCI**, respectively. Some design goals are kept in the developers' mind while writing the LUCKS code. They include:

- The code is well-structured and object-oriented, which make it easy to maintain and build upon for the subsequent users and developers, and written using open source FORTRAN77/99 to make code transportable between computers s
- Where possible, the code is programmed to have modular structures so that increasing functionalities can be easily added and /or replaced with.
- The code is commented on the code usage and the references that indicate the methodologies used.
- The code is designed to be applied across platforms so that it can be compiled and executed under both Windows and UNIX systems.
- The well-established DVODE code is applied to solve the initial value problems in both stiff and non-stiff ODEs systems.

This chapter are presented in two parts. The first part is to present in detail the modeling structure of the LUCKS code and the second part states the use of the computer code. Various aspects of this computer code are discussed.

6.1.1 Why is FORTRAN Used?

FORTRAN computer language is used in coding LUCKS, but the choice may not whet some users' appetite, especially for some of the new numerical programmers. FORTRAN is seemingly losing the ground to be the programmers' primary option

over the alternatives, say, C or C++. However, in the real numerical computing world, FORTRAN still dominates. The following points summarized may explain how FORTRAN surpasses its counterparts in the scientific and engineering community, especially when high performance is required.

- FORTRAN is easier for new programmers to learn than C and C++, because it requires much simpler process of thought of knowing and understanding the language and hence much less time required to learn FORTRAN than either C or C++.
- Modern language features as in C and C++ are embedded and improved in FORTRAN 90, such as useful features of C (column independent code, pointers, dynamic memory allocation, etc) and C++ (operator overloading, primitive objects). FORTRAN 90 helps users write tighter and faster code than either the original FORTRNA 77 or the C and C++. The more important point is that it is easier for existing FORTRNA 77 programmers to change to 90 rather than to C or C++.
- A great deal of FORTRAN codes exist already (CHEMKIN Library, DVODE, etc), much of which is publicly available and of high quality. Learning and rewriting existent programs into another language requires huge cost in programming time and causes difficulties in portability. The use of FORTRAN in LUCKS is consistent with its application in CHEMKIN Library and DVODE, which avoid the rewriting and transition of these existing programs into other languages. The compatibility between user-supplied code and the existing codes should always be regarded as a prerequisite in the selection of programming language.
- Parallel computers have been more and more applied in modern scientific computing. For example, application of a fully detailed chemical mechanism in a multi-zone combustion model or a CFD model may require the use of parallel computers. However, all the programming languages except FORTRAN 90 have the inherent limitation of the linear memory model in achieving parallelism. A linear memory model is one that assumes that consecutive elements of an array are consecutive in memory. This was a reasonable assumption on traditional computers, but it is completely incorrect on a parallel computer. Only Fortran 90 has addressed this problem and

providing standardized language support for parallelism [186].

6.2 Code Structure

Either LUCKS_SI or LUCKS_HCCI code in the LUCKS package is composed of six blocks of FORTRAN code and five input data files:

- Interpreter (code)
- User-Supplied Engine Simulation Subroutine Library (code)
- DVODE Solver (code)
- Simulation Main Program (code)
- Module Library (code)
- The Gas-Phase Subroutine Library (code)
- Input of Initial Conditions (Data File)
- Input of Engine Geometries and Operating Conditions (Data Files)

The LUCKS code has a modular structure composing of multiple blocks of FORTRAN code and input files enabling the users to communicate with the program. The general structure of the LUCKS code is shown in Figure 6-1, wherein a line connecting two routines indicates that the lower routine is called by the upper one. The three blocks on the upper left part of the structure indicates the three input files that interface the users with the code and needs to be supplied by the users, which respectively define the initial mixture conditions (input_#1), and engine geometries and operation conditions (input_#2), and solution method parameters (input_#3). The upper right corner of the structure illustrates the use of the CHEMKIN interpreter to generate the binary file containing chemical and thermodynamic information of the reaction mechanism applied in the simulation. The input files and the generated binary file are input into the main program. The main program interfaces with our blocks on the right, which, from the top, are the user-supplied subroutine library and CHEMKIN subroutine library, and the module block and DVODE solver. The lower part depicts the modelling outputs.

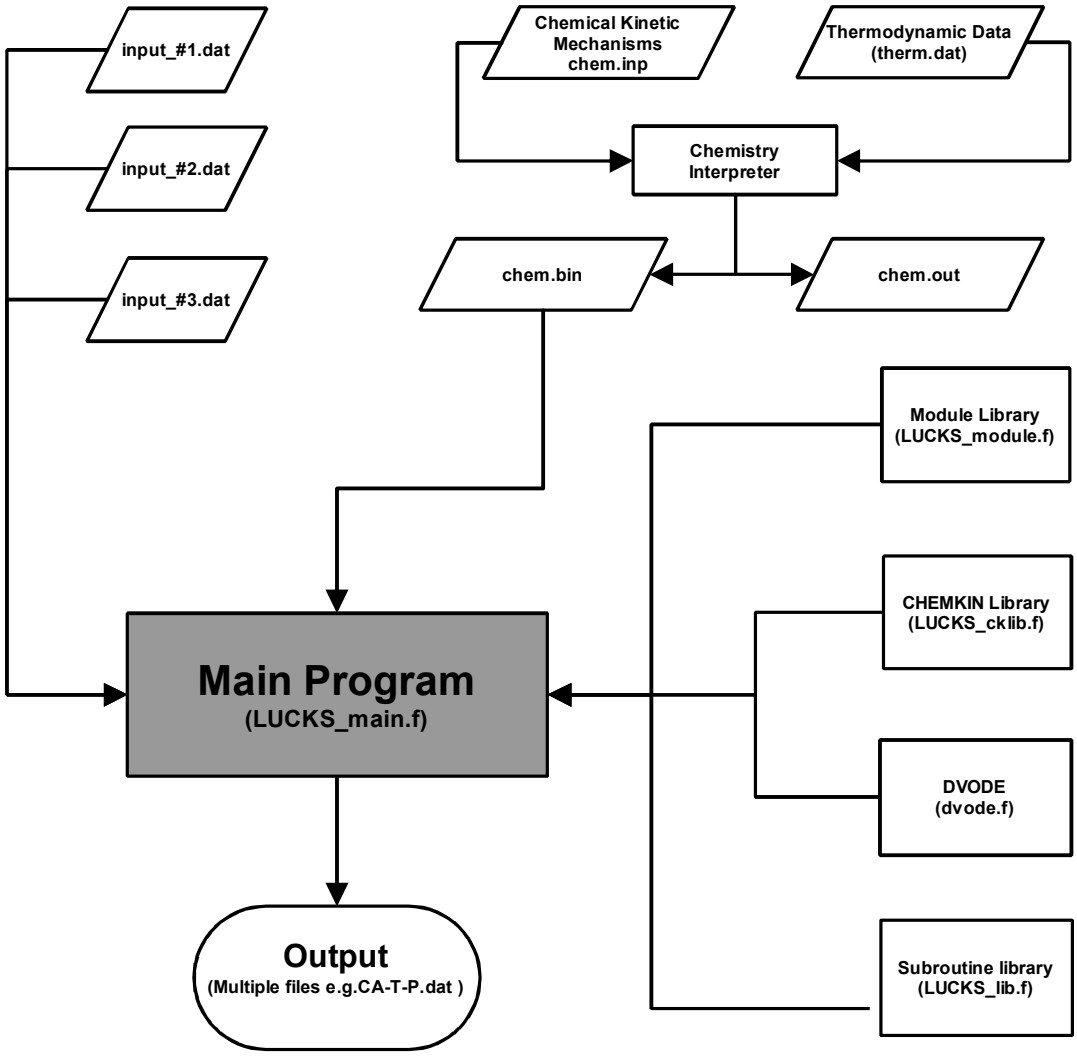

Figure 6-1: The generic structure of the LUCKS code package.

6.2.1 Interpreter

The Interpreter is a FORTRAN program from the CHEMKIN package [187] that reads a symbolic description of a reaction mechanism and then extracts the needed thermodynamic data for each species involved from the Thermodynamic Database. Below is the brief introduction of the input and output of the interpreter. More information about the use of the interpreter and the input and output files can be referred to the CHEMKIN user's manual [188,147].

6.2.1.1 Chem.inp and therm.dat

Two input files are prerequisite to the interpreter. An input file (*chem.inp*) includes information on elements, species and reactions in a reaction mechanism. Input

information in this file is given in 80-column FORTRAN format. Element data are read first, followed by species data and with reactions and reaction rate parameters last.

Another input file to the interpreter is the thermodynamic data file containing the thermodynamic properties for the species in the user's reaction mechanism. The format of *therm.dat* uses the one applied in the CHEMKIN package, which is a minor modification of that used for the Thermodynamic Database in the NASA Chemical Equilibrium code. Consequently, the formatting enables the interpreter to use the NASA database directly without any modification.

6.2.1.2 Chem.bin and chem.out

The primary output from the Interpreter is a binary file called the Linking File (*chem.bin*). This file contains information that contains all required information about the elements, species, and reactions in the user's mechanism, and can be opened and read by the initialization subroutine in the LUCKS code. Hence, the *chem.bin* must be placed in the same directory where the main LUCKS code is put.

In addition to the linking file, another data file (*chem.out*) of FORTRAN's standard output format is produced by the interpreter, which contains a listing of the elements, species, and reactions in the mechanism. The printed output file, though, is not used by the subsequent programs; it is, in contrast to the binary Linking file, of an easily readable file type for the users to recheck the mechanism information and examine the program execution status by providing diagnostic error messages.

Once the Interpreter has been successfully executed to create the linking file, the initialization subroutines in the main program is called to import the information of the reaction mechanism stored in the *chem.bin* into the work arrays in the main program. Then, the work arrays will be used by both the main program and the relevant subroutines.

6.2.2 Main Program

The main program sets up a command procedure to load the subroutines and pass variables and parameters from one process to another. Since the main programs in *LUCKS_SI* and *LUCKS_HCCI* has an analogous structure except the difference in the BLANCE subroutine, in which the mass transfer across flame front in SI engines are modelled by Weibe function and chemical kinetic consumption of unburned gases, which is explained in details in Section 7.2.1.4. The structure of the main

programs of *LUCKS_SI* and *LUCKS_HCCI* is generally illustrated in Figure 6-2, wherein a line connecting two subroutines indicates that the lower routine is called by the upper one. The structure is divided into three sequential levels that are described in the following paragraphs.

The first level marked in light pink first call for the modules used in the main program, which list the defined arguments that will be referenced. Then, all the variables are defined by an implicit type, by which, the variables whose names start with I, J, K, L, M or N is defined as *INTEGER* and all the others are *DOUBLE PRECISION*. Next, the user-supplied subroutine *LUCKS_WRK_ARRAY* is executed to extract into the work arrays the information of the chemical mechanism about the species and chemical reactions for the chosen mechanism from the file *chem.bin* and the subroutine *CKINDX* is next called from the CHEMKIN subroutine library to return a group of indices defining the size of the reaction mechanism. The input file defining the reactor and operating conditions and the parameters for the solver are then loaded and stored in the working space (Subroutines: *LUCKS_INIT_CND, LUCKS_ENG_OPT, and LUCKS_MDL_PAMR*) and the input data are also used to derive the relevant parameters and variables needed by the subsequent subroutines and functions (Subroutines: *VOLUME_FRACTION, VOLUME and MASS*).

The next level (marked in light green) describes the integration loop of the system equations. It starts with the update of the beginning and ending points of the integration and the corresponding crank angles. The subroutine *VOLUME* is called to calculate the geometry properties of both the combustion chamber and each combustion zone. Then, the properties of the gas mixture are updated by the subroutine *STATE_UPDATE* and mass change due to blowby is calculated in *BLOWBY*. Next, the pressure is balanced across all the zones with mass transfer (subroutine: *BALANCE*) and heat transfer coefficients are derived in *HEAT_TRANSFER*. The concentrations of emissions for each zone and the combustion chamber are calculated in the subroutine *EMISSION*. Finally, the subroutine *OUTPUT* is used to writes the calculated results into the output files.

The third level (marked in light yellow) of the structure depicts the execution of the packaged solver code *DVODE* designed for the numerical solution of the system of the first-order ordinary differential equations (ODE'S) given the initial values. The solver code *DVODE* controls the integration and serves as an interface between the calling subroutines and the rest of the package. The solver argument *STATE* is then

checked to specify the state of the calculation.

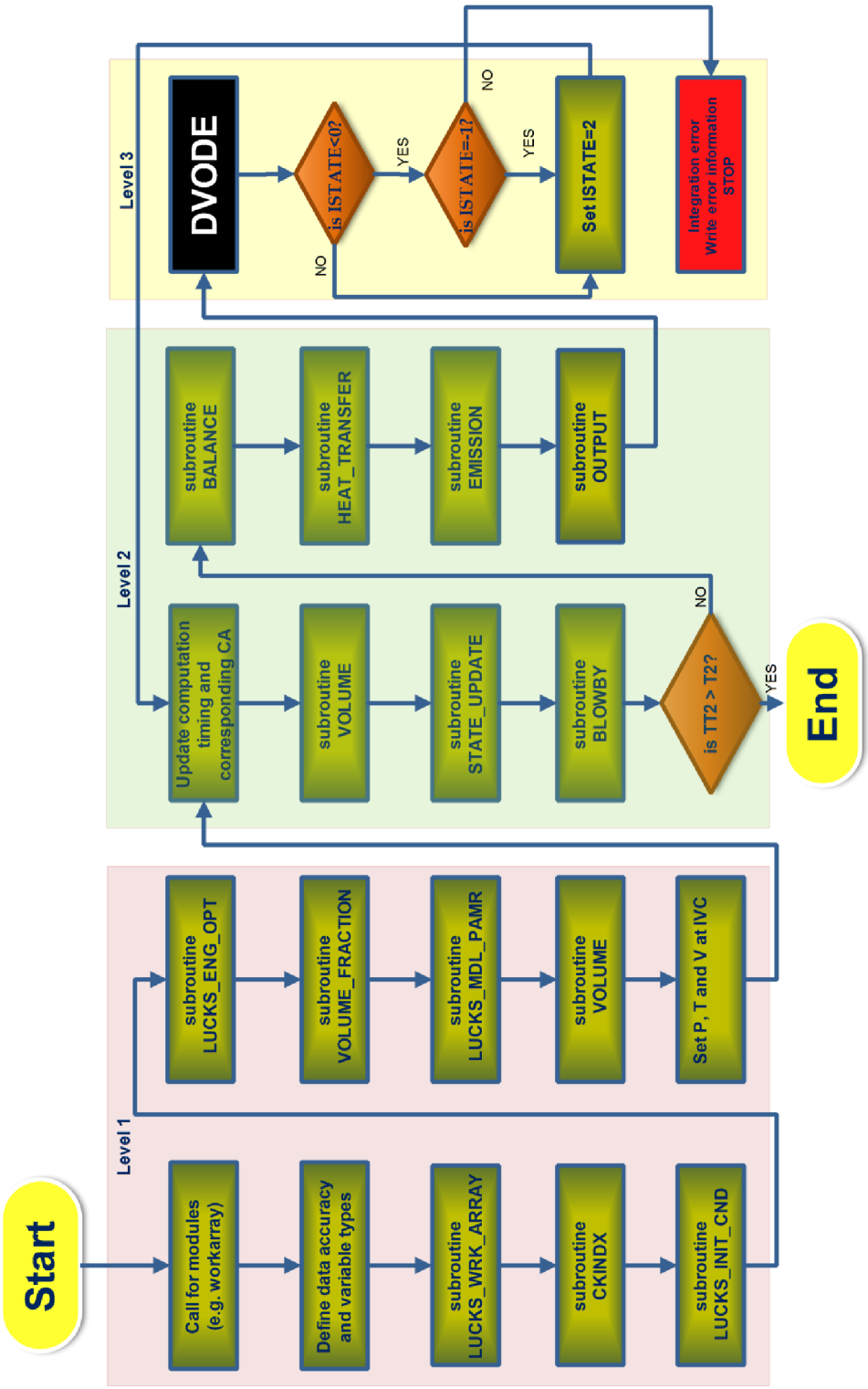

Figure 6-2: The flowchart of the structure of the main program of *LUCKS_HCCI* and *LUCKS_SI.*

6.2.3 Module Library

A new kind of program unit specifically embedded in Fortran 90, *module*, is used in the LUCKS code package. Unlike the main program and the subroutines, modules are not themselves executable program units. Rather, they contain definitions that can be conveniently accessed and used by executable program units. In LUCKS, The parameters and variables are grouped and assigned into different modules according to their use in the related program units, which is a neat and structured way of packaging and categorizing data objects. The data declared in a module can be accessed and used by program, subroutines and functions using the *USE* statements.

6.2.4 Subroutine Libraries

The LUCKS code includes two subroutine libraries: the *user-supplied* subroutine library and the *CHEMKIN* subroutine library. All the subroutines programmed and supplied by the users are packed in the *user-supplied* subroutine library. To enhance the user's understanding of the code, each subroutine contains comment statements on the subroutine's task and the input and output variables into /from the subroutine.

In accordance with the general acceptance of CHEMKIN format in describing the information of chemical kinetic mechanisms, the CHEMKIN format is thus applied in LUCKS to return information on elements, species, and reactions and calculates equations of state, thermodynamic properties, and chemical production rates.

The CHEMKIN Library (LUCKS_cklib.f) is a gas phase subroutine Library, which is a collection of about 100 highly modular FORTRAN subroutines. Generally, the input to these routines will be the state of the gas including pressure or density, temperature(s), and species composition.

Subroutines from this library are called from the main program and user-supplied subroutines. The user's first step must be to dimension three storage arrays: IWORK, RWORK, and CWORK in LUCKS, which are for three data types: integer, floating point and character. Then the initialization subroutine CKINIT must be called to create the storage arrays from the Linking File *chem.bin*. One or more of these arrays is required input to nearly every other subroutine in the CHEMKIN Package. Detailed descriptions of the library are included in the CHEMKIN user's menu [188].

6.2.4.1 Variable-coefficient Ordinary Differential Equation solver

DVODE (Variable-coefficient Ordinary Differential Equation solver) is a double precision version of the VODE package, solving the initial value problem for stiff or non-stiff systems of first order ordinary differentials equations in the forms of,

$$\frac{dy(i)}{dt} = f(i, t, y(1), y(2), ..., y(NEQ)) \qquad \textbf{6-1}$$

Where $i = 1, ..., NEQ$

Communication between the user and the DVODE package is made through calling subroutine DVODE (the same name to the package) to the LUCKS main program at each calculation time step where solutions are desired. Full description of the use of DVODE code is given in [189].

6.3 LUCKS Data File

6.3.1 Input data

To use the LUCKs code, three input files (*input_#1.dat, input_#2.dat,* and *input_ #3.dat*) need to be provided by the user, which define the initial mixture conditions, and engine geometries and operation conditions, and solution method parameters, respectively. The input in the files is in a data-comment-keyword format. On each input line, a numerical number is given first and the description of the number follows the number starting with an exclamation mark. Following the description, an identifying keyword of the argument in the LUCKS code appears after a dash mark (-). The numerical data are read by the code and the data description and keywords are provided for user's information only. All the data in each input files are of fixed orders and any change of the orders or addition of other data have to come with the revise of the genuine code.

6.3.2 Output data

The output from the LUCKS code is printed out into a number of data files: *.dat. As a general rule of the output format, the data in the first column represents the independent variable – crank angle degree (CA^o) and the solutions of the dependent variables are written at each integration step in the following columns. The naming conventions follow the rules that all output files' names starts with letters CA that indicates the crank angle degree as the independent variable in the files and the

remaining letters after the dash represents the generic names of the dependent variables in the files

Writing the solutions at each computation step into each output file raises the execution time, so it is not necessary to print out the solutions that are of no concern to the users in some particular operations. Disabling/enabling the production of output files can be operated by switching from/to the relative command lines to/from the comments lines in the subroutine *OUTPUT* in the user-supplied library.

6.4 Units

Both of the System International (SI) unit system and the Centimetre-Gram-Second (CGS) unit system are used in the LUCKS code. The use of the CGS unit system is to achieve consistence with the units adopted in the CHEMKIN subroutine library, some of whose subroutines are applied to calculate the gas phase properties and reaction rates. In addition, the outputs of the calculation are expressed in SI units. The conversion between SI and CGS systems for the base units encountered in the computation is listed in Table 6-1.

Table 6-1: Definitions and conversion factors of CGS units relevant to SI units

Quantity	CGS unit	CGS unit abbreviation	Definition	Equivalent in SI units
Length, Position	centimeter	cm	1/100 of meter	= 10-2 m
Mass	gram	g	1/1000 of kilogram	= 10-3 kg
Time	second	s	1 second	= 1 s
Velocity	centimeter per second	cm/s	cm/s	= 10-2 m/s
Force	dyne	dyn	g cm / s2	= 10-5 N
Energy	erg	erg	g cm2 / s2	= 10-7 J
Power	erg per second	erg/s	g cm2 / s3	= 10-7 W
Pressure	barye	ba	g / (cm s2)	= 10-1 Pa

Chapter Seven: **Chemical Kinetics Modelling of SI Engine Knock**

7.1 Introduction

Modern spark ignition (SI) engines are being designed to operate close to its limits caused by knock to achieve high brake mean effective pressure (BMEP), optimum brake specific fuel consumption (BSFC) and low emissions. It is generally acknowledged that knock in SI engines is caused mainly by the autoignition of the unburned air and fuel mixture ahead of the flame front. It results in steep pressure gradients that spread in the form of pressure waves in the combustion chamber. These pressure waves then lead to undesirable knocking and ringing noise to the vehicle driver and can cause damages to engine components at sufficiently high intensities.

Chemical kinetic mechanisms play an important role in modelling spontaneous autoignition. These are generally categorized into detailed [159,167], lumped [171], reduced [123,154,177], and global models [174,190] according to the numbers of the reactions and the species [6]. The detailed chemical kinetic mechanisms were developed mostly by adjusting reaction rate parameters and thermal chemical data to fit experimental data. The other types of mechanisms were either extracted from the detailed mechanisms by taking computerized reaction sensitivity analysis like the lumped models, or derived by simplifying the chemical reaction processes into a few generalized chain branching reactions and fitting the reaction parameters for the experimental results like the reduced and global models. The experimental facilities in the study of chemical kinetic mechanisms are mainly engine-like devices such as

closed vessels, flow reactors, shock tubes or rapid compression machines that are operated under homogeneous charge compression ignition (HCCI) conditions. Autoignition behaviour of the unburned mixture under SI engine combustion is different from that under HCCI condition, but mechanisms directly derived from SI engines were scarce due to the complex combustion process. If these HCCI mechanisms are applied to model the autoignition of the unburned mixture under SI engine combustion, certain reaction rate parameters at various operation conditions will have to be tuned to agree with the experimental data.

There are various levels of engine models having the potential to couple chemical kinetics models to simulate SI engine combustion and autoignition, but each comes with inherited advantages and disadvantages. Computational fluid dynamics (CFD) modelling coupled with detailed combustion chemical kinetic mechanisms showed a potential to mimic the engine knock by considering temporal and spatial variance of the properties of the unburned gas mixtures, but requires massive computation resources [25]. Single-step [191,192] and highly simplified multi-step kinetic mechanisms [193-195] have been linked into the CFD simulations to simplify the calculations, but still computationally expensive. Zero-dimensional modelling technique provides much higher computational efficiency and a handy engine design tool that has been extensively developed. However, most conventional zone models incorporate thermodynamic models and chemical equilibrium combustion models [9,196]. They are functionally unable to describe the knock phenomenon. Various combustion chemical kinetic mechanisms, such as Shell autoignition model [197], reduced chemical kinetic mechanism [198], and semi-detailed chemical kinetics [199], have been introduced into zero-dimensional thermodynamic engine models to simulate the knock phenomenon. These zero-dimensional knock models have shown the potential to model and analyze the engine knock behaviour. However, the chemical kinetic mechanism employed was generally based on iso-octane, which is different from the fuel in the real world.

Tanaka mechanism [123,154] uses identical hydrocarbon oxidation schemes for both iso-octane and n-heptane with 12 reactions in each scheme and includes an interaction reaction between n-heptane and iso-octane. By introducing further non-hydrocarbon mechanisms, the Tanaka mechanism consists of 55 reactions with 32 species. It is capable of simulating the combustion and autoignition behaviour of primary reference fuels. The mechanism has been tested in a wide range of HCCI

conditions in a rapid compression machine. It is the interest of this research work to introduce the Tanaka mechanism into an early in-house developed zero-dimensional SI engine model and tune some of its key rate parameters to simulate SI combustion and knock performances.

7.2 The Model

The model developed in the study is a zero-dimensional based SI engine combustion model combined with tuned Tanaka kinetic mechanism. In the model, the in-cylinder gas mixtures are divided into three individual zones according to their different thermodynamic states and compositions as shown in Figure 7-1.

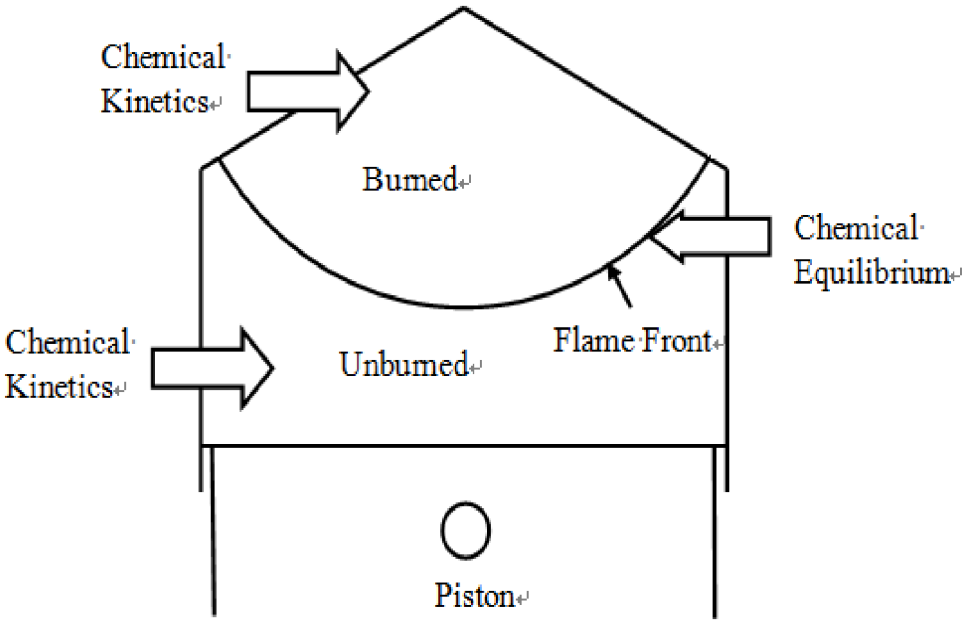

Figure 7-1: Three-zone combustion chamber.

The unburned zone is made of unburned mixture of fuel and air in front of the propagating flame. No burned residuals are considered. The burning zone is the reaction zone of the thin flame front, transporting mass and energy from the unburned to burned gas regions. The burned zone indicates the region consisting of burned products. The combustion chemical kinetic mechanism is applied in both the unburned zone to predict the oxidation reactions of the unburned air and fuel mixture, and in the burned zone to calculate the thermal performance of the burned gas. The burning zone at the thin flame front is assumed to have no volume and regarded as a

transporting process [200,201], which is modelled by chemical equilibrium calculations [202]

7.2.1 Basic Model

The foundation of the zonal model is based on applying the mass and energy conservation principles on both unburned and burned zones. The major assumptions of the basic model are ideal gas engine charge, perfect homogeneous fuel-air mixture, and uniform in-cylinder pressure.

7.2.1.1 Mass Conservation

In the unburned zone, when pressure and temperature are sufficiently high, the air and fuel mixture is no longer stable and cool flame reactions starts. The reactions may further lead to autoignition if the temperature further increases. This is analyzed in the model by introducing chemical kinetics to the unburned zone. Applying the mass conservation principle to the unburned zone, the change rate of the mass fraction of a species i in the unburned zone, $X_{i,u}$, is then expressed as

$$\frac{dX_{i,u}}{dt} = \frac{\overline{M}_i \dot{\omega}_i}{\rho_u} \qquad \textbf{7-1}$$

where, $\overline{M}_i$ is the molecular mass, $\dot{\omega}_i$ is the volume specific molar production rate, and ρ_u is the density of the unburned zone. The subscript i denotes a species in the mixture.

In the burned zone, the mass fraction change of each species is affected by two factors, the formation by the flame reactions, and the formation and consumption by the post flame kinetic reactions. The total mass in the burned zone, m_b', after taking the transferred mass from the burning zone Δm is

$$m_b' = m_b + \Delta m \qquad \textbf{7-2}$$

where m_b is the burned zone mass before taking the transferred mass.

The mass fraction of a species i after mixing with the mass transferred from the burning zone is therefore expressed as

$$X'_{i,b} = \frac{\Delta m \cdot X_{i,f} + m_b \cdot X_{i,b}}{m'_b} \qquad \textbf{7-3}$$

where the $X_{i,f}$ is mass fraction of a species i in the transferred mass from the burning zone which is equal to that in the flame front, and $X_{i,b}$ is the existing fraction before the transfer, the subscript b indicates unburned and burned zone.

Substituting Equation 7-2 into Equation.7-3 yields the mass fraction change of a species i due to formation by the flame reactions. Adding the formation and consumption by the post flame reactions, the mass fraction change of a species i in the burned zone is then obtained

$$\frac{dX_{i,b}}{dt} = \frac{1}{m'_b}\frac{dm_b}{dt} \cdot \left(X_{i,f} - X_{i,b}\right) + \frac{\overline{M}_i \dot{\omega}_i}{\rho_b} \qquad \textbf{7-4}$$

7.2.1.2 Energy Conservation

The energy conservation equation is applied to represent the energy change in the unburned and burned zone. For the unburned zone, it relates the temperature change to the heat transfer $\dot{Q}_{l,u}$, the work due to the volume change, and the energy change due to the chemical kinetic reactions

$$m_u c_{p,u} \frac{dT_u}{dt} = \dot{Q}_{l,u} + V_u \cdot \frac{dp}{dt} - V_u \cdot \sum_{i=1}^{n} \omega_{i,u} \cdot \overline{M}_i \cdot h_{i,u} \qquad \textbf{7-5}$$

where h is the specific enthalpy, c_p is the specific heat capacity at constant pressure, V is the zone volume, p is the cylinder pressure, and T is the zone temperature.

For the burned zone, the effect of the energy transferred from the burning zone, $\dot{m}_b \cdot \left(h_f - h_b\right)$, on the temperature change needs to be taken into account which gives

$$m_b c_{p,b} \frac{dT_b}{dt} = \dot{Q}_{l,b} + V_b \cdot \frac{dp}{dt} + \dot{m}_b \cdot \left(h_f - h_b\right) - V_b \cdot \sum_{i=1}^{N_s} \omega_{i,b} \cdot \overline{M}_{i,b} \cdot h_{i,b} \qquad \textbf{7-6}$$

7.2.1.3 Heat Transfer

The heat transfer of the unburned zone in the model consists of two parts, the heat convection between the unburned gas and the cylinder wall Q_{conv_w} and the heat

convection between the unburned gas and the flame front.

$$\begin{aligned} Q_{l,u} &= Q_{conv\_w} + Q_{conv\_f} \\ &= h_{conv\_w} \cdot A_u \cdot (T_u - T_w) + h_{conv\_f} \cdot A_f \cdot (T_u - T_f) \end{aligned} \quad \textbf{7-7}$$

where A_u and A_f are the contact area between the end gas and the cylinder wall and between the end gas and the flame front. the real front surface area The flame front surface area A_f is estimated by

$$A_f = C_A \cdot A_b \quad \textbf{7-8}$$

Where

Where A_b is the area of burned gases in contact with the cylinder wall, which is calculated by the empirical functions proposed by Fugerson [9],

$$A_b = (\frac{\pi \cdot B^2}{2} + \frac{4 \cdot V}{B}) \cdot x_{flame}{}^{\frac{1}{2}} \quad \textbf{7-9}$$

where x_{flame} is the mass fraction burned by flame propagation and B is the cylinder bore.

C_A in Equation 7.8 is an adjustable constant. As real flame propagates in a turbulent form, the flame front is wrinkles, which lead to a surface area greater than a simple spherical ball of flame. Thus, C_A usually has a value over one. In the work in this chapter, the surface area of flame front is assumed to be twice of the area of burned gases to obtain the best fit to the experimental results.

The heat transfer coefficients h_{conv_w} and h_{conv_f} have been simulated using the Woschni correlation $h = C_h B^{-0.2} p^{0.8} w^{0.8} T^{0.53}$, where C_h is the heat transfer rate constant and w is a characteristic speed [129]. Woschni's correlation was originally determined for a four-stroke, water-cooled, four-valve direct-injection CI without swirl. However, the subsequent upgrade of the formula (Equitation 5.40) for calculation of the characteristic speed with inclusion of swirl effect provided the correlation the ability in predicting the heat transfer at normal and knocking combustion in SI engines at an acceptable accuracy level. This has been proved by the test results by Woschni, et al [222] and recommended by Heywood [1]. Though this correlation has

been widely applied to simulate the heat transfer in SI engines, it was only validated against a certain range of conditions in the test engine. Therefore, when evaluation of heat transfer in any other engine with different specification under various operation conditions, parameters in the correlation need to be adjusted or a more advanced model can be applied. However, the latter is limited by its availability by the current research on heat transfer in SI engines.

The thermal radiation from the burned zone to the cylinder wall is modelled by the Stefan-Boltzmann law $Q_{rad} = A_w \sigma T^4$, where σ is the Stefan-Boltzmann constant $5.67 \times 10^{-8} \left[W/m^2 K^4 \right]$ [1].

7.2.1.4 Mass Fraction Burned

The burned mass in the cylinder consists of two parts, the mass transported from the burning zone due to the flame propagation, and the mass burned in the unburned zone due to the chemical kinetic reactions of the unburned gas autoignition. Thus, the Mass Fraction Burned (MFB), x_b, is expressed as:

$$x_b = x_{flame} + x_{auto-ignition} \quad \textbf{7-10}$$

The mass burned by flame propagation in the model is calculated by the Weibe function [1]. The burned mass in the unburned zone is due to autoignition only, and is therefore equal to the mass that have been consumed by the chemical kinetic reactions. Note that the mass burned due to chemical kinetic reactions will only play a significant part when autoignition starts. This is expressed as

$$x_{auto-ignition} = \sum_{i=1}^{3} \sum_{j=1}^{n} m_u \Delta X_{i,u,j} \Delta t \quad \textbf{7-11}$$

where Δt is the calculation time step, subscript j is the step number, i is species number where 1 denotes fuel, 2 denotes O_2 and 3 denotes N_2.

7.2.2 Kinetic Mechanism

Tanaka combustion chemical kinetic mechanism, as listed in Appendix B, has been employed in this study to model the oxidation of primary reference fuels. It needs to note that the autoignition of the unburned mixture in the SI combustion is different from that of the HCCI combustion. In the HCCI case, the compression, the main driving force of the autoignition, is from the piston only. However, in the SI

combustion, the unburned mixture is compressed by both the piston motion and the flame propagation. The later contributes to faster and stronger compression and is heat transfer intensified. Therefore, it is reasonable to conclude that the autoignition in the SI combustion is stronger than that in the HCCI combustion, and can be characterized by shorter ignition delay and greater burned rate. The original Tanaka mechanism was developed for the HCCI combustion, so it needs to be tuned for the SI engine conditions.

A sensitivity analysis investigating the effect of the reaction rates on the ignition delay and burn-rate [154] indicated that the alkyl radical formation reactions in the Tanaka mechanism (R6 and R18 generally expressed as *RH+OH=>R+H2O*) have the greatest influence on both the ignition delay time and the burn rate. The enhancement of their pre-exponential factors of the rate-constants leads to a shorter ignition delay and a higher burn-rate. This phenomenon is attributed to the role of alkyl radical formation reactions in the oxidation chemistry, where both reactions represent the attack of the active radical *OH* to abstract the atom H from fuel molecules. This is believed to be the primary chemical path that is responsible for fuel consumption [203]. The kinetic parameters in R6 and R18 therefore need to be enhanced in order to tune the mechanism to the level of autoignition under SI conditions.

The enhancement of the kinetic parameters in reactions R6 and R18 have no effects on the low temperature oxidation reactions of the unburned gas mixture before knock occurring or under the conditions that lead to no autoignition. This is because that these two reactions are only actively responsible for the parent fuel decomposition when the temperature rises to the intermediate and high regimes, where OH radicals can be built up and become the critical chain-carrying radicals [12,204]. The modified mechanism is therefore capable to simulate the low temperature reactions of the unburned gas mixture that may or may not lead to knock.

After applying the Tanaka chemical kinetics model into the three-zone engine model, a sensitivity analysis was conducted to study the influence of the pre-exponential factors of reactions R6 and R18 on knock position, peak cylinder pressure, knock intensity and combustion duration. Figure 7-2 shows the calculated knock position and peak cylinder pressure at various enhance factors applied to the pre-exponential factors of R6 or R18. Both reaction rate parameters need to be tuned simultaneously since the two reactions play the same roles in the chain branching mechanisms for n-

heptane and iso-octane, respectively. The modelled engine condition is 900 RPM, spark ignition timing of 6^{o} before top dead centre (BTDC), intake pressure of 1.0 bar, and air to fuel ratio (AFR) of 13:1. The fuel input into the calculation is a primary reference fuel with 95 RON. In the baseline case, the pre-exponential factors are set the same as the ones in the Tanaka mechanism. It can be seen that as the pre-exponential factors increase, the knock occurring position advances towards TDC and the peak in-cylinder pressure increases. This justifies the effect of enhanced factors on the ignition delay. As the ignition delay time is shortened, autoignition occurs early towards the TDC, which leads to higher peak pressure.

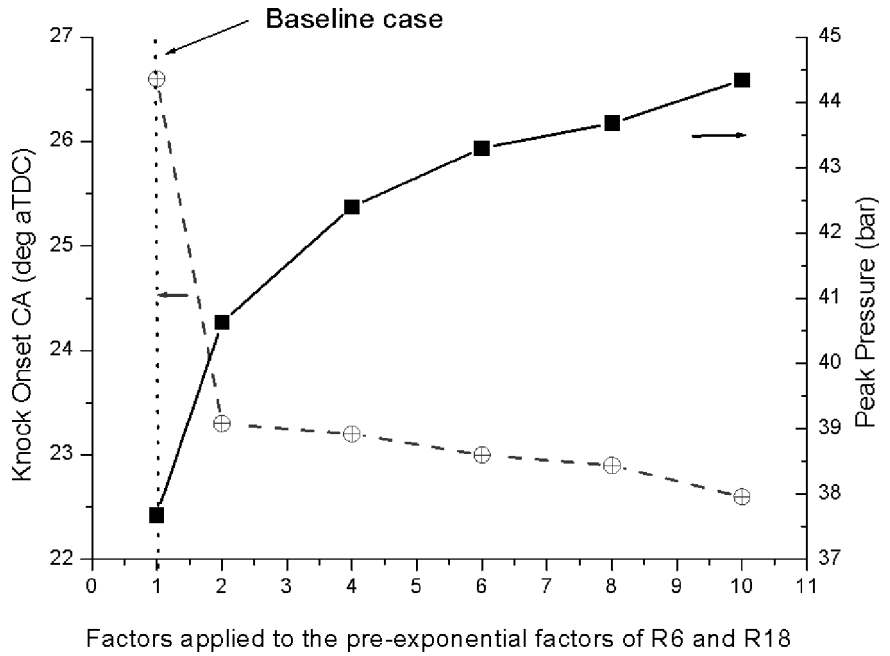

Figure 7-2: Calculated knock position and peak pressure vs. Enhancing Factors in R6 and R18.

Figure 7-3 shows the calculated knock intensity and combustion duration at varying pre-exponential factors of reaction R6 and R18. It can be seen that as the factors increases, the knock intensity increases and the combustion duration decreases attributing to the effects of the factors on accelerating the entire reaction processes.

From Figure 7-2 and 7-3, it shows that the increase of the enhance factors from 1.0 to 6.0 leads to knock position being advanced by about 23%, the peak pressure being increased by around 16% and knock intensity being raised by about 100%. Further increasing the enhance factors from 6.0 to 10.0 can only affect these three parameters by about 3%, 2% and 15%, respectively. Thus, it can be concluded the

enhance factor of the value of 6.0 is the turning point and has been employed in this work.

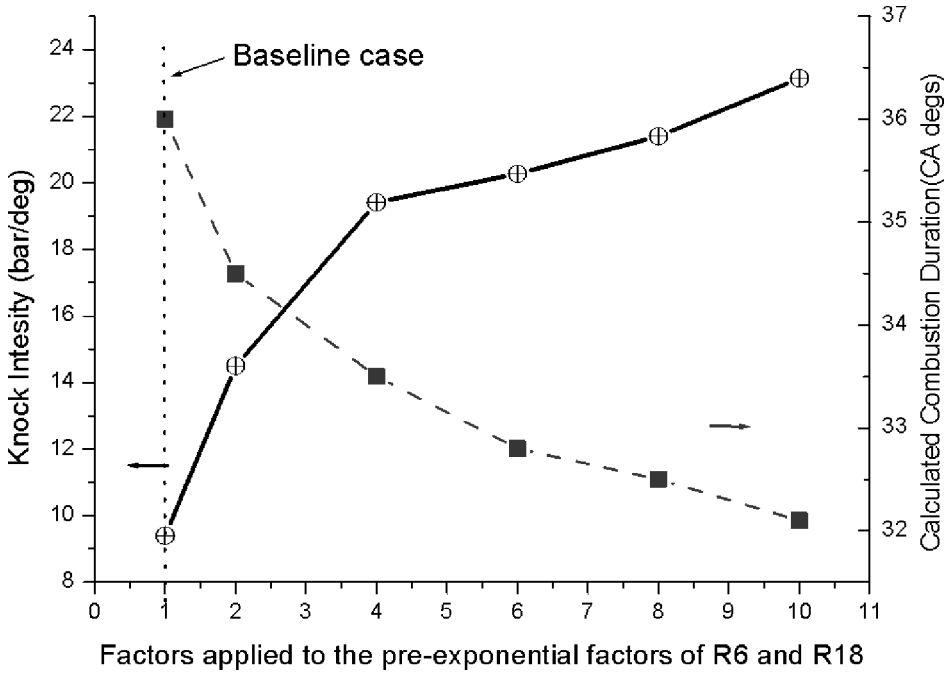

Figure 7-3: Calculated knock intensity and combustion duration vs. Enhancing Factors in R6 and R18.

7.2.3 Equilibrium Burning Zone

The burning zone is the flamelet reaction zone transporting mass and energy from unburned to burned gas regions. In this study, the burning zone is assumed as an adiabatic region at chemical equilibrium. During each calculation step, the mass entrained into the flame front is assumed to be burned and transferred into the burned gases instantaneously.

The same thermodynamic data and chemical species in Tanaka mechanism are selected to be included in the equilibrium chemistry. The equilibrium state of the gas mixture in the burning zone is determined by minimizing the Gibbs free energy $\Delta G \approx 0$, which serves as a criterion of chemical equilibrium. The thermal properties and the equilibrium chemical composition of the burning zone are calculated using the STANJAN equilibrium program [205].

7.2.4 Numerical Solver

The combination of the basic engine model, the mass fraction burned model and the

kinetic combustion model forms a set of coupled Ordinary Differential Equations (ODEs). This includes 66 simultaneous variables for temperatures and species mass fractions as a function of crank angle. Due to the incorporation of chemical kinetics into the combustion system, the set of equations involves enormous disparities in the characteristic time scales for the response of different species during the occurrence of autoignition. These kinetics equations were solved in the model using a Double-precision Variable-coefficient Ordinary Differential Equation (DVODE) solver developed for the solution of both stiff and non-stiff systems.

The previously described in-house FORTRAN code, LUCKS_SI in the LUCKS package integrating the DVODE solver for the ODEs, has been developed to simulate combustion systems with chemical kinetics. Figure 7-4 shows the model flowchart. The simulation is executed from Intake Valve Closing (IVC). A link file with the information of the kinetic mechanism, the thermal data, and an input data file consisting of the initial operating conditions and the engine specifications are input to the function block to calculated the parameters used in the governing equations. The function block includes the subroutines for the calculation of cylinder volume, mass fraction burned, and the zone mixture properties. The governing equations are solved by the DVODE solver and the outputs (zone temperatures and zone species mass fractions) are used to update the in-cylinder pressure and routed back to the function block for the next calculation step. Next, the calculated pressure is also routed back to the function block for the next calculation step. The calculation stops at the timing of Exhaust Valve Opening (EVO). The governing equations are integrated simultaneously at a calculation time step of 0.1 crank angle degrees in the model.

7.3 Model Validation

7.3.1 Tests and Knock Identification

The engine used for the model validation in this work is a single cylinder, 4-stroke Ricardo E6 research SI engine. The engine specifications are detailed in Table 7-1.

The engine was equipped with a pressure transducer and the data was recorded at an interval of one-tenth crank angle degree. A LabVIEW based engine data acquisition system was used to record 50 consecutive engine cycles data at each test condition.

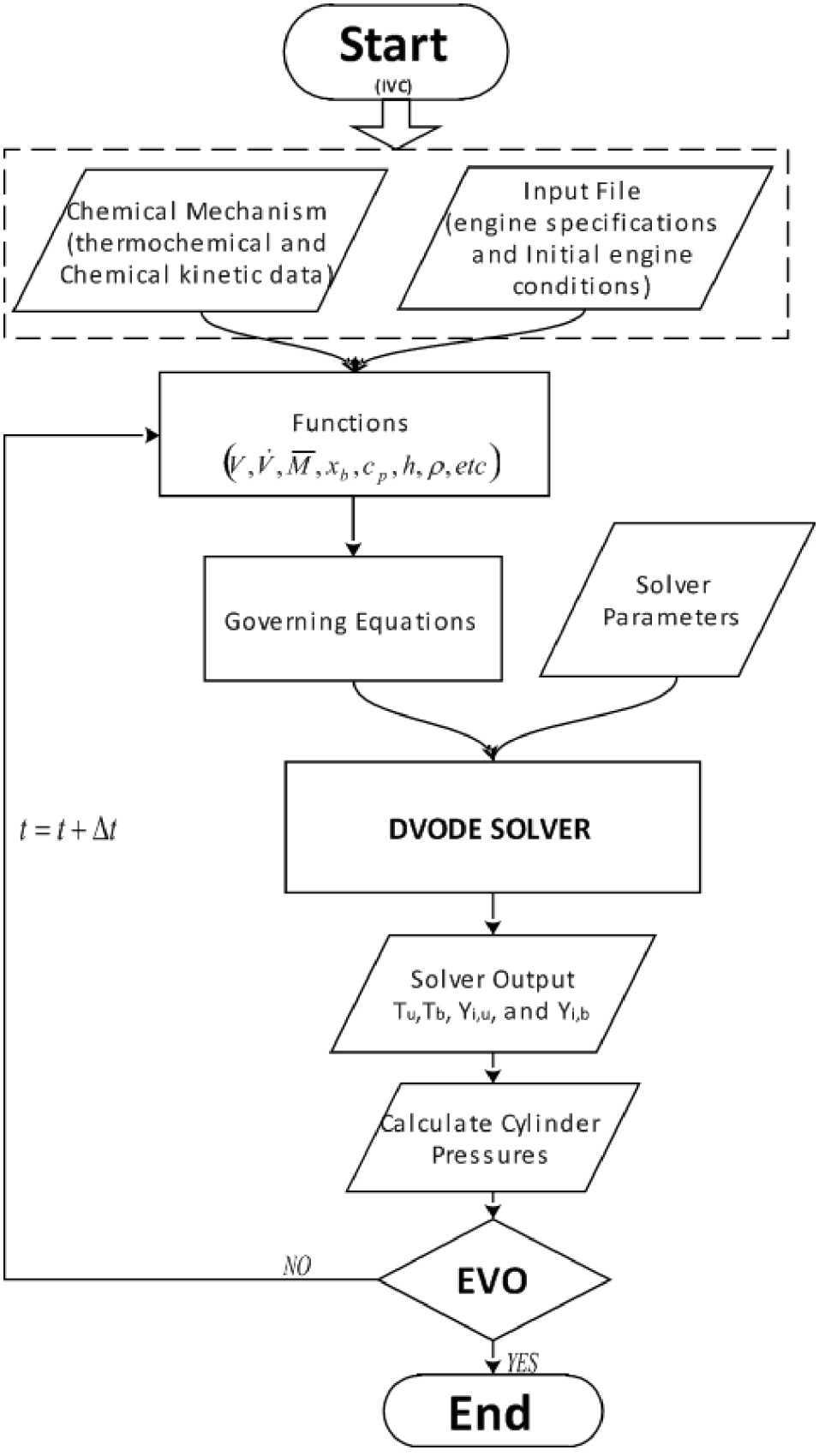

Figure 7-4: The structure of the LUCKS_SI program.

Table 7-1: Engine specification.

Stroke	111.2 mm
Bore	76.2 mm
Con rod length	240.5 mm
Compression ratio	10:1
IVO	9 deg BTDC
IVC	37 deg ABDC
EVO	41 deg BBDC
EVC	10 deg ATDC

Knock detection has been a widely researched subject. It was found that the pressure traces under knocking conditions have two distinct features: the pressure fluctuation and the sharp pressure rise [206,207]. Thus, in this work, the start of the first distinct inflection point in the slope of the cylinder pressure trace, which is followed by consecutive pressure fluctuation, is taken as the knock onset position as shown in Figure 7-5.

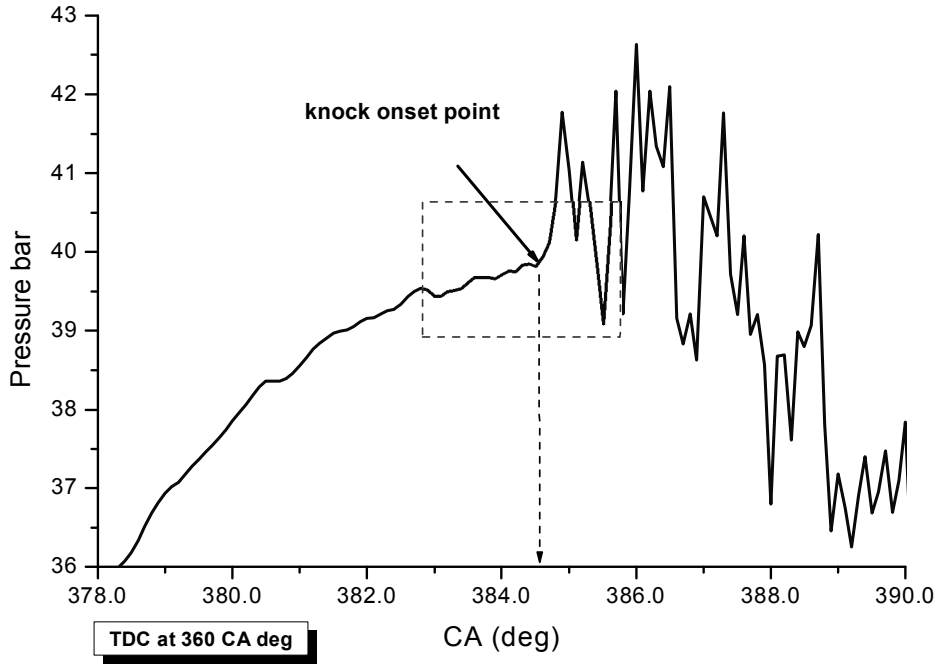

Figure 7-5: Knock position on a typical measured pressure trace.

This inflection point is identified by calculating the pressure slope change rate (K) across every three adjacent values on the pressure curve, which is expressed by Equation 7-12 and Figure 7-6.

$$K = \frac{(p_n - p_{n-1})/\Delta\theta - (p_{n+1} - p_n)/\Delta\theta}{\Delta\theta} \qquad \textbf{7-12}$$

It was found that a threshold value of 30 bar/CA^2 corresponds well with the knock occurrence in the tests and has been used to identify the knock in this study. The cycles with the value of K over this criterion are granted as knocking cycles and the first crank angle where K is greater than this value is termed as knock onset point. Figure 7-7 compares the pressure traces of the knocking cycles (upper part) and non-knocking cycles (lower part) recorded at knocking conditions, which are distinguished in use of the proposed detection approach. It can be seen that among the same set of recorded engine cycles, some cycles exhibit distinct slope change due to knock and the others show smooth pressure traces as in normal combustion, which is attributed to the cycle-by-cycle variation.

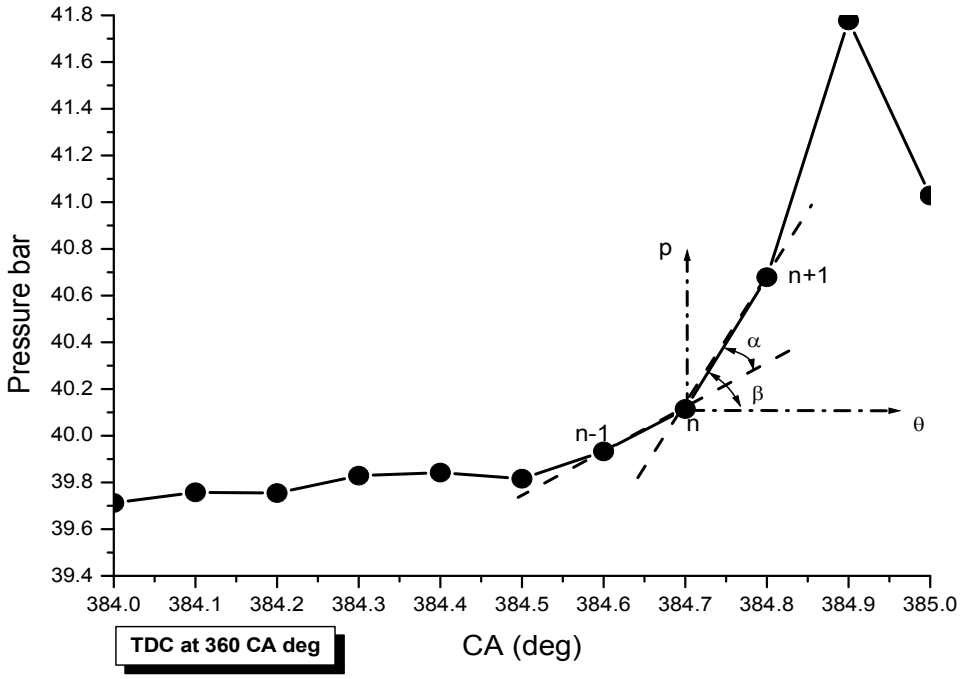

Figure 7-6: Zoom-in image from Figure 7-5 to schematically express the definition of K; $tg\beta = dP_n / d\theta$ and $tg\alpha = dP_{n-1} / d\theta$

As with the simulation results, the corresponding crank angle at which the temperature increase rate is over 100 K/CA that represents the sharp temperature increase, is termed as the knock onset point. This is due to the impossibility of simulating the pressure oscillating variation with time at knock in the current mathematical model, and it has been proven to be convenient and reliable to predict

the autoignition occurrence from the calculated temperature profile as a result of high sensitivity of reaction rates on temperature.

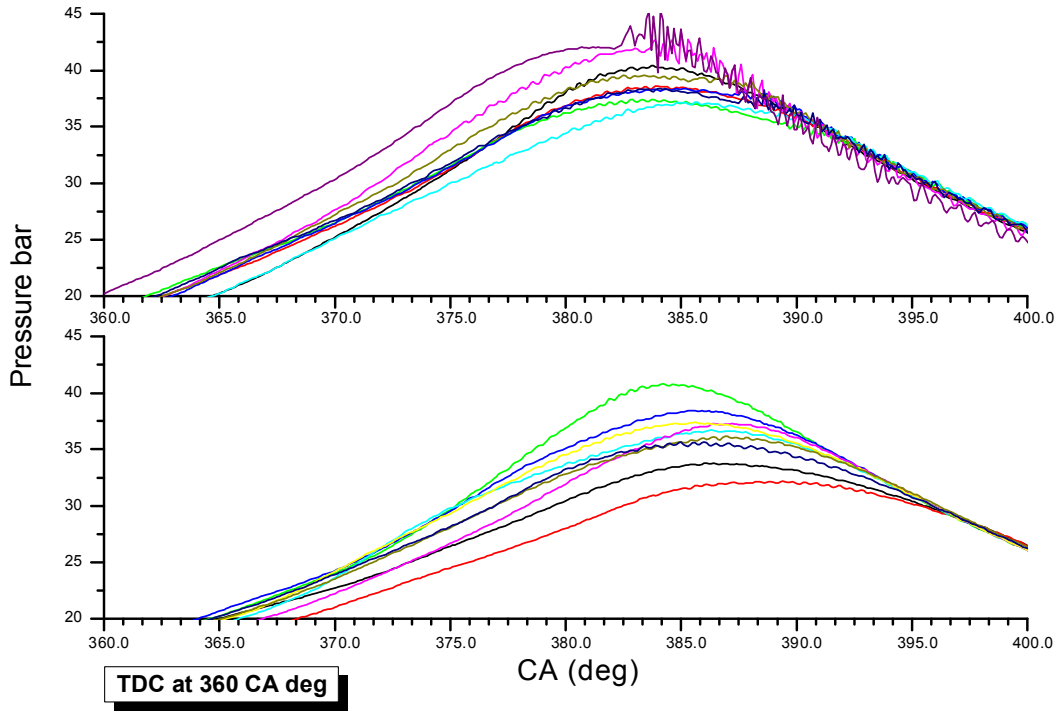

Figure 7-7: Comparison of the pressure traces between knocking cycles (top) and non-knocking cycles (bottom) extracted from the same set of recorded data

The knocking level is evaluated by knock intensity, which is defined as the maximum amplitude of pressure increase rate. Figure 7-8 shows the knock intensity against knock positions of 43 knocking cycles identified from 50 consecutive measured cycles at 900 RPM, 4^{o} BTDC spark timing, AFR of 13 and at wide-open throttle (WOT). It shows that the earlier the knock occurs, the stronger the knock intensity is. This trend agrees with the results reported elsewhere [199,208].

7.3.2 Validation

The model developed in this work was to simulate engine combustion performances under both knock and non-knock conditions. If the engine operates without knocking, the combustion kinetics employed in the model will be low temperature reactions dominated, and thus no autoignition occurs. Figure 7-9 shows the comparison between calculated and measured in-cylinder pressures at a set of non-knock conditions.

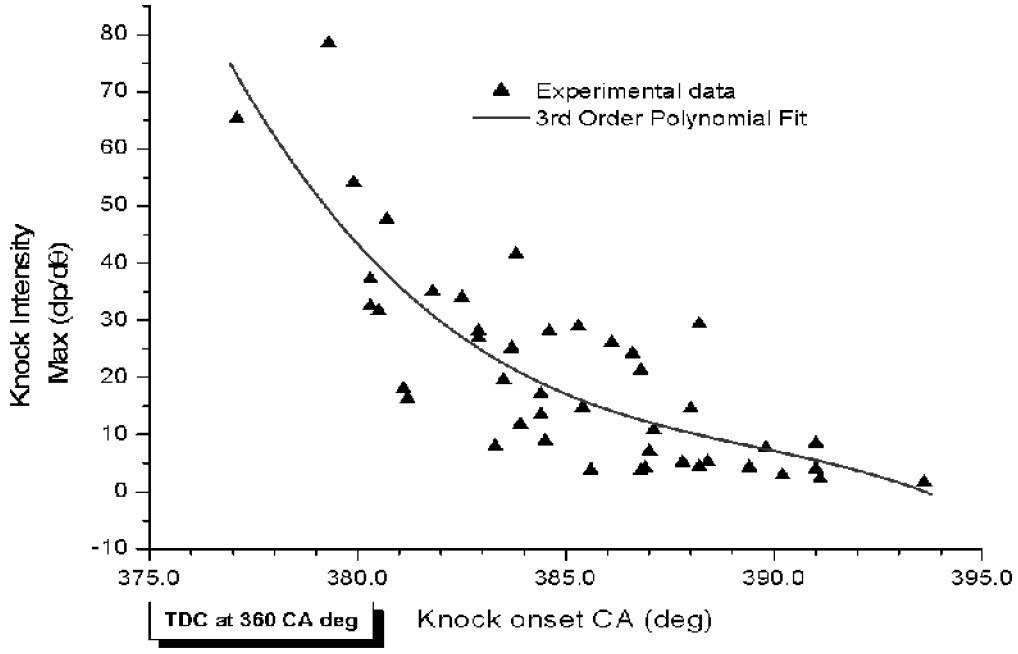

I **g**

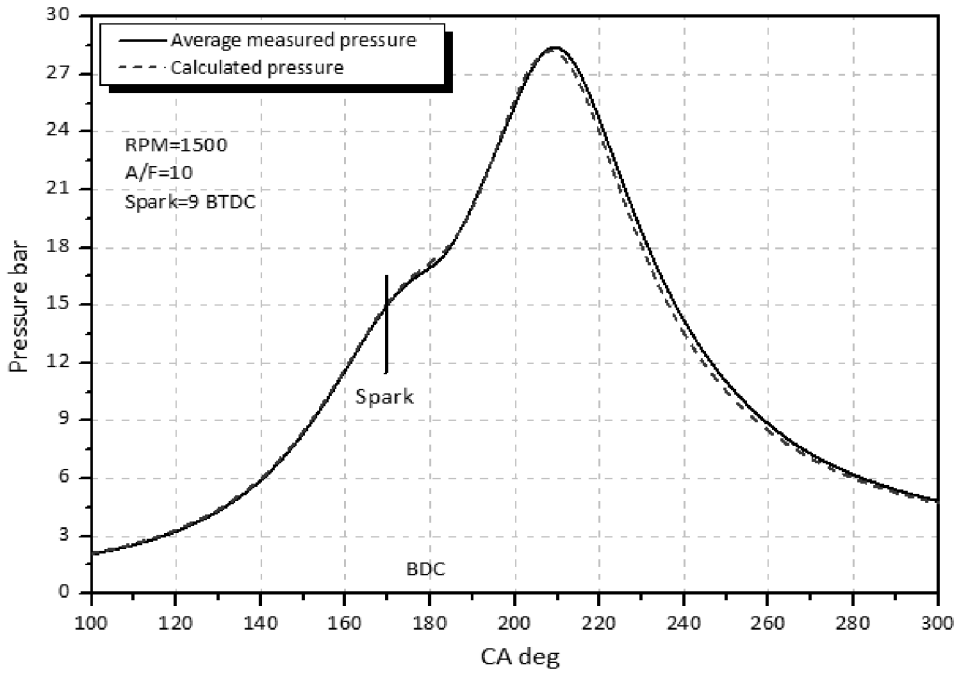

Figure 7-9: Calculated and measured in-cylinder pressure under non-knocking conditions

The measured in-cylinder pressure was averaged over 50 consecutive cycles at WOT condition with a speed of 1500rpm, a spark ignition timing of 9^{o}BTDC, and an AFR of 10. The same engine conditions were used in the model. The fuel rich

mixture decreases the fuel conversion efficiency that leads to a poor combustion without any knock. It can be seen that the calculated in-cylinder pressure agrees well with the measured results. It shows that the model with the modified combustion kinetics does not affect its low temperature reaction mechanism and has the capability to reflect the non-knocking operation conditions.

As the mixture strength reduces, the oxygen availability improves and the combustion temperature increases. With the same engine operation conditions, as the A/F ratio increases, the combustion improves until a level that autoignition of unburned mixture before the flame front starts, which leads to engine knock. To validate the model prediction of knock characteristics (Knock Intensity, Knock Onset and Peak Pressure), the simulation results of these characteristics are compared with the average value of the experimental data of the knocking cycles. Figure 7-10 a-c show the peak pressure, knock intensity and knock onset position of measured values from 50 consecutive measured cycles, the averaged experimental data and the calculated data from the model. The averaged data is calculated through adding up all the measured data of each cycle and dividing the sum by the total cycle number. The engine test conditions are 1500 RPM, 9^{o} BTDC spark timing, AFR of 13 and WOT. The disparity of the measured cycle data is attributed to the significant cycle-to-cycle variation under knocking conditions. The calculated data agrees well with the averaged experimental data, which shows the capability of the developed model in predicting knock characteristics.

Figure 7-11 shows the calculated in-cylinder pressure with various AFR at a fix speed of 1500rpm and a park ignition timing of 9^{o}BTDC. It shows that knock is not detected until the A/F ratio is increased to 11, which is indicated by a smooth pressure curve at AFR=10 and sharp pressure increase at A/F ratio of 11, 12 and 13.

Figure 7-12 summarises the calculated and measured peak cylinder pressure with various AFR. It shows that peak cylinder pressure increases as A/F ratios increase. The model overall slightly under predicted the cylinder peak pressure, by about 5% at the maximum. The difference may due to the heat transfer rate coefficient correlation employed in the model, which may not be sensitive enough to the variation of A/F ratios especially under knock conditions, and the exclusion of the boundary layer from the model, which provides better prediction of the local temperature for the region adjacent to the cylinder wall. Furthermore, the heat transfer across the flame front has been calculated with assumption that the flame front area is twice the

surface area of the burned zone in the model; this causes further errors in predicting the heat transfer.

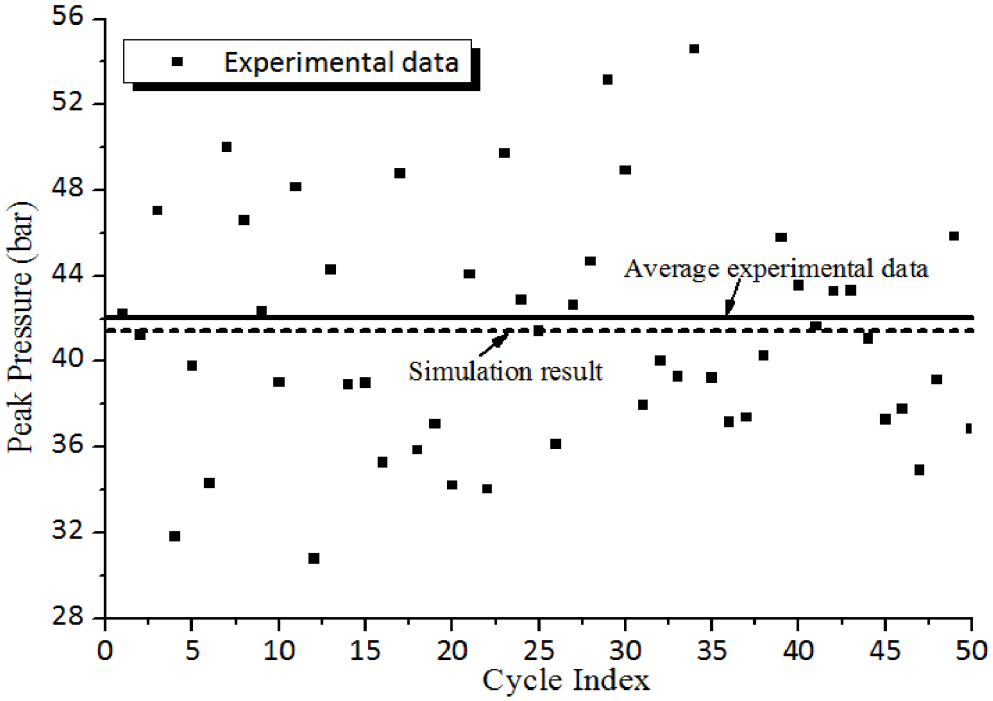

Figure 7-10a

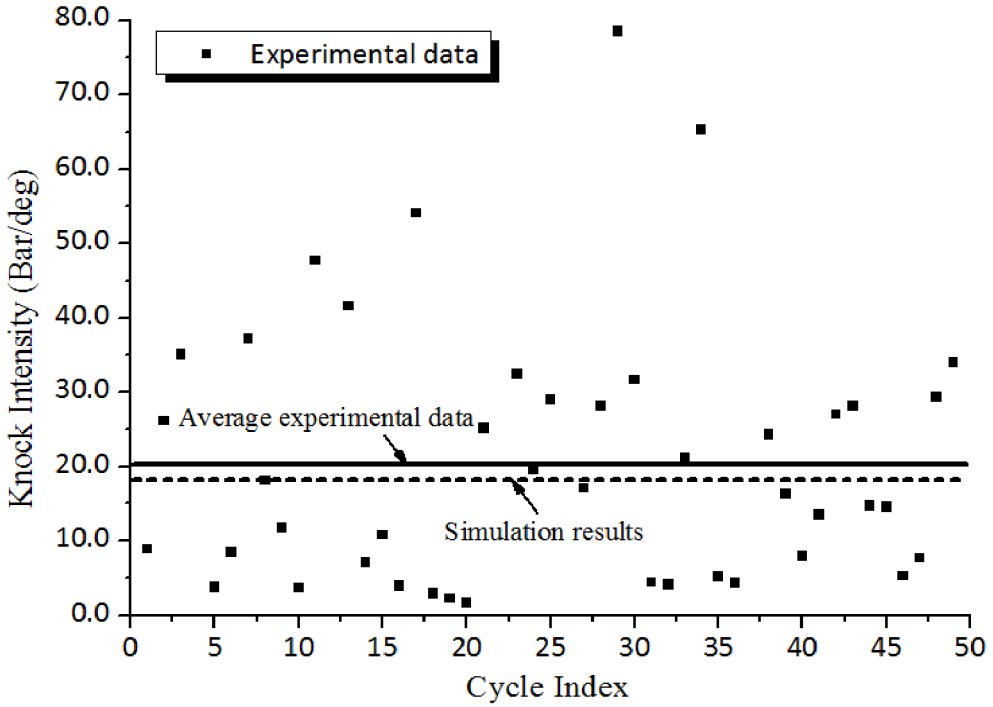

Figure 7-10b

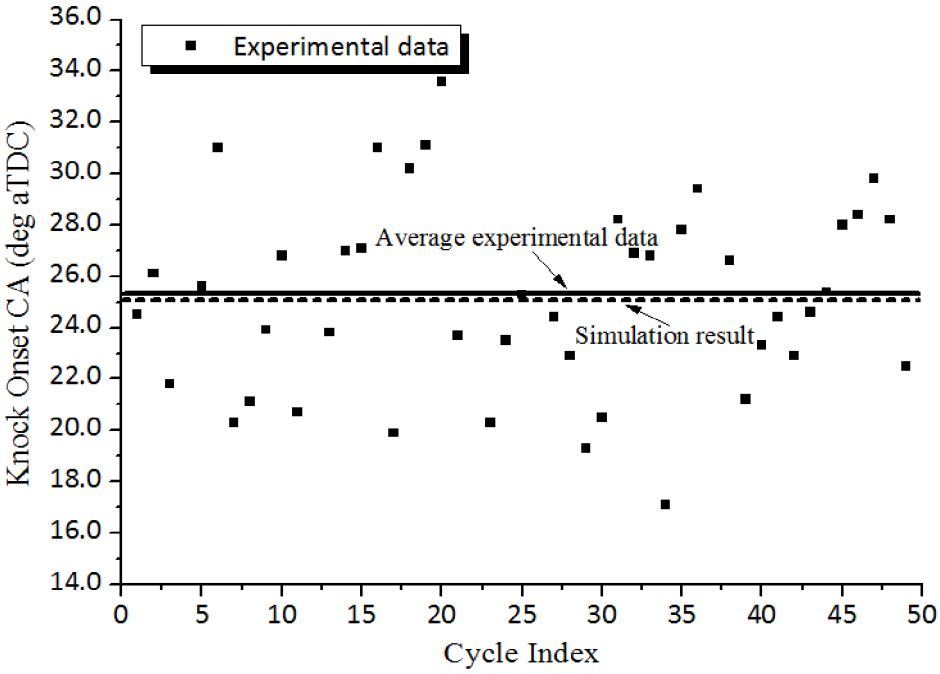

Figure 7-10c

Figure 7-10: Comparison of knock characteristics between calculated and measured data. (a): peak pressure (b): knock intensity (c): knock onset.

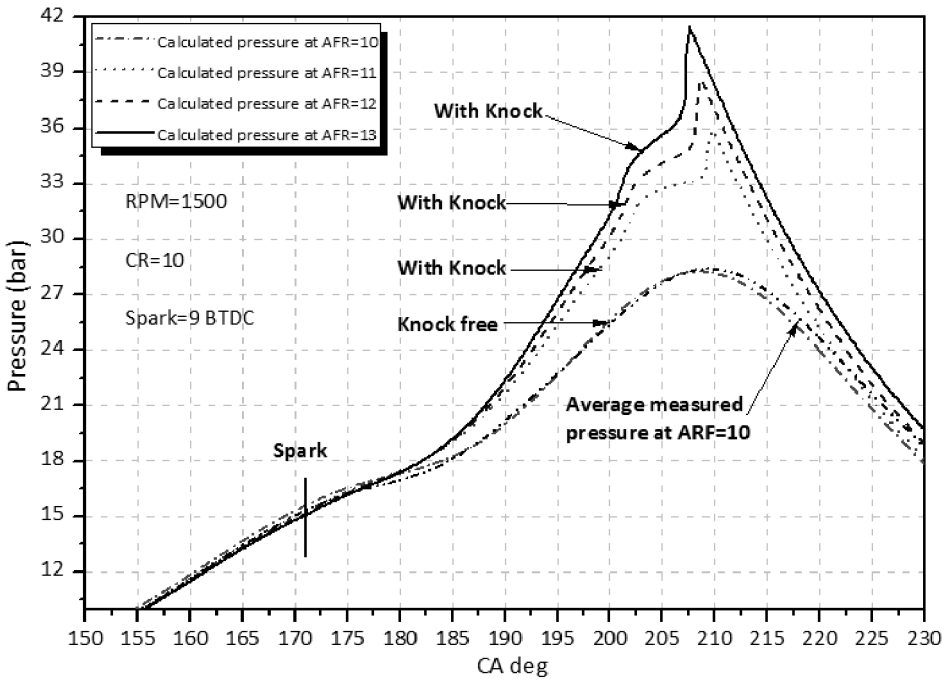

Figure 7-11: Calculated in-cylinder pressure at various AFR.

Engine speed determines the time availability of the combustion cycle. Knock is an autoignition related phenomenon that is dominated by the time dependent chemical

kinetics. It is therefore a logical conclusion that as the engine speed increases, the time availability of the combustion cycle decreases, which leads a delayed knock in terms of engine crank angle. This phenomenon has been tested and simulated in the study and Figure 7-14 shows the calculated and measured results. The engine operating conditions during the test and as the inputs to the model are 4^{o} BTDC fixed spark timing, AFR of 14:1 and WOT. Both the measured and calculated results confirm that the knocking position in terms of engine crank angle is delayed as engine speed increases. The simulated knock position at low engine speed is slightly later than the measured position while at high speed it becomes a bit earlier.

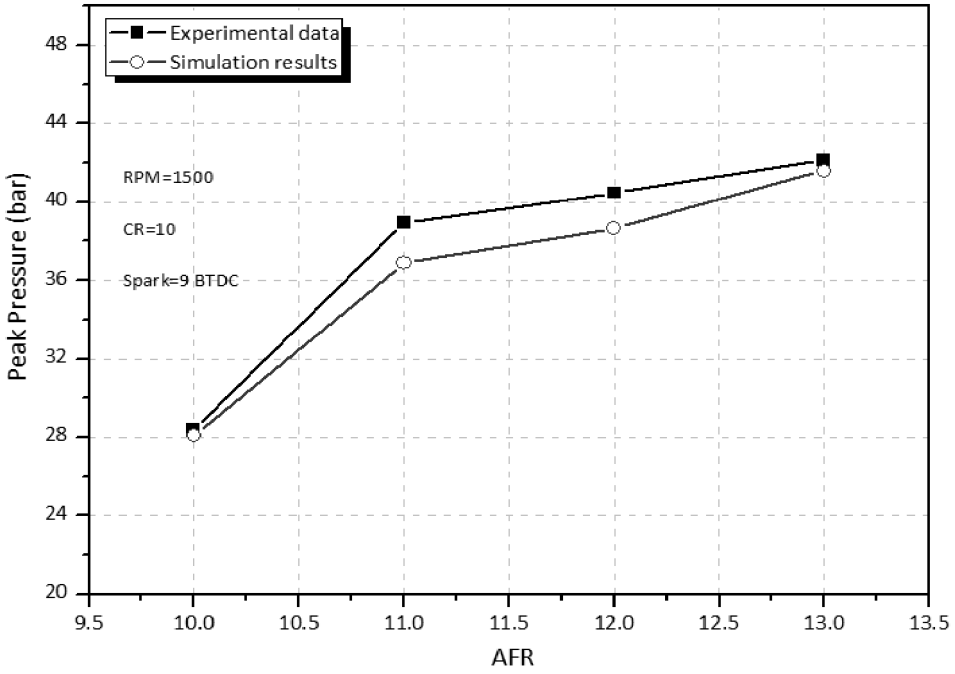

Figure 7-12: Calculated and measured peak pressure at various AFR

Figure 7-13 summarises the calculated and measured knock onset position and knocks intensity at various AFR. Three regions can be identified, the knock region, the non-knock region, and the transition between the two. At the tested engine conditions, the knock region is between the A/F ratios of 11 to 13. When the A/F ratio is lower than 10, there is no knock being detected. In the region of 10 to 11, the engine is under and through the transition. It can be seen that both calculated and measured knock position advances and knock intensity increases as the A/F ratio increases. The simulated knock onset position is slightly less predicted at rich conditions, about 0.6^{o} later than the measured position at AFR of 11. The difference reduces as the mixture getting leaner. As the results, the predicted knock intensity is

about 10% lower than the measured one at lean conditions. Again, the difference may be due to over calculating heat loss at lean conditions.

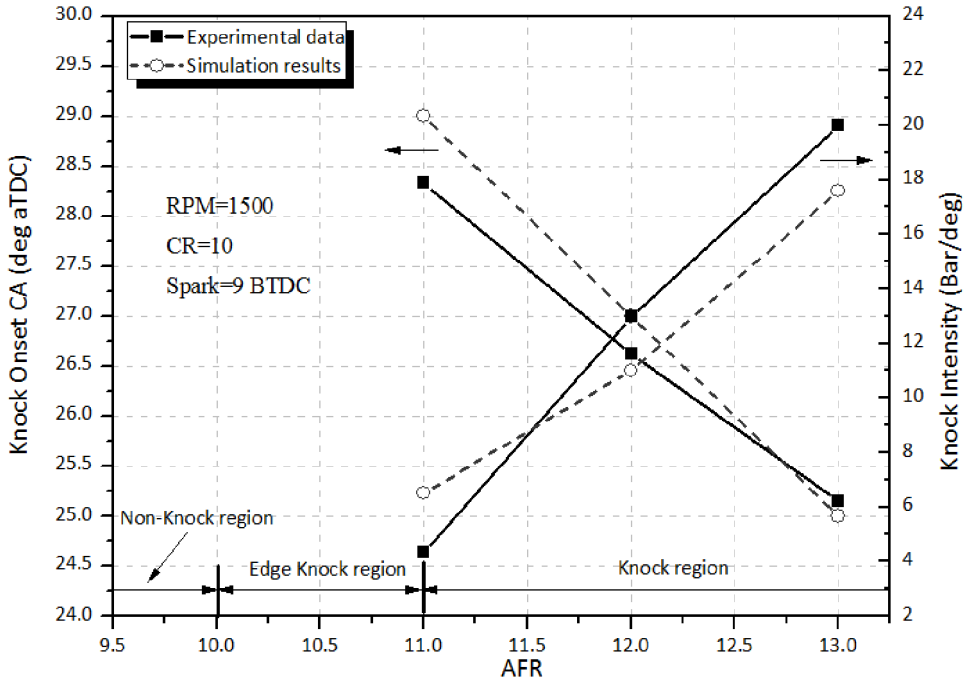

Figure 7-13: Calculated and measured knock onset position and knock intensity at various AFR

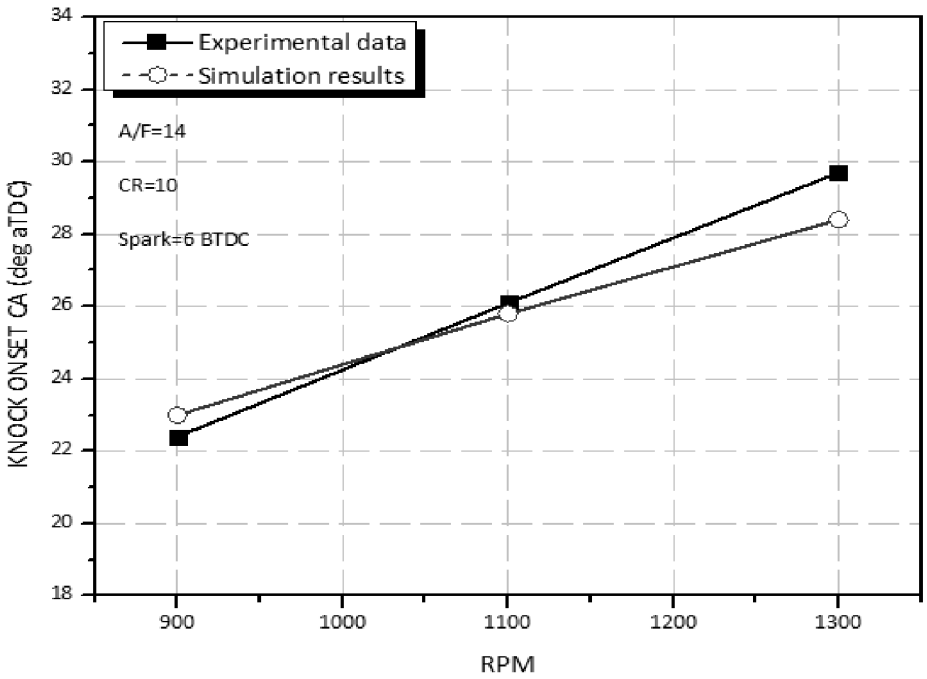

Figure 7-14: Comparison of calculated and measured knock onset positions in respect of RPM

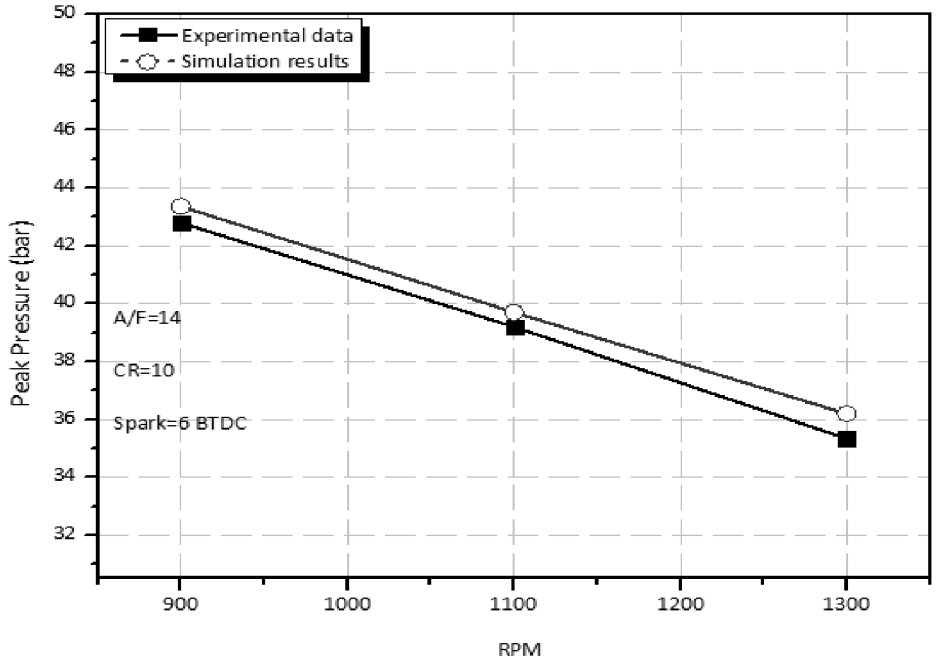

Figure 7-15: Comparison of calculated and measured peak pressures in respect of RPM

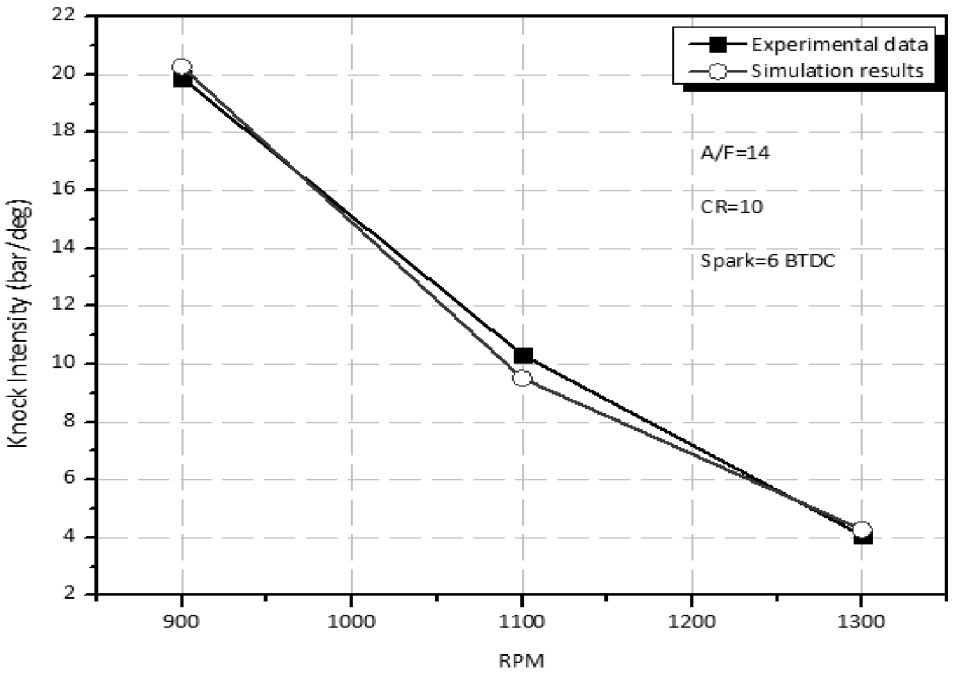

Figure 7-16: Comparison of calculated and measured knock intensity in respect of RPM

Figure 7-15 shows the calculated and measured peak cylinder pressure at knocking conditions at various engine speeds. It shows that peak cylinder pressure decreases as the engine speed increases. The model overall over predicted the cylinder peak

pressure.

Figure 7-16 shows the calculated and measured knock intensity at various engine speeds. Reducing the engine speeds results in an increase of the duration of time for which the end-gas is subjected to high pressure and temperature environment. This leads to the build-up of the radical pool to consume major fraction of the fuel in the gas and causes autoignition. The longer the end gas resides in high temperature and pressure environment, the earlier and harder it is for the end gas to autoignite.

7.4 Model Calculations

Figure 7-17 shows the calculated burned mass fraction with and without autoignition under an engine condition of 1500 RPM, spark timing of 9^{o} BTDC, air to fuel (A/F) ratio of 13, and Wide Open Throttle (WOT) full load condition. The one without autoignition is calculated directly using the Weibe function, and the one with autoignition is calculated by the model with the same Weibe function parameters. It can be seen that the two curves overlap until the level of about 45%. When autoignition, the knock, occurs in the unburned zone, the burned mass fraction suddenly accelerates due to the autoignition of the mixture in the unburned zone. Clearly, to merge the autoignited mass into the burned mass shortens the overall combustion duration than that defined by the Weibe function.

Intake air pressure boosting has been widely used in achieving high BMEP outputs fuel efficiency. The strategy is seriously limited by the knock problem. Spark timing retardation is an efficient method to avoid the knock, but can significantly reduce the engine combustion efficiency. A good understanding in to the relationship among the boost pressure, combustion quality and spark timing retardation is necessary. The zero-dimensional 3-zone model developed in this work offers such a potential. Figure 7-18 shows the calculated peak cylinder and knock timing pressure at various engine intake pressures. The engine conditions for the calculation were 1500 RPM, spark ignition of 9 /BTDC, 1.0 bar intake pressure to simulated the WOT condition and an AFR of 14:1. The results showed that the knock timing advances as the intake pressure increases. This is clearly contributed to the fact that a higher intake pressure increases the in-cylinder effective compression ratio and compresses the unburned mixture harder that improves the fuel autoignition conditions and leads to

an earlier knock.

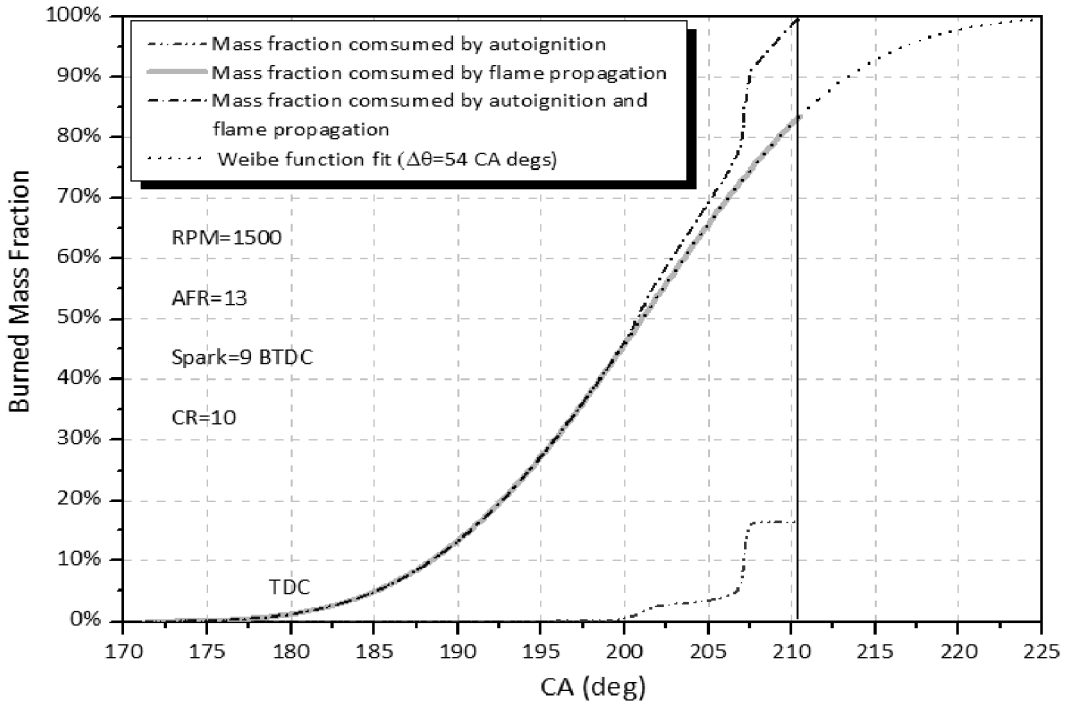

Figure 7-17: MFB with and without unburned mixture autoignition.

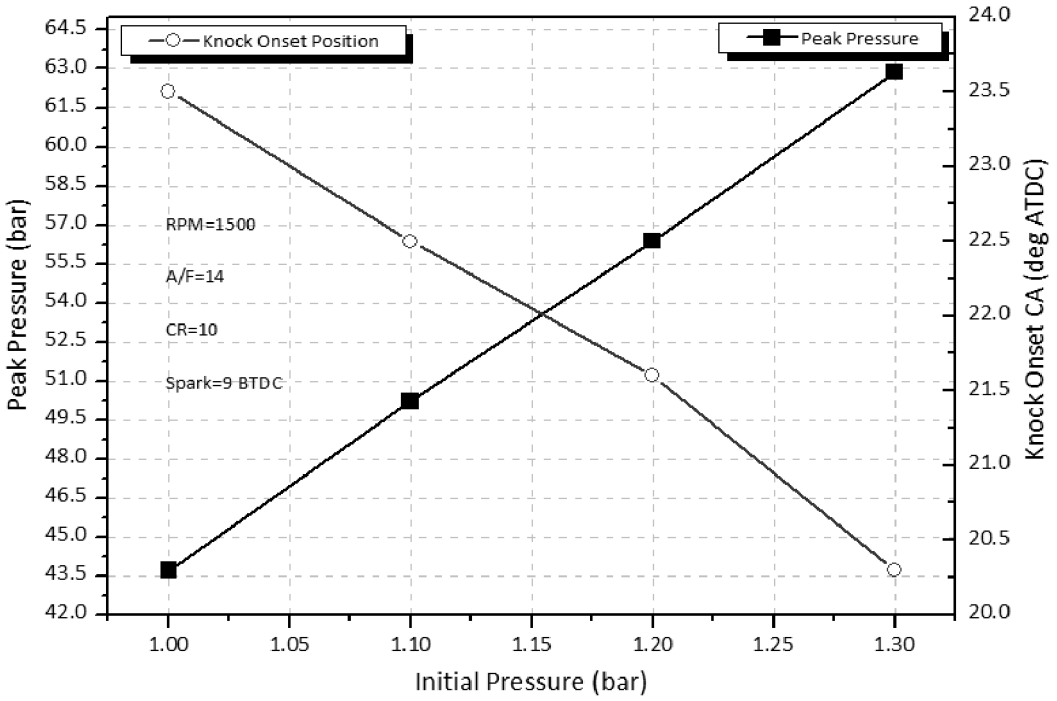

Figure 7-18: Calculated knock onset positions and peak pressures in respect of intake pressure

Figure 7-19: Calculated knock intensity and combustion durations in respect of intake

pressure shows the calculated knock intensity and the combustion duration at various intake pressure. Again, higher intake pressure results in higher knock intensity. The combustion duration calculated in the model is the duration after considering the autoignition of the unburned mixture. It decreases as the intake pressure increases. This is because that the increased effective compression ratio due to intake pressure boost delivers stronger combustion, which pushes the unburned mixture ahead of the flame front harder. This leads to earlier and stronger autoignitions. The enhanced autoignition consumes more unburned mixture and reduces overall combustion duration.

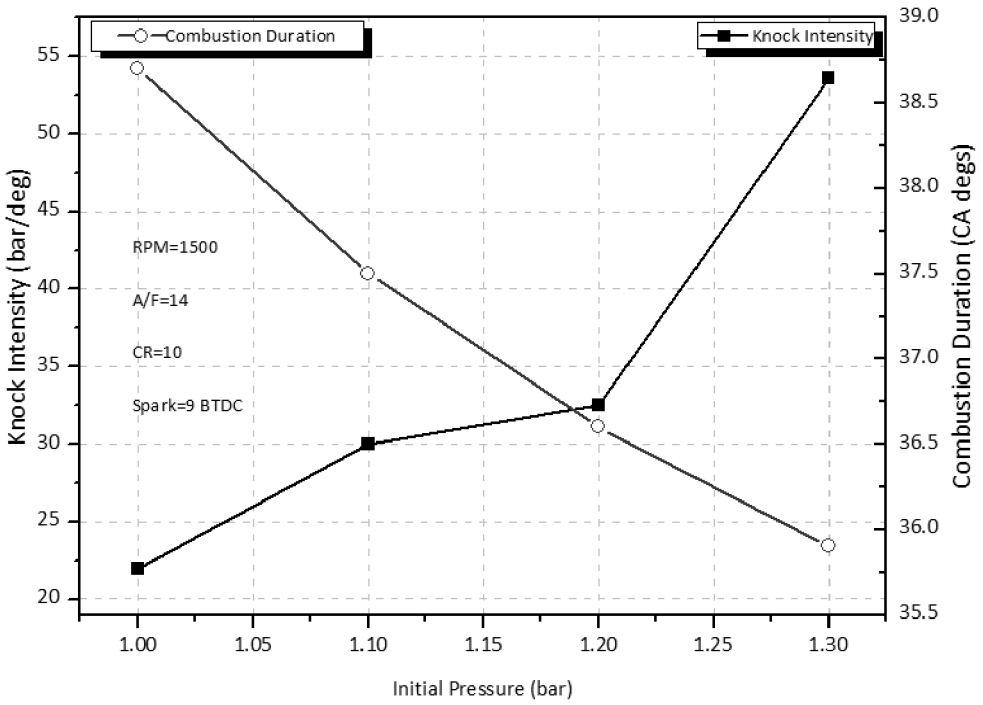

Figure 7-19: Calculated knock intensity and combustion durations in respect of intake pressure

Spark timing retardation is an efficient method to avoid the knock especially under boosted intake conditions. The simulation results in Figure 7-20 shows the influences of the spark timing on the peak pressure and the knock positions at 1500 RPM, the A/F ratio of 14:1 and WOT. It can be seen that as the ignition timing retards towards TDC position, the knock timing delays, too. When the spark timing is delayed to a certain level, no knock occurs and the combustion is safely in the non-knock region. The peak pressure decreases as the ignition timing is retarded, which is simply due to the weakened compression effect on the combustion with delayed ignition timing.

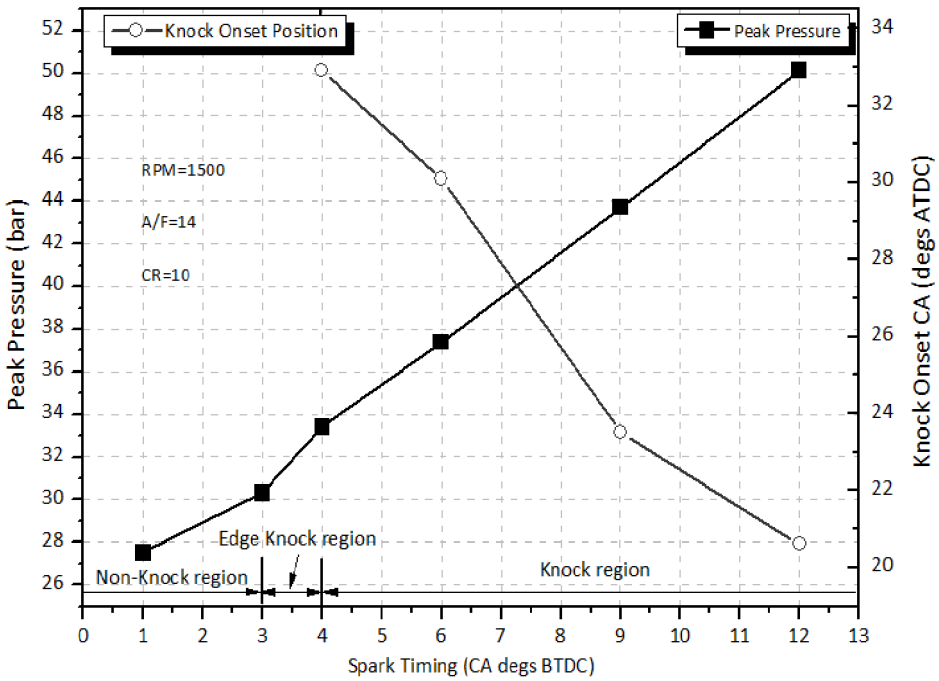

Figure 7-20: Calculated knock onset positions and peak pressures in respect of spark timings

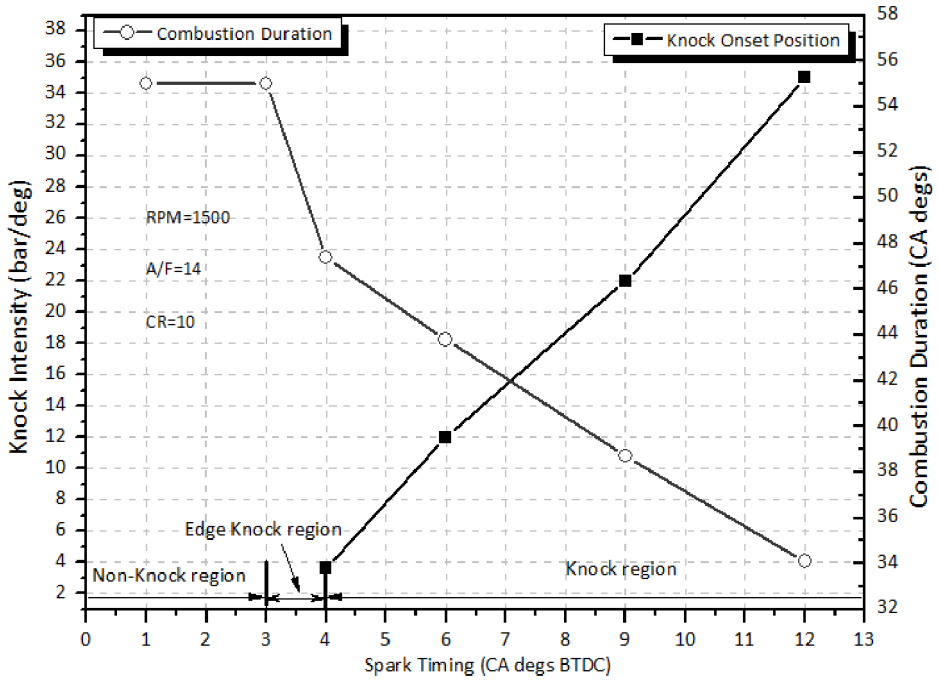

Figure 7-21: Calculated knock intensity and combustion durations in respect of sparking timings

Figure 7-21 shows the simulated knock intensity and combustion duration at various spark timings. It shows that as the spark timing delays, the knock intensity reduces. Again, this is contributed to the fact that the retardation of spark timing delays the

combustion event and smoothes the strength of the flame propagation. The less compression and heat transfer from the delayed combustion reduces the strength of the knock and of course retards knock timing too. On the other side, the combustion duration increases as the spark timing retards. Again, this is mainly due to reduction in flame propagation strength.

7.5 Summary and Conclusions

High load performance and fuel economy of gasoline engines are limited by knocks. Such limitations are becoming worse when the engine is heavily super-charged for high BMEP outputs. Spark ignition timing retardation has been an efficient method to avoid the knock but results in reduced engine performance and poor fuel economy. A better understanding of knock, which could be used to optimize the engine design, ignition timing optimization in particular, is important.

In this chapter, a simulation model for SI engine knock has been developed. The model is based on a three-zone approach (unburned, burning and burned zones). The in-house FORTRAN code, LUCKS_SI in the LUCKS package integrating the DVODE solver for the ODEs, has been developed to simulate combustion systems with chemical kinetics. The Tanaka's reduced chemical kinetics model for a commercial gasoline fuel with an RON of 95 has been modified and applied in both burned and unburned zones. The Tanaka's model used in the model was initially developed for the autoignition of HCCI combustion. The reaction rate constants of the R6 and R18 in the chemical kinetics have been modified to improve the accuracy of autoignition prediction under SI combustion. Applying the Tanaka's reduced chemical kinetics model provides simulation of both post-flame heat release and pre-flame autoignition. The burning zone is modelled by an equilibrium combustion thermodynamic model. A knock detection and process method has been developed to analyze the recorded cylinder pressure, identify the knocking cycles and determine the knock timing. The model has been validated against engine test data. Good agreements have been obtained. The model shows the potential in analyzing the relationship among ignition timing, intake boost pressures and knocks.

Chapter Eight: **Multi-Zone Kinetic Modelling of HCCI Combustion**

8.1 Introduction

The autoignition combustion with homogeneous air and fuel mixture in a Internal Combustion Engine (ICE) offers the potential of high efficiency, low NO_X and low particulate matter emissions. The combustion concept suits to various fuels, but each fuel has a different autoignition behavior, which requires a unique engine control strategy. For fuels with high cetane number, the thermal threshold of the autoignition is low. The high compression ratio of the diesel engine design leads to an undesirable early autoignition. Cooled external Exhaust Gas Re-circulation (EGR) is often needed to dilute the engine charge and delay the autoignition to an acceptable level. The technology is often referred as the Homogeneous Charge Compression Ignition (HCCI) combustion. For fuels with high octane number, the thermal threshold of the autoignition is high. They need extra thermal energy to promote the autoignition. The hot Internal Exhaust Gas Re-circulation (IEGR) achieved using various valve control strategies is a feasible technology to initiate such a combustion. It is often named as Homogeneous Charge compression Ignition (HCCI) combustion, and is the centre of this modeling study.

The autoignition combustion is a chemical-controlled combustion process and is influenced by the in-cylinder turbulence and engine charge mixing. The in-homogeneous in-cylinder conditions affect combustion performance and emissions [53]. In addition, the unburned and partial burned gas mixture transported into or out of the boundary layer and crevice have significant impact on CO and HC emissions.

Modeling study is a valuable tool in understanding the combustion mechanism.

Aceves et al. [53] developed a sequential hybrid approach integrating a Computational Fluid Dynamic (CFD) model (KIVA) with a multi-zone model coupled with detailed chemical kinetics. The CFD model was employed to solve the temperature and mixture composition until a transition angle prior to ignition and Babajimopoulos et al. [209] developed a parallel hybrid approach communicating a CFD model (KIVA) with a multi-zone model solving detailed chemical kinetics at each computational time step, during which the thermodynamic states and composition in both of the models are updated by each other. Orlandini et al. [136] divided the combustion chamber into zones by assuming a constant temperature gradient between the hottest zone and the coldest zone. The methodology simplified the calculation but has limited power in simulating the in-homogeneity of the engine charge. Ogink and Golovitchev [52] and Easley et al [133] divided the cylinder volume into inner core zones, one outer core zone, a boundary layer and a crevice zone at the beginning of the simulation. Mass transfer was considered only between the outer core zone and the boundary layer, and between the boundary layer and the crevice. The in-cylinder mixture was assumed uniform across the combustion chamber. Komninos et al. [131,134] assumed that all zones have an equal thickness at TDC. The in-cylinder temperature and composition at initial calculation point were assumed uniform throughout the cylinder. These previous studies showed that the multi-zone modeling requires less computational resources and has the capability of describing the chemical and physical phenomenon in HCCI engines, making it efficient methodology to study these issues.

In order to describe the chemical and physical processes of the HCCI combustion and to investigate the effect of IEGR on combustion performance and emissions efficiently, the multi-zone modeling technique has been employed in this work. In the model, the combustion chamber is divided in to a number of apportioned volume elements at Inlet Valve Opening (IVO) position. This is to take account of the inhomogeneity of in-cylinder mixture and the IEGR. The apportionment is kept constant throughout the simulation cycle with the exception of the crevice volume. Chemical kinetic mechanism is applied in each zone to simulate the combustion and the heat release. Model results are validated against the experimental observations.

8.2 Model Formulation

8.2.1 Major Assumptions

The major assumptions of the multi-zone model developed in this work are:

- The combustion chamber is divided into ten individual zones: eight core zones, a crevice volume zone, and a boundary layer zone as shown in Figure 8-1.
- The gas mixture in each zone is locally homogeneous. The thermal properties and the compositions of the charge mixture of fresh air-fuel and IEGR have been calculated by a gas mixing model reported in [112].
- The in-cylinder temperature at IVO position is inhomogeneous. It decreases from the innermost core zone to the boundary layer.
- The pressure is uniform throughout the cylinder
- There is no heat transfer between boundary layer and the neighbouring core zone and between adjacent core zones.
- The crevice volume takes 3% of the cylinder clearance volume and has a constant temperature equal to the cylinder wall [1]. Both volume and temperature remain constant throughout the simulation.
- The volume of the boundary layer zone at IVC position is calculated by assuming a thickness of 0.3mm.
- The zones are defined by fixed volume fractions according to a Gaussian-like distribution at the IVC position as shown in Figure 8-2. The fractions remain unchanged throughout the calculation with the exception of the crevice volume.

8.2.2 Governing Equation

The chemical kinetics was introduced into each of the 10 zones. The change rate of the mass fraction of a species, *j*, in the zone, *i*, is calculated by

$$\frac{dY_{i,j}}{dt} = \frac{\dot{\omega}_{i,j} M_j}{\rho_i} \qquad \textbf{8-1}$$

Where M_j is the molar mass $\dot{\omega}_{i,j}$ is the molar production rate, and ρ_i is the zone density.

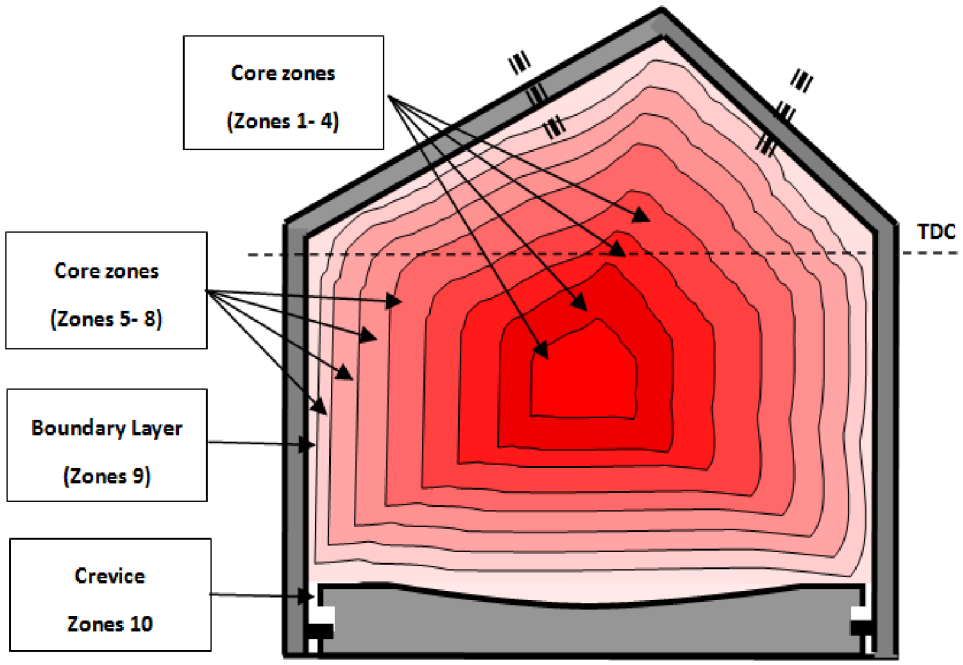

Figure 8-1: Zone configuration

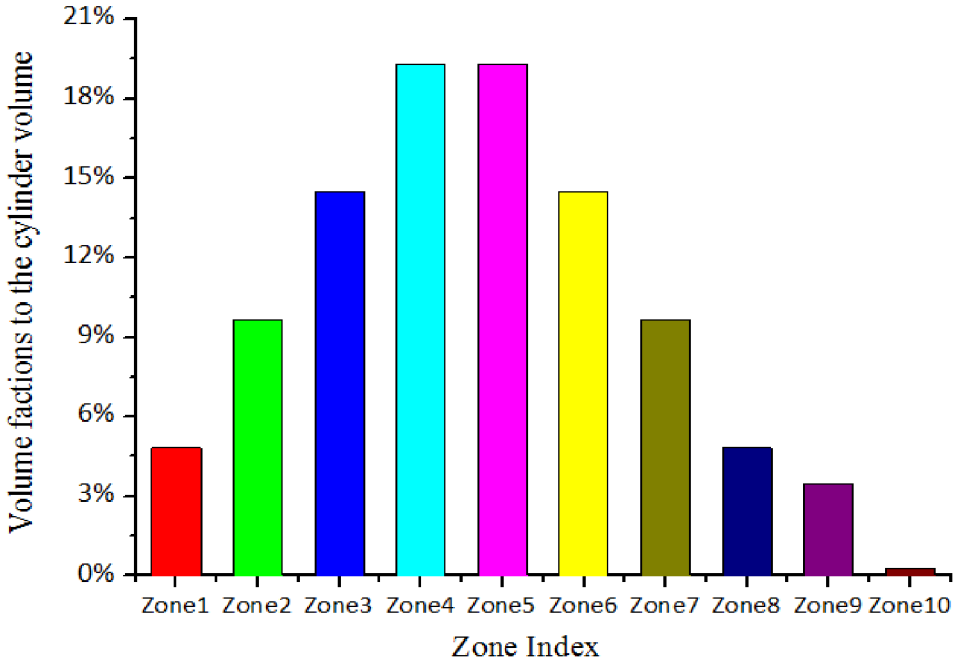

Figure 8-2: Zone fraction distribution in a Gaussian-like shape

The zone energy equation in a general form is

$$\rho_i c_{v,i} \frac{dT_i}{dt} = \frac{\dot{Q}_i}{V_i} + \frac{p}{V_i}\frac{dV_i}{dt} - \rho_i \sum_{j=1}^{n} u_{i,j} \frac{dY_{i,j}}{dt} \qquad \textbf{8-2}$$

where u is the specific internal energy, c, is the specific heat capacity at constant volume, V is the zone volume, p is the cylinder pressure, T is the zone temperature, $\dot{Q}$ is the heat transfer. Note that for the core zones $\dot{Q}$, is assumed to be zero. The heat transfer between the boundary layer zone and the cylinder wall is modelled using the Woschni heat transfer correlation modified by Chang et al. [210].

8.2.3 Mass Mixing

Since the zone apportionment is kept constant, different zone ends with a different volume change rate after each calculation step. This results in different zone thermal properties and zone pressure. In order to keep the pressure uniform across the cylinder, mass has to transfer from higher-pressure zones to the lower-pressure ones. Associating with the mass transfer, energy is transported across zones as well. In this work, the modelling of the mass transportation is carried out at the end of each calculation step. For the zones exporting mass, the thermal properties and gas composition of the zone mixture remain unchanged before and after the mass transportation. The formula of ideal gas law is employed as:

$$P_H^{'}V_H^{'} = \left(m_H^{'} - \Delta m\right) \cdot \frac{RT_H}{M_H} \qquad \textbf{8-3}$$

where subscript H denotes the zones with higher pressure, Δm is the mass transportation between the two neighbouring zones, M_H is the zone molecular mass, P',V' are the zone pressure and volume before the pressure balancing.

For the importing zones, the intake mass mixes with the original mixture and therefore changes the gas properties. The formula of ideal gas law is employed as:

$$P_L^{'}V_L^{'} = \left(\frac{m_L^{'}}{M_L} + \frac{\Delta m}{M_H}\right) \cdot RT_L \qquad \textbf{8-4}$$

where subscript L denotes the zones with lower pressure

For any given two adjacent zones, Thermodynamic and energy equations are applied.

$$m_L c_{p,L} T_L = m_L' c_{P,L}' T_L' + \Delta m c_{p,H}' T_H' \qquad \textbf{8-5}$$

The mixture-averaged specific heats are

$$c_{p,L} = \frac{m'_L \cdot c'_{p,L} + \Delta m \cdot c'_{p,H}}{m_L} \quad \textbf{8-6}$$

Then a system of four equations (8-3-8-6) with four unknowns: $\mathrm{m_L}, \mathrm{c_{p,L}}, \mathrm{T_L}$ and $\Delta \mathrm{m}$, is obtained. With substitution and rearrangement, a quadratic equation of Δm is derived as

$$A \cdot \Delta m^2 + B \cdot \Delta m + c = 0 \quad \textbf{8-7}$$

Where the coefficients of A, B and C are

$$A = \frac{c'_{p,H} \cdot P'_H \cdot T'_H}{M'_H} \cdot \left(1 + \frac{V'_L}{V'_H}\right)$$

$$B = m'_H \cdot c'_{p,H} \cdot T'_H \cdot \left(\frac{V'_H - V'_L}{M'_L \cdot V'_H}\right) + m'_L \cdot c'_{p,L} \cdot T'_L \cdot \left(\frac{V'_H + V'_L}{M'_H \cdot V'_H}\right)$$

$$C = \frac{{m'_H}^2 \cdot c'_{p,L} \cdot T'_L}{M'_L} - \frac{V'_L \cdot m'_H \cdot m'_L \cdot c'_{p,L} \cdot T'_H}{V'_H \cdot M'_H}$$

The solutions to Equation 8-7 are

$$\Delta m = \frac{-B \pm \sqrt{B^2 - 4AC}}{2A}$$

Since Δm indicates the mass transfer from the higher-pressure zones to the lower-pressure zones, its value should not be negative. Thus, the positive root should be taken as the solution of Δm. With the obtaining of Δm, the thermal conditions and mixture compositions of every two adjacent zones can be calculated to keep the pressure uniform. A sequential calculation is then applied to balance the pressure between every two neighbouring zones till the difference of pressure in each zone is within the preset tolerance (0.00001 bars in this work), by which the in-cylinder pressure is regarded as uniform

$$P'_H = P'_L = P \quad \textbf{8-8}$$

8.2.4 Blowby

The blow-by mass flow rate is determined from the isentropic compressible flow relationships [211,212], which is expressed by

$$\dot{m}_{bl} = \frac{C_{bl} \cdot A_{pc} \cdot p}{\sqrt{\overline{R} \cdot T}} \cdot f(p) \qquad \textbf{8-9}$$

where when $\frac{p_o}{p} > \left(\frac{2}{\gamma+1}\right)^{\frac{\gamma}{\gamma-1}}$

$$f(p) = \left(\frac{p_o}{p}\right)^{\frac{1}{\gamma}} \cdot \left\{\frac{2 \cdot \gamma}{\gamma - 1}\left[1 - \left(\frac{p}{p_o}\right)^{\frac{\gamma-1}{\gamma}}\right]\right\}^{\frac{1}{2}}$$

and when $\frac{p_o}{p} \le \left(\frac{2}{\gamma+1}\right)^{\frac{\gamma}{\gamma-1}}$

$$f(p) = \gamma^{\frac{1}{2}} \cdot \left(\frac{2}{\gamma+1}\right)^{\frac{\gamma+1}{2(\gamma-1)}}$$

where subscript bl indicates the engine blowby, A_{pc} is the area of the piston-cylinder gap calculated from measured redial ring clearance, $\overline{R}$ is the specific gas constant. C_{bl} is the model constant, p_o is the atmosphere pressure and γ is the heat specific ratio.

8.2.5 Chemical Kinetic Mechanism

The chemical kinetic mechanism applied in this work is a reduced model for primary reference fuels (PRF) developed by Tanaka et al. [123,154]. The mechanism consists of only 52 reactions with 32 species. It has been tested to reproduce the main features of HCCI combustion under a wide range of conditions but contains no NO_X mechanism. In order to simulate NO_x emissions, a sub-mechanism of NOx formation, derived from Golovithcev's iso-octane mechanism [213], has been added to the Tanaka model. The sub-mechanism includes 4 species and 12 reactions as shown in Appendix C. The addition of the NO_X mechanism should not affect the original model's capability of simulating the main HCCI features.

To verify the new combined model, both the modified and original mechanisms were tested in a single-zone HCCI combustion model at various inlet temperatures. Four calculated combustion performance parameters, ignition timing, peak pressure, maximum pressure increase rate and temperatures at EVO were compared as

shown in Figure 8-3, where the results from the mechanism with NO_X sub-mechanism were normalized by the ones from the mechanism without NO_X sub-mechanism. It can be seen that the addition of NO_X formation chemistry has no effect on the prediction of the ignition timing, and little influence (+/-0.3%) on the maximum pressure increase rate. The addition of the NO_X sub-mechanism lowers the predicted temperature at EVO by about 1% and reduces the maximum pressure increase rate by up to 1.5%. Such reductions may be due to the endothermic character of the NO_X mechanism.

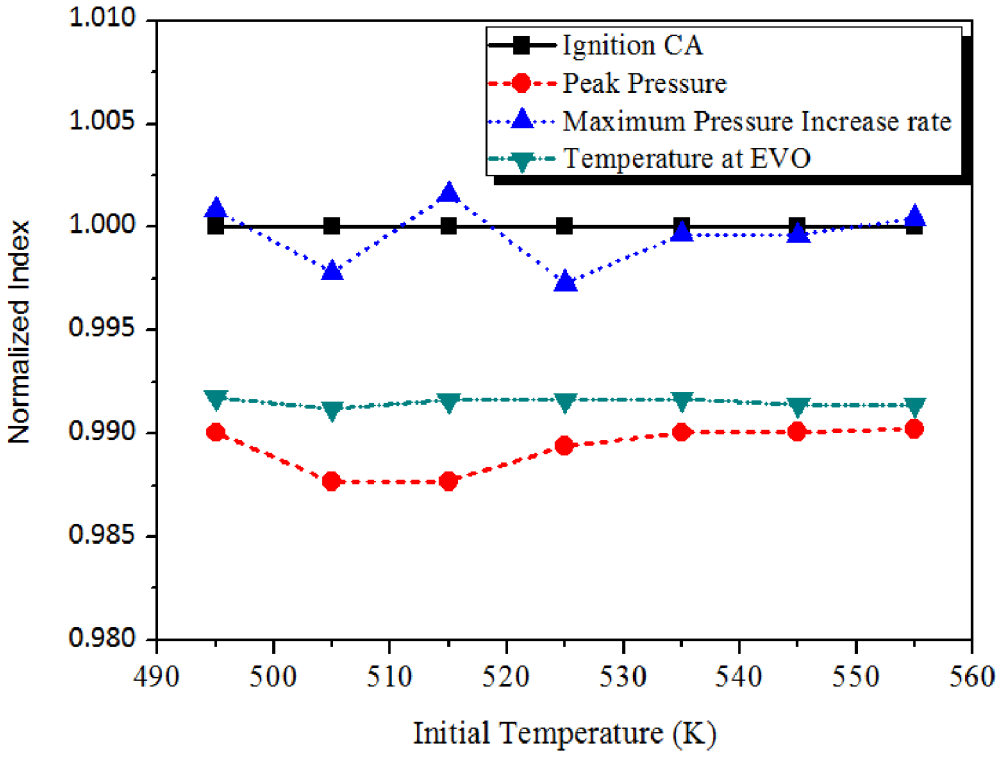

Figure 8-3: Influence of the additive sub-mechanism on the main combustion characters.

8.2.6 Numerical Solution Strategy

Applying the chemical kinetics model and the thermodynamic model on the in-cylinder mixtures forms a set of coupled Ordinary Differential Equations (ODE), which describes the time evolution of the mass fraction of every species and the zone temperatures. For each zone, 36 differential equations are used to express the mass fraction change rates of the 36 species in the combined mechanism and an additional differential equation for the change rate of the zone temperature. Therefore, the ODE system for all the 10 zones comprises a total of 370 equations

with 370 variables.

The previously described in-house FORTRAN code, LUCKS (Loughborough University Chemical Kinetics Simulation), integrating a Double-precision Variable-coefficient Ordinary Differential Equation (DVODE) code has been applied to the model. The numerical procedure the code follows is briefly described in Figure 8-4. The outputs are used to update the pressure of each zone. Then a pressure balance model is applied to simulate the mass exchange among the zones in order to keep the in-cylinder pressure uniform across the zones. The thermal properties and mixture compositions are recalculated and updated after the pressure balance. The simulation is executed from the timing of Intake Valve Closing (IVC) to the timing of Exhaust Valve Opening (EVO), which requires approximately 5-minute CPU calculation time on a Pentium 4 2.4 GHz PC operating on Window XP OS.

8.2.7 Thermodynamic Mixing Model

When Internal Exhaust Gas Recirculation (IEGR) is simulated, the thermodynamic mixing model presented in [112] is used. Given the compositions and temperatures of the fuel-air charge and the IEGR before mixing, the model calculates the thermal properties and compositions of the mixture, and vice versa. In the model, the IEGR gases trapped inside the engine cylinder is assumed to consist of combustion products that are in thermodynamic equilibrium.

8.2.8 Initial Calculation Conditions

The multi-zone model starts the calculation at Intake Valve Closing (IVC) position and ends at EVO. The gas mixture properties and engine conditions at the beginning of the calculation have to be quantified as the initial input conditions.

The heat loss from in-cylinder gas to engine components has a direct impact on the in-cylinder temperature distribution. Due to temperature difference between the in-cylinder gases and the engine components (e.g. the cylinder wall, the piston head and the cylinder head, etc.), heat is transferred out of the in-cylinder gases through the thermal boundary layer and the crevice. As a result, this causes lower temperatures in the outer regions that are close to the cylinder body and higher temperature in the inner regions close to the cylinder centre. This is true to both the IEGR gases trapped inside the cylinder before mixing with fresh engine charge and the mixture of the IEGR, fresh air, and fuel at the IVC position.

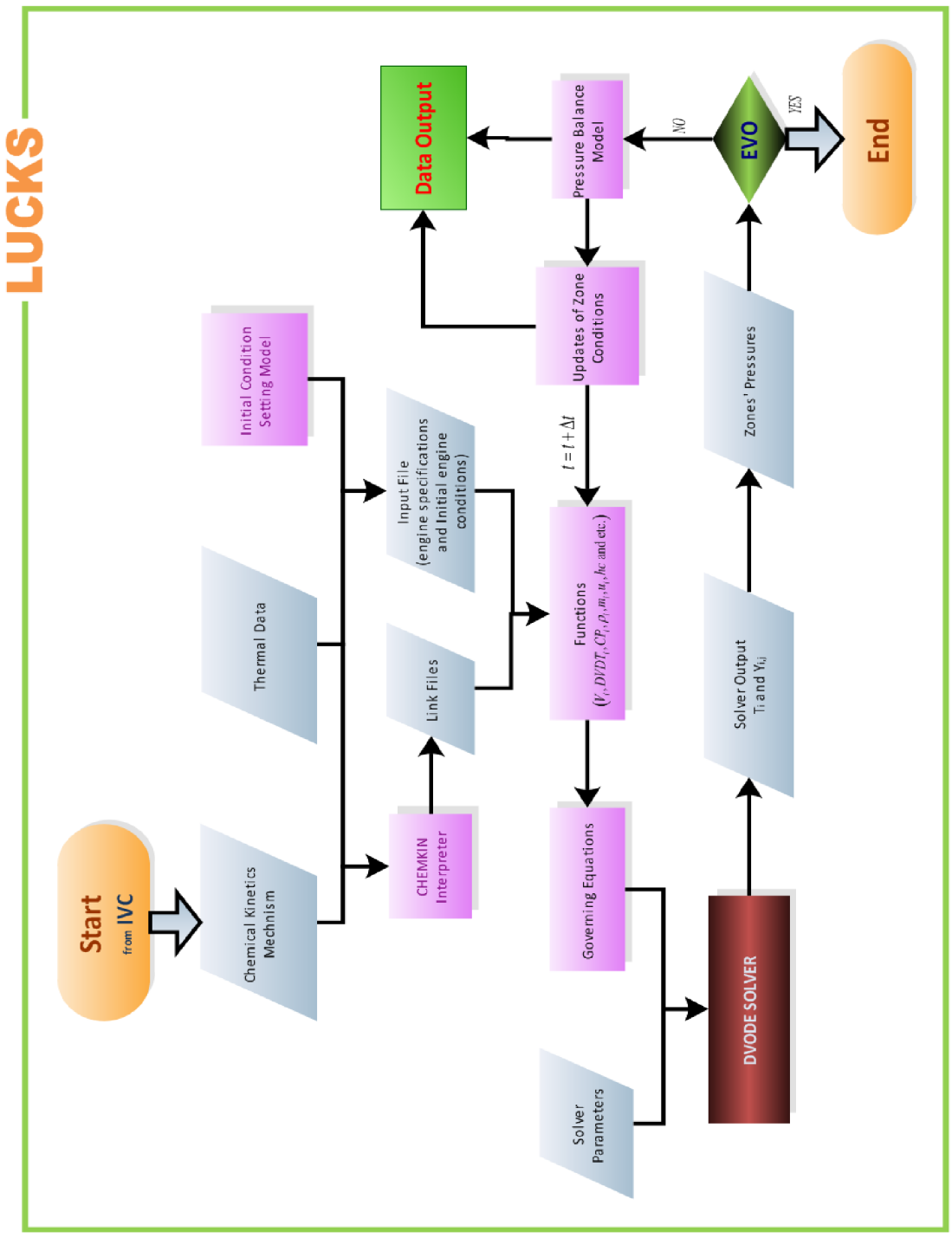

Figure 8-4: The flowchart of numerical procedures in Multi-Zone HCCI engine Simulation.

The gas motion also plays a critical role in temperature and IEGR inhomogeneities. As the inlet air-fuel mixture enters the combustion chamber and mixes with IEGR gases, the flow of the fresh charge primarily moves towards the outer regions and concentrates around the outer regions due to the centrifugal effect of swirls [138].

This leads to both the inhomogeneous distribution of IEGR and temperatures with lower IEGR density and temperature in the outer regions and higher IEGR density and temperature in the inner regions. The results from CFD calculation by Aristotelis [214] also reveal the same pattern of IEGR distribution that the regions with higher residual gas fraction are more close to the cylinder wall and have higher temperature.

However, the spatial distribution of the in-cylinder temperature cannot be obtained through experimental measurement and no general rules have been developed and reported in respect of setting the non-uniform temperature distribution. Therefore, the zone temperatures have to be specified by the users. In this work, these initial conditions were derived from the measured experimental data: the average exhaust temperature, $T_{EGR\_measured}$, the average residual gas fraction (RGF), $f_{EGR\_measured}$, and the inlet air-fuel temperature T_{in}. Making use of these test data provides a genuine condition match between the experiments and the modeling, which avoids arbitrary adjustment of modeling initial conditions. To simplify the case, a linear temperature distribution with a fixed increment ΔT has been assumed in this work. The core zone temperature is

$$T_i = T_{BL} + (NZ - 1 - i)\Delta T \qquad \textbf{8-10}$$

where NZ is the total number of zones.

Since the crevice temperature is set to be the same as the wall temperature, the temperature inhomogeneity starts from the boundary layer zone. With the assumption that the boundary layer temperature equals the cylinder wall temperature being the boundary condition ($T_{BL} = T_{wall}$), the temperature distribution gradient ΔT in Equation 8-10 is therefore the only unknown to solve.

As aforementioned, the mixtures inside very individual zone are assumed to be homogeneous and have the ideal gas properties, so a relation between the average in-cylinder temperature and the zonal temperatures exits when the temperature distribution over the zones is assigned a function. To derive this relation, ideal gas equation is expressed as

$$n = \frac{p \cdot V}{RT} \qquad \textbf{8-11}$$

Based on the molecular conservation of the in-cylinder mixture ($n_{total} = \sum n_i$) and

the assumption of uniform in-cylinder pressure and gas constant across the chamber, the following equation is obtained

$$\sum_{i=1}^{n} \frac{V_i}{T_i} = \frac{V_{cyl}}{T_{ave}} \quad , \quad (\mathrm{i} = 1, \mathrm{NZ}) \qquad \textbf{8-12}$$

The cylinder volume V_{cyl} at IVC is calculated in use of the traditional Slider-Crank Model. The average in-cylinder temperature $T_{average}$ at IVC is calculated through the thermodynamic mixing model with the measured overall EGR temperature $T_{EGR\_measured}$ and inlet temperature T_{in} as the inputs. Solving the two correlative equations 8-10 and 8-12 provides the solution of the temperature distribution gradient ΔT so that the zone temperatures T_i can be calculated from Equation 8-10.

In reality, the mixing of the intake charge and residual gases is a kinetic process starting from the moment of IVO to the beginning of compression stroke at IVC. However, in this study, this process has to be assumed a perfect mixing process happening instantaneously right at IVC so that the initial zone temperatures and zone mixture compositions can be calculated. The intake charges are assumed to have uniform properties over the zones, but temperature inhomogeneity in the residual gases before mixing needs to be taken into account due to the significant temperature difference between residual gas and cylinder wall. The same temperature distribution principles as the ones for the in-cylinder temperature are applied and a linear function is assigned to zone EGR temperature as

$$T_{EGR\_i} = T_{EGR\_Bl} + (NZ - 1 - x) \cdot \Delta T_{EGR} \qquad \textbf{8-13}$$

In Equation 8-13, to define the EGR temperature of a specified zone, three unknowns need to solve and they are the zone EGR temperature T_{EGR_i}, the EGR temperature in the boundary layer T_{EGR_BL} and EGR temperature gradient ΔT_{EGR}. Again, it is assumed that the in-cylinder gases have ideal gases properties and based on the molecular conservation of the in-cylinder residual gases ($n_{EGR\_total} = \sum n_{EGR\_i}$), the following equation is yielded

$$\sum \frac{V_i}{T_{EGR\_i}} = \frac{V_{cyl}}{T_{EGR\_measured}} \quad , \quad (i = 1, NZ) \qquad \textbf{8-14}$$

With Equation 8-13 and 8-14, one more condition is needed to form a solvable equation system with three equations and three unknowns. Herein exits another relation between the cylinder and the zones that the total EGR volume equals the sum of the zone EGR volume. This can be expressed as

$$\sum f_{EGR\_i} \cdot V_i = f_{EGR\_measured} \cdot V_{cyl} \qquad \textbf{8-15}$$

Though Equation 8-15 does not directly involve either of the unknowns in Equation 8-13, it can function as a computation condition. The algorithm is depicted in the flowchart in Appendix D, in which, the measured $T_{EGR\_measured}$, T_{in} and $f_{EGR\_measured}$ were used as the input conditions. First, these input conditions were used in the thermodynamic mixing model to obtain the average in-cylinder temperature $T_{average}$. Numerical iterations of the zone temperature increment ΔT , shown on LHS of the flowchart, were implemented till Equation 8-12 is fulfilled. The derived ΔT then imported to Equation 8-12 to decide the zone temperature T_i and the zone EGR temperatures T_{EGR_i}.

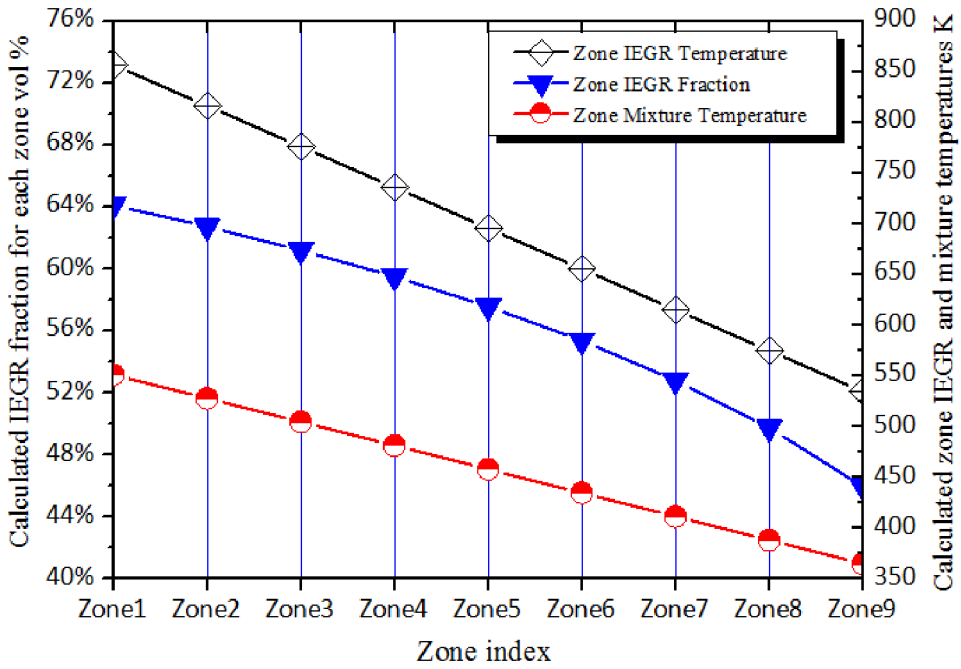

Figure 8-5: Calculated IEGR fraction, IEGR temperature and mixture temperature for each zone at 58% IEGR.

In parallel, two nested iteration loops illustrated on RHS were implemented. The

outer loop used T_{EGR_BL} as iteration variable and Equation 8-15 as the iteration condition. The inner iteration loop corresponding to the Equations 8-13 and 8-14 was used to derive the zone EGR temperature T_{EGR_i} at each T_{EGR_BL}. Next, the zone temperatures T_i and the zone EGR temperatures T_{EGR_i} were used in the thermodynamic mixing model to yield the zone EGR fractions f_{EGR_i} at each T_{EGR_BL}. Finally, Equation 8-15 was examined as the iteration condition. The match to the condition indicates the solutions of zone temperatures, zone EGR temperatures and zone EGR fractions at IVC, which were then imported to the thermodynamic mixing model to obtain the zone mixture compositions, $Y_{i,j}$. It is noteworthy that, with the above algorithm, only approximate solutions can be achieved and iteration tolerances have to be defined, and multiple solutions are avoided by specifying specified iteration bounds based on empirical estimate and verifying the physical meanings of the solutions according to the real engine conditions.

The calculated zone EGR temperatures, zone mixture temperatures and zone EGR fractions at 58% IEGR are shown in Figure 8-5. It can be seen that with the linear zone temperature increase from outer zone to inner ones as assumed, the zone EGR fraction increases non-linearly with higher EGR fractions in the hotter zones, which agree with the discussion in the early context.

8.2.9 Average In-cylinder Temperature

The average in-cylinder temperature is calculated by applying the ideal gas equation to the in-cylinder bulk mixture and the mixture in each zone, respectively, which gives

$$n_{total} = \frac{p \cdot V_{cyl}}{R \cdot T_{average}} \text{ and } n_i = \frac{p \cdot V_i}{R \cdot T_i}$$

As $n_{total} = \sum n_i$, $T_{average}$ is then expressed as:

$$T_{average} = \sum \frac{V_i}{T_i} \qquad \textbf{8-16}$$

8.3 Results and Validation

The engine that the calculation referring to is a single cylinder, four-stoke research engine based on the architecture of the 1.8-litre GM Family One engines. A Research Active Valve Train (AVT) system is applied to allow the variable valve timing strategy to be used. The predefined quantity of residual gases are trapped by implementing the early exhaust valve closure (EVC) event coupled with the late inlet valve opening (IVO) event. The general principle of the valve timing strategy is illustrated in Figure 8-6. In that way, a major amount of the available residual gas was trapped inside cylinder (up to 80%) and a rest was discharged through the exhaust system. Trapping the exhaust gases on this way is normally termed Internal Exhaust Gas Recirculation (IEGR) process. A detailed description of the test engine and the fitted AVT system were reported in [90,215].

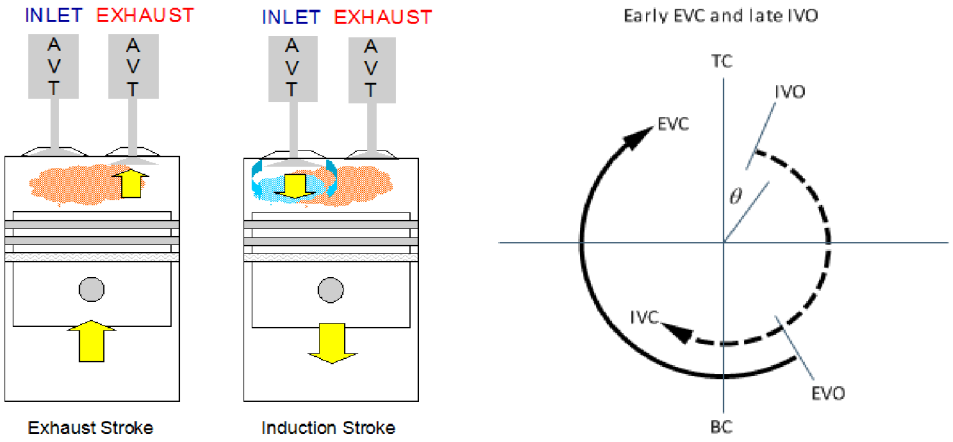

Figure 8-6: The general principle of the valve timing strategy.

The quantity of IEGR is defined as the volume percentage of exhaust gasses trapped inside the cylinder by closing exhaust valves relatively early in the exhaust stroke. The stoichiometric equivalence ratio in this work is referred to the property of fresh air-fuel mixture before mixing with IEGR. The major engine specifications and operating conditions imported into the model calculation are listed in Table 8-1.

The engine test data used to validate the model are those with IEGR levels between 50% and 58%, where stable HCCI combustion has been achieved. The fuel used in the test was commercial gasoline with RON of 95. The engine was tested with a fixed speed of 2000rpm, a fixed air to fuel equivalence ratio of $\phi = 1$, and a fixed load of 2 bar BMEP. Each set of experimental results are taken from an average of 300 consecutive cycles. The engine specification and conditions used in the simulation were the same as those used in the experiment and summarized in Table 8-1. The

zone temperatures and mixture composition at IVC were estimated using the approach presented in the previous section. For the simulation of gasoline fuel with 95 RON, a mixture of isooctane and n-heptane fuels (95% of iso-octane and 5% of n-heptane by volume) is used.

Table 8-1: Engine parameters and operating conditions

Parameter	Value
Bore	80.5
stroke	88.2
Swept volume	450 cm^3
Compression Ratio	11
Speed	2000
Load range	2bar (BMEP)
Number of valves per cylinder	4
Valve Control	Electro-hydraulic Lotus AVT-FVVT system
Fuel Injection	Port fuelled
Fuel	Gasoline (RON 95)
Equivalence ratio	Stoichiometric
Intake Temperature	25^{O}C
Inlet pressure	Natural Aspirated
IEGR	Up to 80% (by volume)
IVC	37 CA degree aBDC
EXO	324 CA degree aBDC

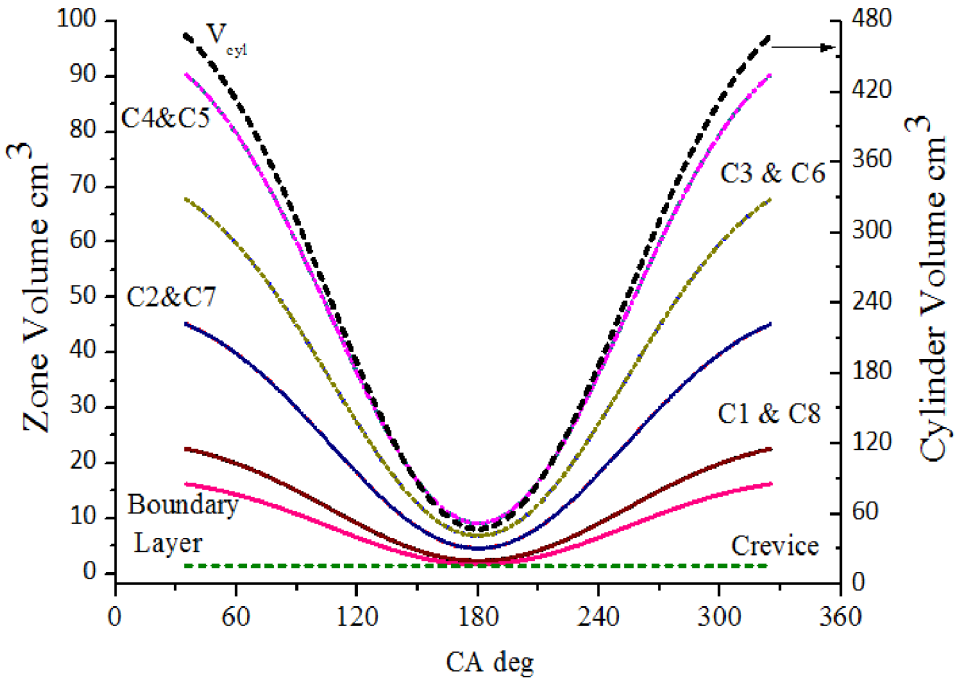

Figure 8-7: Zone volume and cylinder volume in respect of crank angle.

Figure 8-7 shows the calculated zone volumes and the overall cylinder volume in respect of crank angle. It shows that the volume of each zone, except the crevice volume, changes with the piston movement. Again, the zone volumes were distributed according to the Gaussian-like shape, and the boundary layer volume was calculated based on the fixed ratio to overall cylinder volume at IVC. The TDC is positioned at 180 deg CA in the model.

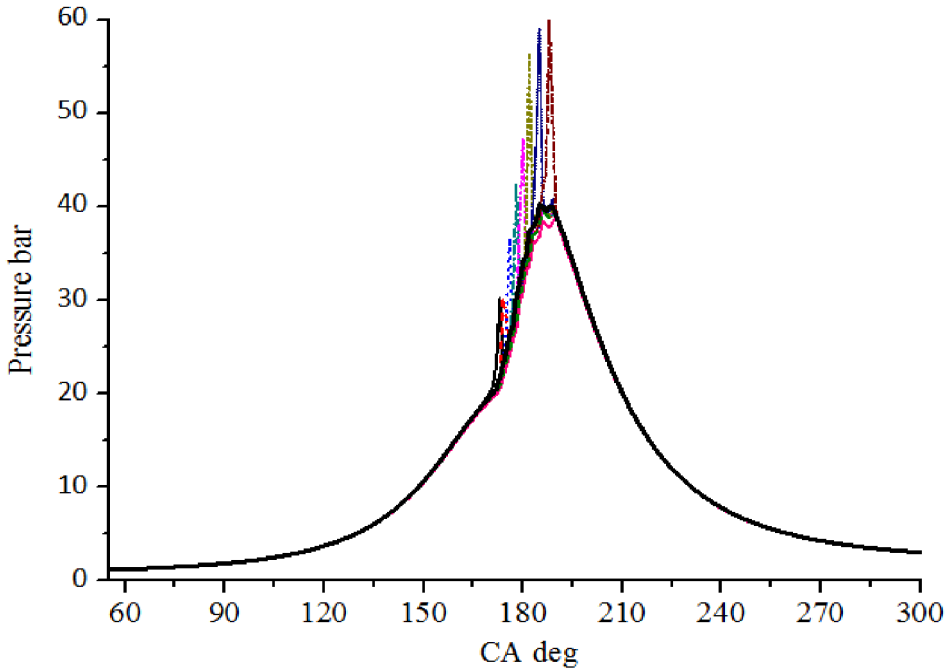

Figure 8-8: Zone pressure and average cylinder pressure (Refer to Figure 8-9 for an enlarged view).

Figure 8-8 and Figure 8-9 show the pressure history of each zone before the zone pressure is balanced to the overall cylinder pressure at the end of each calculation step. It shows that the ignition occurs first in the innermost core zone (C1). This is clearly due to the fact that the innermost zone has the highest temperature. After the ignition in the innermost zone, the rest of the zones ignite sequentially from the inner zones to the outer ones. The boundary zone and crevice zone have no ignition due to the low temperatures in these zones. The overall in-cylinder pressure curve showed in Figure 8-9 exhibits a wave shape curve during the combustion phase. This is of course due to the limitation of zone number. Increase in the number of zones would smooth the pressure wave but at the expense of longer simulation times [133].

The temperature of each zone and the average in-cylinder temperature are depicted in Figure 8-10. Again, it shows the ignition sequence from inner hot zones to outer

cooler ones. Figure 8-10 also shows the low temperature of the boundary layer and the crevice, in which no ignition occurs. One of the reasons for the lower temperature in boundary layer and crevice is that the high contact area ratios between the two zones and engine components (cylinder wall, piston head, etc.) result in high heat transfer rate. Another reason is that the mixtures in boundary layer and crevice are thermally less affected by IEGR due to the lower IEGR fractions as compared with the core zones as explained above. Successfully simulating the low temperature history of the boundary layer and crevice allows the prediction of the HC and CO emissions that both mainly resulted from the mixtures trapped in the boundary and crevice.

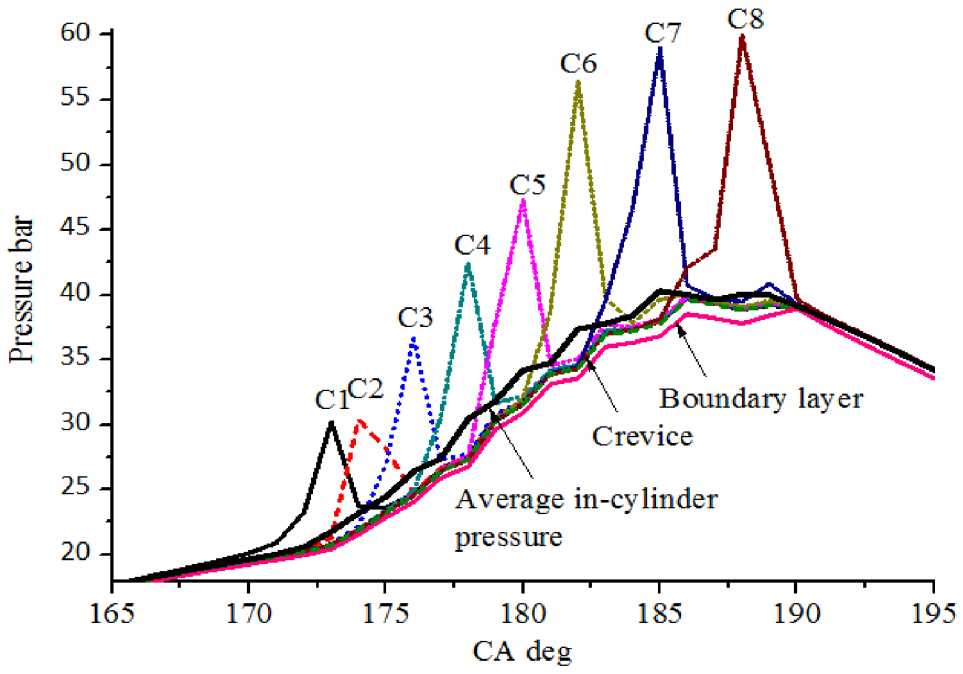

Figure 8-9: Zone pressure and average cylinder pressure – the enlarged image of Figure 8-8.

Figure 8-11 illustrates the mass exchange between neighbouring zones. As mentioned previously, the in-homogeneity of the in-cylinder mixture results in thermal properties which leads to different zone pressure. The difference in pressure then causes mass transfer across neighbouring zones to balance the zone pressures to a uniform in-cylinder pressure. During the compression, the mass in each core zone slightly decreases and the mass in the boundary layer and crevice increases. This is because the core zones have higher initial temperature and thus higher pressure increase rate, which lead to the mass flow out of the core zones into the boundary

layer and then into the crevice. With ignition sequentially occurring from inner core zones, mass is compelled out of the inner zones to the outer zone during the early combustion phase, which is illustrated in Figure 8-11 by the mass decrease of inner core zones (C1, C2, C3 and C4) and the mass increase of outer zones (C5, C6, C7 and C8). When ignition takes place in the outer core zones, the burst of the zone pressure leads to the backward mass flow to the inner core zones during the later stage of combustion, which can be noticed from the increase of the mass in the inner core zones and decrease of the mass in the outer core zones. The mass in the boundary layer and the crevice keep increasing during the combustion phase until all the core zones ignite their mixtures and then gases starts flowing back to the inner core zones. During the expansion, the mass from the crevice flows into the boundary layer leading to the mass increase in the boundary layer, which consists of unreacted and partially reacted mixtures that are regarded as the main source of the HC and CO emission.

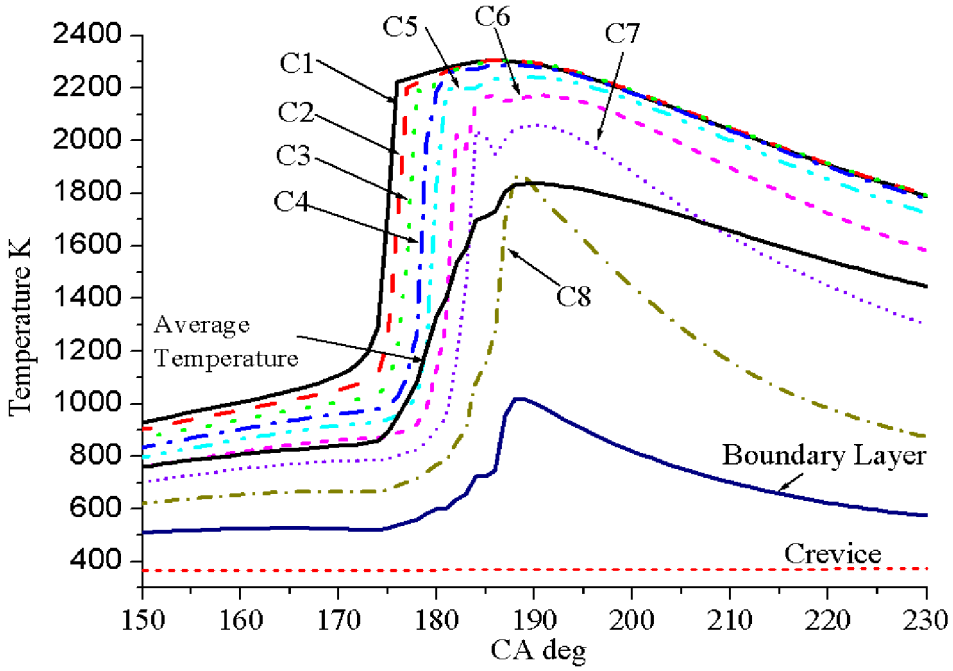

Figure 8-10: Zone temperature and average cylinder temperature.

The calculated cylinder pressure histories are compared to the cylinder pressure histories recorded in the test with an IEGR of 50% and 58% in Figure 8-12 and Figure 8-13. It can be seen that the general shape of the experimental cylinder pressure curve is well reproduced over the closed cycle, except that the calculated pressure curve is not as smooth as the pressure curve averaged from 300 cycles.

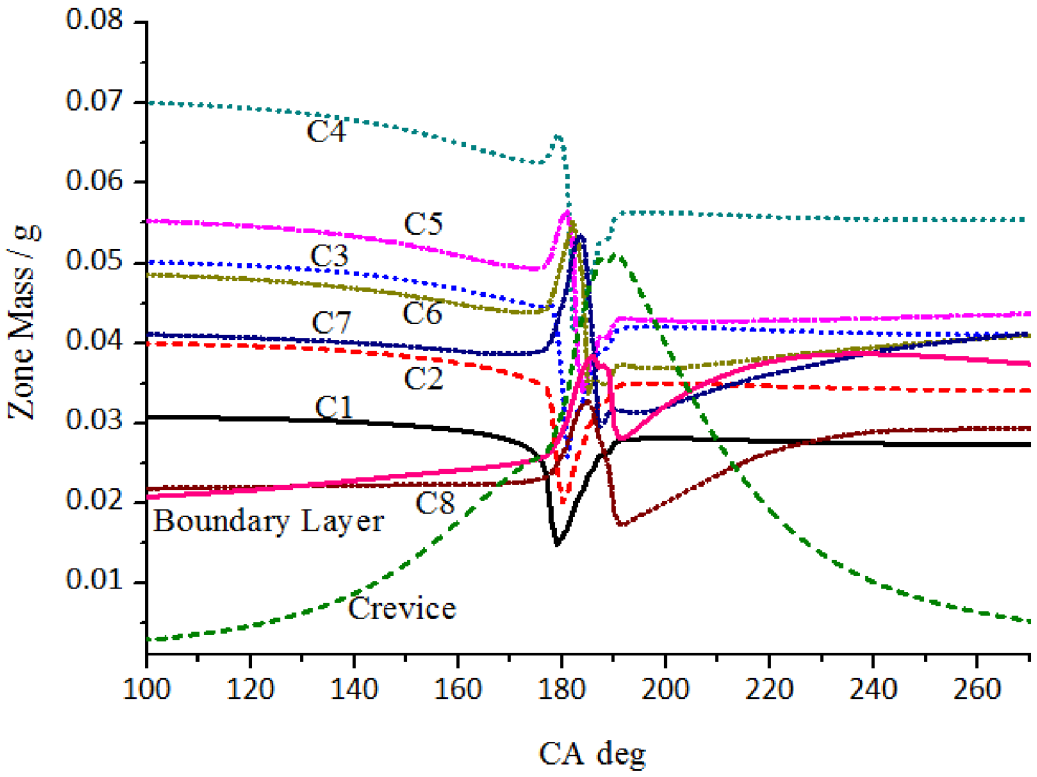

Figure 8-11: Zone mass histories in respect of crank angle.

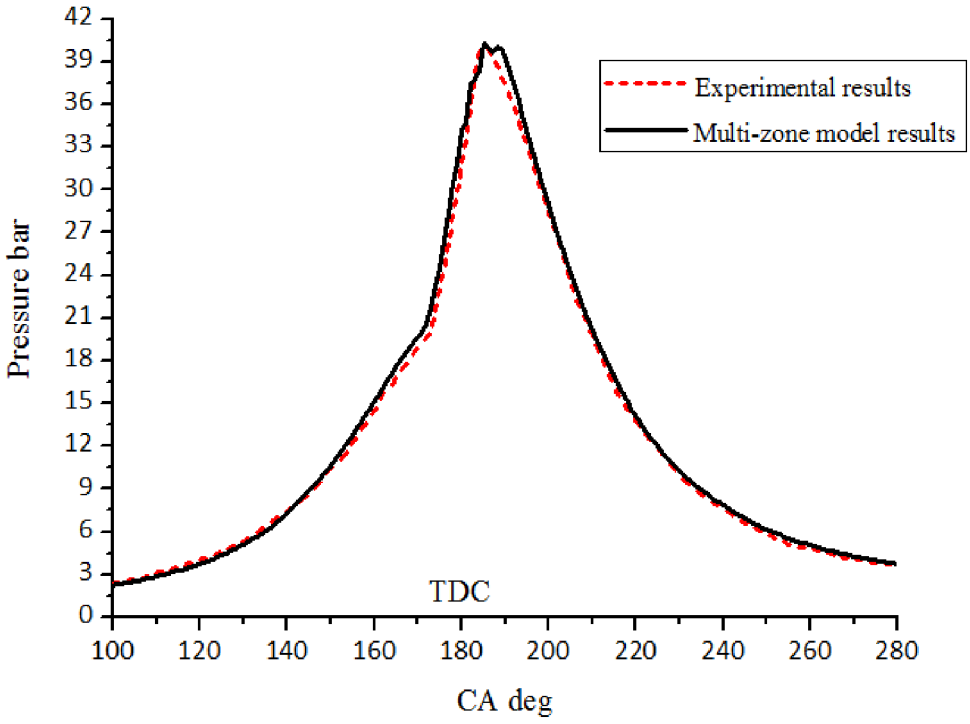

Figure 8-12: Comparison of the calculated pressure curve with experimental results at 58% IEGR.

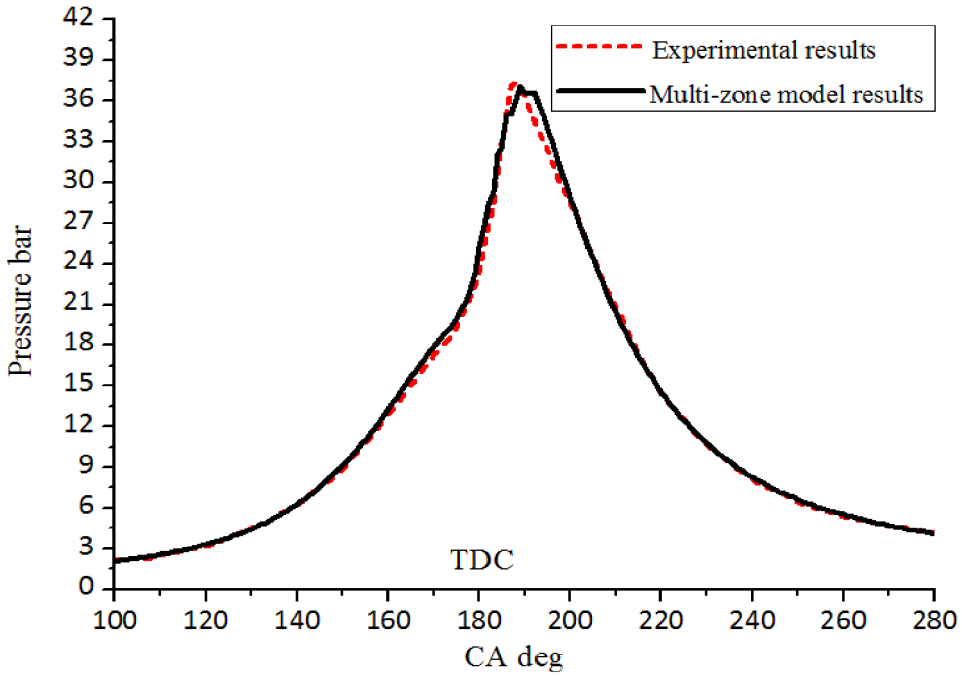

Figure 8-13: Comparison of the calculated pressure curve with experimental results at 50% IEGR.

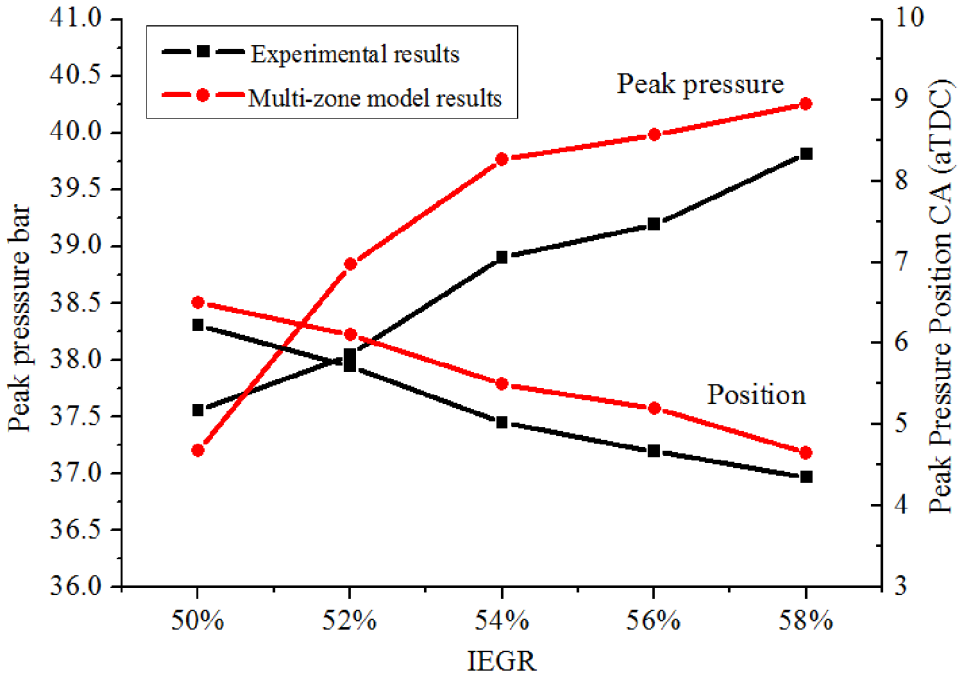

Figure 8-14: Comparison of calculated and measured peak pressure and peak pressure position at various IEGR.

Figure 8-14 compares the measured peak pressure and peak pressure positions with the predictions by the multi-zone model. The peak cylinder pressure is a bit over predicted, which probably results from the omission of the heat transfer between the

neighbouring zones and the prediction of boundary layer volume during the combustion. The effect of IEGR on the in-cylinder pressure is well depicted in Figure 8-14. It can be seen that as the IEGR amount increases, peak cylinder pressure increases and the peak pressure position advances. This may attribute to the thermal effect of IEGR due to its high temperature. When the hot IEGR is mixed with cool air fuel mixture, it improves the temperature of the entire inlet charge and helps the initiation of the ignition of the mixtures, so ignition timing advances and peak pressure increases.

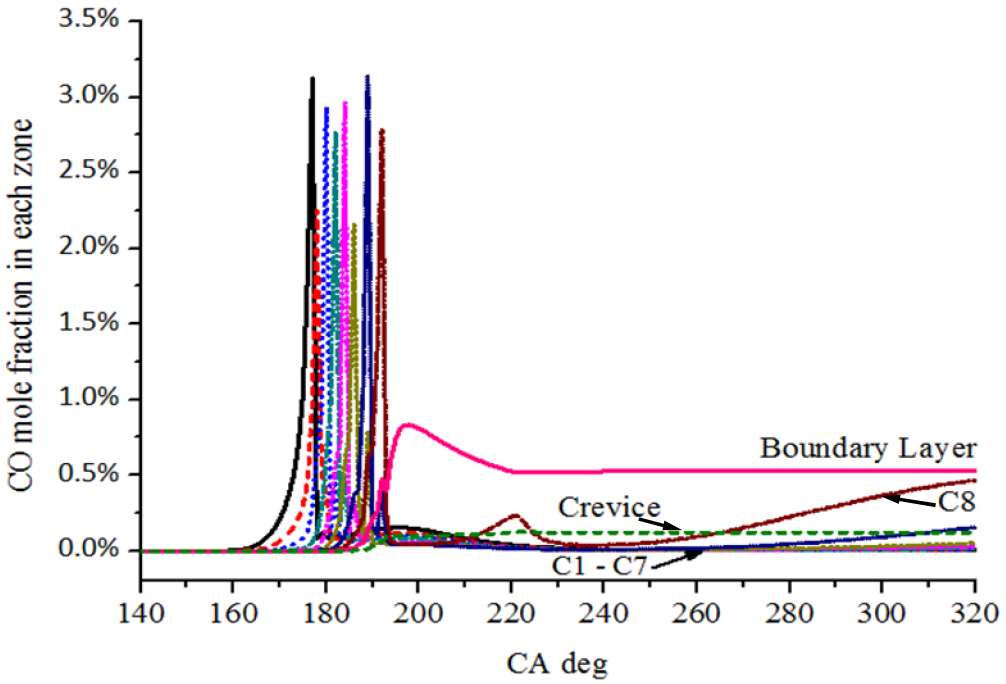

Figure 8-15: CO mole fraction history for each zone against crank angle at 58 % IEGR.

The CO emission distribution over the zones is shown in Figure 8-15. It can be seen that CO product in each core zone starts to build up with the ignition of the zone mixtures and reaches the peak values during the initial oxidation of the fuel molecules, and then sharply reduced to the lowest level due to the further oxidation of CO to CO2 at high temperature. In the boundary layer, fuel oxidation freezes early in the expansion stroke, resulting in a high concentration of CO. Owe to the high pressure during the combustion process, a part of the mixtures containing CO is compelled into the boundary layer and the crevice during the main combustion period. This is clearly illustrated by the increase of the CO fraction in the boundary layer and the crevice during the later stage of combustion. With the gases cooling

down during the expansion stroke, the reactivity of CO oxidation is weakened in the boundary layer so CO cannot be further converted into CO2. As the pressure of the core zones further decreases during the expansion stroke, the unreacted and partially reacted mixtures trapped in the boundary layer and the crevice during the main combustion flows back to the core zones. The CO in the backward flow contributes to the increase of CO fraction in the core zones and some of the unburned or partially burned HC in the backward flow can be further oxidized in the core zones to produce additional CO, which also causes the increase of the CO fraction in the core zones.

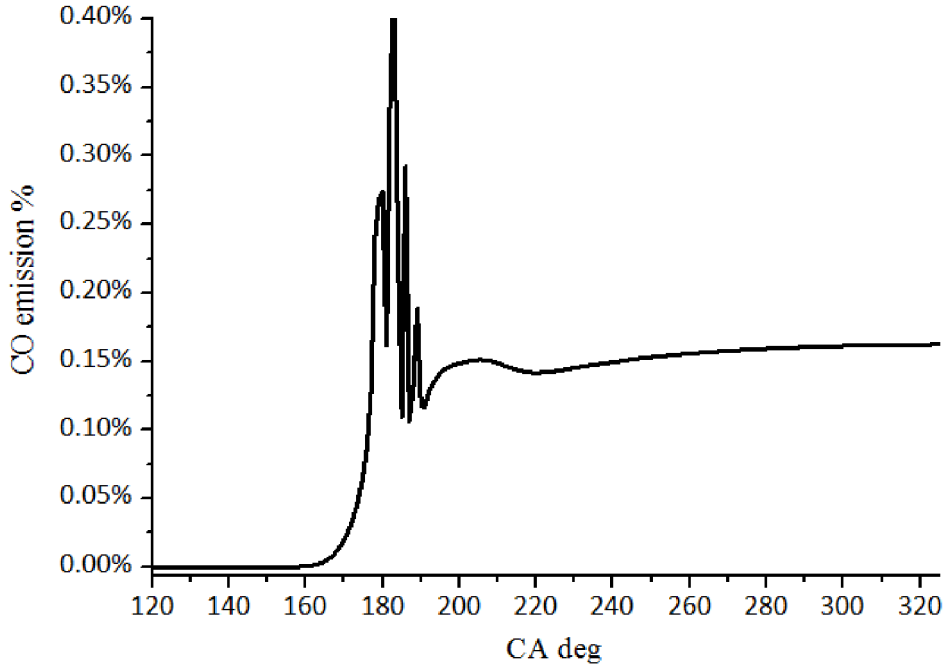

Figure 8-16: In-cylinder CO history against crank angle at 58 % IEGR.

Figure 8-16 depicts the overall in-cylinder CO concentration against crank angle. The results obtained are consistent with the trend found from the CO histories in each zone. The overall CO starts to increase from the beginning of combustion and peaks several times during the combustion due to the sharp CO increase in each zone. Then, CO is further oxidized to CO_2 to reach a low level during the early stage of the expansion. As the mixture is further cooled down, the HC in the outflow from the boundary layer and the crevice cannot be completely oxidized to CO_2 resulting in the increase of CO in the later expansion stroke.

Figure 8-17 shows the comparison between the calculated and measured CO

emission at various IEGR. The agreement between the two is good. The calculated results showed the trend of slightly increase in CO emissions as IEGR increases. Such a trend is reasonable since the IEGR dilutes the engine charge and lowers the combustion temperature which further leads to a reduction in oxidation of CO. The measured results shows a similar trend, judged from the results with 50%, 56% and 58% of IEGR. The measured results with 52% and 54% appear differently, which may be due to a change of test conditions. The overall CO emission has been under predicted by the model. This may attribute to the fact that the lack of the heat transfer between the neighbouring zones in the model which leads to the prediction of a higher in-cylinder temperature. In addition, the boundary layer volume fraction is calculated at IVO, which may not reflect the real scenario accurately.

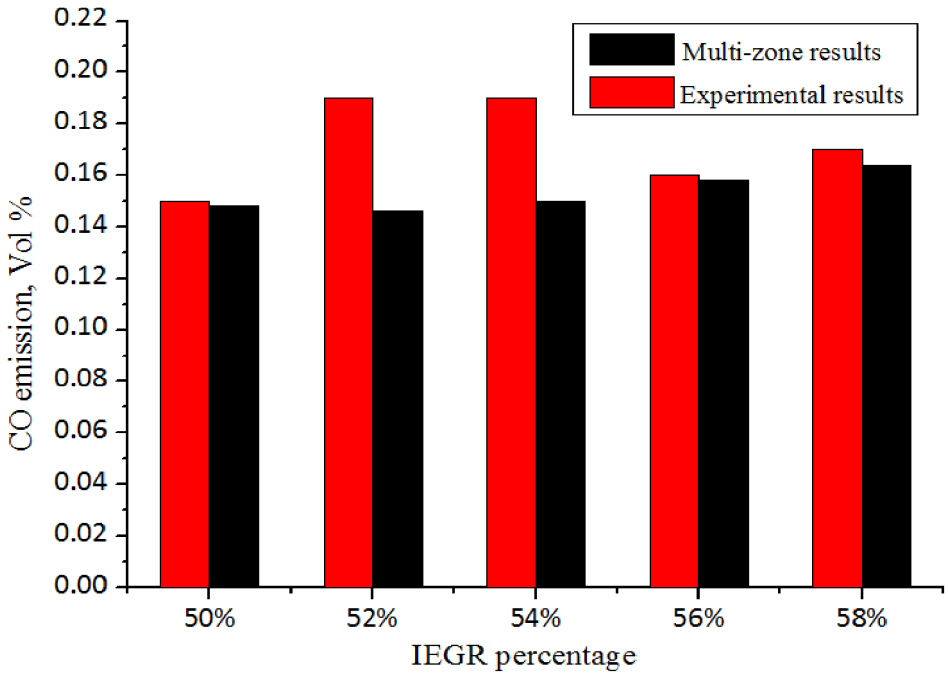

Figure 8-17: Comparison of the calculated CO emission with the experimental results at various IEGR.

The calculated HC concentrations of each zone are given in Figure 8-18. It shows that the majority of the formed HC in core zones have been oxidized during the main combustion event. However, the HC concentration remains high in the boundary layer and the crevice. This agrees with the fact that a portion of unburned and partially burned HC were compelled into the boundary layer and the crevice during the main combustion event and could not be further oxidized due to the low temperature in these two regions

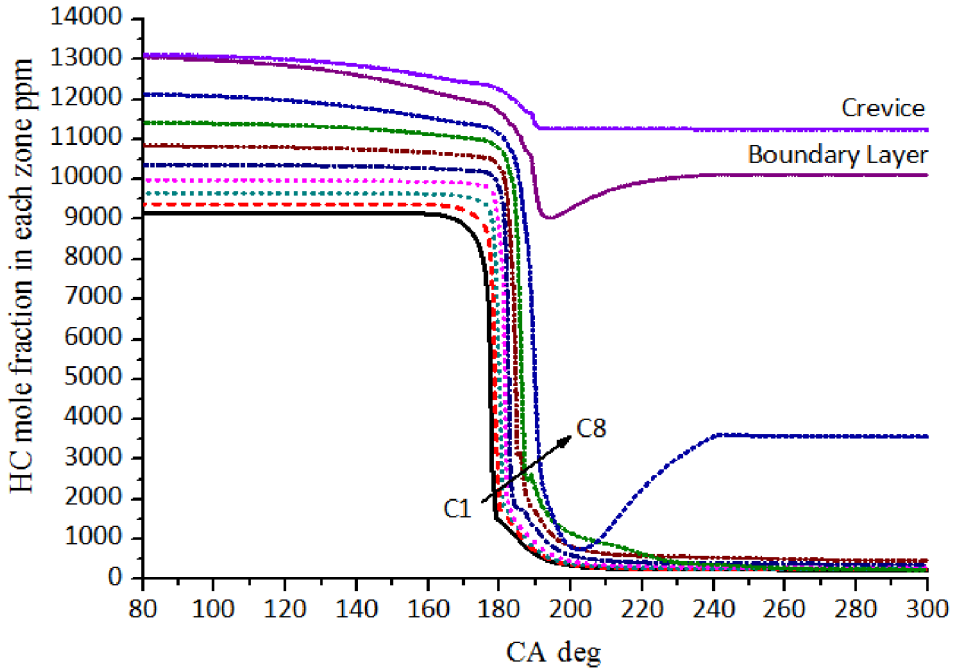

Figure 8-18: HC mole fraction histories for each zone against crank angle at 58 % IEGR.

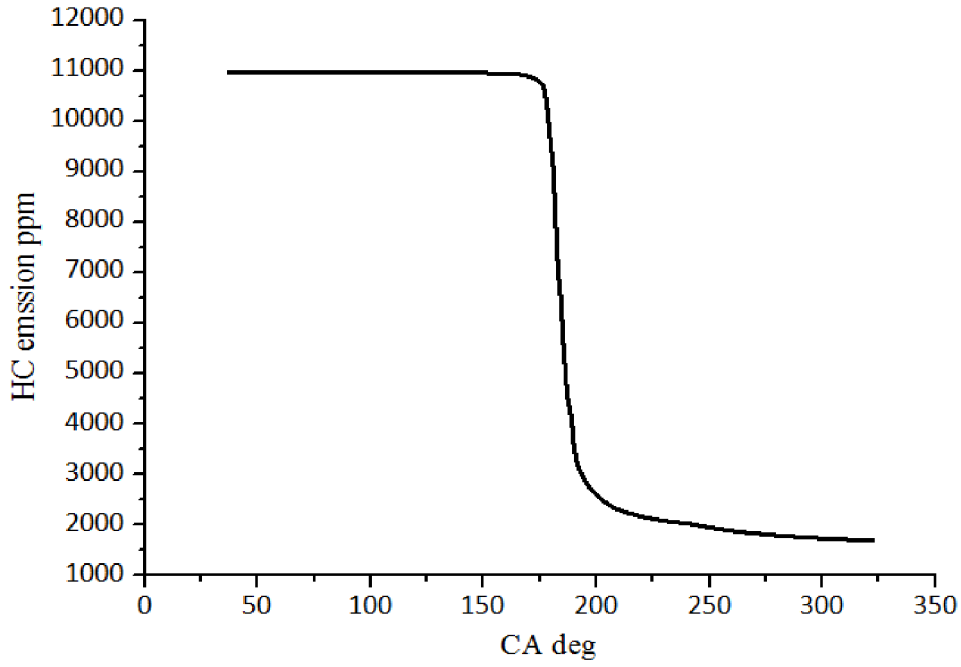

Figure 8-19: In-cylinder HC history against crank angle at 58 % IEGR.

The overall HC concentration is illustrated in Figure 8-19. It shows the major portion of the hydrocarbon species are fast consumed during the main combustion, a small part of HC is further oxidized during the expansion stroke, and HC concentration

reaches a lowest level at EVO.

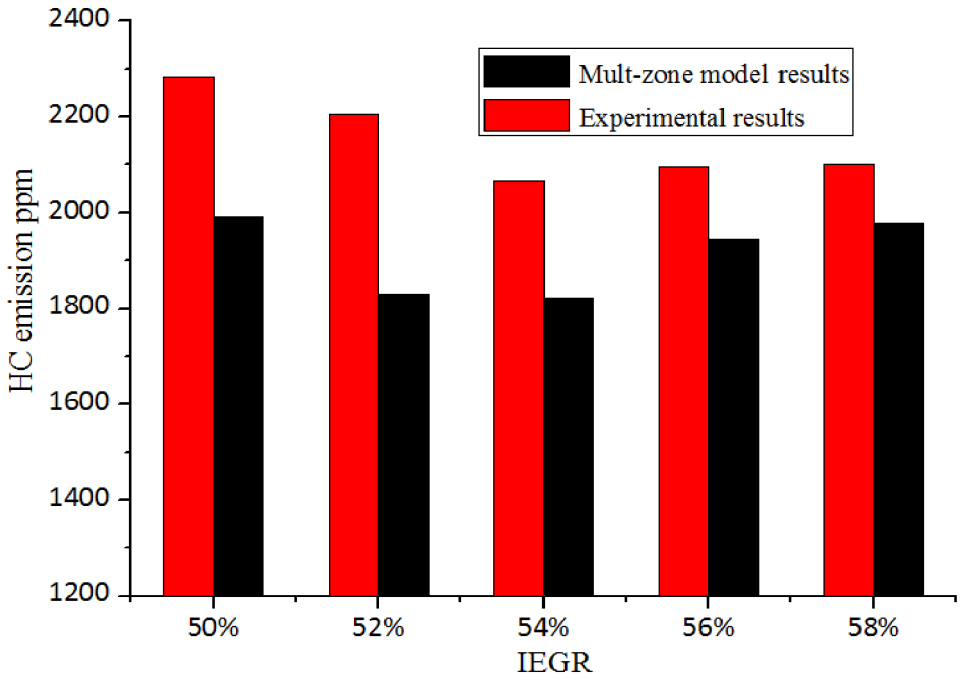

Figure 8-20: Comparison of the calculated HC emission with the experimental results at various IEGR.

The calculated and measured HC emission at various IEGR is compared in Figure 8-20. Again, the agreement between the two is good with the accuracy of 91% to 94%. It is interesting to note that both measured and calculated results showed a potential optimum IEGR level of approx 54% in terms of HC emission. This may be due to the effect of the IEGR on the strength of combustion. As the IEGR level reduces from 54% to 50 %, peak pressure position delays and peak pressure reduces as shown in Figure 8-14. The reduced peak pressure reflects the fact that the combustion strength reduces as the IEGR level decreases. Such a reduction of combustion strength deteriorates the HC oxidation and leads to an increase in HC emission. As the IEGR level further increases from 54% to 58%, the EGR dilutes the engine charge, and leads to a reduction in combustion temperature and therefore a reduction in HC oxidation capability, which is represented by the plot of the calculated temperatures at various IEGR levels shown in Figure 8-21.

NO_X mole fraction histories of each zone are depicted in Figure 8-22. It can be seen the core zones with higher temperature have higher NO_X concentrations and almost no NO_X species in the boundary layer and the crevice due to the relatively low zone temperature.

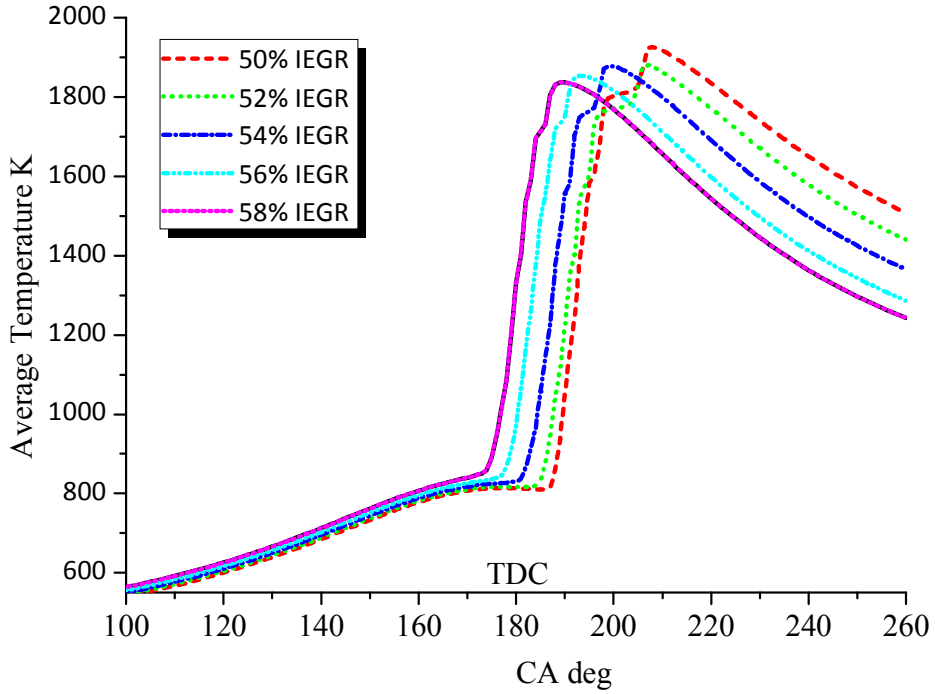

Figure 8-21: Calculated average in-cylinder temperature at various IEGR levels

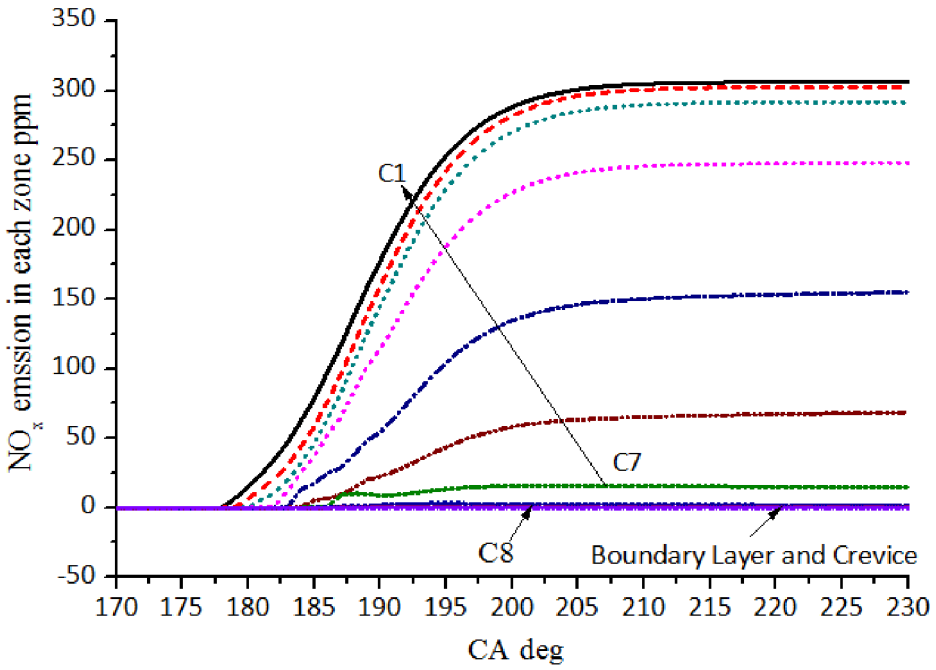

Figure 8-22: NO_X mole fraction histories for each zone against crank angle at 58 % IEGR

The overall NO_X mole fraction in the cylinder at various crank angles is shown in Figure 8-23. NO_X starts to build up at the beginning of combustion and then reach the peak value at the end of combustion and stays at the peak value till the end of the

expansion process.

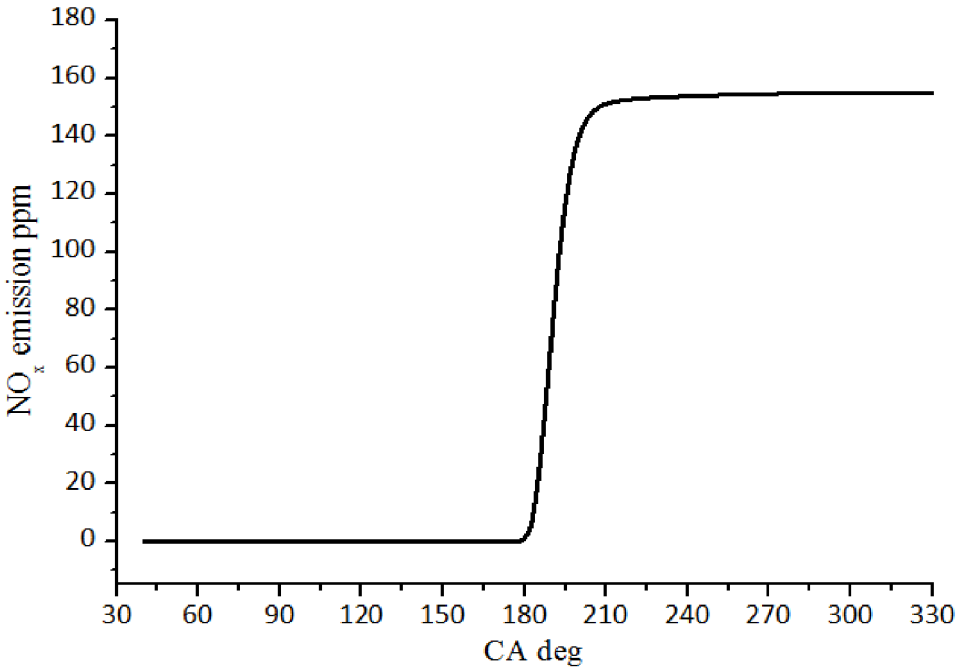

Figure 8-23: In-cylinder NO_X histories against crank angle at 58 % IEGR

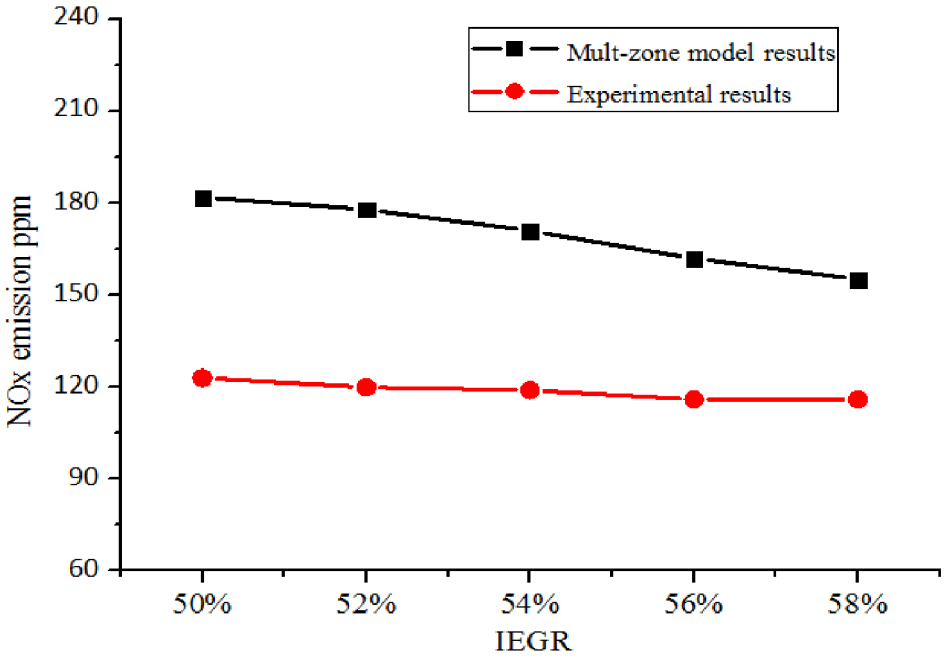

Figure 8-24: Comparison of the calculated NO_X emission with the experimental results at various IEGR

Figure 8-24 shows the comparison between calculated and measured NO_X emissions. The calculated results match the trend obtained from the experiment,

which is that NO_x emission reduces as more IEGR is applied. Again, this attributes to the fact that the more IEGR is applied, the peak average in-cylinder temperature reduces as shown in Figure 8-21. The predicted NO_X emission at various IEGR level is overall higher than the measured results. The disagreement ought to attribute to the overpredicted in-cylinder temperature, which may be because that heat transfer across the zones is not included in the simulation, which will be addressed in the future work.

8.4 Summary and Conclusions

A thermodynamic-based multi-zone model coupled with reduced chemical kinetics for the simulation of HCCI combustion has been developed and reported in this chapter. The model takes into account the effects of the boundary layer, crevice volume, and blowby. In order to investigate the influences of in-cylinder inhomogeneity, the main cylinder chamber has been divided into multiple core zones with various temperature and composition. The mass and energy transfer across the zones is simulated by balancing the calculated zone pressure. A reduced chemical kinetic mechanism was implemented in each zone to simulate the HCCI combustion chemistry and emission formation. An in-house code, the LUCKS_HCCI code in the LUCKS package was employed to solve the coupled differential equations of the system. Measured IEGR fraction, IEGR temperature, and inlet temperature of fresh engine charge are used in a thermodynamic mixing model to calculate the initial gas mixture condition of the simulation. The model was validated against experimental results at various Internal Exhaust Gas Re-circulation (IEGR) levels and then used to analyze the thermal and chemical effect of the IEGR on the HCCI combustion. The calculated results from the developed model were compared with some experimental data at various IEGR level in terms of in-cylinder pressure histories and emissions (HC, CO and NO_X). Good agreements have been obtained for pressure, and HC and CO emissions, and a similar tendency has been identified for NO_X emission.

Chapter Nine: **Concluding Remarks**

9.1 Summary

This research work has been concerned with the development, validation and application of multi-zone chemical kinetic engine models in the simulation of autoignition driven combustion in SI and HCCI engines. The contribution of this work is primarily made to establish a mathematical model based on the underlying physical and chemical principles of autoignition of the fuel-air mixture in SI and HCCI engines. Then, a computer code package has been developed to numerically solve the model. The developed model aims at improving the understanding of autoignition behaviour under engine-like conditions and providing an investigative tool to autoignition characteristics. Furthermore, as part of the ongoing program in the research of free piston engines, the results of this work will significant aid in the investigation and simulation of the constant volume autoignition applied in free piston engines.

Autoignition has been closely related with gasoline engine combustion. Its role is played either as a limitation to SI engines or a solution to HCCI engines. Autoignition is a self-ignited combustion phenomenon that is kinetically driven by the chemical reactions of fuel-air mixture. Autoignition occurs in different scenarios In SI and HCCI engines. In SI engines, autoignition chemistry is initiated by chemical reactions with heat release as the result of compression work from both piston upward motion and flame front propagation. However, in HCCI engines, autoignition is applied as the ignition approach, which is dominated by local chemical-kinetic reactions with no requirement of flame propagation.

Therefore, chemical kinetics modelling has been implemented to study the kinetic chemistry of autoignition that can be interpreted as a process of hydrocarbon oxidation involving a series of chemical paths in chains. Chemical kinetics modeling is a numerical tool to calculate the rate of this chemical process.

Multi-zone thermodynamic combustion modelling has been regarded as a functional simulation approach to study the combustion process in IC engines and a decent compromise between computation accuracy and efficiency. Integration of chemical kinetics models into multi-zone models is therefore a potential modelling method to investigate the chemical and physical processes of autoignition in SI and HCCI engines. The benefits of multi-zone chemical kinetics modeling can be summarized as

- In contrast to the single zone models, the multi-zone approach takes account of inhomogeneity of the in-cylinder mixture such as temperature, composition etc.
- By adopting a model for blowby, the multi-zone approach can capture the effect of blowby on the combustion process.
- Zone division of the cylinders includes the crevice and boundary layer so that the effect of these regions on combustion can be captured and investigated.
- Multi-zone modelling is capable to describe the processes of heat transfer and mass transfer across in-cylinder regions with different properties.
- Multi-zone modelling represents much lower computational cost in comparison with the CFD approach.
- When coupled with chemical kinetics models, multi-zone modelling is competent to depict the chemical process of autoignition so that the major characteristics of autoignition such as ignition timing and heat release rate etc. can be predicted. With chemical kinetics modelling, in addition, emissions e.g. CO and HC can be better modelled in multi-zone models.

The major assumptions made and principles applied to establish the mathematical model for multi-zone chemical kinetics modeling are summarized as:

- The cylinder volume is split into a series of zones of different thermal and composition properties.
- Each zone is treated as a variable volume combustion reactor, filled with

homogeneous mixtures that act as a perfect gas, to which kinetic chemistry and mass and energy conservation are applied

- The multi-zone engine model handles distribution of temperature and composition through setting different initial temperatures and compositions in each zone.
- Pressure is assumed spatially uniform throughout the cylinder.
- The zones can interact with each other through compression work, heat and mass transfer.
    - In HCCI combustion, compression work is caused by the expansion work of hotter zones on the colder zones. However, in SI engine combustion, compression work originates from both upward piston motion and flame propagation.
    - In HCCI combustion, mass is transferred from high-pressure zones to low-pressure zones to balance the zone pressure and in SI engines, mass is entrained by the flame front and transferred from unburned zone to burned zone
    - Heat transfer between in-cylinder mixtures and the cylinder wall is considered in the type of convection in HCCI engine combustion and convection and radiation in SI engine combustion.

The code package of LUCKS (Loughborough University Chemical Kinetics simulation) has been developed for the numerical solution of the system equations. The LUCKS code has been designed with inclusion of the following modeling features:

- Combustion system with the volume being a specified function of time parameters (e.g. IC engines)
- Simulation of open combustion systems via modelling of blowby
- Multi-zone modelling of inhomogeneity of in-cylinder gas mixture (burned, burning and unburned zones for SI engines and crevice zone, boundary layer and core zones for the HCCI engines)
- Modelling the effects of IEGR on combustion and pollutant formation in HCCI engines

- Simulation of locally homogeneous gas-phase chemical kinetics
- Compatible with either detailed or reduced chemical kinetic mechanisms

In the development of the LUCKS code, the following design principles are applied to make the code efficient and easy-to-use.

- The code is well-structured and object-oriented, which make it easy to maintain and build upon for the subsequent users and developers, and written using open source FORTRAN77/99 to make code transportable between computers s
- Where possible, the code is programmed to have modular structures so that increasing functionalities can be easily added and /or replaced with.
- The code is commented on the code usage and the references that indicate the methodologies used.
- The code is designed to be applied across platforms so that it can be compiled and executed under both Windows and UNIX systems.
- The well-established DVODE code is applied to solve the initial value problems in both stiff and non-stiff ODEs systems.

The LUCKS code is first applied to investigate knock phenomenon in SI engines. The model is based on a three-zone approach (unburned, burning and burned zones). Wherein, chemical kinetics models are applied in both burned and unburned zones. The burning zone is modelled by an equilibrium combustion thermodynamic model. Major contributions and findings from the study include:

- The Tanaka's reduced chemical kinetics model for a commercial gasoline fuel with an RON of 95 has been modified and applied. Enhancement of the reaction rate constants of R6 and R18 has been justified to enable the model to simulate autoignition under SI combustion. Analysis results showed that the enhance factor of 6.0 has most obvious effect on the major autoignition characteristics.
- Applying the chemical kinetics model provides simulation of both pre-flame chemistry and post-flame heat release
- The burning zone is modelled by an equilibrium combustion thermodynamic model using the STANJAN code.

- A novel knock detection and process method has been developed to analyze the recorded cylinder pressure to identify the knocking cycles and determine the knock timings.
- The simulated results at various AFRs and compression ratios have been validated against experimental results with good agreements being achieved and the following facts revealed
  - For the engine used in the research at a fixed engine speed (1500 rpm) and spark timing (9^o BTDC), the A/F ratio of 11 is found to be the critical point for autoignition occurrence and the A/F ratios of 11 to 13 is indentified as the engine knock region.
  - At knock conditions (fuel rich conditions in this work), as A/F ratios increase, the peak pressure and intensity rise and knock position advances.
  - Both the experimental and simulation results verify the delayed knock position, abated peak pressure and reduced knock intensity as engine speed increase.
- The calculation results quantitatively describe the effect of the autoignition of the end gas on accelerating the burned mass fraction and shortening the overall combustion duration.
- The model shows the potential in analyzing the relationship among ignition timing, intake boost pressures and knocks, which reveals the followings
  - Intake pressure boost leads to advanced knocking timing, shortened combustion duration and boosted knock intensity.
  - As spark timing retards, the knock timing delays and knock is avoided at a critical point. Spark ignition retardation also results in delayed knocking timing, extended combustion duration and depressed knock intensity.

The LUCKS code is also applied to simulate the combustion process in HCCI engines. Major contributions and findings from the study include:

- The model takes into account the effects of the boundary layer, crevice volume and blowby.

- In order to investigate the influence of in-cylinder inhomogeneity, the main cylinder chamber has been divided into multiple core zones with various temperature and composition.
- The mass and energy transfer across the zones is simulated by balancing the calculated zone pressure.
- A reduced chemical kinetic mechanism was implemented in each zone to simulate the HCCI combustion chemistry and emission formation. A submechanism for the NO_X simulation is added to the reduced model, which is verified that has little effect on major autoignition characteristics.
- Measured IEGR fraction, IEGR temperature and inlet temperature of fresh engine charge are used with a thermodynamic mixing model to calculate the initial gas mixture conditions of the simulation.
- In description of the physical behaviour of the in-cylinder mixture, the model reveals the followings
  - Autoignition occurs first in the innermost and hotter core zone and propagate subsequently to the outer and colder zones. No autoignition occurs in both the boundary layer and the crevice zone as a result of locally low temperatures.
  - The locally low temperature in the boundary layer and crevice zone attribute to the high heat loss rate to the cylinder wall due to the high contact area ratios between the two zones and the cylinder wall, and less thermal effect from the IEGR owing to the lower IEGR fraction in these two zones.
  - The modelling results quantitatively illustrate the mass transfer process inside the combustion chamber. During the combustion, the mass in the core zones flow in to the boundary layer and the crevice zone owing to the local pressure difference. With ignition subsequently occurring, mass is compelled out of the inner core zones to the outer core zone during the early combustion phase. As autoignition proceeds into the outer core zones, the burst of the zone pressure leads to the backward mass flow to the inner core zones. The mass in the boundary layer and the crevice keep increasing during the combustion phase until all the core zones ignite their mixtures and

then gases starts flowing back to the inner core zones. During the expansion, the mass from the crevice flows into the boundary layer leading to the mass increase in the boundary layer, which consists of unreacted and partially reacted mixtures that are regarded as the main source of the HC and CO emission.

- The model was validated against experimental results at various Internal Exhaust Gas Re-circulation (IEGR) levels and then used to analyze the thermal and chemical effect of the IEGR on the HCCI combustion and emissions, which reveals the followings
  - As the IEGR amount increases, peak cylinder pressure rises and the peak pressure position advances as result of the thermal effect of IEGR on the in-cylinder mixture
  - The CO emission distribution over the zones is simulated. The CO fraction in each core zone peaks with autoignition occurrence and then reaches a low level due to further oxidation to CO_2 at high temperature. In the expansion stroke, fuel oxidation freezes in the boundary layer and the crevice zone resulting in a high concentration of CO and the unreacted and partially reacted mixtures trapped in the boundary layer and the crevice during the main combustion flowing back to the core zones cause the late increase of CO in the outer core zones.
  - The overall CO fraction reaches the peak value during the major combustion and levels off during the expansion stroke. As the mixture is cooled down further, the HC in the outflow from the boundary layer contributes to the further formation of CO in the later expansion stroke.
  - The CO concentration increases at higher IEGR owing to the dilution effect of IEGR on the engine charge, which leading to the decrease of the overall combustion temperature and therefore a reduction of oxidation of CO.
  - The majority of the formed HC in core zones have been oxidized during the main combustion event. However, the HC concentration remains high in the boundary layer and the crevice.

- The calculation results of the overall HC concentration indicate that the major portion of the hydrocarbon species are fast consumed during the main combustion, then a small part of HC is further oxidized during the expansion stroke, and HC concentration reaches a lowest level at EVO.
- A potential optimum IEGR level of approx 54% between 50% and 58% is observed for the lowest HC emission, at which the thermal and diluting effects of IEGR that play contrary roles in affecting the combustion reaches a balance in determining HC formation.
- Higher NO_X concentration exists in the core zones with higher temperature and almost no NO_X species in the boundary layer and the crevice due to the low local temperatures.
- The overall NO_X starts to build up at the beginning of combustion and then reach the peak value at the end of combustion and stays at the peak value till the end of the expansion process.
- NO_X emission reduces as more IEGR is applied owing to the fact that the more IEGR is applied, the peak average in-cylinder temperature reduces.
- Good agreements between modelling results and experimental data have been obtained for pressure, and HC and CO emissions, and a similar tendency has been identified for NO_X emission.

9.2 Recommendation for Future Work

The work in this research has though provided the practicability and feasibility of incorporation of chemical kinetics model into thermodynamic engine models. However, it is still at the early stage of its evolution to develop the research work into a successful and enduring product in respect of its integrity, validation and efficiency. Based on the experience gained from doing this work, I would like to make the following recommendations to the future work in view of both the establishment of the numerical model and the development of the LUCKS code.

As for mathematical model, the following aspects may be considered in the future

work to expand and strengthen the results

- First, in the SI model, the burned mass fraction model currently applied is of an empirical form, which is originally developed at normal engine operation conditions and specified engine specification. However, when applied for knocking conditions, the flame front accelerates in a much higher speed in comparison with normal. It thus necessitates a flame propagation model that has the engine specification and operating conditions involved, e.g. laminar flamelet models and turbulent flame propagation models.
- Second, the heat transfer across the flame front in the SI model is estimated using a heat convective model whose correlation was not originally developed for such scenario, which leads to the lack of confidence in the use of such a model for the prediction. Research on heat transfer across the flame front is thus is essential and should be carried out by the subsequent researchers.
- Third, addition of a boundary layer model should be able to improve the modelling accuracy, especially when the emissions are studied. This is because the modelling of temperature distribution adjacent to the cylinder wall has strong effect on heat transfer. In the HCCI model, a constant boundary layer thickness is assumed, which diverges from real scenario, in which the thickness varies as the engine operates. Since the boundary layer has a big influence on the formation of HC and CO and thermally affects the heat conductivity of in-cylinder charge to the cylinder wall, a more advanced model for layer thickness is requisite for improving modelling accuracy.
- Fourth, a crevice model involving the simulation of piston ring pack can also be considered a part of future work. In the current HCCI model, the volume of crevice zone is modelled as a fixed portion of cylinder clearance volume, which is a generally empirical evaluation with oversimplification by ignoring the existence of the piston ring pack in the crevice structure.
- Fifth, a reduced chemical kinetics model was applied in for both SI and HCCI engine simulation for the sake of saving of computation time and source. However, a chemical kinetics model involving more reactions and species may better reflect the nature chemical process in terms of reaction rates. Furthermore, it is of interest to investigate the relations of mechanism sizes with computation time scales and simulation accuracy.

- In general, the current models need further validation across a wider range of engine operation conditions and on a variety of engines with different specifications, before it can be considered a reliable and effective tool that can be applied to the real engine design.

As for development of the LUCKS code, I would like to suggest:

- First, at some point, the code is better off being openly released and distributed to the researchers and organizations that will have their practical use of the code. This will surely help maturing the code though gathering the advices and suggestions, which can be called collaborative source development
- Second, Graphical User Interface (GUI) allows quick and easy implementation of the models, which facilitates the establishment of modelling cases and increases the productivity for both non-expert and expert users. This work may involve the transformation of language of the code to GUI scripting languages like C++.
- In general, the LUCKS code should be of a goal to evolve into commercial publication, as only with commercial support, the work of developing the code can gain its requisite manpower and resource and have its value acknowledged through its practical application in the industry.

Appendix A: **Introduction of Internal Combustion Engine**

A.1. Definition and classification of Internal Combustion Engines

From the definition of HCCI engine introduced in the previous section, it can be concluded that in some regards, HCCI incorporates the best features of both SI and CI, as summarized in Table A-1 and illustrated in Figure A-1.

Table A-1: Comparison of SI, CI and HCCI combustion processes

Combustion type	**SI**	**HCCI**	**CI**
Ignition Types	Spark Ignition	Autoignition	
Ignition Point	Single	Multiple	Single
Combustion Characteristics	Flame Propagation	Multi-point Ignition and Combustion	Diffusion Flame
Charge type	Premixed homogeneous charge		In-cylinder mixed inhomogeneous charge
Throttle type	Throttled	Unthrottled	
Injection types	Port Injection	Port or Direct-Injection	Direct-Injection with Swirl
Air-fuel ratios	Stoichiometric	Variable Stoichiometry (lean to rich)	Lean/Dilute Stoichiometry
Major emissions	NO_X , CO and HC	HC and CO	PM, NO_X and HC

An Internal Combustion (IC) engine is an engine, in which chemical energy is converted to mechanical energy as a result of the combustion of an ignitable mixture of air and fuel. A piston internal combustion engine works by burning hydrocarbon or hydrogen fuel that presses on a piston; and a jet engine works as the hot combustion products press on the interior parts of the nozzle and combustion chamber, directly accelerating the engine forwards. The rotary combustion engine uses a rotor instead

of reciprocating pistons.

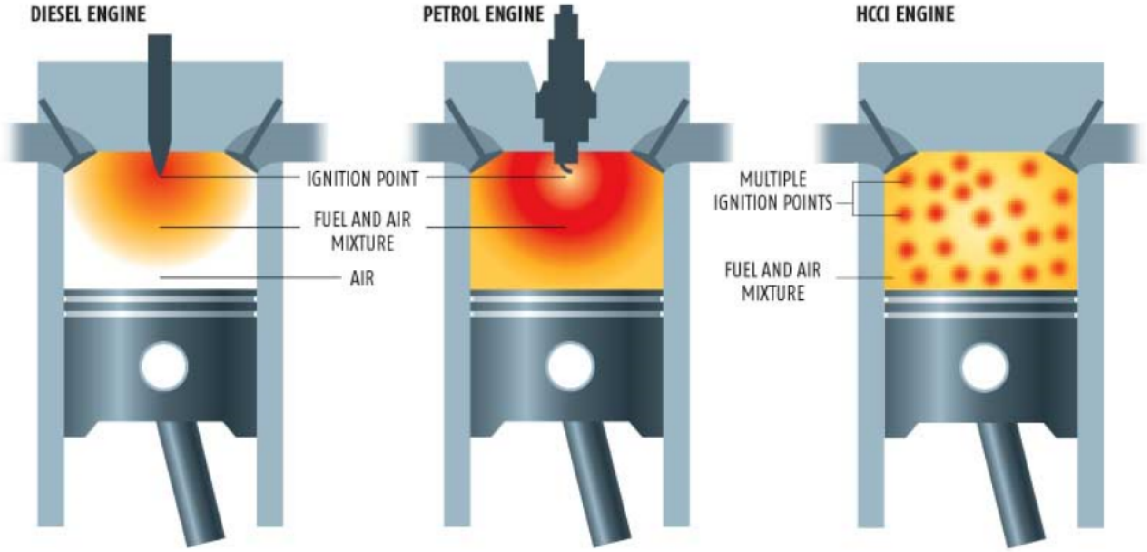

Figure A-1: Pictorial comparison of CI, SI and HCCI engines.

The IC engine contrasts with the external combustion engine, such as a steam or Stirling engine in which the energy is produced outside the working chamber as a result of continuous combustion and transferred to the working fluid. This allows a closed working process and the use of variant types of fuels such as fossil fuel, wood-burning, nuclear, solar etc.

Table A-2: Classification of IC engine

Internal Combustion Engines			
Type of combustion	**Cyclical combustion**		
Engine type	Diesel	HCCI	Gasoline
Fuel	Diesel	Gasoline/Natural gas	
Working cycles	Four-stroke processes		
Type of ignition	Autoignition (CI)		Supplied ignition (SI)
Mixture type	Heterogeneous	Homogeneous	Homogeneous or heterogeneous
Fuel Injection methods	Indirect Injection		
	Direct Injection		

In a piston internal combustion engine, the expansion of the high temperature and pressure gases produced by the combustion applies force to the piston that is connected to the crankshaft by a connecting rod. Through the crankshaft, the linear

motion of the piston is converted into rotational motion. The crankshaft in turn, turns the car's gears, which turns the car's wheels.

There is a wide range of internal combustion engines corresponding to their many varied applications. Likewise there is a wide range of ways to classify internal-combustion engines, some of which are listed below.

IC Engines can and are classified in wide range of ways, by combustion process, by the working cycles, by the source of energy, mixture generation system, or by charging system and etc. Some of them are listed in Table A-2

A.2. Engine Types

Among the combustion processes, classification is made primarily between Spark Ignition (SI) for gasoline engines and Compression Ignition (CI) for both diesel engine and HCCI engines. The term SI engine is used to refer to a combustion engine in which combustion of the compressed fuel and air mixture is ignited by means of synchronized extraneous ignition. In the diesel engine, on the other hand, the liquid fuel injected into combustion chamber mixes with the air charge previously heated by means of compression and auto-ignites at a sufficiently high temperature. Homogenous Charge Compression Ignition (HCCI) process is a promising alternative to combustion in SI and CI and considered as the third definitive class of the IC engine. To achieve HCCI combustion, the engine generally needs to run on a lean, diluted mixture of fuel, air, and combustion products. The mixture is compressed by upward moving piston to a temperature sufficiently to support the production of chemical species, which follows the self-ignition processes [45,46,59]

A.2.1. SI Engines

In a conventional four-stroke SI engine, the fuel is mixed with air in the intake system to form a premixed homogeneous charge with equivalence ratio around stoichiometry and then compressed by the piston. Under normal operating conditions, the fuel and air mixtures are initiated in the combustion chamber at the precise moment towards the end of the compression stroke at the spark plug by an electric discharge. When the spark plug fires, a flame kernel is formed, and then the kernel continues to grow into a fully developed self-sustained flame and propagates through the homogenous charge. As flame propagates, the flame front, a thin flamelet involving intense chemical reaction, is a high temperature region, which leads to significant NO_X

formation in the post -flame [3,4,5].

When flame propagation speeds exceeds a limited value, the end-gas is compressed by both the propagating flame front and upward moving piston to a sufficiently high pressure and temperature for fuel oxidation to spontaneously occur, which starts with pre-flame chemistry and ends with rapid energy release. This phenomenon is generally termed as 'autoignition' [1]. Autoignition of the end-gas limits the compression ratios in a position to achieve higher combustion efficiency and severe autoignition leads to knock, deteriorates engine efficiency, and thereby increases emissions.

Due to the homogenous mixture, SI engines have no PM emissions. However, as introduced early, the high temperature of the propagating flame leads to the formation of NO_X emissions in both the flame front and the post-flame gases. Usually, the term 'NO_X' indicates the nitric oxide (NO) and nitrogen dioxide (NO_2), between which the former one is the predominant component of NO_X. It has been. It has been generally accepted that the extended Zeldovich mechanism presents the principal reactions governing the formation of NO [1].

CO emission in the SI engines is controlled by the fuel-air equivalence ratios. In the exhaust of rich-running engines at full load, CO appears because there is insufficient oxygen to convert all the carbon in the fuel to CO2. CO formation is unavoidable and in the untreated exhaust CO, concentration is the highest of all emissions.

Table A-3: Primary sources for hydrocarbon emissions in SI engines [217].

Source	Unburned Fuel from normal combustion (%)	Unburned fuel leaving with the exhaust (%)
Crevice	5.2	0.76
Liquid Fuel	1.2	0.40
Oil Layer	1.0	0.32
Deposits	1.0	0.32
Exhaust Valve Leakage	0.1	0.10
Flame Quench	0.5	0.10
Total	**9.0**	**2.0**

Unburned Hydrocarbon (UHC) emission representing the unburned fuel in the exhaust gases are the consequence of incomplete combustion of hydrocarbon fuel. In SI engines, nearly 9% of the fuel supplied to an engine is not burned during the major combustion phase. Most of this unburned fuel is consumed by the post

combustion oxidation during the power expansion stroke, including oxidation in the exhaust port during the blow down process. However, approximately 2% of total fuel still exists with the exhaust, including partial reaction products, such as acetaldehyde, formaldehyde, 1, 3 butadiene, and benzene, etc. [217].

Hydrocarbon emissions represent a decrease in engine thermal efficiency and main air pollutions. Six main sources of UHC emissions are summarized in Table A-3

Combustion chamber crevices – the narrow regions in the combustion chamber into which the flame cannot propagate because they are smaller than the quenching distance. Crevices represent about 1 to 3% of the clearance volume. Combustion chamber crevices are major sources of UHC emissions, responsible for about 40% of the UHC. Of the combustion chamber crevices, the piston upper crevice volume is the main contributor to engine-out HC emissions. In general, the sensitivity of the UHC emissions to the combustion-chamber crevices is influenced strongly by the in-cylinder flow field and combustion, which influence the concentration of burned gases in the crevice gases. UHC can further be oxidized during the exhaust stroke when the UHC emit from the crevices and through 3-way catalyst after treatment [6].

Liquid fuel – For some fuel injection systems there is a possibility that liquid fuel is introduced into the cylinder past an open intake valve. The less volatile constituents in the fuel may not vaporize (especially during engine warm-up) and be trapped in the crevices and carbon deposits.

Oil layers - Since the piston rings cannot absolutely seal against the cylinder to preventing oil migration into the cylinder above the piston, the lubricating oil layer exists on the cylinder liner and cyclically absorbs and desorbs the fuel, which is suggested as a significant source of unburned hydrocarbon emissions from spark ignition engines.

Deposits – Carbon deposits build up on the valves, cylinder, and piston crown. These deposits are porous with pore sizes smaller than the quenching distance, with in which trapped fuel cannot burn.

Exhaust valve leakage- Exhaust valves that are normally closed may leak UHC directly into the exhaust port.

Quenching – Most of the hydrocarbon contained in the wall quench layer diffuse into the hot combustion products outside the layer and are consumed during the post combustion oxidation processed. However, bulk gas quenching can occur during the

decompression and blow down processes when the temperature drops to a low enough level.

A.2.2. CI engine

Combustion in CI engines is characterized by the following features. The liquid fuel is injected under high pressure towards the end of the compression stroke, normally shortly before Top Dead Center (TDC), directly into the main (Direct Injection) combustion chamber, or, on older engines, into a pre-chamber (indirect injection). The spray formation, droplet evaporation, and the mixing of fuel vapour with highly compressed air to create ignitable mixture all occurs in a high temperature and high-pressure environment [216]. Due to the high compression ratios (14 -22) applied in CI engine, the gases mixture near the end of compression reaches a temperature high enough so that the fuel autoignites very soon after injection starts. The period between the start of injection and autoignition is called the ignition delay [9]. As the CI engine applies inner mixture formation, the load control of CI engine is achieved via the supplied fuel quantity with the unthrottled and inducted air [216]. The employment of high compression ratios in CI engine leads to the combustion efficiency of CI is up to 40% larger than SI engines [6]

Because of the inhomogeneity of the mixture from charge stratification, there are zones inside the combustion chamber with air-fuel ratios that are less than one. In these areas, high concentrations of CO arise during the main combustion reaction and usually largely re-oxidized later in the combustion process using the excess air [216]. In contrast to SI engines, CI engines, except being operated fuel rich, benefit from substantially lower specific carbon monoxide emissions

A few factors are believed to be primary sources for UHC emission in CI engines. Firstly, the fuel trapped in the injector at the end of injection that incompletely mixes with the air. Then, the mixing of fuel and air occurs outside the main burning area, which leads to the regions with too low air-fuel ratios to be burned. Some of this fuel makes its way out the exhaust. Finally, some fuel is trapped along the walls by crevices, deposits, or oil due to impingement by the spray. Owe to the combustion efficiency and high in-cylinder temperature in CI engines, the UHC emissions are usually much lower compared with SI engines.

While the operational advantages of CI engines are clear regarding combustion efficiency, CO, and UHC emissions, CI engines are a major contributor to NO_X and

PM emissions. NO_X formation is very susceptive to high temperature, so the high temperature regions in CI engines provide the circumstance for the reaction of O-N-NO_X to occur. NO_X is usually formed in the high temperature regions at the diffusion flame interface where both oxygen and nitrogen are available and in the post-combustion hot gas regions while fuel rich oxidation in some regions produces elevated particulate concentrations. As temperature is proportional to load in a CI engine, more NO_X is formed as the load increases. [218]. The most part of PM emissions from CI engines consists of the unburned hydrocarbon, hydrocarbon compound and sulphites particles resulting from the inhomogeneous fuel rich regions.

A.2.3. HCCI combustion

The homogenous charge is used in SI engines where a pre-mixed (homogenous) charge is inducted into the cylinder and that mixture is then ignited using a spark. Inside of a CI engine, only fresh air is brought into the cylinder and then fuel is directly injected into the hot compressed air when the piston is near its top position. The fuel injected initially mixes with the hot air and auto-ignites; then the subsequently injected fuel is sprayed into the hot charge and burns as a diffusion flame. HCCI combines those two ideas and creates a third combustion system. The main difference between the three systems is the control of the combustion. In both SI and CI engines, there is an event, which triggers the combustion (spark timing in SI and injection timing in CI). Such a definitive triggering event is lacking in HCCI, which is controlled by combustion chemical kinetics and the charge thermal environment.

A.3. Fuel

IC engines generally uses fossil in the form of gas, liquid or solid. The classification of major fuels that can be combusted in the IC engine is shown Table A-4. The fuels applied in the SI and CI engine.

Gasoline and diesel are primarily used as fuels in IC engines. Gasoline engines are used in most other road vehicles including most cars, motorcycles, and mopeds. Diesel engines are generally heavier, noisier, and more powerful at lower speeds than gasoline engines. They are also more fuel-efficient in most circumstances and are used in heavy road vehicles, some automobiles (increasingly so for their

increased fuel efficiency over gasoline engines), ships, railway locomotives, and light aircraft. Note that in Europe, sophisticated diesel cars have taken over about 40% of the market since the 1990s.

Table A-4: Classification of fuels used in IC engines [216].

Fuel types		Examples
Gaseous fuels		Methane, propane, butane, natural gas, biogas, and hydrogen
Liquid fuels	**Light**	Gasoline, kerosene, benzene, alcohols (methanol, ethanol), acetone, ether, liquefied gases (LNG, LPG)
	Heavy	Petroleum, diesel fuel, Fatty-acid methyl ester (FAME), biodiesel, vegetable oils, and marine fuel oil
Solid fuels		Pulverized coal

A.3.1. Working cycles

With respect of working cycles, the distinction is made between four-stroke and two stroke processes.

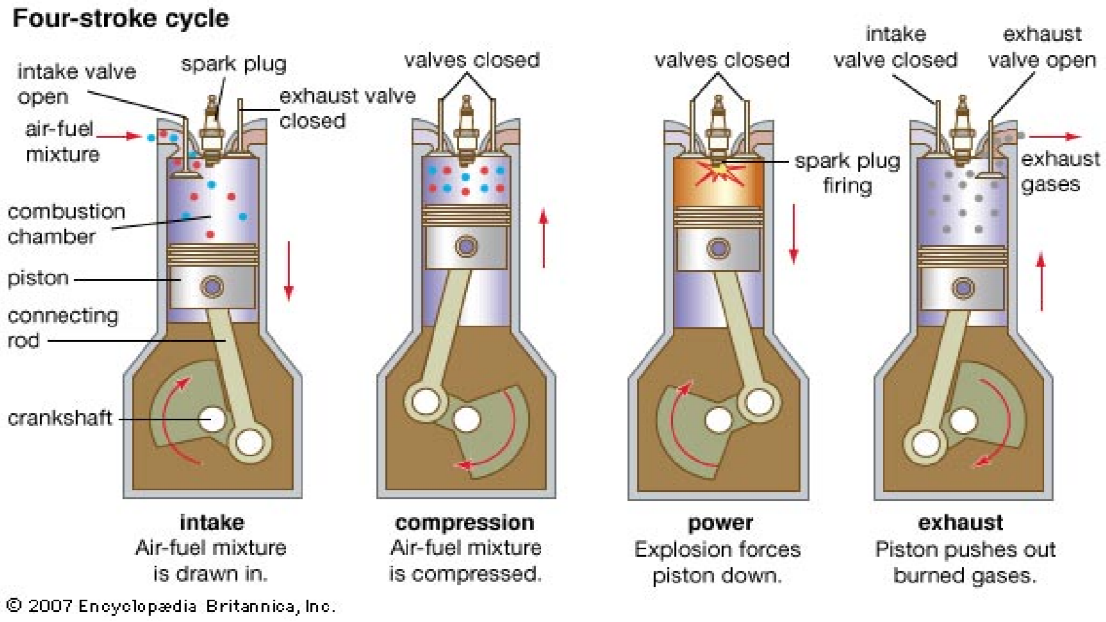

Figure A-2: Working principle of a four-stroke engine [219].

A.3.2. Four-Stroke Engine

A four-stroke engine has its charge (air, or a fuel vapour with air mixture) compressed in the first stroke by the upward moving piston, and ignition occurring

shortly before the reversal of piston motion. Combustion process associated with an increase in pressure up to the maximum cylinder pressure and expansion of the working gas in the subsequent stroke, during which work is applied to the piston. To remove the combustion gas from the working chamber, the exhaust valve is opened by the cam/lifter mechanism at the bottom of the power stroke and the upward stroke of the piston drives the combustion gas out of the cylinder. The working principles of the four-stroke engines are illustrated in Figure A-2.

A.3.3. Two-Stroke Engine

In the two-stroke process depicted in Figure A-3, gas exchange occurs in the vicinity of bottom dead centre as a results of expulsion of the combustion gases by the fresh charge with only a slight change in the working volume, with the results that the complete stroke is not exploited for compression and expansion. An additional scavenging blower is necessary for the scavenging process.

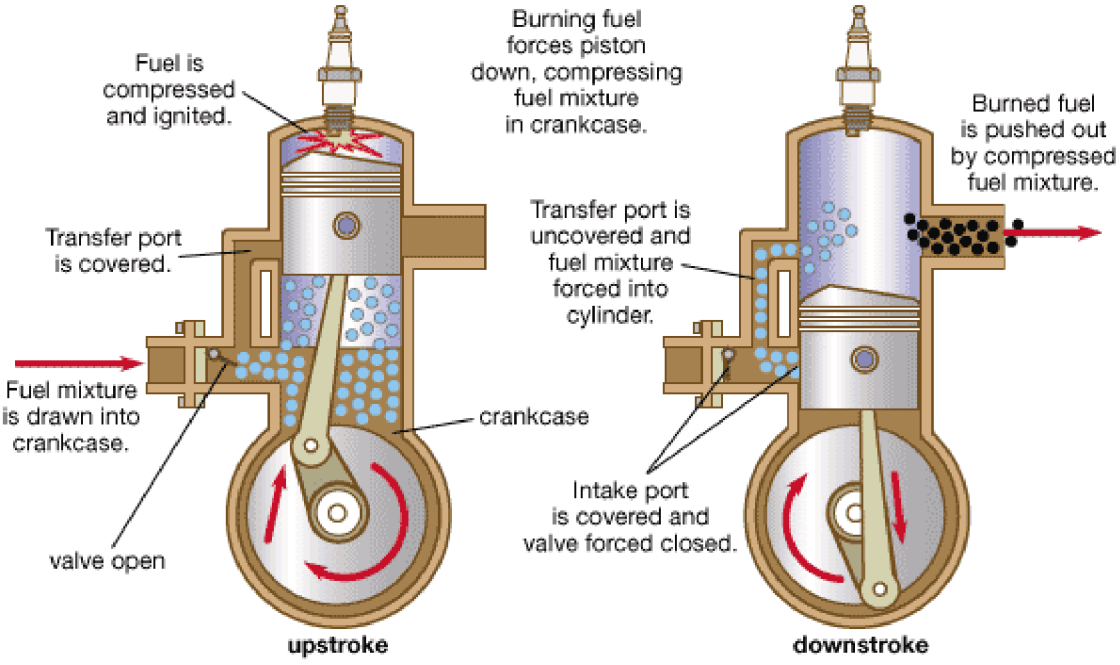

Figure A-3: Working principle of a two-stroke engine [220].

In the two stroke engine, all four strokes in the four-stroke engines are integrated into one simple downward stroke, and one upward stroke. Intake and exhaust are both integrated into the compression and combustion movement of the piston, eliminating the need for valves. This is accomplished by an inlet and exhaust port in the wall of the combustion chamber itself. As the piston travels downward from combustion, the

exhaust port is exposed allowing the spent gasses to rush out of the chamber. The downward stroke also creates suction that draws in new air/fuel through an inlet located lower in the chamber. As the piston rises again, it blocks off the inlet and port, compressing the gasses at the top of the chamber. The spark plug fires and the process start over. Significantly, the engine fires on every revolution, giving the two stroke its power advantage

Since the two stroke engine fires on every revolution of the crankshaft, a two stroke engine is usually more powerful than a four stroke engine of equivalent size. This, coupled with their lighter, simpler construction, makes the two stroke engine popular in chainsaws, line trimmers, outboard motors, snowmobiles, jet-skis, light motorcycles, and model airplanes.

Unfortunately, most two stroke engines are inefficient and are terrible polluters due to the amount of unspent fuel that escapes through the exhaust port. The principle of the operation of working cycle of two-stroke engines is illustrated in Figure A-3.

A.4. Ignition Types

The fuel-gas mixture in IC engines may be ignited by means of supplied ignition or compression ignition. The supplied ignition is generally applied in gasoline engine, which uses an electrical spark ignites the mixture in the cylinder, which thus is thus termed as Spark Ignition (SI). By nature, petrol is a highly volatile liquid, but its self-ignition temperature is high. Hence, for the combustion of this fuel a spark is necessary to initiate its burning process. To generate this spark in SI engines, the spark plug is placed in the cylinder head of the engine. The voltage is provided to the spark plug either from the battery or from the magneto.

Compression Ignition (CI) is an autoignition-initiated combustion process, in which the fuel injected ignites spontaneously in the air preheated by the piston compression. The most prominent difference between spark ignition and compression ignition engines is the type of fuel used in each. In SI engines, gasoline is used as fuel; hence, these engines are also called gasoline engines. In CI engines, diesel is used as fuel; hence, they are also called diesel engines. The self-ignition temperature of diesel is comparatively lower. When diesel fuel is compressed to high pressures,. its temperature also increases beyond the self-ignition temperature of the fuel. Hence, in the case of CI engines, the ignition of fuel occurs due to compression

of the air-fuel mixture and there is no need for spark plugs.

A.5. Mixture Generation

Combustion engine can also be classified in terms of methods applied to generate fuel-air mixture that satisfies the requirements of the engine over its entire operating regime. Table A-5 summarizes the classification of methods of mixture generation in IC engines

Table A-5 Classification of methods of mixture generation

Fuel-air Mixture Generation		
Methods on the basis of	**Categories**	**Characteristics and application**
Type	External mixture generation	Formation of the fuel-air mixture in the inlet system
	Internal mixture generation	Formation of the mixture in the working chamber
Quality	Homogeneous mixture generation	Carburetor and manifold injection in the case of gasoline engine, or gasoline direct injection during the induction stroke
	Non-homogeneous mixture generation	Injection at extremely short intervals in the diesel engine and in gasoline engines with gasoline direct injection (GDI)
Location	Working chamber	Direct injection into the working chamber in the case, for example, of direct injection (DI) diesel engines and GDI engines. Injection may be air-directed, jet-directed, or all directed.
	Subsidiary chamber	Indirect injection into a subsidiary chamber, such as antechamber, swirl-chamber, and air-chamber in diesel engine
	Intake manifold	Intake manifold injection (in gasoline engines)

Appendix B: **The CHEMKIN-Formatted Chemical Kinetic Mechanism by Tanaka, et al.**

```
                                                        (k = A T**b exp(-E/RT))
   REACTIONS CONSIDERED                                   A        b        E

 1. C7H16+O2<=>C7H15+HO2                              1.00E+16    0.0    46000.0
       Reverse Arrhenius coefficients:                1.00E+12    0.0        0.0
 2. C7H15+O2<=>C7H15OO                                1.00E+12    0.0        0.0
       Reverse Arrhenius coefficients:                2.51E+13    0.0    27400.0
 3. C7H15OO<=>C7H14OOH                                1.51E+11    0.0    19000.0
       Reverse Arrhenius coefficients:                1.00E+11    0.0    11000.0
 4. C7H14OOH+O2<=>OOC7H14OOH                          3.16E+11    0.0        0.0
       Reverse Arrhenius coefficients:                2.51E+13    0.0    27400.0
 5. OOC7H14OOH=>OC7H13OOH+OH                          8.91E+10    0.0    17000.0
 6. C7H16+OH=>C7H15+H2O                               1.00E+13    0.0     3000.0
 7. C7H15+O2<=>C7H14+HO2                              3.16E+11    0.0     6000.0
       Reverse Arrhenius coefficients:                3.16E+11    0.0    19500.0
 8. C7H14+HO2+7O2=>7CO+7H2O+HO2                       3.16E+13    0.0    10000.0
 9. OC7H13OOH=>OC7H13O+OH                             3.98E+15    0.0    43000.0
10. OC7H13O+O2<=>OC7H12O+HO2                          3.16E+11    0.0     6000.0
       Reverse Arrhenius coefficients:                3.16E+11    0.0    19500.0
11. HO2+OC7H12O+O2=>H2O2+OC7H10O+HO2                  3.16E+13    0.0    10000.0
12. HO2+OC7H10O+5O2=>7CO+5H2O+HO2                     3.16E+13    0.0    10000.0
13. C8H18+O2<=>C8H17+HO2                              1.00E+16    0.0    46000.0
       Reverse Arrhenius coefficients:                1.00E+12    0.0        0.0
14. C8H17+O2<=>C8H17OO                                1.00E+12    0.0        0.0
       Reverse Arrhenius coefficients:                2.51E+13    0.0    27400.0
15. C8H17OO<=>C8H16OOH                                1.14E+11    0.0    22400.0
       Reverse Arrhenius coefficients:                1.00E+11    0.0    11000.0
16. C8H16OOH+O2<=>OOC8H16OOH                          3.16E+11    0.0        0.0
       Reverse Arrhenius coefficients:                2.51E+13    0.0    27400.0
17. OOC8H16OOH=>OC8H15OOH+OH                          8.91E+10    0.0    17000.0
18. C8H18+OH=>C8H17+H2O                               1.00E+13    0.0     3000.0
19. C8H17+O2<=>C8H16+HO2                              3.16E+11    0.0     6000.0
       Reverse Arrhenius coefficients:                3.16E+11    0.0    19500.0
20. C8H16+HO2+8O2=>8CO+8H2O+HO2                       2.00E+13    0.0    10000.0
21. OC8H15OOH=>OC8H15O+OH                             3.98E+15    0.0    43000.0
22. OC8H15O+O2<=>OC8H14O+HO2                          3.16E+11    0.0     6000.0
       Reverse Arrhenius coefficients:                3.16E+11    0.0    19500.0
23. HO2+OC8H14O+O2=>H2O2+OC8H12O+HO2                  1.58E+13    0.0    10000.0
24. HO2+OC8H12O+6O2=>8CO+6H2O+HO2                     1.58E+13    0.0    10000.0
25. C8H18+C7H15<=>C7H16+C8H17                         5.01E+12    0.0        0.0
26. OH+H2=H+H2O                                       2.14E+08    1.5     3449.0
27. O+OH=O2+H                                         2.02E+14   -0.4        0.0
28. O+H2=OH+H                                         5.06E+04    2.7     6290.0
29. H+O2(+M)=HO2(+M)                                  4.52E+13    0.0        0.0
    Declared duplicate reaction...
    Low pressure limit:  0.10500E+20 -0.12570E+01  0.00000E+00
       H2O              Enhanced by    0.000E+00
       H2               Enhanced by    0.000E+00
       H2O              Enhanced by    0.000E+00
       H2               Enhanced by    0.000E+00
       N2               Enhanced by    0.000E+00
30. H+O2(+N2)=HO2(+N2)                                4.52E+13    0.0        0.0
    Declared duplicate reaction...
    Low pressure limit:  0.20300E+21 -0.15900E+01  0.00000E+00
31. H+O2(+H2)=HO2(+H2)                                4.52E+13    0.0        0.0
```

```
    Declared duplicate reaction...
    Low pressure limit:  0.15200E+20 -0.11330E+01  0.00000E+00
32. H+O2(+H2O)=HO2(+H2O)                          4.52E+13    0.0        0.0
    Declared duplicate reaction...
    Low pressure limit:  0.21000E+24 -0.24370E+01  0.00000E+00
33. OH+HO2=H2O+O2                                 2.13E+28   -4.8     3500.0
    Declared duplicate reaction...
34. OH+HO2=H2O+O2                                 9.10E+14    0.0    10964.0
    Declared duplicate reaction...
35. H+HO2=OH+OH                                   1.50E+14    0.0     1000.0
36. H+HO2=H2+O2                                   8.45E+11    0.7     1241.0
37. H+HO2=O+H2O                                   3.01E+13    0.0     1721.0
38. O+HO2=O2+OH                                   3.25E+13    0.0        0.0
39. OH+OH=O+H2O                                   3.57E+04    2.4    -2112.0
40. H+H+M=H2+M                                    1.00E+18   -1.0        0.0
       H2O              Enhanced by    0.000E+00
       H2               Enhanced by    0.000E+00
41. H+H+H2=H2+H2                                  9.20E+16   -0.6        0.0
42. H+H+H2O=H2+H2O                                6.00E+19   -1.2        0.0
43. H+OH+M=H2O+M                                  2.21E+22   -2.0        0.0
       H2O              Enhanced by    6.400E+00
44. H+O+M=OH+M                                    4.71E+18   -1.0        0.0
       H2O              Enhanced by    6.400E+00
45. O+O+M=O2+M                                    1.89E+13    0.0    -1788.0
46. HO2+HO2=>H2O2+O2                              2.00E+10    0.0     5000.0
47. H2O2+M=>OH+OH+M                               1.00E+16    0.0    48000.0
48. H2O2+H=HO2+H2                                 1.98E+06    2.0     2435.0
49. H2O2+H=OH+H2O                                 3.07E+13    0.0     4217.0
50. H2O2+O=OH+HO2                                 9.55E+06    2.0     3970.0
51. H2O2+OH=H2O+HO2                               2.40E+00    4.0    -2162.0
52. O+CO(+M)<=>CO2(+M)                            1.80E+10    0.0     2385.0
    Low pressure limit:  0.60200E+15  0.00000E+00  0.30000E+04
       H2               Enhanced by    2.000E+00
       O2               Enhanced by    6.000E+00
       H2O              Enhanced by    6.000E+00
       CO               Enhanced by    1.500E+00
       CO2              Enhanced by    3.500E+00
       AR               Enhanced by    5.000E-01
53. O2+CO<=>O+CO2                                 2.50E+12    0.0    47800.0
54. CO+OH<=>CO2+H                                 4.76E+07    1.2       70.0
55. HO2+CO<=>OH+CO2                               4.76E+13    0.0    23600.0
```

NOTE: A unit - mole-cm-sec-K, E unit - cal/mole

Appendix C: **The sub-mechanism Reactions for Simulating NO_X Chemistry**

SPECIES	1. N 2. NO 3. N_2O 4. NO_2			
REACTIONS	$k = A \cdot T^{n} \cdot \mathrm{EXP}(-E/RT)$	A (mol cm s K)	n (-)	E (cal/mole)
1	N+NO=N2+O	3.50E+13	0.0	330.0
2	N+O2=NO+O	2.65E+12	0.0	6400.0
3	N+OH=NO+H	7.33E+13	0.0	1120.0
4	N2O+O=N2+O2	1.40E+12	0.0	10810.0
5	N2O+O<=>2NO	2.90E+13	0.0	23150.0
6	N2O+H<=>N2+OH	4.40E+14	0.0	18880.0
7	N2O+OH<=>N2+HO2	2.00E+12	0.0	21060.0
8	N2O+M<=>N2+O+M	1.30E+11	0.0	59620.0
9	NO+HO2=NO2+OH	2.11E+12	0.0	-480.0
10	NO2+O<=>NO+O2	3.90E+12	0.0	-240.0
11	NO2+H<=>NO+OH	1.32E+14	0.0	360.0
12	NO+O+M<=>NO2+M	1.06E+20	-1.4	0.0

Appendix D: **Flowchart of Algorithm of Initial Condition Setting**

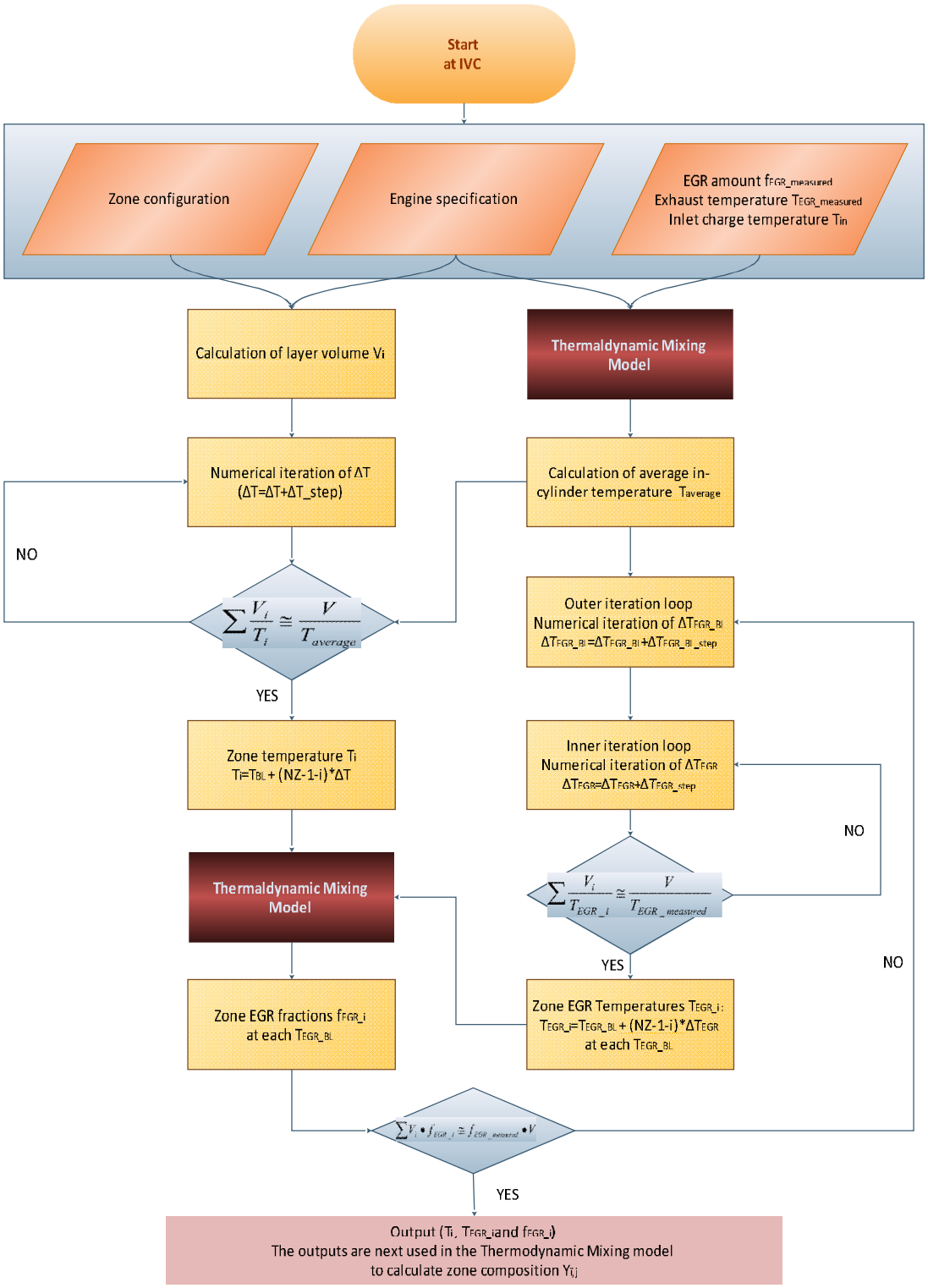

Bibliography

[1] Heywood,J.B., "Internal Combustion Engine Fundamentals". McGraw-Hill International Editions. 1988.

[2] "Engine Detonation or Knock". Available at: http://www.thor-racing.co.uk/Detonation_or_Knock-36.asp. Accessed on: 06/04, 2009.

[3] Gatowski,J.A., Heywood,J.B. and Deleplace,C., "Flame photographs in a spark-ignition engine". Combustion and Flame. Vol. 56. Issue: 1. 1984. pp: 71-81.

[4] Kalghatgi,G.T., "Early flame development in a spark-ignition engine". Combustion and Flame. Vol. 60. Issue: 3. 1985. pp: 299-308.

[5] Aoyama,T., Hattori,Y., Mizuta,J. and Sato,Y., "An Experimental Study on Premixed-Charge Compression Ignition Gasoline Engine". Society of Automotive Engineers. SAE 960081. 1996.

[6] Zheng,J., "A study of homogeneous ignition and combustion processes in CI, SI, and HCCI engine systems". Degree Type: PhD, Philadelphia, Pa. USA. Drexel University. 2005.

[7] Gerty,M.D., "Effects of operating conditions, compression ratio, and gasoline reformate on SI engine knock limits". USA. Massachusetts Institute of Technology. 2005.

[8] Revier,B.M., "Phenomena that determine knock onset in spark-ignited engines". Massachusetts Institute of Technology. 2006.

[9] Ferguson,C.R., "Internal combustion engines: applied thermosciences". New York ; Chichester. Wiley. 1986.

[10] Cernansky,N.P., Green,R.M., Pitz,W.J. and Westbrook,C.K., "Chemistry of Oxidation Preceding End-Gas Auto-ignition". Combustion Science and Technology. Vol. 50. 1986. pp: 3-25.

[11] Green,R.M., Cernansky,N.P., Pitz,W.J. and Westbrook,C.K., "The Role of Low Temperature Chemistry in the Auto-Ignition of n-Butane". Society of Automotive Engineers. SAE 872109. 1987. pp: 575-591.

[12] Westbrook,C.K., "Chemical Kinetics of Hydrocarbon Ignition in Practical Combustion Systems". July 30 - August 4. 2000. 28th International Symposium Combustion, Edinburgh, Scotland.

[13] Pan,J. and Sheppard,C.G., "A Theoretical and Experimental Study of the Modes of End Gas Autoignition Leading to Knock in S.I. Engines". Society of Automotive Engineers. SAE942060. 1994.

[14] Sheppard,C.G. and Konig,G., "End Gas Autoignition and Knock in a Spark Ignition Engine". Society of Automotive Engineers. SAE 902135. 1990.

[15] Hajireza,S., Mauss,F. and Sundén,B., "Hot-spot autoignition in spark ignition engines". Symp.Int.Combust. Vol. 28. Issue: 1. 2000. pp: 1169-1175.

[16] Griffiths,J.F., Jiao,Q., Schreiber,M., Meyer,J. and Knoche,K.F., "Development of thermokinetic models for autoignition in a CFD code: Experimental validation and application of the results to rapid compression studies". 24th Symposium (International) On Combustion: The Combustion Institute. 1992.

[17] Schreiber,M., Sadat,S.A., Poppe,C., Griffiths,J.F., Halford-Maw,P. and Rose,D.J., "Spatial Structure in End-Gas Autoignition". Society of Automotive Engineers. SAE 932758. 1993.

[18] Kawahara,N., Tomita,E. and Sakata,Y., "Auto-ignited kernels during knocking combustion in a spark-ignition engine". Proceedings of the Combustion Institute. Vol. 31. Issue: 2. 2007. pp: 2999-3006.

[19] Christensen,M., Bradley,D., Gu,X.J. and Emerson,D.R., "Amplified Pressure Waves During Autoignition: Relevance to Cai Engines". Society of Automotive Engineers. SAE 2002-01-2868. 2002.

[20] Pan,J., Sheppard,C.G.W., Tindall,A., Berzins,M., Pennington,S.V. and Ware,J.M., "End Gas Inhomogeneity, Autoignition and Knock". Society of Automotive Engineers. SAE 982616. 1998.

[21] Zeldovich,Y.B., "Regime classification of an exothermic reaction with nonuniform initial conditions". Combust.Flame. Vol. 39. 2. 1980. pp: 211-214.

[22] Leppard,W.R., "The Auto-Ignition Chemistry of Iso-Butane: A Motored Engine Study". Society of Automotive Engineers. SAE 881606. 1988. pp: 658-680.

[23] Leppard,W.R., "The Auto-Ignition Chemistry of Primary Reference Fuels, Olefin/Paraffin Binary Mixtures, and Non-Linear Octane Blending". Society of Automotive Engineers. SAE 922325. 1992. pp: 1683-1705.

[24] Li,H., "Auto-Ignition Chemistry Studies of Primary Reference Fuels and Their Mixtures with Oxygenates in a Research Engine". Degree Type: Ph.D. Thesis, Drexel University. 1995.

[25] Oran,E.S. and Boris,J.P., "Numerical approaches to combustion modeling". First Edition. Washington, DC. USA. American Institute of Aeronautics and Astronautics.

1991.

[26] Dryer,F.L., The Phenomenology of Modelling Combustion Chemistry. New York Fossil Fuel Combustion-A Source Book - (Bartok, W and Sarofim, A.F. eds.), Wiley Inter-Science. 1991. pp: 121-213.

[27] Gong,X.H., "The Effects of DTBP on the Oxidation of SI Primary Reference Fuels - A Study in an HCCI Engine and in a Pressurized Flow Reactor ". Degree Type: Ph.D. Thesis, Drexel University. 2005.

[28] Walker,R.W. and Morley,C., Chapter 1 Basic chemistry of combustion. In: M.J. Pilling, editor. " Comprehensive Chemical Kinetics". Elsevier. 1997. pp: 1-124.

[29] Smith,J.R., Green,R.M., Westbrook,C.K. and Pitz,W.J., "Experimental and Modelling Studies of Engine Knock". Proceedings of Combustion Institute. Vol. 20. 1984. pp: 91-100.

[30] Minetti,R., Carlier,M., Ribaucour,M., Therssen,E. and Sochet,L.R., "A rapid compression machine investigation of oxidation and auto-ignition of n-Heptane: Measurements and modeling". Combust.Flame. Vol. 102. Issue: 3. 1995. pp: 298-309.

[31] By,A., Kempinski,B. and Rife,J.M., "Knock in Spark Ignition Engines". Society of Automotive Engineers. SAE 810147. 1981.

[32] Douaud,A.M. and Eyzat,P., "Four-Octane-Number Method for Predicting the Anti-Knock Behavior of Fuels and Engines". Society of Automotive Engineers. SAE 780080. 1978.

[33] Warnatz,J., Mass U. and Dibble R.W., , "Combustion". Third Edition. Springer Verlag. 2001. pp:299.

[34] Westbrook,C.K. and Dryer,F.L., "Chemical kinetic modeling of hydrocarbon combustion". Progress in Energy and Combustion Science. Vol. 10. Issue: 1. 1984. pp: 1-57.

[35] Curry,S., "A Three-Dimensional Study of Flame Propagation in a SparkIgnition Engine". Vol. 71. SAE Transaction. 1963. pp: 628.

[36] Wheeler,R.W., Abnormal Combustion Effects on Economy. Plenum Press, J.C Hilliard and G.S. Springer Edition. 1984. pp: 225-276.

[37] Howard,F.A. and Wood,L.A., "The Birth of an Industry". New York. D. van Nostrand Company, Inc., 1947.

[38] Hamilton,B. "What fuel property does the Octane Rating measure?". 2009. Available at: http://stason.org/TULARC/vehicles/gasoline-faq/index.html. Accessed on: 06/04, 2009.

[39] Perdih,A. and Perdih,F., "Chemical Interpretation of Octane Number". Vol. 53. Acta Chimica Slovenica. 2006. pp: 306-315.

[40] Puzinauskas,P.V., "Examination of Methods Used to Characterize Engine Knock". Society of Automotive Engineers. SAE 920808. 1992.

[41] Brecq,G., Ramesh,a., Tazerout,M. and Le Corre,O., "An Experimental Study of Knock in a Natural Gas-Fuelled Spark Ignition Engine". Society of Automotive Engineers. SAE 2001-01-3562. 2001.

[42] Karim,G.A., "A Dimensionless Criterion for Predicting the Onset of Knock in Spark Ignition Engines". Society of Automotive Engineers. SAE 2004-01-1992. 2004.

[43] U.S. Department of Energy. "Homogeneous Charge Compression Ignition (HCCI) Technology. A Report to the U.S. Congress". April 2001.

[44] Thring,R.H., "Homogeneous-Charge Compression-Ignition (HCCI) Engines". Society of Automotive Engineers. SAE 892068. 1989.

[45] Onishi,S., Jo,S.H., Shoda,K., Jo,P.D. and Kato,S., "Active Thermo-Atmosphere Combustion (ATAC) - A New Combustion Process for Internal Combustion Engines". Society of Automotive Engineers. SAE 790501. 1979. pp: 1851-1860.

[46] Najt,P.M. and Foster,D.E., "Compression-Ignited Homogeneous Charge Combustion". Society of Automotive Engineers. SAE 830264. 1983. pp: 1.964-1.979.

[47] Iida,N., "Alternative Fuels and Homogeneous Charge Compression Ignition Combustion Technology". Society of Automotive Engineers. SAE 972071/JSAE 9734043. 1997. pp: 5-14.

[48] Oguma,H., Ichikura,T. and Iida,N., "A Study on Adaptability of Alternative Fuels for Lean Burn Two-Stroke ATAC Engine". Society of Automotive Engineers. SAE 972097/JSAE 9734304. 1997. pp: 173-180.

[49] Hultqvist,A., Christensen,M., Johansson,B., Franke,A., Richter,M. and Alden,M., "A Study of the Homogeneous Charge Compression Ignition Combustion Process by Chemiluminescence Imaging". Society of Automotive Engineers. SAE 1999-01-3680. 1999.

[50] Richter,M., Franke,A., Alden,M., Hultqvist,A. and Johansson,B., "Optical Diagnostics Applied to a Naturally Aspirated Homogeneous Charge Compression Ignition Engine". Society of Automotive Engineers. SAE 1999-01-3649. 1999.

[51] Hultqvist,A., Christensen,M., Johansson,B., Richter,M., Nygren,J., Hult,J. and Alden,M., "The HCCI Combustion Process in a Single Cycle – Speed Fuel Tracer LIF and Chemiluminescence Imaging". Society of Automotive Engineers. SAE 2002-01-0424. 2002.

[52] Ogink,R. and Golovitchev,V., "Gasoline HCCI Modelling: An Engine Cycle Simulation Code with a Multi-Zone Combustion Model". Society of Automotive Engineers. SAE 2002-01-1745. 2002.

[53] Aceves,S.M., Flowers,D.L., Westbrook,C.K., Smith,J.R., Pitz,W., Dibble,R., Christensen,M. and Johansson,B., "A Multi-Zone Model for Prediction of HCCI

Combustion and Emissions". Society of Automotive Engineers. SAE 2000-01-0327. 2000.

[54] Aceves,S., Flowers,D., Martinez,J., Espinosa,F. and Dibble,R., "Homogeneous Charge Compression Ignition (HCCI) R&D". August 28. 2002. DEER Meeting.

[55] Kelly-Zion,P.L. and Dec,J.E., "A computational study of the effect of fuel type on ignition time in homogenous charge compression ignition engines". Symposium (International) on Combustion. Vol. 28. Issue: 1. 2000. pp: 1187-1194.

[56] Christensen,M., Johansson,B. and Einewall,P., "Homogeneous Charge Compression Ignition (HCCI) Using Isooctane, Ethanol and Natural Gas - A Comparison with Spark Ignition Operation". Society of Automotive Engineers. SAE 972874. 1997.

[57] Kontarakis,G. and Collings,N., "Demonstration of HCCI Using a Single Cylinder Four-stroke SI Engine with Modified Valve Timing". Society of Automotive Engineers. SAE 2000-01-2870. 2000.

[58] Oakley,A., Zhao,H. and Ladommatos,M., T., "Dilution Effects on the Controlled Auto-Ignition (CAI) Combustion of Hydrocarbon and Alcohol Fuels". Society of Automotive Engineers. SAE 2001-01-3606. 2001.

[59] Ryan III,T.W. and Callahan,T.J., "Homogeneous Charge Compression Ignition of Diesel Fuel". Society of Automotive Engineers. SAE 961160. 1996. pp: 157-166.

[60] Gray III,A.W. and Ryan III,T.W., "Homogeneous Charge Compression Ignition (HCCI) of Diesel Fuel". Society of Automotive Engineers. SAE 971676. 1997.

[61] Fiveland,S.B., Agama,R., Christensen,M., Johansson,B., Hiltner,J., Mauss,F. and Assanis,D.N., "Experimental and Simulated Results Detailing the Sensitivity of Natural Gas HCCI Engines to Fuel Composition". Society of Automotive Engineers. SAE 2001-01-3609. 2001.

[62] Chen,Z., Konno,M., OGUMA,m. and yANAI,t., "Experimental Study of CI Natural Gas/DME Homogeneous Charge Engine". Society of Automotive Engineers. SAE 2000-01-0329. 2000.

[63] Morimoto,S.S., Kawabata,Y., Sakurai,T. and Amano,T., "Operating Characteristics of a Natural Gas-Fired Homogeneous Charge Compression Ignition Engine (Performance Improvement Using EGR)". Society of Automotive Engineers. SAE 2001-01-1034. 2001.

[64] Satot,S., Yamasakit,Y., Kawamura,H. and lidatl,N., "Research on the Influence on Natural Gas HCCI Combustion of Hydrogen and Carbon Monoxide". Proceedings of the sixth international symposium on diagnostics and modelling of combustion in internal combustion engines; COMODIA 2004, August 2-5, Yokohama, Japan August 10. : COMODIA. 2004. The Sixth International Symposium on Diagnostics and Modeling of Combustion in Internal Combustion Engines.

[65] Aceves,S.M., Flowers,D.L., Martinez-Frias,J., Smith,J.R., Westbrook,C.K.,

Pitz,W.J., Dibble,R., Wright,J.F., Akinyemi,W.C. and Hessel,R.P., "A Sequential Fluid-Mechanic Chemical-Kinetic Model of Propane HCCI Combustion". Society of Automotive Engineers. SAE 2001-01-1027. 2001.

[66] Flowers,D., Aceves,S., Smith,R., Torres,J., Girard,J. and Dibble,R., "HCCI in a CFR Engine: Experiments and Detailed Kinetic Modelling". Society of Automotive Engineers. SAE 2000-01-0328. 2000.

[67] Flowers,D., Aceves,S.M., Martinez-Frias,J., Smith,J.R., Au,M., Girard,J. and Dibble,R., "Operation of a Four-Cylinder 1.9L Propane Fuelled Homogeneous Charge Compression Ignition Engine: Basic Operating Characteristics and Cylinder-to-Cylinder Effects". Society of Automotive Engineers. SAE 2001-01-1895. 2001.

[68] Christensen,M., Hultqvist,A. and Johansson,B., "Demonstrating the Multi-Fuel Capability of a Homogeneous Charge Compression Ignition Engine with Variable Compression Ratio". Society of Automotive Engineers. SAE 1999-01-3679. 1999.

[69] Christensen,M. and Johansson,B., "Homogeneous Charge Compression Ignition with Water Injection". Society of Automotive Engineers. SAE 1999-01-0182. 1999.

[70] Olsson,J.O., Tunestal,P., Haraldsson,G. and Johansson,B., "A Turbo Charged Dual Fuel HCCI Engine". Society of Automotive Engineers. SAE 2001-01-1896. 2001.

[71] Christensen,M. and Johansson,B., "Supercharged Homogeneous Charge Compression Ignition (HCCI) with Exhaust Gas Recirculation and Pilot Fuel". Society of Automotive Engineers. SAE 2000-01-1835. 2000.

[72] Stanglmaier,R.H., Ryan III,T.W. and Souder,J.S., "HCCI Operation of a Dual-Fuel Natural Gas Engine for Improved Fuel Efficiency and Ultra-Low NOx Emissions at Low to Moderate Engine Loads". Society of Automotive Engineers. SAE 2001-01-1897. 2001.

[73] Blank,D.A., Pouring,A.A. and Lu,J., "Methanol Combustion in Low Compression Ratio D.I. Engines Enabled by Sonex Piston Design". Society of Automotive Engineers. SAE 2001-01-1197. 2001.

[74] Hultqvist,A., Engdar,U., Johansson,B. and Klingmann,J., "Reacting Boundary Layers in a Homogeneous Charge Compression Ignition (HCCI) Engine". Society of Automotive Engineers. SAE 2001-01-1032. 2001.

[75] Kaimai,T., Tsunemoto,H. and Ishitani,H., "Effects of a Hybrid Fuel System with Diesel and Premixed DME/Methane Charge on Exhaust Emissions in a Small DI Diesel Engine". Society of Automotive Engineers. SAE 1999-01-1509. 1999.

[76] Lida,N. and Igarashi,T., "Auto-Ignition and Combustion of n Butane and DME/Air Mixtures in a Homogeneous Charge Compression Ignition Engine". Society of Automotive Engineers. SAE 2000-01-1832. 2000.

[77] Ogawa,H., Miyamoto,N., Kaneko,N. and Ando,H., "Combustion Control and Operating Range Expansion With Direct Injection of Reaction Suppressors in a

Premixed DME HCCI Engine". Society of Automotive Engineers. SAE 2003-01-0746. 2003.

[78] Lida,N., "Combustion Analysis of Methanol-Fuelled Active Thermo-Atmosphere Combustion (ATAC) Engine Using a Spectroscopic Observation". Society of Automotive Engineers. SAE 940684. 1994.

[79] Ishibashi,Y. and Asai,M., "Improving the Exhaust Emissions of Two-Stroke Engines by Applying the Activated Radical Combustion". Society of Automotive Engineers. SAE 960742. 1996. pp: 113-123.

[80] Suzuki,H., Koike,N., Ishii,H. and Odaka,M., "Exhaust Purification of Diesel Engines by Homogeneous Charge with Compression Ignition Part 1: Experimental Investigation of Combustion and Exhaust Emission Behaviour Under Pre-Mixed Homogeneous Charge Compression Ignition Method". Society of Automotive Engineers. SAE 970313. 1997.

[81] Christensen,M. and Johansson,B., "Influence of Mixture Quality on Homogeneous Charge Compression Ignition". Society of Automotive Engineers. SAE 9824541. 1998.

[82] Milovanovic,N., "A study of controlled autoignition (CAI) combustion in internal combustion engines". Degree Type: PhD, Loughborough University. 2003.

[83] Bisetti,F., Chen,J., Hawkes,E.R. and Chen,J.H., "Probability density function treatment of turbulence/chemistry interactions during the ignition of a temperature-stratified mixture for application to HCCI engine modeling". Combust.Flame. Vol. 155. Issue: 4. 2008. pp: 571-584.

[84] Harada,A., Shimazaki,N., Sasaki,S., Miyamoto,T., Akagawa,H. and Tsujimura,K., "The Effects of Mixture Formation on Premixed Lean Diesel Combustion Engine". Society of Automotive Engineers. SAE 980533. 1998.

[85] Noguchi,M., Tanaka,Y., Tanaka,T. and Takeuchi,Y., "Study on Gasoline Engine Combustion by Observation of Intermediate Reactive Products during Combustion". Society of Automotive Engineers. SAE 790840.

[86] Sharke P. "Otto or Not, Here it Comes".Mechanical Engineers . June 2000;Vol: 122. pp: 62-69.

[87] Zur Loye AO, Akinyemi OC, Durrett RP, Flynn PF, Hunter GL, Moore GA, et al, inventors. AnonymousPremixed Charge Compression Ignition Engine with Optimal Combustion Control . 6286482. 3 June 2004 .

[88] Law,D., Kemp,D., Allen,J., Kirkpatrick,G. and Copland,T., "Controlled combustion in an IC-engine with a fully variable valve train". Society of Automotive Engineers. SAE 2001-01-0251. 2001.

[89] Milovanovic,N., Chen,R. and Turner,J., "Influence of variable valve timings on the gas exchange process in a controlled auto-ignition engine". Professional Engineering Publishing. Proceedings of the Institution of Mechanical Engineers --

Part D -- Journal of Automobile Engineering. Vol. 218. Issue: 5. 2004. pp: 567-583.

[90] Law,D., Kemp,D., Allen,J., Kirkpatrick,G. and Copland,T., "Controlled Combustion in an IC Engine with a Fully Variable Valve Train". Society of Automotive Engineers. SAE 2000-01-0251. 2000.

[91] Allen,J. and Law,D., "Variable Valve Actuated Controlled Auto-Ignition: Speed Load Maps and Strategic Regimes of Operation". Society of Automotive Engineers. SAE 2002-01-0422. 2002.

[92] Mahrous,A.M., Potrzebowski,A., Wyszynski,M.L., Xu,H.M., Tsolakis,A. and Luszcz,P., "A modelling study into the effects of variable valve timing on the gas exchange process and performance of a 4-valve DI homogeneous charge compression ignition (HCCI) engine". Energy Conversion and Management. Vol. 50. Issue: 2. 2009. pp: 393-398.

[93] Lavy,J., Dabadie,J.C., Angelberger,C., Duret,P., Willand,J., Juretzka,A., Schaflein,J., Ma,T., Lendresse,Y., Satre,A., Schulz,C., Kramer,H., Zhao,H. and Damiano,L., "Innovative Ultra-low NOx Controlled Auto-Ignition Combustion Process for Gasoline Engines: The 4-SPACE Project". Society of Automotive Engineers. SAE 2000-01-1837. 2001.

[94] Shaver,G.M., Roelle,M.J. and Christian Gerdes,J., "Modeling cycle-to-cycle dynamics and mode transition in HCCI engines with variable valve actuation". Control Eng.Pract. Vol. 14. Issue: 3. 2006. pp: 213-222.

[95] Ohyama,Y., "Simultaneous Control of Air/fuel Ratio and Intake, Exhaust Valve Timing for HCCI Operation". Society of Automotive Engineers. SAE 2003-01-1084. 2003.

[96] Hyvönen,J., Haraldsson,G. and Johansson,B., "Supercharging HCCI to Extend the Operating Range in a Multi-Cylinder VCR-HCCI Engine". Society of Automotive Engineers. SAE 2003-01-3214. 2003.

[97] Canakci,M., "An experimental study for the effects of boost pressure on the performance and exhaust emissions of a DI-HCCI gasoline engine". Fuel. Vol. 87. Issue: 8-9. 2008. pp: 1503-1514.

[98] Richter,M., Engstrom,J., Franke,A., Alden,M., Hultqvist,A. and Johansson,B., "The Influence of Charge Inhomogeneity on the HCCI Combustion Process". Society of Automotive Engineers. SAE 2000-01-2868. 2000.

[99] "Fuel mixture stratification as a method for improving homogeneous charge compression ignition engine operation". Available at: http://www.patentstorm.us/patents/7128046/fulltext.html. Accessed on: 03/02, 2009.

[100] Zheng,Z. and Yao,M., "Charge stratification to control HCCI: Experiments and CFD modeling with n-heptane as fuel". Fuel. Vol. 88. Issue: 2. 2009. pp: 354-365.

[101] Berntsson,A.W. and Denbratt,I., "HCCI Combustion Using Charge Stratification for Combustion Control". SAE Paper 2007-01-0210. 2007.

[102] Mase,Y., Kawashima,J., Sato,T. and Eguchi,M., "Nissan's New Multivalve DI Diesel Engine Series". Society of Automotive Engineers. SAE 981039. 1998.

[103] Su,H., Vikhansky,A., Mosbach,S., Kraft,M., Bhave,A., Kim,K., Kobayashi,T. and Mauss,F., "A computational study of an HCCI engine with direct injection during gas exchange". Combust.Flame. Vol. 147. Issue:1-2. 2006. pp: 118-132.

[104] Standing,R., Kalian,N., Ma,T., Zhao,H. and Wirth,M., "Effects of Injection Timing and Valve Timings on CAI Operation in a Multi-Cylinder DI Gasoline Engine". Society of Automotive Engineers. SAE 2005-01-0132. 2005.

[105] Leach,B., Zhao,H., Li,Y. and Ma,T., "Control of CAI Combustion Through Injection Timing in a GDI Engine With an Air- Assisted Injector". Society of Automotive Engineers. SAE 2005-01-0134. 2005.

[106] Hasegawa,R. and Yanagihara,H., "HCCI Combustion in DI Diesel Engine". Society of Automotive Engineers. SAE 2003-01-0745. 2003.

[107] Tao,F., Liu,Y., RempelEwert,B.H., Foster,D., Reitz,R.D., Choi,D. and Miles,P.C., "Modelling the Effects of EGR and Injection Pressure on Soot Formation in a High-Speed Direct-Injection (HSDI) Diesel Engine Using a Multi-Step Phenomenological Soot Model". Society of Automotive Engineers. SAE 2005-01-0121. 2005.

[108] Ra,Y. and Reitz,R.D., "The Use of Variable Geometry Sprays With Low Pressure Injection for Optimization of Diesel HCCI Engine Combustion". 2005-01-0148. 2005.

[109] Nishijima,Y., Asaumi,Y. and Aoyagi,Y., "Impingement spray system with direct water injection for premixed lean diesel combustion control". Society of Automotive Engineers. SAE 2002-01-0109. 2002.

[110] Su,W., Wang,H. and Liu,B., "Injection Mode Modulation for HCCI Diesel Combustion". Society of Automotive Engineers. SAE 2005-01-0117. 2005.

[111] Koopmans,L. and Denbratt,I., "A Four Stroke Camless Engine, Operated in Homogeneous Charge Compression Ignition Mode with Commercial Gasoline". Society of Automotive Engineers. SAE 2001-01-3610. 2001.

[112] Chen,R., Milovanovic,N., Turner,J. and Blundell,D., "The Thermal Effect of Internal Exhaust Gas Recirculation on Controlled Auto Ignition". Society of Automotive Engineers. SAE 2003-01-0751. 2003.

[113] Christensen,M., Johansson,B., Amneus,P. and Mauss,F., "Supercharged Homogeneous Charge Compression Ignition". Society of Automotive Engineers. SAE 980787. 1998. pp: 1-16.

[114] Dec,J.E., "A Computational Study of the Effects of Low Fuel Loading and EGR on Heat Release Rates and Combustion Limits in HCCI Engines". Society of Automotive Engineers. SAE 2002-01-1309. 2002.

[115] Chen,R. and Milovanovic,N., "A computational study into the effect of exhaust gas recycling on homogeneous charge compression ignition combustion in internal combustion engines fuelled with methane". Elsevier. International Journal of Thermal Sciences 41. 11 October 2002. pp: 805-813.

[116] Aroonsrisopon,T., Hayashi,M., Foster,D. and Martin,J., "The Effect of Intake Air Temperature, Compression Ratio and Coolant Temperature on the Start of Heat Release in an HCCI (Homogeneous Charge Compression Ignition) Engine". Society of Automotive Engineers. SAE 2001-01-1880. 2001.

[117] Fiveland,S.B. and Assanis,D.N., "A Four-Stroke Homogeneous Charge Compression Ignition Engine Simulation for Combustion and Performance Studies". Society of Automotive Engineers. SAE 2000-01-0332. 2000.

[118] Peng,Z., Zhao,H. and Ladommatos,N., "Effects of Air/Fuel Ratios and EGR Rates on HCCI Combustion of n-Heptane, a Diesel Type Fuel". Society of Automotive Engineers. SAE 2003-01-0747. 2003.

[119] Amano,T., Morimoto,S. and Kawabata,Y., "Modelling of the Effect of Air/Fuel Ratio and Temperature Distribution on HCCI Engines". Society of Automotive Engineers. SAE 2001-01-1024. 2001.

[120] Milovanovic,N., Blundell,D., Pearson,R. and Turner,J. ; .C., R., "Enlarging the Operational Range of a Gasoline HCCI Engine By Controlling the Coolant Temperature". Society of Automotive Engineers. SAE 2005-01-0157. 2005.

[121] Lü,X., Chen,W. and Huang,Z., "A fundamental study on the control of the HCCI combustion and emissions by fuel design concept combined with controllable EGR. Part 2. Effect of operating conditions and EGR on HCCI combustion". Fuel. Vol. 84. Issue: 9. 2005. pp: 1084-1092.

[122] Aceves,S.M., Flowers,D., Martinez-Frias,J., Espinosa-Loza,F., Fitz,W.J. and Dibble,R., "Fuel and Additive Characterization for HCCI Combustion". Society of Automotive Engineers. SAE 2003-01-1814. 2003.

[123] Tanaka,S., Ayala,F., Keck,J.C. and Heywood,J.B., "Two-stage ignition in HCCI combustion and HCCI control by fuels and additives". Combust.Flame. Vol. 132. 1-2. 2003. pp: 219-239.

[124] Agarwal,A. and Assanis,D.N., "Multi-Dimensional Modelling of Natural Gas Ignition Under Compression Ignition Conditions Using Detailed Chemistry". Society of Automotive Engineers. SAE 980136. 1998.

[125] Yarnaya,Y., Furutani,M. and Ohta,Y., "Advanced/Retarded Criterion on Ignition of Fuel/Air Mixtures with Formaldehyde Doping". Proceedings of the sixth international symposium on diagnostics and modelling of combustion in internal combustion engines; COMODIA 2004, August 2-5, Yokohama, Japan August 2 - 5. : COMODIA. 2004. 6th International Symposium on Diagnostics and Modeling of Combustion in Internal Combustion Engines.

[126] Flowers,D.L., Aceves,S.M., Westbrook,C.K., Smith,J.R. and and Dibble,R.W.,

"Sensitivity of Natural Gas HCCI Combustion to Fuel and Operating Parameters Using Detailed Kinetic Modeling". : American Society of Mechanical Engineers. 1999. Proceedings of the ASME Advanced Energy Systems Division, Edited by Aceves, S.M.; Garimella, S.; and Peterson, R.

[127] Zheng,J., Yang,W., Miller,D.L. and Cernansky,N.P., "A Skeletal Chemical Kinetic Model for the HCCI Combustion Process". Society of Automotive Engineers. SAE 2002-01-0423. 2002.

[128] Zhao,H., Peng,Z., Williams,J. and Ladommatos,N., "Understanding the Effects of Recycled Burnt Gases on the Controlled Auto-ignition (CAI) Combustion in Four-Stroke Gasoline Engines". Society of Automotive Engineers. SAE 2001-01-3607. 2001.

[129] Woschni,G., "A Universally Applicable Equation for the Instantaneous Heat Transfer Coefficient in the Internal Combustion Engine". Society of Automotive Engineers. SAE 670931. 1967. pp: 3065-3083.

[130] Flowers,D., Aceves,S., Martinez-Frias,J., Hessel,R. and Dibble,R., "Effect of Mixing on Hydrocarbon and Carbon Monoxide Emissions Prediction for Isooctane HCCI Engine Combustion Using a Multi-zone Detailed Kinetics Solver". Society of Automotive Engineers. SAE 2003-01-1821/JSAE 20030127. 2003.

[131] Komninos,N.P., Hountalas,D.T. and Kouremenos,D.A., "Development of a New Multi-Zone Model for the Description of Physical Processes in Hcci Engines". Society of Automotive Engineers. SAE 2004-01-0562. 2004.

[132] Fiveland,S.B. and Assanis,D.N., "Development of a Two-Zone HCCI Combustion Model Accounting for Boundary Layer Effects". Society of Automotive Engineers. SAE 2001-01-1028. 2001.

[133] Easley,W.L., Agarwal,A. and Lavoie,G.A., "Modelling of HCCI Combustion and Emissions Using Detailed Chemistry". Society of Automotive Engineers. SAE 2001-01-1029. 2001.

[134] Komninos,N.P., Hountalas,D.T. and Kouremenos,D.A., "Description of In-Cylinder Combustion Processes in HCCI Engines Using a Multi-Zone Model". Society of Automotive Engineers. SAE 2005-01-0171. 2005.

[135] Komninos,N.P. and Hountalas,D.T., "Improvement and validation of a multi-zone model for HCCI engine combustion concerning performance and emissions". Energy Conversion and Management,. Vol. 49. Issue: 10. 2008. pp: 2530-2537.

[136] Orlandini,I., Kulzer,A., Weberbauer,F. and Rauscher,M., "Simulation of Self Ignition in HCCI and Partial HCCI Engines Using a Reduced Order Model". Society of Automotive Engineers. SAE 2005-01-0159. 2005.

[137] Aceves,S.M., Martinez-Frias,J., Flowers,D.L., Smith,J.R., Dibble,R.W., Wright,J.F. and Hessel,R.P., "A Decoupled Model of Detailed Fluid Mechanics Followed by Detailed Chemical Kinetics for Prediction of Iso-Octane HCCI Combustion". Society of Automotive Engineers. SAE 2001-01-3612. 2001.

[138] Kongsereeparp,P. and Checkel,M.D., "Novel Method of Setting Initial Conditions for Multi-Zone HCCI Combustion Modeling ". Society of Automotive Engineers. SAE 2007-01-0674. 2007.

[139] Li,G., Bo,T., Chen,C. and Johns,R.J.R., "CFD Simulation of HCCI Combustion in a 2-Stroke DI Gasoline Engine". Society of Automotive Engineers. SAE 2003-01-1855. 2003.

[140] Kong,S.C. and Reitz,R.D., "Multidimensional Modeling of Diesel Ignition and Combustion Using a Multistep Kinetics Model". Journal of Engineering for Gas Turbine and Power, ASME Transactions. Vol. 115. 1993. pp: 781-789.

[141] Ali,A., Cazzoli,G., Kong,S.C. and Reitz,R.D., "Improvement in Computational Efficiency for HCCI Engine Modeling by Using Reduced Mechanisms and Parallel Computing". 2003. Central State Section Meeting.

[142] Aceves,S., Martinez-Frias,J., Flowers,D., Smith,J.R., Dibble,R. and Chen,J.Y., "A Computer Generated Reduced Iso Octane Chemical Kinetic Mechanism Applied to Simulation of HCCI Combustion". Society of Automotive Engineers. SAE 2002-01-2870. 2002.

[143] Iwashiro,Y., Tsurushima,T., Nishijima,Y., Asaumi,Y. and Aoyagi,Y., "Fuel Consumption Improvement and Operation Range Expansion in HCCI by Direct Water Injection". Society of Automotive Engineers. SAE 2002-01-0105. 2002.

[144] Iida,S., Kusaka,J. and Daisho,Y., "Numerical Study on Iso-Octane Homogeneous Charge Compression Ignition". Society of Automotive Engineers. SAE 2003-01-1820. 2003. pp: 1-6.

[145] Kusaka,J. and Daisho,Y., "Multi-Dimensional Modelling Combined with a Detailed Kinetics (Application for HCCI of Natural Gas)". July 1-4. : COMODIA. 2001. The Fifth International Symposium on Diagnostics and Modelling of Combustion in Internal Combustion Engines.

[146] Ogink,R., "Computer Modeling of HCCI Combustion". Division of Thermo and Fluid Dynamics, CHALMERS UNIVERSITY OF TECHNOLOGY. 2004.

[147] "Reaction Mechanism - elementary process " 2000. Available at: http://www.science.uwaterloo.ca/~cchieh/cact/c123/elmntary.html. Accessed on: 19/05, 2009.

[148] Laidler,K.J., "*Chemical Kinetics*". Third Edition. UK. Benjamin-Cummings. 1997.

[149] Borman,G.L. and Ragland K.W., "Combustion engineering". First. New York. McGraw-Hill. 1998.

[150] Ophardt,C.E. "What is Gasoline?'' 2003. Available at: http://www.elmhurst.edu/~chm/vchembook/514gasoline.html. Accessed on:06/26, 2006.

[151] Violi,A., Yan,S., Eddings,E.G., Sarofim,A.F., Granata,S., Faravelli,T. and Ranzi,E., "EXPERIMENTAL FORMULATION AND KINETIC MODEL FOR JP-8 SURROGATE MIXTURES". Taylor & Francis. Combustion Sci.Technol. Vol. 174. Issue: 11. 2002. pp: 399.

[152] Lenhert DB, Khan AR, Cernansky NP, Miller DL, Owens KG. "The Oxidation of an Isf Surrogate and Its Components in the Negative Temperature Coefficient Region". 2003;Volume: RIC Engines III.

[153] Eng,J.A., Leppard,W.R. and Sloane,T.M., "The Effect of Di-Tertiary Butyl Peroxide (DTBP) Addition to Gasoline on HCCI Combustion". Society of Automotive Engineers. SAE 2003-01-3170. 2003.

[154] Tanaka,S., Ayala,F. and Keck,J.C., "A reduced chemical kinetic model for HCCI combustion of primary reference fuels in a rapid compression machine". Combustion and Flame. Vol. 133. 2003. pp: 467-481.

[155] Yelvington,P.E. and Green,W.E., "Prediction of the Knock Limit and Viable Operating Range for a Homogeneous-Charge Compression-Ignition (HCCI) Engine". Society of Automotive Engineers. SAE 2003-01-1092. 2003.

[156] Steacie,E.W.R., , "*Atomic and Free Radical Reactions*". 2nd Edition. Reinhold, New York. 1954.

[157] Robertson,S.H., Seakins,P.W. and Pilling,M.J., Chapter 2 Elementary reactions. In: M.J. Pilling, editor. " Comprehensive Chemical Kinetics". Elsevier. 1997. pp: 125-234.

[158] Ranzi,E., Gaffuri,P., Faravelli,T. and Dagaut,P., "A wide-range modeling study of n-heptane oxidation". Combust.Flame. Vol. 103. Issue: 1-2. 1995. pp: 91-106.

[159] Curran,H.J., Gaffuri,P., Pitz,W.J. and Westbrook,C.K., "A Comprehensive Modeling Study of n-Heptane Oxidation". Combust.Flame. Vol. 114. Issue: 1-2. 1998. pp: 149-177.

[160] Cox,R.A. and Cole,J.A., "Chemical Aspects of the Autoignition of Hydrocarbon-Air Mixtures". Combustion and Flame. Vol. 60. 1985. pp: 109-123.

[161] Westbrook,C.K., Pitz,W.J., Boercker,J.E., Curran,H.J., Griffiths,J.F., Mohamed,C. and Ribaucour,M., "Detailed chemical kinetic reaction mechanisms for autoignition of isomers of heptane under rapid compression". Proceedings of the Combustion Institute. Vol. 29. Issue: 1. 2002. pp: 1311-1318.

[162] Bozzelli, J.W. and Sheng, C., ''Thermochemistry, Reaction Paths, and Kinetics on the Hydroperoxy-Ethyl Radical Reaction with O2: New Chain Branching Reactions in Hydrocarbon Oxidation'', The Journal of Physical Chemistry A 2002 106 (7), 1113-1121

[163] Westbrook,C., Warnatz,J. and Pitz,W., "A Detailed Chemical Kinetic Reaction Mechanism for the Oxidation of Iso-Octane and n-Heptane over an Extended Temperature Range and its Application to Analysis of Engine Knock". 22th

Symposium (International) on Combustion: The Combustion Institute. 1988. 22th Symposium (International) on Combustion.

[164] Amneus,P., Nilsson,D., Mauss,F., Christensen,M. and Johansson,B., "Homogeneous Charge Compression Ignition Engine: Experiments and Detailed Kinetic Calculations". : COMODIA. 1998. The fourth International Symposium COMODIA.

[165] Dagaut,P., Reuillon,M. and Cathonnet,M., "High Pressure Oxidation of Liquid Fuels From Low to High Temperature. 1. n-Heptane and iso-Octane.". Taylor & Francis. Combustion Sci.Technol. Vol. 95. Issue: 1. 1994. pp: 233.

[166] Pitz,W.J., Westbrook,C.K. and Leppard,W.R., "Auto-Ignition Chemistry of n-Butane in a Motored Engine: A Comparison of Experimental and Modelling Results". Society of Automotive Engineers. SAE 881605. 1988. pp: 648-657.

[167] Curran,H.J., Gaffuri,P., Pitz,W.J. and Westbrook,C.K., "A comprehensive modeling study of iso-octane oxidation". Combust.Flame. Vol. 129. Issue: 3. 2002. pp: 253-280.

[168] Yamasaki,Y. and Lida,N., "Numerical Analysis of Auto Ignition and Combustion of n-Butane and Air Mixture in the Homogeneous Charge Compression Ignition Engine by Using Elementary Reactions". Society of Automotive Engineers. SAE 2003-01-1090. 2003. pp: 1-12.

[169] Yamasaki,Y. and Lida,N., "Numerical Simulation of Auto-Ignition and Combustion of n-Butane and Air Mixtures in a 4 Stroke HCCI Engine by Using Elementary Reactions". Society of Automotive Engineers. SAE 2000-01-1834. 2000. pp: 1-14.

[170] Westbrook,C.K., Pitz,W.J., Thornton,M.M. and Malte,P.C., "A kinetic modeling study of n-pentane oxidation in a well-stirred reactor". Combust.Flame. Vol. 72. Issue:1. 1988. pp: 45-62.

[171] Agosta,A., Cernansky,N.P., Miller,D.L., Faravelli,T. and Ranzi,E., "Reference Components of Jet Fuel: Kinetic Modeling and Experimental Results". Exp. Therm. Fluid. Sci. Vol. 28. 2004. pp: 701-708.

[172] Wang,H. and Frenklach,M., "Detailed reduction of reaction mechanisms for flame modeling". Combust.Flame. Vol. 87. Issue: 3-4. 1991. pp: 365-370.

[173] Halstead,M.P., Kirsch,L.J. and Quinn,C.P., "The Autoignition of Hydrocarbon Fuels at High Temperatures and Pressures-Fitting of a Mathematical Model". Combustion and Flame. Vol. 30. 1977. pp: 45-60.

[174] Halstead,M.P., Kirsch,L.J., Prothero,A. and Quinn,C.P., "A Mathematical Model for Hydrocarbon Autoignition At High Pressures". Proceedings of the Royal Society of London. Vol. A.346. 1975. pp: 515-538.

[175] Griffiths,J.F., "Reduced Kinetic Models and Their Application to Practical Combustion Systems Progress in Energy and Combustion Science". Progress in

Energy and Combustion Science. Vol. 21. 1995. pp: 25-107.

[176] Hu,H. and Keck,J., "Autoignition of Adiabatically Compressed Combustible Gas Mixtures". Society of Automotive Engineers. SAE 872110. 1987.

[177] Li,H., Miller,D.L. and Cernansky,N.P., "A Study on the Application of a Reduced Chemical Reaction Model to Motored Engines for Heat Release Prediction". Society of Automotive Engineers. SAE 922328. 1992.

[178] Li,H., Miller,D.L. and Cernansky,N.P., "Development of a Reduced Chemical Kinetic Model For Prediction of Preignition Reactivity and Autoignition of Primary Reference Fuels". Society of Automotive Engineers. SAE 960498. 1996.

[179] Zheng,J., Yang,W., Miller,D.L. and Cernansky,N.P., "Prediction of Pre-ignition Reactivity and Ignition Delay for HCCI Using a Reduced Chemical Kinetic Model". Society of Automotive Engineers. SAE 2001-01-1025. 2001.

[180] Müller,C.U., Peters,N. and Liňán,A., "Global Kinetics for n-Heptane Ignition at High Pressures". Proceedings of the Combustion Institute. Vol. 24. 1992. pp: 777-784.

[181] Annand,W.J.D., "Heat transfer in the cylinder of reciprocating internal combustion engines". Proceedings of the IMechE, Part D: Journal of Automobile Engineering. Vol. 177. 1963. pp: 973-990.

[182] Petzold,L.R., , "Computer Methods for Ordinary Differential Equations and Differential-Algebraic Equations". SIAM: Society for Industrial and Applied Mathematics. 1998.

[183] Press,W., Flannery B., Teukolsky S. and Vetterling W., "Numerical Recipes in C : The Art of Scientific Computing". Cambridge University Press. 1992.

[184] Gear,C.W., "Numerical Initial Value Problems in Ordinary Differential Equations". Upper Saddle River, NJ, USA. Prentice Hall PTR. 1971.

[185] Brown,P.N., Byrne,G.D. and Hindmarsh,A.C., "VODE: A Variable-Coefficient ODE Solver". SIAM. SIAM J.Sci.and Stat.Comput. Vol. 10. Issue: 5. 1989. pp: 1038-1051.

[186] John Prentice. "Fortran 90 for Science Students". 1995. Available at: http://www.lahey.com/PRENTICE.HTM. Accessed on: 09/09, 2009.

[187] Kee RJ, Rupley FM, Meeks E. "CHEMKIN-III: A FORTRAN CHEMICAL KINETICS PACKAGE FOR THE ANALYSIS OF GAS-PHASE CHEMICAL AND PLASMA KINETICS". 1996;Volume: SAND96-8216.

[188] Kee RJ, Rupley FM, Meeks E, Miller JA. "CHEMKIN-III: A Fortran Chemical Kinetics Package For The Analysis of Gas-Phase Chemical and Plasma Kinetics". May 1996;

[189] Brown,P.N. and Hindmarsh,A.C. "Variable-coefficient Ordinary Differential

Equation solver (VODE) FORTRAN code". Available at: http://www.netlib.org/ode/vode.f. Accessed on: 09/01, 2009.

[190] Zheng,J., Miller,D.L. and Cernansky,N.P., "A Global Reaction Model for the HCCI Combustion Process". Society of Automotive Engineers. SAE 2004-01-2950. 2004.

[191] Kaario,O., Larmi,M. and Tanner,F., "Comparing single-step and multi-step chemistry using the laminar and turbulent characteristic time combustion model in two diesel engines". Society of Automotive Engineers. SAE 2002-01-1749. 2002.

[192] Liu,J., Gong,J. and Cai,L., "Multi-dimensional simulation of air=fuel premixing and stratified combustion in a gasoline direct injection engine with combustion chamber bowl offset". Society of Automotive Engineers. SAE 2006-32-0006. 2006.

[193] Blunsdon,C.A. and and Dent,J.C., "The Simulation of Autoignition and Knock in a Spark Ignition Engine with Disk Geometry". Society of Automotive Engineers. SAE 940524. 1994.

[194] Eckert,P., Kong,S.C. and Reitz,R.D., "Modeling Autoignition and Engine Knock Under Spark Ignition Conditions". Society of Automotive Engineers. SAE 2003-01-0011. 2003.

[195] Kong,S.C., Han,Z. and Reitz,R.D., "The Development and Application of a Diesel Ignition and Combustion Model for Multidimensional Engine Simulation". Society of Automotive Engineers. SAE 950278. 1995.

[196] Ferguson,C.R. and Kirkpatrick A.T., , "Internal combustion engines : applied thermosciences". 2nd. New York ; Chichester. Wiley. 2001.

[197] Najt,P.M., "Evaluating threshold knock with a semi-empirical model-initial results". Society of Automotive Engineers. SAE 872149. 1987.

[198] Moses,E., Yarin,A.L. and Bar-Yoseph,P., "On knocking prediction in spark ignition engines". Combust.Flame. Vol. 101. Issue: 3. 1995. pp: 239-261.

[199] Noda,T. and Kazuya,H., "Development of transient knock prediction technique by using a zero-dimensional knocking simulation with chemical kinetics". Society of Automotive Engineers. SAE 2004-01-0618. 2004.

[200] Hajireza,S., Mauss,F. and Sunden,B.A., "Investigation of end-gas temperature and pressure increases in gasoline engines and relevance for knock occurrence". Society of Automotive Engineers. SAE 971671. 1997.

[201] Hajireza,S., Sunden,B. and Mauss,F., "A Three-Zone Model for Investigation of Gas Behaviour in the Combustion Chamber of SI Engines in Relation to Knock". Society of Automotive Engineers. SAE 1999-01-0219. 1999.

[202] Gordon S, McBride BJ. "Computer Program for Calculation of Complex Chemical Equilibrium Compositions and Applications I. Analysis". 1994; Vol. E-8017.

[203] Li,H., Prabhu,S.K., Miller,D.L. and Cernansky,N.P., "Auto-Ignition Chemistry Studies on Primary Reference Fuels in a Motored Engine". Society of Automotive Engineers. SAE 942062. 1994.

[204] Callahan,C.V., Curran,H.J., Dryer,F.L., Pitz,W.J. and Westbrook,C.K., "Oxidation of automotive primary reference fuels at elevated pressures". Conference: Twenty-Seventh International Conference on Combustion Mar 01. : Boulder, Co. 1999.

[205] Reynolds WC. "The element potential method for chemical equilibrium analysis: Implementation in the interactive program STANJAN-III". 1986.

[206] Arrigoni,V. and Cornetti,G.M., "High speed knock in SI engines". Society of Automotive Engineers. SAE 741056. 1974.

[207] Swarts,A., Yates,A. and Viljoen,C., "Standard knock intensity revisited: Atypical burn rate characteristics identified in the CFR octane rating engine". Society of Automotive Engineers. SAE 2004-01-1850. 2004.

[208] Takagi,Y. and Itoh,T., "An analytical study on knocking heat release and its control in a spark ignition engine". Society of Automotive Engineers. SAE 880196. 1988.

[209] Babajimopoulos,A., Assanis,D., Flowers,D., Aceves,S. and Hessel,R., "A fully coupled computational fluid dynamics and multi-zone model with detailed chemical kinetics for the simulation of premixed charge compression ignition engines". International Journal of Engine Research. Vol. 6. Issue: 5. 2005. pp: 497-512.

[210] Chang,J., Guralp,O., Filipi,Z. and Assanis,D., "New Heat Transfer Correlation for an HCCI Engine Derived from Measurements of Instantaneous Surface Heat Flux". Society of Automotive Engineers. SAE 2004-01-2996. 2004.

[211] Kouremenos,D., Rakopoulos,C., Hountalas,D. and Yfantis,E., "A model Calibration and Constants Determination Procedure Based on the Elaboration of the Measured Pressure Crank Angle Diagram in a Divided Chamber Diesel Engine". Proc. ASME-WA Meeting. Vol. 21. 1990. pp: 21-31.

[212] Kouremenos,D., Rakopoulos,C., Hountalas,D. and Yfantis,E., "Evaluation Results of the Application of an Engine Diagnosis Simulation Model on Different Types of Diesel Engines". 3rd Int. Conf. on Innovation and Reliability in Automotive Design and Testing. Vol. Issue: 1. 1992. pp: 615-627.

[213] Golovitchev,V. "N-heptane Mechanism". Available at: http://www.tfd.chalmers.se/~valeri/MECH.html. Accessed on: 11/11, 2006.

[214] Babajimopoulos,A., Assanis,D.N. and Fiveland,S.B., "An Approach for Modelling the Effects of Gas Exchange Processes on HCCI Combustion and Its Application in Evaluating Variable Valve Timing Control Strategies". Society of Automotive Engineers. SAE 2002-01-2829. 2002.

[215] Chen,R. and Milovanovic,N., "A computational study into the effect of exhaust

gas recycling on homogeneous charge compression ignition combustion in internal combustion engines fuelled with methane". International Journal of Thermal Sciences. Vol. 41. Issue: 9. 2002. pp: 805-813.

[216] Van Basshuysen,R. and Schֿfer, F., "Internal combustion engine handbook : basics, components, systems and perspectives". Warrendale, PA. SAE International. 2004.

[217] Cheng,W., Hamrin,D., Heywood,J., Hochgreb,S., Min,K. and Norris,M., "An Overview of Hydrocarbon Emissions Mechanisms in Spark Ignition Engine". SAE Internaltional. 1993.

[218] Miller,J.A. and Bowman,C.T., "Mechanism and modeling of nitrogen chemistry in combustion". Progress in Energy and Combustion Science. Vol. 15. Issue: 4. 1989. pp: 287-338.

[219] Encyclopædia Britannica Online. . "Working principle of four-stroke engines". Available at: http://cache-media.britannica.com.cdnetworks.net/eb-media/72/93572-034-26C16785.jpg. Accessed on: 03/02, 2009.

[220] Encyclopædia Britannica Online. "Working principle of two-stroke cycle engines". Available at: http://cache-media.britannica.com.cdnetworks.net/eb-media/10/310-004-58E43DBF.gif. Accessed on: 03/02, 2009.

[221] Nobuyuki,K., Eiji,T., Yoshitomo,S., ‘’Auto-ignited kernels during knocking combustion in a spark-ignition engine’’. Proceedings of the Combustion Institute, Vol. 31, Issue 2, January 2007, pp: 2999-3006,

[222] Woshni,G., and Fieger,J., ‘’Experimental investigation of the heat transfer at normal and knocking combustion in Spark Ignition engines’’. MTZ. vol.43, pp.63-67, 1982.